Urban growth and its impact on urban heat sink and island formation in the desert city of Dubai

Ahmed Khalaf Nassar

M.Sc., B.Sc.,

A thesis submitted to Lancaster University in fulfilment of the requirements for

the degree of Doctor of Philosophy

September, 2015

Lancaster University

ProQuest Number: 11003592

ProQuest 11003592

Urban growth and its impact on urban heat sink and heat island formation in the desert city of Dubai

Ahmed Khalaf Nassar

A thesis submitted to Lancaster University in fulfilment of the requirements for the degree of Doctor of Philosophy

Lancaster Environment Centre, Faculty of Science and Technology

Lancaster University, United Kingdom

September, 2015

Supervised by:

Dr. G. Alan Blackburn and Dr. J. Duncan Whyatt

Lancaster University

Urban growth and its impact on urban heat sink and island formation in the desert city of Dubai

Ahmed Khalaf Nassar M.Sc., B.Sc.

Submitted in fulfilment of the requirements for the degree of Doctor of Philosophy.

September 2015

Abstract

The rapid pace of urban growth in Dubai has attracted the attention of economists, environmentalists and urban planners. This thesis quantifies the extent of urbanisation within the Emirate since the discovery of oil and investigates the impacts of such growth on urban temperatures. The study used remotely-sensed imagery in the absence of publicly available data on city growth and microclimate.

The study used a hybrid classification method and landscape metrics to capture historical urban forms, rates and engines of growth in the Emirate. Stepwise multiple regression analysis techniques were subsequently used to investigate the relationship between the rate and form of urbanisation and the intensity of the urban heat sink between 1990 and 2011. Local Climate Zones were then developed to specifically investigate the impacts of urban geometry variables and proximity to water on both urban heat sinks during the day-time and urban heat islands during the night.

The study revealed a significant increase in urban area over time (1972-2011) with accelerated phases of growth, linked to local and global economic conditions, occurring during specific periods. Physical urban growth has now outpaced population growth, indicating urban sprawl. This growth has occurred at the expense of sand and has included a significant increase in vegetation and water bodies unlike other desert cities in the Gulf region.

The results demonstrated that urban growth has promoted a heat sink effect during daytime and that all urban land use types contributed to this effect. Urban albedo was not responsible for the daytime urban heat sink; other factors including the specific heat capacity of urban materials, urban geometry and proximity to the Gulf were mainly responsible. Furthermore, increases in vegetation cover and impervious surface cover

i

over time have contributed to the daytime (morning) urban heat sink. At night-time, urban geometry and proximity to the Gulf were the major influences upon the formation of urban heat islands.

This research contributes to better understanding of urbanisation in desert cities as demonstrated through Dubai, revealing previously unknown spatiotemporal variations in urban areas across the city through the use of a time-series of satellite images. The findings provide new insights into the impacts of land cover, land use, proximity to water and urban geometry on the formation of urban heat sinks and urban heat islands in the desert environment.

Table of Contents

List of Figures

List of Tables

List of abbreviations

Abbreviation	Meaning
BHV	Building Height Variations
BSF	Building Surface Fraction
CMR	Compact Midrise
GIS	Geographic Information System
HRE	Heights of Roughness Elements
IRS	Indian Remote Sensing
ISF	Impervious Surface Fraction
Landsat ETM+	Landsat Enhanced Thematic Mapper plus
Landsat MSS	Landsat Multi Spectral Scanner
Landsat TM	Landsat Thematic Mapper
LC	Land Cover
LCZs	Local Climate Zones
LLR	Large Low-rise
LST	Land Surface Temperature
LU	Land Use
LULC	Land Use Land Cover
MODIS	Moderate-Resolution Imaging Spectroradiometer
OHR	Open High-rise
OLR	Open Low-rise
OMR	Open Midrise
PSF	Pervious Surface Fraction
SB	Sparsely Built
SUHI	Surface Urban Heat Island
SUHS	Surface Urban Heat Sink
SVF	Sky View Factor
TIR	Thermal Infrared
UHI	Urban Heat Island
UHS	Urban Heat Sink
USGS	United States Geological Survey

Acknowledgement

Declaration

I declare that, except where explicit reference is made to the contribution of others, that this thesis is the result of my own work and has not been submitted for any other degree at the Lancaster University or any other institution.

Signature

Ahmed Khalaf Nassar

September 2015

Chapter 1 Introduction

1.1 Rationale

Dubai, like many desert cities, has witnessed great economic change resulting in rapid urbanisation in the last two decades which has turned the desert into residential, commercial, sports and tourism projects. Cities within a city are a particular characteristic of this Emirate, and a number of mini cities have been developed including Dubai Festival City, Sports City, Media City, Internet City and Healthcare City. This rapid urbanization has raised many concerns by environmentalists about the impacts of such rapid growth on the environment and inhabitants (Intercon, 2010; Kelbaugh, 2011). Figure 1.1 depicts the rapid pace of urbanisation along a major road in Dubai over a 13-year period.

Figure 1.1 Urban developments along Sheikh Zayed Road (Courtesy: weburbanist1).

One of the environmental impacts of urbanisation can be the increase of near-surface temperature which has negative effects on human health and comfort, particularly during the summer (Johnson et al., 2011; Taha, 1997; US EPA, 2008a). In Dubai, it could be argued that the large urban development has been accompanied by an increase in the amount of vegetation and inland water which tend to decrease surface temperature. These changes in land cover differ from those in other desert cities such as Muscat in Oman (Al-Awadhi, 2007) and Doha in Qatar (Al-Manni et al, 2007) which have experienced a decrease in vegetation cover with increased urbanisation.

However, there is no publicly accessible information on the urban expansion of Dubai and changes in land cover, likely due to a paucity of data overall and governmental restrictions on data that do exist. This research sought to solve this problem by making use of freely accessible medium-high spatial resolution satellite data to investigate the change of land cover types in Dubai covering the full period from the start of the Landsat mission in 1972 to 2011. The study employed landscape metrics and other data sources to explore the drivers of the spatiotemporal dynamics of urban growth based on socio-economic information and local/regional events, and then linking the findings to recent empirical urban growth theory (Dietzel et al., 2005a).

Consequently, the impact of changes in land cover/use and albedo on daytime land surface temperature were explored using three Landsat thermal images from 1990 to 2011 and statistical analysis techniques. The findings of this study prompted an in-depth study of the effects of urban geometry (i.e. building heights, sky view factor, etc.) on the diurnal and seasonal changes of land surface temperature using primarily Moderate Resolution Imaging Spectroradiometer (MODIS) data. This study employed a Local Climate Zones (LCZ) classification schema to explain the inter-zone surface temperature variations in Dubai. This study was also driven by the fact that the dramatic

14

urban growth of Dubai has extended horizontally as well as vertically with more than 403 buildings above 100m tall, with Dubai being ranked second in the world in terms of average height of buildings, after Busan in South Korea (Gerometta, 2009). This makes Dubai an interesting case study to investigate how the combination of urban geometry, land cover and proximity to water impact upon land surface temperature variations in desert environments.

1.2 Study area

1.2.1 Location and size

Dubai emirate is located in the Northern region of the United Arab Emirates, on the southeast coast of the Arabian Gulf (Fig. 1.2). Dubai is one of seven emirates forming the United Arab Emirates, being the second largest after Abu Dhabi Emirate in terms of population and area. The total area of the emirate before the development of the islands was 3885 km^2 excluding Hatta which is an exclave city that has no boundary with Dubai Emirate (Department of Finance, 2009). Dubai Creek runs south from the Arabian Gulf for 13km with a width ranging from 0.2km to the north and 1.8km to the south, dividing the city into Deira to the east and Bur Dubai to the west.
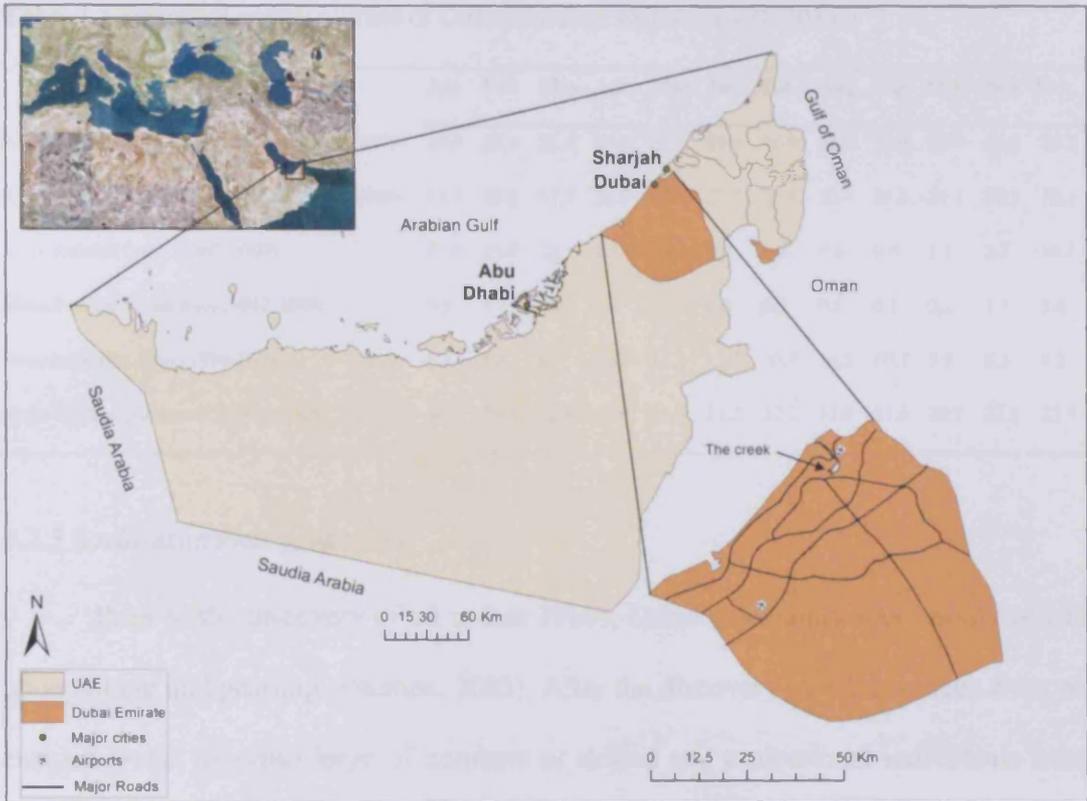
Figure 1.2 Study area, Dubai Emirate, United Arab Emirates. The map of Dubai Emirate shows the major roads that exist in 2014 (Sources: Vector data: Dubai municipality; Raster data: ESRI online within the ArcMap software).

1.2.2 Physical properties and climate

Dubai is generally flat with an average altitude of 8 meters above sea level and is surrounded on three sides by hundreds of kilometres of red sand dunes except the northern side which overlooks the Arabian Gulf. Dubai is classified as hyper-arid environment (Böer, 1997) with an annual average rainfall of approximately 8mm falling mostly in winter and late autumn (Dubai Airport, 2010). The warmest months in Dubai are June to August with an average maximum temperature of 40°C and average minimum of 28°C; the coldest months are December to February with an average maximum temperature of 25°C and average minimum of 15°C (Table 1.1).

16

Table 1.1 Historical annual climate of Dubai (Source: Dubai airport, 2014[2]).

	Jan	Feb	Mar	Apr	May	Jun	Jul	Aug	Sep	Oct	Nov	Dec
Average Maximum Temperature °C (1984-2009)	23.9	25.4	28.4	33.0	37.7	39.5	40.9	41.3	38.9	35.4	30.6	26.2
Average Minimum Temperature °C (1984-2009)	14.3	15.5	17.7	21.0	25.1	27.3	30.0	30.4	27.7	24.1	20.1	16.3
Mean Rainfall (mm) (1967-2009)	18.8	25.0	22.1	7.2	0.4	0.0	0.8	0.0	0.0	1.1	2.7	16.2
Mean # of Days with Rain (1967-2009)	5.5	4.7	5.8	2.6	0.3	0.0	0.5	0.5	0.1	0.2	1.3	3.8
Sunshine Hours / day (1974-2009)	8.1	8.6	8.7	10.2	11.3	11.5	10.7	10.5	10.3	9.9	9.3	8.2
Mean Sea Temperature °C (1987-2009)	20.9	20.6	22.3	25.0	28.5	31.2	32.2	32.8	31.9	29.7	27.1	23.3

1.2.3 Socio-economic properties

Prior to the discovery of oil in late 1960s, Dubai's economy was heavily reliant upon fishing and pearling (Pacione, 2005). After the discovery of oil, revenues from oil enabled Dubai to attract large of numbers of skilled and professional individuals from overseas that played a critical role in the urbanization process in the city. As a result, Dubai's total population increased dramatically from 183,187 inhabitants in 1975 to 2,213,000 inhabitants in 2013 (Dubai Statistical Centre, 2013) (Fig.1.3) with expatriate residents forming about 90% of the total population. In general, the Gulf cities never accomplished a high urban status prior to the discovery of the oil because of their poor environmental conditions and low population. During the last decade, Dubai has diversified its economy by establishing itself as a major economic, transportation, tourism and real estate centre in the Middle East which enhanced the urbanisation process in the emirate.

---

[2] https://services.dubaiairports.ae/dubaimet/MET/Climate.aspx
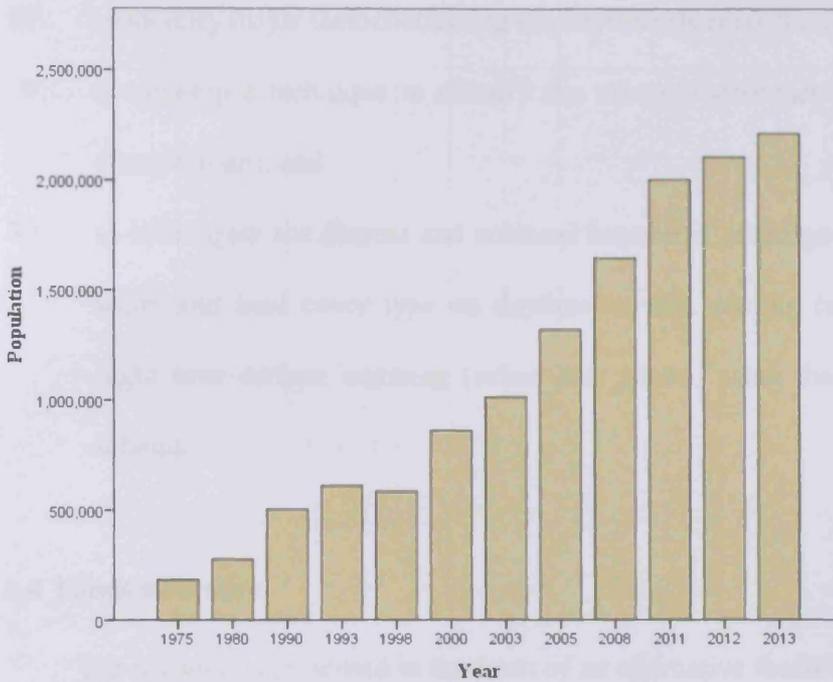
Figure 1.3 Historical changes in the population of Dubai (Collected from several national and Dubai statistics reports).

1.3 Aim and objectives

Using the city of Dubai as a case study, this research aims to study spatiotemporal change in a desert city and examine whether urbanisation has contributed to the variations in surface thermal conditions.

1.3.1 Objectives

The following are the objectives of this research:

I. to identify the spatiotemporal change of urban and other land cover types for an extended time series (1972- 2011);

II. to study Dubai's urban evolution in the context of recent empirical urban growth theory and to investigate the historical engines and patterns of urban expansion;

III. to investigate the impact of changes in land use/land cover and albedo on the daytime thermal variations in Dubai using Landsat data;

18

IV.   to identify major factors effecting the daytime thermal change in Dubai,

V.   to develop a technique to classify the urban environment in Dubai into local climate zones, and

VI.   to investigate the diurnal and seasonal impact of urban geometry, proximity to water and land cover type on daytime surface cooling (urban heat sink) and night time surface warming (urban heat island) using the local climate zones schema.

1.4 Thesis structure

The research is presented in the form of an alternative thesis format. It is made up of seven chapters, incorporating three empirical chapters that were written in journal manuscript format, and have been published or submitted for publication in relevant internationally-recognised scientific journals. In addition to the references at the end of each journal-style paper, a comprehensive reference list is provided at the end of the thesis. The thesis is outlined as follows:

Chapter 1 introduces the research, provides the rationale behind the research, introduces the study area and identifies the aims and objectives of the research.

Chapter 2 reviews urban growth studies with special focus on desert cities. It specifically introduces the reader to the locations, time scales and spatial extents of previous research on urban growth. It then moves on to discuss the data used in urban studies and common ways in which these data have been manipulated. It then reviews urban classification methods and accuracy assessment techniques used in urban studies and discusses the importance of spatial metrics in urban studies for understanding how urban areas evolve over time. The chapter concludes with a discussion and synthesis which provides the basis for the first empirical chapter.

Chapter 3 describes the urban heat island phenomenon (UHI) and reviews factors affecting its intensity. It goes on to discuss the existence of both urban heat sinks (UHS) and UHI in desert cities and reviews the use of satellite data in urban thermal studies. Following this, UHI mitigation strategies are discussed. The chapter concludes with a discussion and synthesis of the literature which forms the basis of the second and third empirical chapters.

Chapter 4 is a replication of a paper published in the journal "Computers, Environment and Urban Systems". It focusses upon quantifying historical urban growth and associated changes in land cover across Dubai using an extended Landsat data series from 1972-2011. Rates of urbanization in Dubai were then compared to rates experienced by other desert cities and other highly urbanized cities in the world. The chapter then discusses the drivers of the urban growth by relating them historical socio-economic and political factors. Spatial metrics were applied to quantify urban form and the possible existence of urban sprawl. The spatial metrics were also used to compare and contrast Dubai's experience of urban growth to that of other cities using empirically based models.

Chapter 5 discusses the use of the Landsat thermal data to study the impact of urbanisation on the daytime surface urban heat sink (SUHS) in Dubai. The intensity of the surface SUHS was then related to the changes in albedo, land use and land cover from 1990-2011. The chapter is a replication of a paper submitted for publication in the Journal "Landscape and Urban Planning".

Chapter 6 describes how Local Climate Zone (LCZ) were combined with MODIS land surface temperature (LST) data to explore diurnal and seasonal variations in UHS and UHI across Dubai. Urban geometry, proximity to water and land cover types were investigated and related to the intensity of both UHS and UHI using multivariate

statistics. The chapter is a replication of the paper based on this aspect of the research, which has been submitted for publication in the "Journal of Arid Environments".

Chapter 7 concludes the thesis by summarising the key outcomes of the research and contributions to knowledge. It highlights the methods used in the research and the results obtained. It further discusses the limitations of the research and identifies avenues that may be explored in the future.

Chapter 2 Remote sensing in urban growth studies

2.1 Background

This review focusses on how remote sensing has been used to investigate changes in urban environments over time. Remote sensing offers essential capture, classification and analysis of the earth's surface properties, including urban surfaces. In addition, satellite remote sensing produces reliable and accurate spatial data that may be used to quantify urban growth and form over time.

Satellite remote sensing has developed significantly over the last 40 years and there have been parallel developments in image processing and analysis. The spatial, spectral, and temporal resolution of space-borne imagery has improved significantly over time. For example, spatial resolution increased from 80 metres in the 1970s to less than 1 metre in the year 2000 (Lillesand et al, 2004). Over the same time period spectral resolution increased from 4 bands (Landsat Multi-Spectral Scanner) to several hundred bands with hyperspectral sensors. Furthermore, temporal resolution has improved from 18 days to 1 day (Cheng & Sustera; 2009) in response to imaging acquisition speed and on-demand imaging services (Avery & Berlin, 1992). When compared to other conventional methods of surveying, remote sensing is cost-effective and time-saving (Jat et al., 2008; Masser, 2001). All these factors make monitoring urban growth more accurate, easier and relatively cost effective.

In addition to the importance of remote sensing in monitoring and analysis of land cover over time, GIS has become an essential tool for mapping, modeling and analysing remotely-sensed data in a spatial context (Maktav & Erbek, 2005; Mundia & Aniya, 2005). Remote sensing and GIS can be integrated in urban studies in a number of ways: Firstly, remote sensing can be used to build datasets for use in GIS. Secondly,

GIS can be used to add precision to the information derived from remote sensing by adding ancillary data (Mundia & Aniya, 2005). The analytical capabilities of the GIS can then be used for further analysis. Finally, the GIS environment can be used to produce high quality cartographic outputs.

2.2 Location and extent of urban growth studies

Most previous studies on urban growth monitoring and analysis have focused on newly industrialized countries such as India and China or developing regions in Africa and the Middle East. These areas have experienced a rapid increase in urbanization due to various factors including the economy, population pressure or/and policy regulating urbanization process where they seek to develop more areas and extend urban facilities. Conversely, urbanization in developed countries has progressed at a much slower rate in recent years (Barredo & Demicheli, 2003; Bhatta, et al. 2010; Cohen, 2006; United Nations, 2014: p. 9). However, a small number of studies have reported on an increase in urban areas in some developed cities in the 1980s, 1990s and early 2000s such as Las Vegas (Xian et al. 2005) and Atlanta, USA (Yang & Lo 2003) which have grown through business-led urban development.

Some researchers have expanded the scope of urban growth detection to continental and global scales. For example, Kasimu and Tateishi (2008) used coarse resolution satellite imagery (MODIS) to monitor urban growth globally at 1km resolution using Landsat imagery as a reference. Knight and Voth (2010) used MODIS imagery to study and monitor urban growth at continental and global scales and to check the accuracy of their results at these scales, whilst Schneider et al. (2003) used remote sensing to study urban growth across the continent of North America.

Furthermore, Angel et al. (2010) used a global sample of 30 cities to study urban sprawl using Landsat as the main source of data.

Other researchers have limited their scope to individual countries or parts of a country. For example, Tian et al. (2005) carried out a study to monitor the dynamics of urban growth for the whole China.

The next section discusses the time span of urban growth studies using remote sensing imagery and other data sources.

2.3 Time span of urban growth studies

Numerous urban studies that have used satellite-based imagery as inputs are available. Some researchers study urban growth over short time periods whereas others extend their analysis over much longer time periods. For example, Angel et al. (2010) investigated the urbanization of a global sample of 30 cities (e.g. Buenos Aires, Cairo, Paris, Bangkok) between the years 1800 and 2000 using a combination of historical maps and Landsat satellite images. Others, such as, Moeller and Blaschke (2006), carried out a study to detect urban change in the North American city of Phoenix, USA from 2003 to 2005. The majority of studies, however, have focused on urban change over the medium term.

In spite of the above categorization, there is no specific standard for the classification of studies in terms of timeframe. However, a classification does emerge if we consider the timeframes of previous studies and the sources used in their research. Table 2.1 summarizes the longest-term span of urban studies that have used satellite-based imagery as inputs (along with other cartographic sources).

Table 2.1 Longest-term span of urban growth studies.

Authors	City	Time span of the study	Number of years studied
Angel et al. (2010)	Global sample	1800-2000	200
Rajendran et al. (2002)	Tamil State, India	1928-1998	70
Hara et al. (2005)	Bangkok	1955-1998	43
Kurucu & Kucukyilmaz (2008)	Torbali, Turkey	1965-2001	36
Yang et al. (2001)	Atlanta, USA	1966-1998	32

2.4 Data used in urban growth studies

The ability to study and monitor urban growth is highly dependent on various multi-date data, including optical satellite imagery, aerial photographs, LIDAR (Light Detection And Ranging) imagery, thematic maps, topographical maps and other forms of spatial information. With the availability of imagery from a variety of different optical sensors including the Landsat Multi-Spectral Scanner (MSS), Landsat Thematic Mapper (TM), Landsat Enhanced Thematic Mapper (ETM+), Moderate Resolution Imaging Spectroradiometer (MODIS), Advanced Land Observing Satellite (ALOS), Satellite Pour l'Observation de la Terre (SPOT), Indian Remote Sensing system (IRS), Advanced Spaceborne Thermal Emission and Reflection Radiometer (ASTER) and IKONOS, urban growth detection through image combination or 'fusion' becomes increasingly attractive.

Five of the most essential concerns when using remote sensing imagery in urban growth studies include cost, availability, spatial, spectral and temporal resolution (Ji et al., 2001; Tole, 2008). Cost is the first concern, determining which satellite data may be used, especially in studies that are not funded or which have a limited budget. In addition, several studies require near-anniversary date repeat images when studying urban growth to help to minimize the effects of sun azimuth and atmospheric distortions during analysis. However, near- anniversary date images are not always available (e.g.

Basith et al., 2010; Haack et al., 1997). Furthermore, due to technical constraints of satellites, high spatial resolution tends to be related with low spectral resolution and vice versa (Jensen, 2007), see Table 2.2 for optical satellites that have been mostly used in urban growth studies.

Satellite images captured by the Landsat series of satellites provide the longest continuously acquired collection of moderate-resolution remote sensing data for urban study applications and are widely used due to their availability from 1972 to the present date with adequate spatial and spectral resolution. Furthermore, these data are now freely available and widely accessible through organisations such as the USGS via their GLOVIS service. Prior to the 1970s, studies used aerial photographs to manually detect urban growth for relatively small areas. For example, Kurucu and Kucukyilmaz (2008) used aerial photographs of the year 1965 to digitize urban areas and major land cover areas using the knowledge of experienced researchers from shape and texture of urban features.

Studies of urbanization that focus upon the 1970s by necessity have to use images from the Landsat MSS sensor. This images are particularly useful for places lacking accurate base maps or past surveys (Bhatta, 2009; Dewan & Yamaguchi, 2009; Jat et al., 2008; Ma & Xu, 2010; Mundia & Aniya, 2005).

Table 2.2 Most often used optical satellites in urban studies (Sources: collected from various imagery suppliers' websites).

Satellites	Sensors	Spectral Resolution	Temporal Resolution (Days)	Spatial Resolution (meters)	Launched	Decommissioned	Availability
Landsat 1-3	MSS	5 bands	18	80 (visible & infrared bands); 240 (thermal band)	1972	1983	
Landsat 4-5	MSS & TM	7 bands (TM); 5 bands (MSS)	16	30 (visible & infrared bands) for TM; 60 (thermal band) for TM	1982 (Lan.4); 1984 (Lan.5)	2001; 2013	
Landsat 7	ETM+	9 bands	16	30 (visible & infrared bands); 60 (thermal bands); 15 (panchromatic band)	1999		Free
Landsat 8	OLI; TRIS	11 bands	16	30 (visible & infrared bands); 100 (thermal bands); 15 (panchromatic band)	2013		
Terra	MODIS	36 bands	daily	250 (bands 1-2); 500 (bands 3-7); 1000 (bands 8-36)	1999		
Aqua	MODIS	36 bands	daily	250 (bands 1-2); 500 (bands 3-7); 1000 (bands 8-36)	2002		
Terra	ASTER	14 bands	16	15 (visible bands); 30 (infrared bands); 90 (thermal bands)	1999		Free upon request (education)
IRS-1C	LISS-III	5 bands	24	23.5 (multispectral bands); ~6 (panchromatic band)	1995		
SPOT 1-3	HRV	4 bands	26	20 (visible & infrared bands); 10 (panchromatic band)	1986	2007; 2009	
SPOT-4	HRVIR	5 bands	26	20 (visible & infrared bands); 10 (panchromatic band)	1998	2013	
IKONOS	IKONOS	4 bands	3	4 (multispectral bands); 1 (panchromatic band)	1999		
QuickBird-2	QuickBird-2	5 bands	3	2.4 (multispectral bands); 0.6 (panchromatic band)	2001	2015	Commercial
SPOT-5	HRVIR	5 bands	26	20 (Shortwave-IR band); 10 (visible & near-IR bands); 2.5 to 5 (panchromatic band)	2002		
SPOT-6	NAOMI	5 bands	26	6 (visible & near infrared bands); 1.5 (panchromatic band)	2012		

In 1984 the Landsat TM sensor was launched which offered better overall radiometric sensitivity and higher spatial resolution than the MSS it replaced. For example, Ward et al. (2000) used two Landsat TM images to quantify urban growth in Southeast Queensland, Australia between 1988 and 1995.

From 2000 onwards, urban growth studies have tended to use Landsat ETM+ imagery (e.g. Taubenböck et al., 2009). However, on May 31, 2003, the Scan Line Corrector (SLC) of the ETM+ instrument failed resulting in a striping effect on the images acquired after this date, which affected the quality of the data (USGS, 2013). Fortunately, Operational Land Imager (OLI) and Thermal Infrared Sensor (TIRS) were included onboard Landsat 8 which was launched in February, 2013 as part of Landsat Data Continuity Mission. It has nine spectral bands similar to ETM+ with 30m resolution; however with an extra deep blue visible band to study coastal zones and infrared band 9 for the detection of cirrus clouds.

Another source of imagery used in urban studies after 2000 is ASTER. Although ASTER is mainly useful to retrieve land surface temperature and emissivity, several researchers have used ASTER imagery to detect urban areas. Crane et al. (2005) combined ASTER imagery with Landsat to detect changes in urban areas within Las Vegas from 1984 to 2002. However, ASTER data is not widely used in urban studies due to its high cost and limited availability for many cities including Dubai.

Another source of imagery widely used after 2000 to monitor urban growth at relatively coarse scales is MODIS which provides 36 spectral bands at spatial resolutions of 250m, 500m and 1km (Kasimu & Tateishi, 2008; Knight & Voth, 2010). MODIS imagery is ideally suited for monitoring urban growth over large areas, especially when the use of higher spatial resolution data is impractical on grounds of cost or availability. However, such studies suffer from inaccuracies because of the

mixture of different land cover types per pixel in urban areas. In addition, it is also difficult to assess the accuracy of the results due to the coarse resolution of the extracted information compared to real world data. However, using MODIS imagery to study the impact of land cover change on the environment at global scale is more practical than using alternate imagery (Reeves et al., 2006; Song & Le, 2009).

Conversely, the use of high resolution images in urban growth studies has been challenging because of their relatively low spectral resolution and coverage (Gamba et al., 2011). The high financial cost and lack of a sufficiently long archive have also limited the use of high resolution images in urban studies. Nevertheless, several researchers have studied the feasibility of using very high resolution imageries in urban growth studies (e.g. Moeller & Blaschke, 2006).

Other researchers combine various high spatial resolution imageries with medium resolution data. For example, some researchers have combined SPOT imagery at 20m resolution with Landsat imagery at 30m resolution to detect urban growth (Belaid, 2003). However, in order to combine images, the higher resolution image needs to be usually transformed to a lower resolution through the process of resampling (Banzhaf et al., 2009; Ward et al., 2000; Xian et al., 2005; Yuan, 2008).

Supplementary data such as topographical maps, thematic maps, aerial photographs and high resolution images have been used in previous urban growth studies as reference and to aid in the visual interpretation to evaluate the accuracy of the results (Bhatta, 2009; Mundia & Aniya, 2005; Tian et al., 2005; Yin et al. 2005). Bhatta (2009), for example, used topographical maps and previous land use maps as reference and evaluated the accuracy of the land cover classification derived from satellite images.

Finally, due to the fact that satellite imagery and other optical images are not usually captured in poor weather conditions or at night time, various studies have used Synthetic Aperture Radar (SAR) and LIDAR to study urban areas. LIDAR and SAR can be used under cloudy conditions at any time during day or time, thus several studies have used SAR to study and map urban areas (Grey et al., 2003; Thiel et al., 2008). Conversely, LIDAR has been used mainly to extract 3D image output of urban areas (Vilanova et al., 2008)

Table 2.3 lists the number of studies published up to year 2013 that have used only Landsat or medium to high spatial resolution imagery such as IKONOS, SPOT, IRS and Quickbird. The following keywords were used in Web of Knowledge search engine to retrieve these studies (urban change; urban growth; land use; land cover; urban expansion; urban sprawl; urbanization).

Table 2.3 Number of urban studies based on satellite imagery published up to 2013.

Imageries as primary data	Number of reviews	Percentage
Only Landsat (MSS, TM, ETM+)	58	55%
SPOT, IKONOS, IRS & Quickbird	16	15%
Mix of imageries	31	30%
Total	105	100%

It appears from the above table that more than half of the studies adopted Landsat imagery for the following reasons:

1- Free to download for all Landsat series as from January 2009. NASA reported that this led to a 60-fold increase in data downloads (NASA, 2013);

2- Landsat was the only source of high resolution satellite imagery in the 1970s and 1980s hence researchers studying urban growth over this time period had little option other than to use these data;

3- The cost and security constraints of using high resolution alternatives (Haack et al., 1997; Rajendran et al., 2002). This is in addition to the technical challenges of using high resolution images to retrieve urban areas.

2.5 Data preparation and methods

One of the main difficulties facing researchers when using satellite remote sensing in studies of urban growth is that analytical techniques cannot easily be transferred from one location or study to another (Haack et al., 1997). Therefore, the satellite image analyst should first study the available data and investigate the study area from all aspects and then come up with appropriate techniques to solve and achieve the objectives of the study. In urban studies, some researchers give particular attention to pre-processing of satellite images prior to image classification. It is essential that these are applied in order to correct sensor and platform radiometric and geometric distortions of images (Jensen, 2005).

In order to correct images from atmospheric effects various methods are employed. The most common are relative and absolute atmospheric correction techniques. For the relative technique, no prior knowledge about the atmospheric conditions of the scene at a specific time is required; this is a relatively straight forward technique (San & Suzen, 2010). The absolute technique, in contrast, is complex and prior knowledge of atmospheric characteristics and sensor calibration data are required at the time of data acquisition. Both techniques are based on estimating the atmospheric

effect on the image (scattering and absorption). The atmospheric effect is then removed pixel by pixel in the image for each band. Most researchers recommend using the absolute atmospheric correction technique, especially when most of the atmospheric information is known (Nikolakopoulos et al., 2002; San & Suzen, 2010). However, Song et al. (2001) stated that the relative technique is sufficient in urban studies and leads to highly accurate results. One example of a relative atmospheric correction technique is the darkest-pixel subtraction technique which is considered the simplest because it does not require atmospheric characteristics and sensor calibration information (San & Suzen, 2010; Song et al., 2001).

Absolute atmospheric correction techniques are mainly based on MODTRAN or LOWTRAN modeling (San & Suzen, 2010). Two of the most commonly used commercial techniques are the Fast Line-of-sight Atmospheric Analysis of Spectral Hypercubes (FLAASH) module within ENVI software, and the Atmospheric CORrection module (ATCOR) within ERDAS software.

After atmospherically correcting the data, studies usually include operations of geometric correction and registration for the satellite image into local coordinate systems. Geometric correction is a crucial step for remote sensing data to correct the systematic and non-systemic errors introduced during image acquisition process (Gonçalves et al., 2009). It is typically implemented by using ground control points (GCP's) from the field or from positions on existing rectified maps or images. After geometric correction, Root Mean Square Error (RMSE) is typically calculated to verify the accuracy of registration and quantify geometric distortion. It is recommended that RMSE should be less than half of image pixel size (Jensen, 2005).

2.6 Classification Systems (schema) in urban growth studies

The first system mentioned in the literature was developed by the US Bureau of Census in 1874 where land use was classified into binary classes; urban and rural (Hailu & VanEenwyk, 2009). More recently, Anderson et al. (1976) developed a classification system based on levels for standardization purposes; with level-1 representing urban/built-up areas and level-2 representing a more detailed classification of level-1 such as residential, commercial, industrial, transportation and so on. Anderson left this system open ended so that subsequent researchers could develop their own sub-levels describing further detail if necessary.

Although the Anderson system (also known as the USGS system) was developed for American states, many researchers have adopted this system or a modified version to reflect the nature of their particular study areas. The chosen classification system and level depends on several factors, including the spatial extent of the study area, the spatial resolution of the images and the nature of the land and the objectives of the study (Anderson et al., 1976; Bhatta et al., 2010; Maselli et al., 2002; Rajendran et al., 2002).

Generally speaking, it is more feasible to adopt level-2 systems when using high resolution imagery (Al-Awadhi & Azaz, 2005; Salman et al., 2008). However, some studies using high resolution imageries have adopted a level-1 classification approach (Banzhaf et al., 2009; Chi et al., 2009; Jong et al., 2000), while others have used Landsat images to map urban growth using a level-2 approach. Ward et al. (2000), for example, classified urban areas into residential and industrial areas using Landsat TM data for the Queensland State, Australia. Nevertheless, a number of published articles have reported highly accurate results using medium spatial resolution imagery (such as Landsat) to monitor urban growth in cities at level 1 (Gillies et al., 2003; Liu et al., 2010; Martinuzzi et al., 2007; Niero et al., 1982; Tole, 2008; Weng, 2001; Xian et al.

2005). Anderson et al. (1976) recommended using the higher level of classification with high resolution imagery.

Another classification schema was adopted for low spatial resolution satellite imagery such as MODIS at 250m to 1000m. The International Geosphere-Biosphere Program Land-Cover Classification System is used for regional land cover classification and includes a single class for built up areas (Strahler et al., 1999).

Several factors could limit the use of remote sensing in urban studies. Firstly, the spatial and spectral resolutions of imagery could greatly affect the quantification accuracy of land cover and 'confusion' between different land cover types (Jensen, 2007). For example, using higher spatial resolution imagery greatly improves the detection and quantification of urban areas. However, lower spectral resolution could increase the chance of confusion between different land cover types such as sand and urban areas within desert environments as will be discussed in section 2.9. Other factors that could limit the use of remote sensing include cloud cover, especially in tropical cities (Thiel et al., 2008). However, this factor is negligible in desert cities such as Dubai where sand storms are likely to have a greater impact on image quality.

2.7 Image classification methods and accuracy assessment

Accurate classification of the urban environment is valuable in many applications (socio-economic, urban planning and environmental) hence various algorithms and techniques have been developed to extract information on the extent of urban areas from remotely- sensed images to provide the highest accuracy possible. The first step is to classify the images then an accuracy assessment is implemented on the resulting thematic map to verify its accuracy and to eliminate or minimize errors in classification. Several methods have been adopted in urban growth studies including manual

digitization, unsupervised, supervised, sub-pixel classification, neural network, object based, texture and hybrid techniques. The selected method depends on many variables such as the level of classification required, and both the spatial and spectral resolution of the image.

Classification methods are generally grouped into either manual or automated methods. Manual methods are based on visually digitizing the images or aerial photography on screen. A number of researchers have adopted manual digitization techniques for classification and this technique is much preferred when using aerial images where automated methods are challenging or unfeasible. For example, Rajendran et al. (2002) manually digitized urban areas from historical aerial photographs. These areas were extracted by the knowledge of experienced researchers from the shapes and textures of urban features.

Other studies have adopted automatic classification methods that are based primarily on the spectral characteristics of urban features where similar spectral pixels are grouped together. Two major methods fall in this category, namely per-pixel and sub-pixel classification methods. Two major per-pixel classification methods are widely used: unsupervised and supervised in which each single pixel is assigned to one class. Unsupervised methods tend to be used when there is no prior knowledge of the study area. In this case a set of pixels are clustered by the software into different groups based on their spectral characteristics. The user subsequently assigns the groups to classes. The supervised method is based on selecting training areas for each class either from field visits or local knowledge then asking the software to group the pixels based on the spectral characteristics of these samples. However, Lo and Choi (2004), for example, used a hybrid classification technique (supervised and unsupervised) to overcome

spectral confusion between different classes for the city of Atlanta, USA, and achieved a good separation of urban land cover from other land cover classes.

Per-pixel classification methods can be of limited value in heterogeneous regions where one pixel could contain more than one class. Consequently, sub-pixel classification approaches such as fuzzy classification or neural networks can be used instead. These approaches are based on estimating the percentage of urban area and other types of land cover in each pixel and are thought to provide a more accurate means of classification (Crane et al., 2005; McMahon et al., 2005; Yang et al., 2003). Xian et al. (2005), for example, used a fuzzy classification approach to calculate the percentage of impervious areas in each image pixel.

With the advent of a very high resolution imagery such as IKONOS, simple reliance upon spectral properties was not seen to be good enough for classification purposes due to the limited number of bands. Consequently, object-oriented classification techniques were developed which classified images into objects rather than pixels based on a combination of their spectral, spatial and textural features (e.g. Bhaskaran et al., 2010; Taubenbock et al., 2009).

Thematic maps generated from the classification process are assessed through a procedure called accuracy assessment. It is a quantitative method used to assess the quality of a classification derived from remotely-sensed imagery through comparison with ground truth data (reference samples) (Jensen, 2005). These samples can be acquired from high resolution images, topographical maps and local knowledge when ground truth samples are unavailable. The reference samples should be taken at the same time as the satellite image to avoid errors due to landscape change. Furthermore, they should be randomly selected and should be independent from the data used for training in order to avoid the risk of bias (Verbyla & Hammond, 1995). However, it

should be recognized that the resulting accuracy statement may be significantly distorted by errors in the reference data (Foody, 2002). A confusion matrix is commonly used to evaluate the accuracy of classification which includes the following measures: overall accuracy, user's accuracy, producer's accuracy, error of omission and error of commission. The overall accuracy is computed by dividing the number of pixels that are correctly classified by the total number of reference pixels (Xiuwan, 2002). Therefore, this measure calculates the accuracy for all classes and does not tell the accuracy of individual class. For this reason, user's and producer's accuracies are used alongside the overall accuracy for evaluating the classification performance of each individual class. User's accuracy refers to the error of commission that measures the probability that a given pixel of a certain land cover class in the classified image will appear on the ground as it is classed (Congalton & Green, 2009; Foody, 2002). Producer's accuracy refers to the error of omission that measures the probability that a certain land cover type of an area on the ground is classified as such. It is calculated by dividing the total number of correctly classified pixels in a given class by the total number of pixels that actually belong to that class.

Based on summarizing all previous urbanisation studies that have used optical remote sensing sensors up to year 2013, the following graphs are plotted: 1) Fig. 2.1 summarizes the accuracy assessments based on both user's and producer's accuracies; 2) Fig. 2.2 summarizes the overall accuracy; and 3) Figs. 2.3 and 2.4 summarize the accuracies based on classification methods.
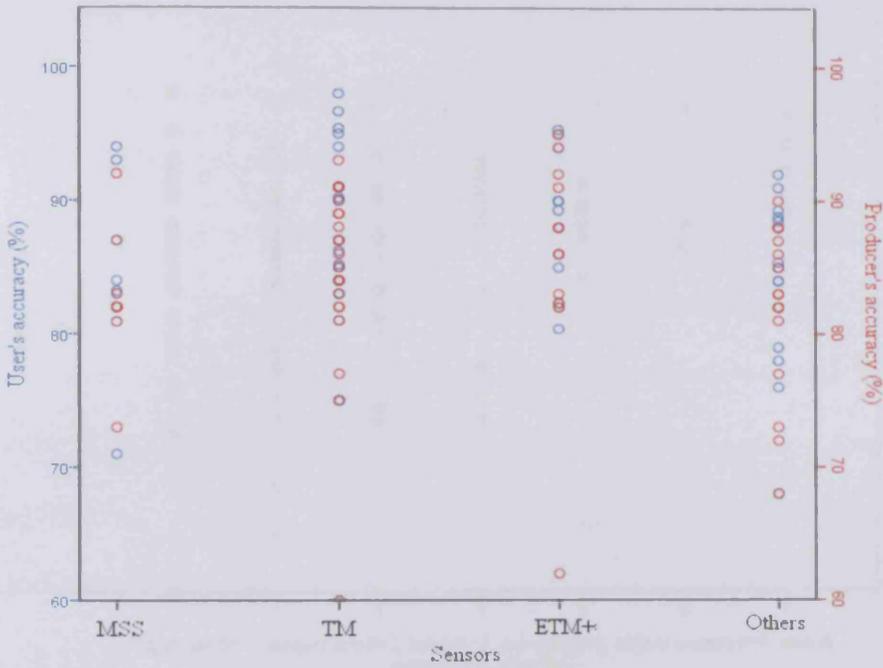
Figure 2.1 Relationship between satellite sensors and user's (blue) and producer's (red) accuracies for urban classes, based on 41 studies.
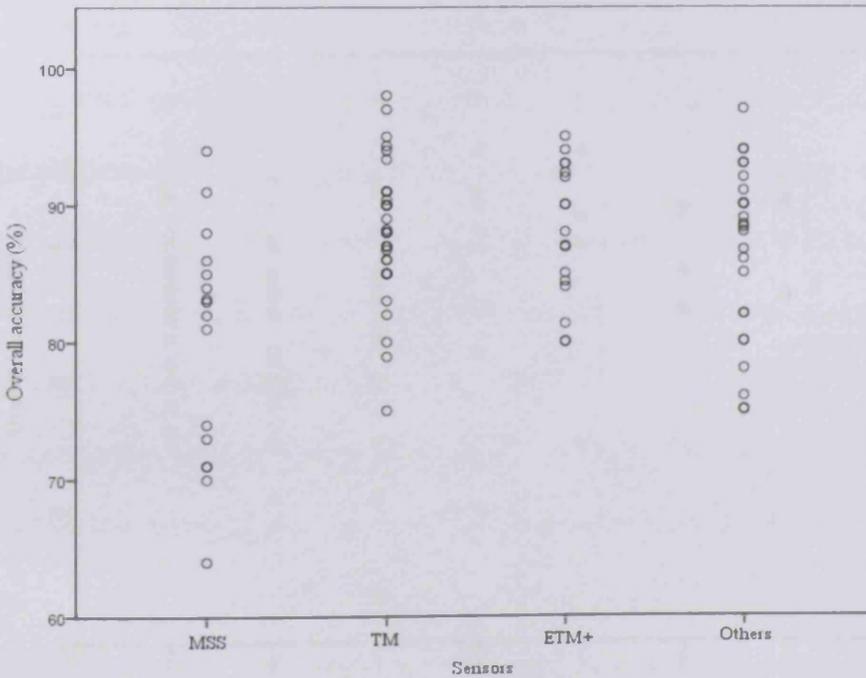
Figure 2.2 Relationship between types of sensor and the overall classification accuracy of all land cover classes, including urban classes, based on 79 studies.

Accuracy (%)

100 —

90 —

80 —

70 —

60 —

Supervised=1, unsupervised=2, hybrid=3, sub-pixel=4, object oriented=5, neural network=6, others=7
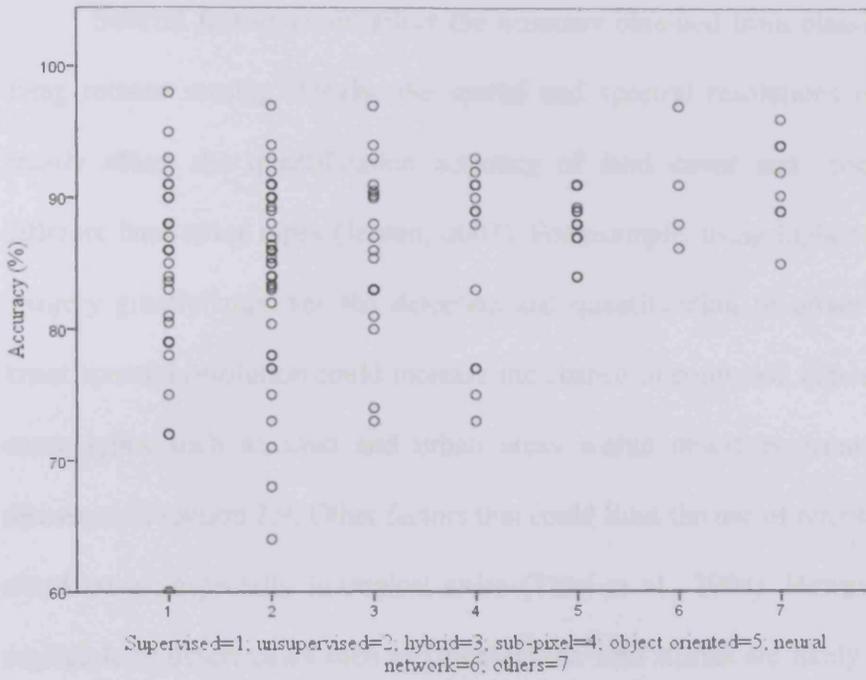
Figure 2.3 Classification accuracy (with both user's and producer's accuracies when applicable) of urban classes based on classification method.

Overall Accuracy(%)

100 —

90 —

80 —

70 —

60 —

Supervised=1, unsupervised=2, hybrid=3, sub-pixel=4, object oriented=5, neural network=6, others=7
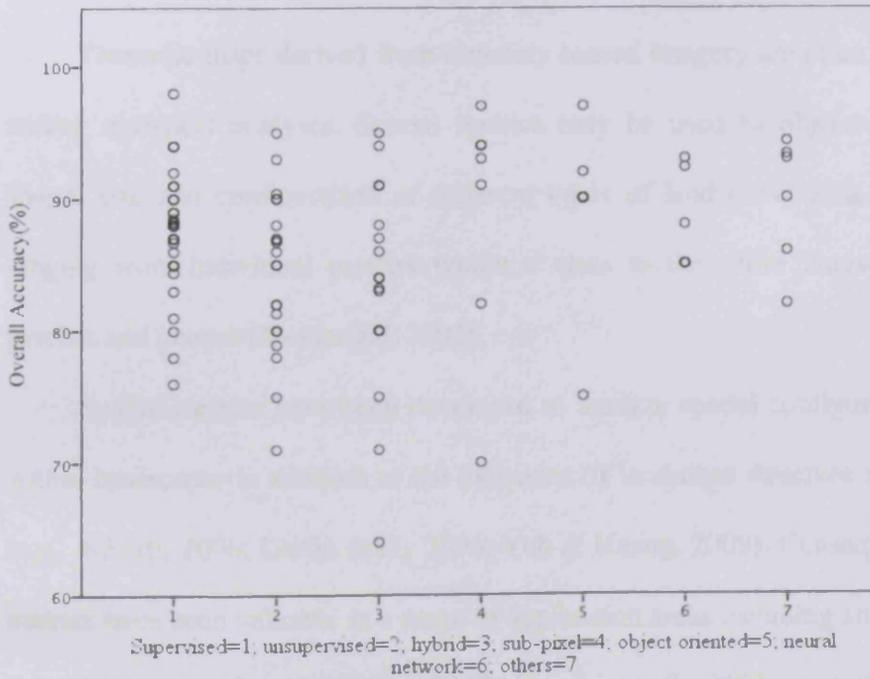
Figure 2.4 Overall classification accuracy for all land cover classes, including urban classes, based on classification method.

Several factors could affect the accuracy obtained from classification methods using remote sensing. Firstly, the spatial and spectral resolutions of imagery could greatly affect the quantification accuracy of land cover and 'confusion' between different land cover types (Jensen, 2007). For example, using higher spatial resolution imagery greatly improves the detection and quantification of urban areas. However, lower spectral resolution could increase the chance of confusion between different land cover types such as sand and urban areas within desert environments as will be discussed in section 2.9. Other factors that could limit the use of remote sensing include cloud cover, especially in tropical cities (Thiel et al., 2008). However, this factor is negligible in desert cities such as Dubai where sand storms are likely to have a greater impact on image quality.

2.8 Spatial metrics used in urban studies

Thematic maps derived from remotely sensed imagery are often subject to spatial and/or statistical analyses. Spatial metrics may be used to objectively describe the shape, size and configuration of different types of land cover at a variety of scales ranging from individual patches within a class to the entire landscape of different patches and classes (McGarigal, 2006).

Spatial metrics have been developed to analyze spatial configuration and pattern within landscapes in addition to the dynamics of landscape structure and heterogeneity (e.g., Alberti, 2008; Leitão et al., 2006; Yeh & Huang, 2009). Consequently, landscape metrics have been valuable in a range of application areas including studies of plant and animal diversity (e.g., Hanberry, 2007; Honnay et al., 2003), and the environmental impacts of natural disasters on landscape fragmentation (Lin et al., 2006).

There has been a growing interest in the use of spatial metrics to study urban structures and sprawl (Aguilera et al., 2011; Araya & Cabral, 2010; Taubenböck et al., 2008; Wu et al., 2011). Spatial metrics have been used in urban studies to help urban planners and policy makers understand the dynamics of change associated with urban growth within entire landscapes (Lowry & Lowry, 2014). Various metrics (indices) have been used in urban growth studies to describe the spatial characteristics of urban form and to reveal hidden information of urban growth patterns that could not be determined from visual interpretation alone. Some researchers draw conclusions about urban pattern and structure based on a single index. For example, Liu et al (2010) investigated the complexity of the urban environment in Xingjiang city, China using a compactness index. The higher the value of the index, the more compact the urban environment. When the city becomes more compact the cost of urban infrastructure including transportation networks and other construction decreases; however above certain threshold traffic congestion becomes problematic. Furthermore, Shannon's Entropy Index has been widely used by researchers to investigate urban sprawl in cities (e.g. Jat et al., 2008; Sudhira et al., 2010; Tole, 2008). Studying urban sprawl (dispersion) is essential in urban growth studies "because it causes problems in the allocation of basic needs and increases risk to life and property in the face of disasters", (Verzosa & Gonzalez, 2010, P.269).

Other studies use Fragstats, a widely used public domain program to study landscape composition and configuration for categorical maps, to compute a large number of metrics ranging from each patch within a class to the entire landscape (McGarigal et al., 2002). Many metrics computed by Fragstats are correlated so the user needs to define what metrics to use depending on the objectives of the study. For example, Herold et al. (2002) used eleven metrics to study the urban form of Santa

41

Barbara. The metrics chosen included: Patch Density (number of patches of urban fabric divided by sum of total landscape area); Largest Patch Index (area of largest patch of urban class divided by total areas the class multiplied by 100); Mean Patch Size (mean size of patches of a urban class); Area Standard Deviation Patch Size (standard deviation of in size of the patches of urban class) and Edge Density (total length of all edges in the urban class divided by the total area of landscape area). However, several factors could affect the values of these metrics such as the spatial resolution of the landscape classification, the extent of the study area and level of detail in the landscape (Herold et al., 2003).

A more recent use of spatial metrics is to examine the harmonic-oscillation theory of urban growth in cities through diffusion and coalescence phases (Dietzel et al., 2005a, b). These phases can be revealed through the comparison of several metrics such as the number of urban patches, mean nearest neighbour distance of patches (average of the shortest distance from one urban patch to another) and largest patch index (percent of the total landscape covered by the largest patch). For example, if there is an increase in both the number of urban patches and the mean nearest neighbour distance with the decrease of largest patch index then the city experiences a diffusion phase.

2.9 Urban studies in sandy desert cities

This part of the review will focus on studies of desert cities that share similarities with the City of Dubai. A table is built to summarize these studies, highlight the particular challenge of each study, and explain how these challenges were overcome. Some of these studies have been situated in the Gulf region, namely: Seeb Wilayat in Oman, Al Ain in UAE, and Al Ahsa in Saudi Arabia.

For example, urban growth in Seeb Wilayat occurred at the expense of both desert and vegetation with vegetation decreasing by 53% over a 12 year period (Al-Awadhi and Azaz, 2005). Conversely, Belaid (2003) reported that urban and vegetated surfaces increased in Al-Ahsa city by 75% and 22% respectively at the expense of sabkha (salt flat) and sand dunes.

In other regions where desert land is dominant, Yin et al. (2005), in their study of Cairo, concluded that urban growth occurred at the expense of desert and farm land. In developed countries, the desert cities of Las Vegas and Phoenix have witnessed the fastest rates of urban growth in the United States. In these cities the urban fabric (and to a lesser extent, vegetation) increased at the expense of desert land (Moeller, 2005; Xian et al., 2005).

In order to quantify rates of urbanization in desert cities a variety of classification approaches have been adopted, however, some researchers have faced challenges in detecting urban areas in such environments (Table 2.4).

Table 2.4 Classification methods adopted by researchers in desert cities.

Authors	City	Classification method	Challenges identified in the literature	Challenges overcome
Al-Awadhi & Azaz (2005)	Seeb Wilayat,	Digitization	---	---
Yagoub (2004)	Al Ain, city, United Arab Emirate	Supervised	Misclassification of urban areas	Manual digitization & then grouping using GIS
Belaid (2003)	Ahsa city, Saudi Arabia			
	Moroccan cities	Digitization	---	---
Zhou et al.(2008)	Xinjiang	Supervised	---	---
Yin et al (2005)	Cairo	Unsupervised	Similar spectral characteristic between the mix of urban areas/farmland and other mix types	Manual classification of mixed lands using high resolution imageries and maps.
Stewart et al. (2004)	Cairo	Supervised	difficulty in discriminating urban and desert features	Extracting only urban areas to reduce the uncertainty by aid of high res. images
Wu et al. (2003)	Nouakchott	various methods	urbanized areas and bare land appear similar by using automative method	Manual digitization method
Xian et al. (2005)	Las Vegas	Sub-pixel classification	---	---
Moeller (2005)	Phoenix	object oriented	---	---
Moeller & Blaschke (2006)	Phoenix	Principle component analysis	---	---
Flores et al.(2008)	Ciudad Juarez, Mexico	Object oriented	interstitial of bare soil areas within urban areas	---
Qian and Zhou (2009)	Xinjiang	Object oriented	detecting urban areas from bare soil and desert	---

From the above table it is obvious that most researchers faced the challenge of separating urban areas from desert areas because most houses are constructed from very similar material, mainly sand (e.g. Stewart et al., 2004). Furthermore, in desert environments urban features such as roads and walkways can be partially covered with sand which makes the separation of urban areas from sand more challenging. However, most researchers have overcome these challenges by grouping the misclassified categories manually. Although different researchers have used different methods of classification and different images, it is still unclear what data or/and method is the best used in desert areas to separate urban areas from other land cover types most effectively.

2.10 Causes and implications of urban growth

While remote sensing and GIS are mainly used to quantify urban growth, other sources of data are required to explain the causes of such growth. Understanding the drivers of growth is necessary for urban planning and forecasting the needs of the city. As a result of the integration of urban data and other ancillary data, most researchers conclude that various factors influence urban growth and contribute to the different pattern and dynamics of urban growth. These influential factors include economic, total population, topography, gross domestic product (GDP), governmental intervention, industrial development, political boundaries and traffic infrastructure, such as roads.

For example, Bhatta (2009); Tole et al. (2008); and Yin et al. (2005) studied the relationship between population growth and urbanization. They concluded that the increase in population led to the urban growth in Kolkata, Toronto and Cairo respectively. However, Yin et al. (2005) found that the urban growth in Cairo was slower than the population growth due to economic factors during the period of study.

The study of this relationship is important to investigate whether or not the increase in urban growth in a city is a natural consequence of the increase of population or is it driven by other factors. Indeed, Ma and Xu (2010) found that urban expansion in the Guangzhou city, China was more affected by the increase in gross domestic product and urban residents' income, while Zhao et al. (2007) concluded that population growth was the top most influencing factor on urbanization in the city of Xuzhow city, China.

On the other hand, several factors constrain the rate, form and direction of urban growth including water bodies, upland areas and political boundaries. Barredo and Demicheli (2003) concluded that urban expansion in Lagos, Nigeria did not continue to the south-west of the city due to the presence of water bodies which constrained development in these directions. Moreover, road networks and topography influence the direction of the urban growth (Mundia & Aniya, 2005).

The relationship between urban growth and the aforementioned factors has been studied using a variety of different approaches. Several researchers have used multivariate regression analysis including linear and logarithmic regression (Jat et al., 2008; Wu et al., 2003; Zhao et al., 2007) and Pearson's correlation (Yang et al., 2001). Pearson's correlation is typically used to find the correlation between two variables, for instance urban growth and population. Conversely, multivariate regression analysis is used to find the relationship between multiple variables (e.g. population and economy) and urban growth.

Other studies have given special attention to the encroachment of urban growth onto other types of land cover including vegetation, forests, and water bodies which has important ecological and environmental consequences. Ji et al. (2001), for example, found that 40km^2 of agricultural land was lost for residential developments within less than 10 years in one municipality in China. Similarly, many studies have shown that

vegetated land was lost to urban development (Maktav & Erbek, 2005; Rajendran et al., 2002; Tole, 2008; Yin et al., 2005). Other studies have shown a decrease in both vegetated areas and water bodies (Liu et al., 2010; Ramadan et al., 2004). Dewan and Yamaguchi (2009) revealed that the urban area in Dhaka, Bangladesh had increased considerably during 30 years; this growth came at the expense of cultivated land, vegetation and water bodies. Conversely, Mundia and Aniya (2005) found that vegetated land increased around in Nairobi, Kenya over a 10-year period because the government chose to protect these lands.

2.11 Conclusions

The aforementioned review may be summarized as follows:

1- Urban developments do not arise in a vacuum, but rather from the need of the country and through the influence of multiple variables (section 2.10). In some countries urban development has occurred due to economic factors, while in other countries it has occurred in response to internal problems caused by the need for housing because of a rapidly increasing population. In this study, the driver for urban development is a desire to diversify from an oil-based economy since oil reserves will ultimately become depleted hence the economy should focus on other sources of revenue such as real estate.

2- A wide range of different data sources have been used to study urban growth. However, satellite remote sensing data is preferred over conventional methods such as surveying because it is cost-effective and time-saving. The accuracy assessments of urban areas classification from previous studies using Landsat imagery clearly show acceptable levels of accuracy as seen in graphs 2.1 and 2.2. Therefore, it can

be concluded from previous sections that Landsat data is preferred in the following cases:

A. When studying urban growth in the 1970s and 1980s because Landsat sensors were the only ones in operation over this period with acceptable spatial and spectral resolution.

B. When studying urban growth at level-1, Landsat is efficient in terms of both spatial and spectral resolutions.

C. When studying urban growth at a large scale because Landsat is available to download at no cost, while higher resolution images are costly and cover smaller areas

D. The cost of using high resolution imagery which is prohibitively expensive hence unaffordable to most researchers, especially those based in developing countries.

3- Various methods have been used to detect urban growth (section 2.7). These show that what works for one study areas does not necessarily work for another. Accuracy assessment of classified outputs in desert environments suggests that the results are reasonably consistent irrespective of method adopted.

4- It is useful to use spatial metrics in studies of urban growth to analyse and reveal hidden information about urban patterns such as urban sprawl as mentioned in section 2.8. In the context of the present study, spatial metrics provide a means of quantifying specific spatial characteristics of urban patches within the entire landscape and therefore have value in helping to understand the historical process of urban development.

5- The studies have presented different causes and implications of urban growth (section 2.10). It is important to understand historical causes of urbanisation (drivers or engines) whether due to increase in population, as is normally the case, or due to other

factors. On the other hand, the implications of urbanisation should be identified in order to assess its effect on the environment and future urban developments.

2.12 Summary

This chapter essentially discussed the importance of studying urban growth, its drivers and the use of spatial metrics to understand the spatial form and characteristics of the growth. It also discussed data sources, classification techniques and accuracy assessment, focussing specifically on the challenges of multi-spectral classification in desert environments.

Based on previous studies, no study has been conducted on Dubai which has grown dramatically over the last few decades and thus there is a need for a comprehensive work on this area. The difficulty in accessing urban and other land cover information in Dubai justifies the need for satellite detection of urbanization.

The next chapter focuses on the urban heat island formation and the urbanization impact on the formation of this phenomenon.

Chapter 3 Urban heat islands

3.1 Background

Global warming has received unprecedented attention from governments, agencies, scientists and the media in recent decades. One contributor to global warming is thermal change as a consequence of urbanization, with artificial surfaces replacing natural surfaces (Vargo et al., 2013). Indeed, the impact of urbanization on the global warming change is considered by some to be as important as the release of greenhouse gas emissions (GHEs) (McCarthy et al., 2010; Pielke, 2005).

Some of the consequences of altering land surfaces through urbanization include reduced rates of evapotranspiration and changes in the thermal properties and wind flow in the urban environment. This leads to an increase in surface temperatures in cities and can affect the quality of life and human health (Frumkin, 2002; Lo, 1997; Speak et al., 2013; Stathopoulou et al., 2012). According to Kalnay and Kai (2003), almost half of the change in the global temperature is linked to urbanization. Others, however, have contested this (e.g. Grimmond, 2007) since urban areas only cover small part of the Earth's surface hence are more likely to have local as opposed to global effects. Nevertheless, there are some similarities between thermal increases in urban environments and global warming in that both can increase energy demand during hot seasons thus elevating air pollution from air-conditioning units and Green House Effects (US EPA, 2008b).

The mean global surface temperature has increased by 0.74 ± 0.18°C from 1906–2005 with the rate of warming doubling over the last 50 years using the most reliable data available (IPCC, 2007). Knowledge of surface temperatures is important in a variety of different applications including local to global scale climate modelling and

other forms of environmental assessment (e.g. Pitman, 2003; Vargo et al., 2013). Examples include urban environmental quality (UEQ) studies (e.g. Liang & Weng, 2011); urban climatology and sustainable urban development studies (Weng & Larson, 2005) and summer heat-related health studies (e.g. Johnson et al., 2011). For example, Mirzaei and Haghighat (2010) reported that almost 50,000 people died because of heat-related illnesses across Europe during the summer of 2003. Consequently, there has been a considerable amount of research on the causes and effects of enhanced heating in urban areas in recent years.

Undoubtedly, the most widely studied thermal phenomena in urban areas is the heat island effect. Oke (1987) defines this as the increase in temperature in urban areas relative to suburban or rural surroundings.

3.2 Urban heat island (UHI)

The study of UHI goes back to the early 19th century when Howard (1833) made use of air temperature measurements to study changes in temperature between the centre of London and surrounding areas. More recently, Voogt and Oke (2003) have identified three types of UHI namely (i) the canopy layer heat island (CLHI) (ii) the boundary layer heat island (BLHI) and (iii) the surface (skin) urban heat island (SUHI). The CLHI extends from the surface upwards to approximately mean building height, whilst the BLHI extends above the canopy layer. SUHI, in contrast, is a broader term used to describe the detection of urban heating using remote sensing techniques.

The term UHI is mostly commonly associated with changes in air temperature within the canopy layer, which extends from the ground to the tops of buildings or trees, and is usually measured via traverses across an urban area or from a series of weather stations located within and around such areas (Emmanuel & Kruger, 2012; Pichierri et

al., 2012). In contrast, SUHI or land surface temperatures (LST) are derived from satellite or air-borne thermal sensors. It is important to note that LST and air temperature are different, with LST usually warmer than air temperature, especially during summer and winter months (Yuan & Bauer, 2007). A number of studies have shown that patterns of LST (derived from remotely sensed images) and air temperature are similar, albeit with differences in absolute values (e.g. Coutts & Harris, 2012; Schwarz et al., 2012). Differences between LST and air temperatures are most pronounced during the daytime and least pronounced during the night (US EPA, 2008a) (Fig. 3.1).
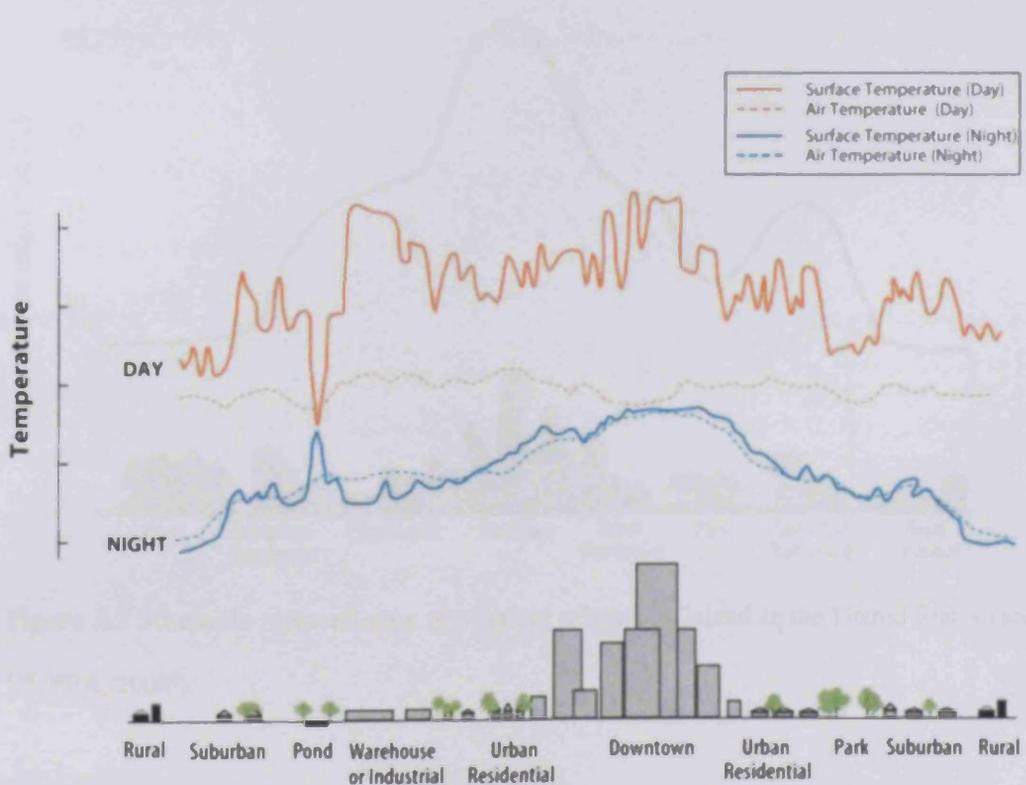
Figure 3.1 Variations in land surface temperature (LST) and air temperature during daytime and night-time for different types of land cover (source: US EPA, 2008[3]). Higher temperatures are associated with denser urban areas and lower temperatures with suburban and rural areas.

---

[3] United Stated Environmental Protection Agency: http://www.epa.gov/heatislands/about/index.htm

LST measurements have been widely adopted in studies of UHI since the advent of thermal remote sensing technology because data from these sensors can cover a larger spatial extent and produce more frequent measurements at lower cost than traditional techniques (e.g. Hamdi, 2010; Kharol et al., 2013; Ngie et al., 2014; Sobrino et al., 2013; Tomlinson et al., 2012; Xu & Chen, 2004).

The intensity of the UHI effect is determined by the form and composition of the urban area; consequently, no two UHI are the same. Figure 3.2 illustrates how the late afternoon temperature varies spatially across an urban area in response to different types of land cover and land use.
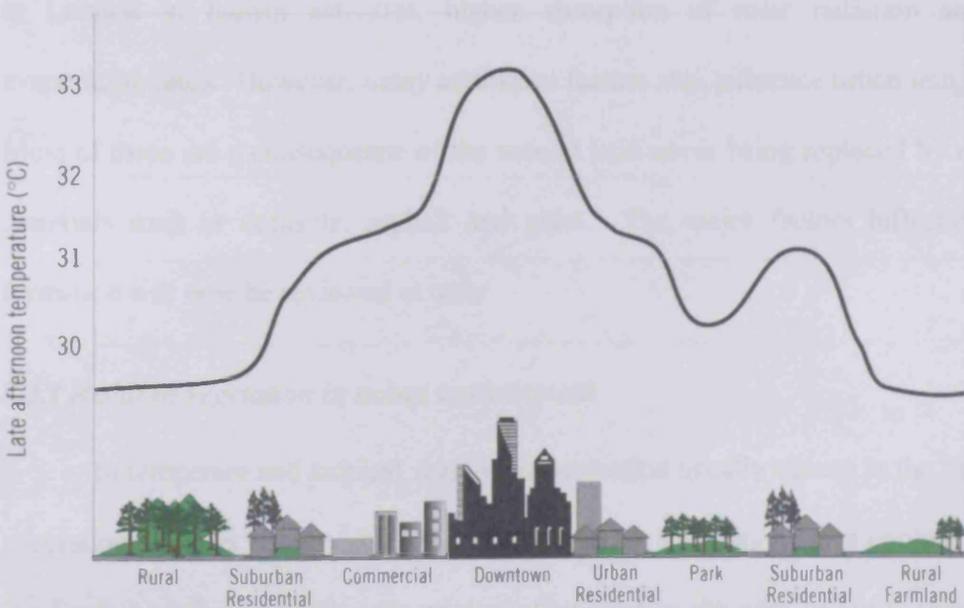
Figure 3.2 Schematic representation of a typical urban heat island in the United States (source: US EPA, 2008[4]).

UHI intensity typically increases from mid-noon to its maximum intensity a few hours after sunset. Temperatures in urban areas at night-time can be 7-12°C warmer

---

[4] United Stated Environmental Protection Agency: http://www.epa.gov/heatislands/resources/pdf/BasicsCompendium.pdf

than in surrounding rural areas. By day, temperature variations are more modest, typically in the range 1-3°C (Goward, 1981). The UHI effect is most pronounced during calm and clear nights as the built surface materials tend to absorb and store significant amounts of heat during the daytime and slowly release this at night (Gartland, 2008).

3.3 Factors affecting UHI intensity

Although UHI in cities generally share similar characteristics, their intensity and time of occurrence can vary considerably based upon local urban physical characteristics, geographical location and weather conditions (Chen et al., 2014; Gartland, 2008; Shashua-Bar & Hoffman, 2000). Howard (1833) related the UHI effect in London to human activities, higher absorption of solar radiation and lower evaporation rates. However, many additional factors also influence urban temperatures. Most of these are a consequence of the natural land cover being replaced by manmade materials such as concrete, asphalt and glass. The major factors influencing UHI formation will now be reviewed in turn:

3.3.1 Reduced vegetation in urban environment

In temperate and tropical regions, urbanization usually occurs at the expense of vegetation which is replaced by impervious surfaces. Vegetation has a cooling effect on the Earth's surface through evapotranspiration (and in the case of trees, shade) while impervious surfaces such as roads, pavements, rooftops and car parks absorb less water (Akbari, 2002; Voogt & Oke, 2003; Weng et al., 2004). The change from pervious to impervious surface increases the dryness of the surface which leads to an increase in the absorption of solar energy and production of sensible as opposed to latent heat, leading to elevated surface temperatures in urban areas in comparison to rural areas where

vegetated/natural surfaces are dominant (Streutker, et al., 2003; US EPA, 2008a; Weng et al., 2004) (Fig. 3.3).
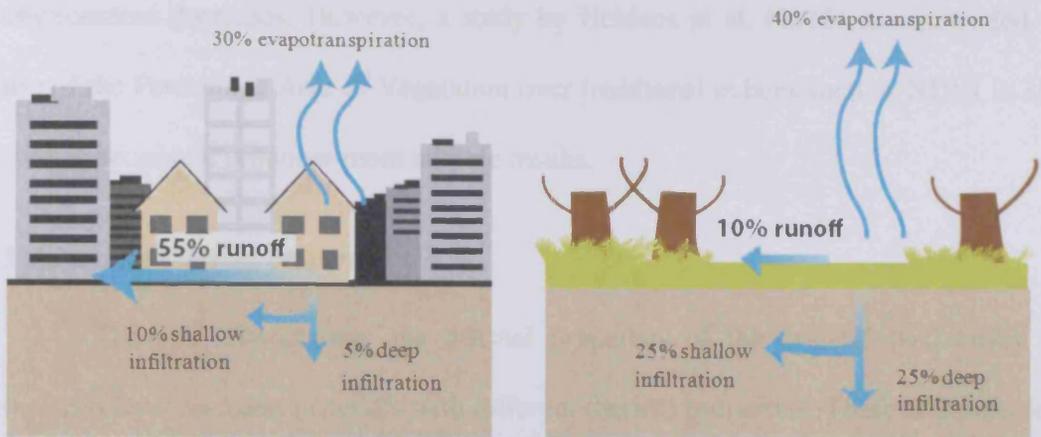
Figure 3.3 Comparison between highly urbanized areas (left) and rural areas (right). The higher proportion of impervious surfaces decreases the surface moisture available for evapotranspiration in the urban environment. This characteristic contributes to the increase in both air and surface temperatures in urban areas which increases the intensity of the UHI (source: US EPA, 2008[5]).

Due to the importance of this factor many researchers have studied the influence of vegetation on UHI intensity by relating the percentage area of vegetation or vegetation indices in urban areas to surface temperature. Vegetation indices combine two or more characteristics of vegetation such as water content and pigments to provide meaningful information about the relative density and greenness or health of vegetation (Exelis, 2013). Examples include the Normalized Difference Vegetation Index (*NDVI*) (e.g. Cui & Shi, 2012; Julien, et al., 2006), Enhanced Vegetation Index (*EVI*) (e.g. Khandelwal & Goyal, 2010; Zhou et al., 2014) and Leaf Area Index (*LAI*) (e.g. Loughner et al., 2012; Ren et al. 2013). Other indices include Vegetation Fraction (*VF*) (e.g. Cui & Foy, 2012, Weng et al., 2004) and Percentage Area of Vegetation (*V*) (e.g.

---

[5] United Stated Environmental Protection Agency: http://www.epa.gov/heatislands/resources/pdf/BasicsCompendium.pdf

Coseo & Larsen, 2014; Zhang et al., 2009). These studies confirm that UHI intensity increases when vegetation indices or the percentage of vegetation within the urban environment decreases. However, a study by Heldens et al. (2013) recommended the use of the Percentage Area of Vegetation over traditional indices such as NDVI in UHI studies because it produces more reliable results.

3.3.2 Urban thermal properties

Through urbanization, the thermal properties of the original land cover are replaced by man-made materials with different thermal properties. These materials tend to promote heat storage through the combination of two properties: thermal conductivity and heat capacity (Gartland, 2008; Kaloush et al., 2008). These properties interact in two different ways with the higher thermal conductivity of man-made materials tending to conduct heat to a greater depth and materials with high heat capacity tending to store more heat in their volume. Many man-made materials, such as steel, asphalt, concrete and glass have higher heat capacities than natural materials such as dry soil and sand hence more solar energy is stored as heat in the urban environment (Christen & Vogt, 2004; US EPA, 2008a).

A third material property called thermal diffusivity is calculated by dividing thermal conductivity by heat capacity (Erell et al., 2011). As Figure 3.4 shows, the thermal diffusivity of man-made materials are clearly higher than those of natural materials indicating that solar heating penetrates deeper into the urban environment and is stored for longer periods of time (Gartland, 2008; Oke, 1987). For this reason, more heat is stored by the urban fabric during the day then released slowly back at night to the atmosphere causing an increase in temperature in urban areas relative to their more rural surrounds (US EPA, 2008a).

Chart data (Thermal Diffusivity, m^2 / s x 10-6):

- Dry Peat Soil: 0.10
- Wet Peat Soil: 0.12
- Dense Wood: 0.13
- Water @ 4°C: 0.14
- Dry Clay Soil: 0.18
- Gypsum board: 0.18
- Light Wood: 0.20
- Dry Sandy Soil: 0.23
- Aerated Concrete: 0.29
- Built-up Roofing: 0.32
- Asphalt: 0.39
- Glass: 0.45
- Clay Tile: 0.47
- Wet Clay Soil: 0.51
- Brick: 0.61
- Dense Concrete: 0.72
- Wet Sandy Soil: 0.74
- Stone: 0.97
- Polystyrene Insulation: 1.50
- Fiberglass Insulation: >> 10.93
- Steel: >> 11.56
- Still Air @ 10°C: >> 20.83

Figure 3.4 Thermal diffusivity of various materials and cover types (Source: Gartland, 2008).

3.3.3 Low solar reflectivity

Generally, man-made materials tend to absorb more net radiation from the sun than natural materials due to the fact that they have low solar reflectivity or low albedo, which is defined as the ratio of the amount of radiation reflected from a surface to the total amount of radiation received by that surface (Strugnell & Lucht, 2001). Albedo is a dimensionless quantity that ranges from 0.0 for a non-reflective surface (perfectly black) to 1.0 for a perfectly reflective surface (white) (Gosling et al., 2014). For example, typical albedo values for asphalt surfaces range between 0.10 – 0.15; concrete surfaces between 0.10-0.35; bricks between 0.20-0.40; dry sand between 0.20 – 0.30 and dry grass around 0.30 (Assimakopoulus et al., 2001).

Man-made materials with low solar reflectivity such as roads, car parks and pavements tend to absorb more of the sun's energy than other urban materials, thus

57

contributing to an increase in LST and intensification of the UHI (Oke, 1987; Radhi et al., 2014). However, albedo varies considerably between cities and within cities, ranging from 0.15-0.20 in most European and North American cities to 0.30-0.45 in North African cities because of differences in construction materials (i.e. sand and bricks) (Taha, 1997).

3.3.4 Urban Geometry

Urban geometry is considered one of the most important factors controlling the UHI (Oke, 1987; p.293). The effect of urban geometry on UHI is governed by many factors including variations in building height, building density, building layout and building structure (Kakon et al., 2010; Martin et al., 2012; Tonkaz & Çetin, 2007; Xiao et al., 2008). For example, urban canyons (tall buildings separated by narrow streets) alter the amount of solar energy reaching the surface and being re-emitted to the atmosphere as they are effective at trapping the radiation, particularly at night-time (Stewart et al., 2014; US EPA, 2008a) (Fig. 3.5). Furthermore, net radiation absorption is enhanced in urban areas through multiple reflections between buildings (Oke, 1982). However, during the day, tall buildings can provide more shade thus some cooling in urban areas (Nichol, 1996; US EPA, 2008a).

Johansson and Emmanuel (2006) noted that buildings with similar heights (small height variation) caused wind speeds to decrease at street level hence promote UHI formation, whereas a group of buildings with different heights tended to increase wind circulation within urban areas and assist in cooling. However, tall buildings can act as wind breaks which can in turn elevate the temperatures in nearby urban areas. Nichol (1996) noted that a group of buildings with small mass accumulated heat more

easily during the daytime than a group of buildings with a larger mass due to lower thermal inertia.

Red Arrows – Heat released by buildings and pavement at night. Constantly being reflected and thus, trapped in the city.
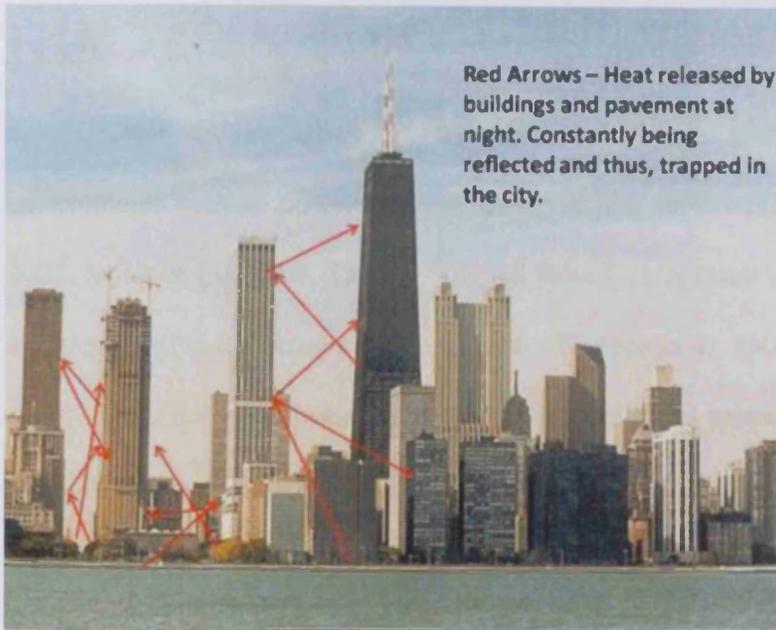
Figure 3.5 Multiple reflections and trapping of heat within a city during the night causing the UHI to intensify (Source: Ephraimrc, 2012[6]).

Another urban geometry metric that has been widely used in UHI studies is the Sky View Factor (e.g. Hwang et al., 2011; Lin et al., 2012). This represents a dimensionless quantity of visible sky at a specific location in the city. It is defined as the ratio of solar radiation received by a planar surface compared to that received from the entire hemispheric radiating environment (Watson & Johnson, 1987). Generally, high levels of urbanization lead to low sky view factors in cities which increases the intensity of the UHI during the night-time (Svensson, 2004). However, Svensson's study was based only on night temperature measurements performed in Goteborg,

6 https://ephraimchaney.wordpress.com/2012/10/22/a-failure-to-think-systematically/

Sweden. Similarly, Gal et al. (2009) found that sky view factor relates strongly and negatively to UHI intensity in Szeged, Hungary based on annual temperature data.

3.3.5 Other factors

Other factors affecting UHI intensity include heat sources in the urban environment such as power stations, transport and air conditioning units (Kato et al., 2005; Sailor & Lu, 2004; Taha, 1997). All these factors result in increased temperatures in cities relative to surrounding rural areas (Tiangco et al. 2008). Heat release from air conditioning units has been found to increase the mean temperature of urban areas by 1°C during the night in Arizona, USA (Salamanca et al., 2014),

Additional factors include the geographic location of the city and local weather conditions. For example, cities that are close to large water bodies tend to experience lower daytime UHI intensity because of breezes that convect heat away from urban areas hence contribute to cooling (Nasrallah et al., 1990; US EPA, 2008a). Mountain ranges can also influence the intensity of the UHI either by acting as natural barrier to the wind reaching the city, thus increasing UHI intensity, or by creating mountain wind circulation that results in a reduction in UHI intensity especially during the night-time (Miao et al., 2014; US EPA, 2008a).

3.4 UHI in sandy desert environments

Most published studies of this phenomenon are based on temperate cities where vegetation is dominant. The results of such studies indicate that because impervious surfaces (i.e. urban areas) replace natural vegetation cover, the surface temperature of the urban area increases relative to the surrounding rural area during the daytime, and

this effect is intensified during night-time (e.g. Imhoff et al., 2010; Li et al., 2012; Sobrino et al., 2013). However, in desert cities where sand is the dominant land cover an inverse phenomena is noted in which the city exhibits lower surface temperatures than the desert during the daytime (Urban Heat Sink, UHS) and higher temperatures than the desert during night-time (i.e. UHI) (Frey et al., 2007; Lazzarini et al., 2013; Lougeay et al., 1996).

Numerous factors that control the UHS phenomenon have been investigated in desert cities. The UHS has mainly been attributed to an increase in vegetated areas associated with urbanization leading to an increase in cooling due to the increase in latent heat flux through evapotranspiration and a decrease in sensible heat in the urban environment compared to desert surroundings (Lazzarini et al., 2013). However, Frey et al. (2007) noted that even industrial non-vegetated urban areas exhibited more cooling than surrounding areas in desert cities. Conversely, Lougeay et al. (1996) has attributed the UHS in Phoenix, Arizona to the water bodies.

Another metric, the Impervious Surface Area Fraction (ISA) has been used to show that the higher the proportion of impervious surfaces in the urban area the higher the surface temperature and vice versa (Lazzarini et al., 2013). However, Imhoff et al. (2010) noted that despite some desert cities being highly urbanized (high proportion of impervious surfaces) they still show an UHS during the day. This disparity in the literature highlights the need for further research to understand the relationships between land cover/use and LST in desert cities.

3.5 Satellite thermal data used in urban thermal studies

All objects on earth emit thermal infrared (TIR) electromagnetic radiation that can be detected by TIR satellite sensors within the atmospheric window that ranges between 3 to 14μm in the in the electromagnetic spectrum (Jensen, 2007) (Fig. 3.6).
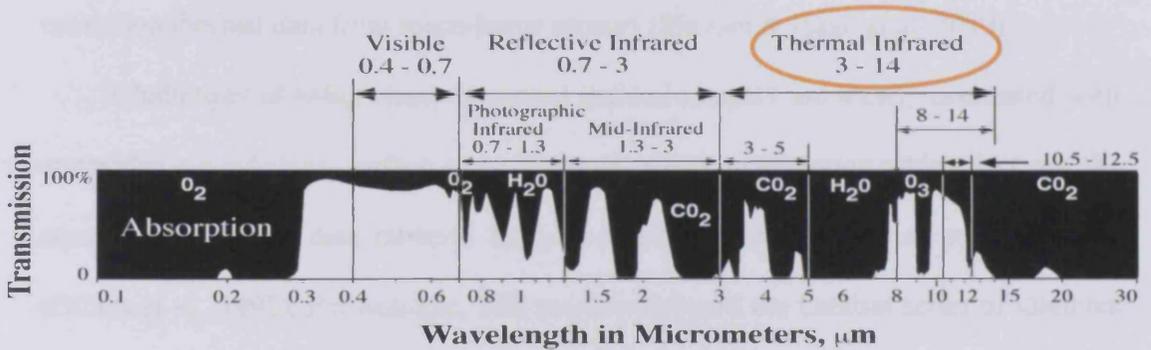
Figure 3.6 Atmospheric windows in the electromagnetic spectrum. Most satellite TIR sensors operate within the ~8-12μm window apart from MODIS which has an extended range (source: Jensen, 2007).

Over the last 50 years, there have been significant developments in thermal sensor technology as well as improvements in thermal image processing algorithms which have significantly increased the use of thermal data in UHI studies. The scientific aims of studying UHI are not limited to quantification of magnitude and spatial extent, but also consider cause and effects of this phenomenon. Therefore, studying operational and long-term surface temperature is receiving more scientific attention than ever before.

Since early attempts to derive surface temperature information from space by Wark et al. (1962) using the Television Infrared Observation Satellite (TIROS-2), the spatial, spectral and temporal resolution and coverage of satellite-mounted thermal sensors has improved considerably (Table 3.1).

Large scale acquisition of surface temperature data from satellite-based thermal sensors offer an attractive, cost effective and timely means of obtaining data (Cristobal, 2011). Furthermore, remote sensing technology allows researchers to study areas that are not necessarily accessible through conventional methods (Chen et al., 2014). The high cost and limited (spatial and temporal) availability of high resolution air-borne thermal imagery has meant that researchers have turned instead to medium-low resolution thermal data from space-borne sensors (Mirzaei & Haghighat, 2010).

Challenges of using remotely-sensed thermal imagery are mostly associated with atmospheric conditions, surface emissivity and radiance calibration which decrease the accuracy of thermal data retrieval by 1-2k relative to air temperature measurements (Gillies et al., 1995). For example, TIR sensors on-board the Landsat series of satellites (except the recent Landsat-8) use only one TIR band which makes it challenging to implement atmospheric correction for more accurate LST retrieval when compared to other TIR sensors which utilise more than one band such as ASTER or MODIS (Cristobal et al., 2009).

With the availability of various TIR sensors on board different satellite platforms a choice has to be made between either using thermal data at high spatial resolution or high temporal resolution (Table 3.1). A further choice is whether to choose a thermal sensor that operates at day and/or at night. For example, one could choose medium scale (~60m) thermal data from sensors mounted on Landsat and ASTER platforms with relatively long repeat cycles or small scale (~1km) thermal data from sensors mounted on MODIS and AVHRR platforms with short repeat cycles of approximately 12 hours. It is currently unfeasible to estimate LST at both high spatial resolution and high temporal resolution (Sattari & Hashim, 2014).

Nevertheless, various satellites and thermal instruments have been used in SUHI studies: Advanced Very High Resolution Radiometer (AVHRR) images have been used at both the local scale, only one country is studied, (e.g. Ouaidrari et al., 2002; Streutker, 2003) and global scale, to study the entire Earth, (e.g. Jin, 2004). MODIS has been used at city scales (e.g. Hu & Brunsell, 2013; Tomlinson et al., 2012), continental scales (e.g. Imhoff et al., 2010; Schwarz et al., 2011) and global scales (e.g. Jin & Dickinson, 2010). However, medium resolution TIR sensors have been primarily used at city scales such as Landsat TM (e.g. Carnahan & Larson, 1990; Sobrino et al., 2004), Landsat ETM+ (e.g. Li et al., 2012) and ASTER (e.g. Jinghui et al., 2006; Nichol et al., 2009) or in conjunction with other sensors operating at different scales (e.g. Lazzarini et al., 2013).

Table 3.1 Primary operational satellite sensors used in UHI studies (Sources: Collected from various imagery suppliers' websites).

Satellite	sensor	Time of the day	Number of thermal bands	Spatial resolution	Revisit interval (days)	TIR bands and Spectral range μm	Service year
NOAA 6,8,10			2			B4: 10.50 - 11.50 B5: B4 repeated	
NOAA 7,11,12,14	AVHRR	Day and night	4	1.1km	daily	B4: 10.30 - 11.30 B5: 11.50 - 12.50	1979-present (full series)
Terra	MODIS	Day and night	6 for Surface temperature with different spectral radiance. Other 5 more bands used for LST retrieval.	1km	daily	B20: 3.660 - 3.840 B21: 3.929 - 3.989 B22: 3.929 - 3.989 B23: 4.020 - 4.080 B31: 10.780 - 11.280 B32: 11.770 - 12.270	1999-
Aqua							2002-
Terra	ASTER	Day and night	5	90m	16	B10-B11: 8.125-8.825 B12: 8.92 :9.275 μm B13-B14: 1.25-11.65 μm	1999-
Landsat 5	TM	Day	1	120m	16	B6: 10.4–12.5 μm	1984-
Landsat 7	ETM+	Day	1	60m	16	B6: 10.4–12.5 μm	1999-
Landsat 8	TIRS	Day	2	100m	16	B10: 10.60 - 11.19 μm B11: 11.50 - 12.51 μm	2013-

3.6 Satellite thermal Infrared (TIR) remote sensing

With the limitations of conventional temperature retrieval methods from weather stations due to the sparse availability of temperature records for many cities (Knight et al., 2010), TIR data retrieval from space-borne satellites has received increasing attention. In addition, thermal data from remotely sensed images has been widely adopted as an alternative to conventional techniques as they do not suffer from problems of uncertainty introduced by interpolating between a limited number of fixed points (Li et al., 2013). Satellite TIR images are particularly useful for isolated locations where weather stations are not present (Czajkowski et al., 2005).

Earth surface temperature detection from space is based on Planck's Law, which states that the temperature of a blackbody determines the type of spectral radiation it emits (Jensen, 2007). However, the land surface is highly heterogeneous, being composed of many different types of land cover hence estimating surface temperature from satellite thermal infrared sensor (TIR) data is highly complex (Weng & Larson, 2005). In order to use long term and reliable estimates of LST for thermal studies, LST must be retrieved at an accuracy of 1-2 kelvin (Li et al., 2013). Therefore, in order to retrieve LST as accurately as possible from TIR sensors four major requirements need to be met (Fig. 3.7). Firstly, TIR images must be screened for clouds since the amount of cloud influences the quality of thermal electromagnetic signals and ultimately the final LST retrieval (Wan et al., 2004). For example, cloud cover of 10% could result in an estimate of LST that is 20°C lower than the actual land beneath it (Weng & Larson, 2005).

Cloud screening

Spectral radiance to at-sensor brightness temperature

Atmospheric correction

Land surface emissivity retrieval
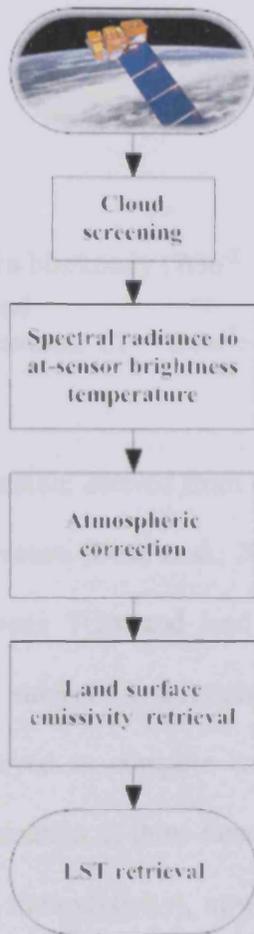
LST retrieval

Figure 3.7 Typical LST retrieval steps followed by thermal urban studies using space-borne sensors.

The second step in LST retrieval is the conversion of spectral radiance received by the sensor to at-sensor brightness temperature. Satellite TIR sensors determine 'top of the atmosphere' (TOA) radiances, from which TOA blackbody temperatures (at-sensor brightness temperatures) can be derived based on Planck's radiation function (equation 3.1) (Dash, 2002). It assumes that all objects with more than absolute zero kelvin temperatures and emissivity of 1 (blackbodies) emit radiation. Emissivity (ε) is the radiance emitted by an object divided by that emitted by a black body at the same temperature.

$$BT = \frac{C_1}{\lambda^5 \left[\exp\left(\dfrac{C_2}{\lambda T} \right) - 1 \right]}$$

(3.1)

Where

BT is the spectral radiance of a blackbody (Wm^{-2} μm^{-1} sr^{-1}) (Plank's function);

λ is the wavelength (μm); and

C_1, C_2 are Plank's radiation constants, $C_1 = 2\pi hc^2 = 3.7418.10^{-16}$ Wm^2; $C_2 = hc/k = 1.4388.10^{-2}$mk.

The TOA brightness temperature derived from equation 3.1 is usually lower than the land surface brightness temperature (Dash et al., 2002). Prata et al. (1995) stated that the temperature difference between TOA and land surface brightness temperatures could range from 1°C to 5°C, subject to atmospheric conditions. For this reason, atmospheric correction is employed to compute land brightness temperature. TOA brightness temperature is a combination of three factors, namely emitted radiance from the Earth's surface (atmospheric transmissivity), upwelling atmospheric radiance from the atmosphere, and down-welling atmospheric radiance. Therefore, in order to derive surface brightness temperature all atmospheric factors must be corrected (Li et al., 2013; Prata et al., 1995; Wan and Dozier, 1996). For this reason, atmospheric information at the time of image acquisition must be known in order to correct the image. However, in the 8–12μm (thermal infrared) region of the electromagnetic spectrum covered by most TIR satellite sensors, absorption and scattering of aerosol is relatively insignificant and usually ignored with water vapour essentially responsible for the atmospheric effect (Dash et al., 2002; Prata et al., 1995).

Finally, land surface emissivity (LSE) retrieval is required to eventually derive LST from brightness temperature. Because most of the natural bodies are grey (0< ε <1), emissivity must be known for each pixel in the image before land surface

temperature is computed (Dash et al., 2002; Voogt & Oke, 2003). Jin (2004) highlighted that a 1% uncertainty in the emissivity of a surface could increase or decrease the estimated land surface temperature by 0.7 ^{0}C, thus LSE retrieval is critical in thermal studies.

Depending on the type of thermal sensors and availability of atmospheric and land surface emissivity information for the TIR data acquired, different methods have been developed to retrieve LST. LST retrieval is considered to be one of the most exciting yet challenging topics in thermal studies of urban environments. LST retrieval methods are based on employing several assumptions and estimates for the atmospheric factors and LSE (Li, et al., 2013).

For priori known LSE, two major methods are widely used for atmospheric correction: single-channel algorithm methods (e.g. Jimenez-Munoz et al., 2014; Lamaro et al., 2012; Qin et al., 2001) and multi-channel (split window) algorithm methods (e.g. Jimenez-Munoz, 2014; Wan & Dozier, 1996; Zhou et al., 2014). Single channel methods are generally suitable for one TIR channel sensors such as Landsat TM and ETM+ while multi-channel methods are better suited to sensors with two or more TIR channels such as Landsat 8 TIR and ASTER. Both algorithms are based on the separation of atmospheric factors which are highly correlated and dependant on atmospheric water vapour content (Jimenez-Munoz & Sobrino, 2006). However, the single-channel algorithm requires water vapour to be accurately known at the time of image acquisition. This is unavailable in most cases (Li et al., 2013). For this reason, the split-window algorithm is preferred as the atmospheric profiles derived from the two adjacent TIR channels yield more accurate results in order to eliminate the atmospheric influence (Wan & Dozier, 1996).

The second group of methods are used when the emissivity is unknown. Three major methods are widely used, namely classification based emissivity methods (Synder et al., 1998), NDVI based emissivity methods (Sobrino et al., 2004; Valor & Caselles, 1996; Van de Griend & Owe; 1993) and temperature emissivity separation methods (TES) (Gillespie et al., 1998; Wang et al., 2011). The first two methods do not require accurate atmospheric corrections unlike the TES method (Li et al., 2013). Furthermore, TES methods are only used when 3 or more TIR channels are available, such as is the case with ASTER and MODIS.

Classification-based emissivity methods break a study area down into different land cover classes (assuming each land cover class has similar surface materials) then assign emissivity values to each class (Synder et al., 1998). In contrast, NDVI-based emissivity methods assume that the study aras is composed of only soil and vegetation, with each class assigned an emissivity value accordingly. Sobrino et al. (2004) modified this in order to produce a Normalized Difference Vegetation Index Threshold Method in which the emissivity retrieval was based on three NDVI threshold value cases. TES methods are mainly employed by separating LST and LSE using atmospherically corrected TIR images by relying on the empirical relationship between the spectral contrast and the minimum emissivity measured from field spectra library (Gillespie et al., 1998).

3.7 UHI intensity mitigation

Humans can adapt to increasing temperatures in their homes and work places by adjusting their air conditioning units, however, this results in more heat being released into the urban environment and further intensifies the UHI effect. Therefore, other

mitigation measures that have no negative impacts on local and global heat release need to be considered.

A number of measures have been adopted to reduce the intensity of the UHI effect. Three have been widely used in practice: (i) increases in the amount of urban vegetation cover (ii) increases in the albedo (reflectivity) of urban materials (iii) changes in urban structure.

By increasing the amount of vegetation urban areas become cooler through increased evapotranspiration and shade (e.g. Rosenthal et al., 2008; US EPA, 2008b). Furthermore, green roofs can be adopted to reduce the amount of heat stored at the top of the urban canopy (e.g. Li et al., 2014; Peng & Jim, 2013). Green roofs are special multi-layer structures that are installed on existing roofs to support the growth of plants and promote natural drainage of water to mimic natural surfaces (Vayda, 2010)

Increasing solar reflectivity by using new materials or painting existing materials with high albedo colours (high solar reflectivity) can help reduce heat gain during the day and re-radiation during the night. Some cities have made use of highly reflective urban materials (e,g., Bretz et al., 1998; Mackey et al., 2012). Mackey et al. found that increasing the surface reflectivity in urban areas of Chicago had a stronger cooling effect than increasing the vegetation coverage. Taha et al. (1997) found that white surfaces with an albedo of 0.72 were 45°C cooler than other black surfaces with an albedo of 0.08 during clear daytime summer conditions at noon.

Other mitigation strategies are related to manipulating the urban geometry and design of buildings during the urban planning process or redevelopment process (Emmanuel, 2005). For example, it is possible to increase the amount of shade and wind circulation through careful choice of street alignment and building arrangement relative to dominant weather patterns (Emmanuel et al., 2007). Oke (1988) suggested that a

building height to width ratio (urban canyon) of between 0.4 and 0.6 would reduce the UHI intensity during summer daytime and provide suitable air circulation in urban environments during the night-time.

3.8 Conclusions

UHI is an important phenomenon that reflects the negative human intervention on natural landscape. While the alteration of the landscape through urbanization is inevitable, a variety of mitigation measures could reduce the consequences of this phenomenon.

Several types of data are available to investigate temperature gradients in UHI studies; however, TIR remote sensing data is becoming more popular, particularly for cities that have limited weather recording capabilities such as Dubai. Nevertheless TIR data are hampered by either low spatial or low temporal resolution, hence a decision has to be made whether to focus primarily on the spatial or temporal properties of this phenomenon when planning research.

Many UHI studies have been conducted in temperate and tropical regions; however, more research emphasis needs to be placed on studies in desert cities since these are growing rapidly in response to planned and projected changes in population. For example, the city of Dubai has rapidly expanded horizontally and vertically over the last two decades. Urbanization has been accompanied by an increase in the amount of vegetation and water in the built environment at the expense of desert sand. On examining the literature it becomes apparent that few studies have focused on desert cities to date. One exception to this is the study of Abu Dhabi reported by Lazzarini et al. (2013) whose analysis was based on simple correlations between LST, NDVI and Impervious Surface Index for three sample areas across the city containing a high

proportion of vegetation, a low proportion of vegetation and no vegetation. They

concluded that LST correlated negatively with the amount of vegetation and positively

with the percentage area of impervious surfaces. Their findings are applicable to all

cities, however, their approach does not determine what other factors are responsible for

UHI or/and UHS in desert cities or the relative importance of such factors.

Furthermore, other UHI studies in desert cities have raised questions about the actual

causes of cooling in some urban areas in the absence of vegetation (section 3.4);

therefore other approaches need to be adopted to address such questions. Knowledge of

the factors controlling UHI or/and UHS formation in desert cities will ultimately assist

the development of appropriate mitigation strategies.

3.9 Summary

This chapter discussed the history, importance and different types of UHI. It then

introduced the factors influencing the change in UHI intensity in cities before going on

to discuss UHI in temperate and desert regions and presenting methods used to study

UHI in desert environments. The chapter then discussed the value of satellite TIR data,

retrieval algorithms for land surface temperature and mitigation strategies.

The next three chapters present empirical studies covering: the historic urban

growth of Dubai, its drivers and characteristics (Chapter 4), daytime urban heat island

effects in Dubai and contributing factors using Landsat data (Chapter 5) and an

investigation of diurnal and seasonal variations in UHI and UHS derived from MODIS

data for local climate zones composed from different proportions of land cover and

different types of urban geometry (Chapter 6).

Chapter 4 Developing the desert: The pace and process of urban growth in Dubai

Ahmed K. Nassar, G. Alan Blackburn and J. Duncan Whyatt

Lancaster Environment Centre, Lancaster University, Lancaster, UK

Statement of Authorship

I, Ahmed Khalaf Nassar, in my capacity as the first author of the above publication, researched, acquired, pre-processed, processed and compiled all the Landsat images and other data such as the population data and other ancillary data that were used in the paper. I tested the technique and methods presented, and subsequently applied the technique to obtain historical urban growth, drivers and form of the city, and compared it to recent urban growth theory. I carried out the analysis of the results and drafted the manuscript, including the preparation of all figures and tables. I undertook the revisions of the manuscript following comments and advice from the co-authors and referees and submitted the final version to the journal. This constitutes approximately 85% of the work involved with this publication.

Please find hereunder signatures of the co-authors confirming my contribution to the above publication, as described above.

Yours sincerely,

74

Ahmed Khalaf Nassar

Signature *Ahmed Khala/*

Co- authors:

Name   G. Alan Blackburn

Signature   *G. A Black...*

Name   J. Duncan Whyatt

Signature   *J. D Whyatt*
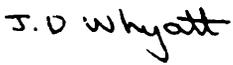
Context

In order to investigate the relationship between urban growth and thermal change in Dubai it is first necessary to quantify the rate and form of urbanisation over an extended time period. Unfortunately, no publicly accessible information exists concerning the rate or form of the urbanisation process in Dubai. Therefore, in this chapter timeseries of remotely sensed data were used to quantify changes in urban and other land cover in the emirate between 1972 and 2011. These data are preferred over conventional data for reasons discussed in section 2.11. Landsat imagery was utilised because the archive extended over the period of this study and the sensors provided data of acceptable spatial and spectral resolution.

A hybrid classification method was employed to classify the Landsat images into different land cover types. This method accurately discriminated between urban and other types of land cover and compared favourably to other methods previously used to determine land cover in other desert cities (section 2.9).
Spatial metrics were used to quantify the spatial evolution of the emirate over time to identify different phases of urban growth and to better understand the drivers for growth as discussed in section 2.8.

The results indicate a dramatic increase in urban area, with a compound annual growth rate of 10.03% over the study period, with a peak of 13.03% during 2003–2005, making Dubai one of the fastest growing cities in the world. While the population growth rate was high, this has been outpaced by the rate of increase in urban area and the declining population density is indicative of urban sprawl. The spatiotemporal dynamics of urban growth are closely associated with prevailing local and global economic conditions and the ambitious development strategies of the government. Notable aspects of this growth include the substantial increase in vegetation and water

bodies, and the unprecedented rate of construction of offshore islands. Dubai has undergone oscillating phases of urban diffusion and coalescence, but with much more rapid transitions than other cities. Superimposed on these phases are spatial patterns of development which have been recognised elsewhere, but the sequence of patterns appears unique to Dubai

The findings of this chapter have provided new insights into the pace and process of urban growth in Dubai which have necessitated the study of the impact of such growth on the surface thermal characteristics of the emirate in the following chapter.

4.1. Introduction

Over the last decade Dubai Emirate has witnessed great economic growth resulting from rapid urbanization which has turned the desert into residential, commercial, sports and tourism projects. In addition, the offshore environment has been developed with artificial islands, such as Palm Jumairah, Palm Deira and the World Islands. Cities within a city are a particular characteristic of this Emirate, and a number of mini cities have been developed in Dubai including Dubai Festival City, Sports City, Media City, Internet City and Healthcare City. The scale of development in recent years is evidenced by the estimate that 25% of the world's construction cranes operate in Dubai (Badouri, 2007). Indeed, the rapid pace of urban growth in Dubai has attracted the attention of economists, environmentalists and urban planners (Intercon, 2010; Kelbaugh, 2011). However, there is no publicly accessible information on the expansion of Dubai, likely due to a paucity of data overall and governmental restrictions on data that do exist. Therefore, the present research presents us with the opportunity to develop and apply an accurate and objective method for quantifying urban growth in order to

understand the spatiotemporal characteristics of the development process in this rapidly changing landscape.

Urban development often takes place as a consequence of factors such as industrial expansion, economic prosperity and population growth (Li et al., 2003; Yin et al., 2005). Conversely, urban growth can be constrained by a range of factors including differential patterns of land ownership and physical barriers such as coastlines (e.g. Taubenböck et al., 2009). In Dubai, the main driver for recent urban development has been a political strategy to diversify the basis of the economy via inward investment in real estate, in the face of diminishing oil reserves. This policy has resulted in a ten-fold increase in the population of Dubai since 1975 (National Bureau of Statistics, 2010; Dubai Statistical Centre [DSC], 2011) mainly due to the increase in expatriate workers with locals forming only 8.8% of the total population in 2010 (National Bureau of Statistics, 2011). Moreover, in Dubai, urban growth has not been constrained by physical boundaries such as the desertified terrestrial environment or the Gulf coast, or by issues of land ownership. Hence, this makes Dubai an interesting and important site for investigating the characteristics of urban development under a unique combination of drivers and apparent lack of constraints.

Satellite remote sensing has been widely used in studies of urban growth and offers a cost effective and time saving alternative to other conventional methods such as surveying (Patino & Duque, 2013). Over the last 40 years there have been significant advances in sensor technologies as well as digital image processing methods and analytical tools. The spatial, spectral and temporal resolution and coverage of satellite imagery has improved considerably, however there are often operational trade-offs between these parameters which can limit the applicability of the data for studying urban growth. For example, Gamba et al. (2011) discussed the limitations of using high

spatial resolution images to monitor urban growth due to their relatively low spectral resolution and coverage, in addition to their high financial cost and lack of a sufficiently long archive of imagery. The timescale over which urban growth has been investigated using remotely sensed imagery also varies considerably between studies; some researchers study urban growth over short time periods, for example, Moeller and Blaschke (2006) tested the feasibility of using Quickbird imagery to monitor Phoenix, USA from 2003 to 2005, while Rajendran et al. (2002) used IRS-1A & 1C imagery in combination with old aerial photographs and topographic maps to study urban growth in Tiruchirapalli, India between 1928 and 1998. However, the most appropriate timescale is likely to be determined by achieving a balance between the known period and pace of urban development in an area and the availability of remotely sensed data of suitable temporal and spatial coverage and resolution for that area.

Data from the Landsat satellite series, considered medium-high spatial resolution, is available at no cost, with near-global coverage from 1972 to the present date. The higher spatial and spectral resolutions of the later Landsat TM and ETM+ sensors make them very useful for detecting urban areas and other forms of land cover. The earlier Landsat MSS sensor has lower spatial and spectral resolutions, but is the only accessible source of imagery for the period 1972-1984. The three sensors combined provide the longest time series of images with a relatively short revisit time (nominally 16 days) over the period in which Dubai has grown most rapidly, and therefore represent a potentially valuable source of information for understanding the process of development in the emirate. Previous researchers using remotely sensed data to study urban growth in arid environments have faced considerable challenges in discriminating urban areas from sand using multispectral imagery and a range of different techniques have been proposed. For example, Stewart et al. (2004) used an

automated relative reflectance enhancement technique to aid discrimination, while Yagoub (2004) and Yin et al. (2005) used manual classification, but no universal solution has emerged. Hence, an appropriate method needs to be applied in order to achieve adequate levels of discrimination for Dubai using the Landsat data.

There has been a long-standing interest in the study of urban form and the analysis of urban growth in relation to demography and economy. Early urban growth theories included the Concentric Zone Theory (Burgess, 1924), the Sector Theory (Hoyt, 1939), the Multiple Nuclei Theory (Harris & Ullman, 1945) and the Wave Theory Analog Approach (Boyce, 1966). Increased computing power enabled the development of urban growth simulation models such as SLEUTH (Clarke et al., 1997) to account for the key drivers of urbanization. More recently, empirically based models of growth have been developed as a result of advances in monitoring capabilities offered by remote sensing and analytical tools to quantify urban development (Dietzel, Herold et al., 2005; Dietzel, Oguz, et al., 2005). For details regarding the empirical model background and previous urban growth theories, see Dietzel et al. (2005). There has been a growing interest in the use of landscape metrics to study urban structures and patterns of urban evolution (Aguilera et al., 2011; Araya & Cabral, 2010; Taubenböck et al., 2009; Wu et al., 2011). These metrics have been developed to analyse spatial configuration and pattern within landscapes in addition to the dynamics of landscape structure and heterogeneity (e.g., Alberti, 2008; Leitão et al., 2006; Yeh & Huang, 2009). In the context of the present study, landscape metrics provide a means of quantifying specific spatial characteristics of landscape patches, classes of patches of particular land cover types, or entire landscape mosaics and therefore have value in helping to understand the process of urban development at a range of scales.

The outputs from remotely sensed mapping exercises have been analysed using landscape metrics for a number of cities in order to inform models of urban growth (Dietzel, Herold, et al., 2005; Dietzel, Oguz, et al., 2005; Martellozzo & Clarke, 2011). These studies suggest that cities are developed through harmonic oscillation of two phases, diffusion and coalescence, with each phase consisting of multiple waves over different time periods. Dietzel, Oguz, et al. (2005) indicate that this harmonic behaviour can be reflected by landscape metrics such as number of patches and Euclidian nearest neighbour distance for urban patches, but other metrics may not exhibit any harmonic behaviour. The oscillation of phases has been measured over different periods of time, such as the 11 oscillations over a 100 year period evidenced in Central Valley cities of California (Dietzel, Herold, et al., 2005) or the 3 oscillations over 28 years found in Houston (Dietzel, Oguz, et al., 2005). Given the distinctive drivers and styles of development found in Dubai, this city provides us with an interesting opportunity to examine the extent to which these existing models of urban growth are applicable in a rapidly developing coastal landscape that is typical of a number of cities that are emerging in the Middle East.

The objectives of this study are firstly to quantify land cover change in Dubai by conducting a spatiotemporal analysis of remotely sensed data and relate this to the economic, population and political drivers; secondly, to quantify changes in the spatial structure of the emirate through the use of landscape metrics; finally, to evaluate the extent to which the process of urban growth in Dubai conforms with the diffusion-coalescence theory (Dietzel, Herold, et al., 2005; Dietzel, Oguz, et al., 2005).

4.2. Materials and methods

4.2.1. Study area

Dubai is one of seven emirates forming the United Arab Emirates, being the second largest after Abu Dhabi in terms of population and area (Fig. 4.1). The total area of the emirate before the development of the islands was 3885 km^2 excluding Hatta which is an exclave city that has no boundary with Dubai Emirate (Department of Finance, 2009). Dubai Creek runs south from the Arabian Gulf for 13km, dividing the city into Deira to the east and Bur Dubai to the west. Dubai is considered as hyperarid with an annual average rainfall of approximately 8mm falling mostly in winter and late autumn (Dubai Airport, 2010).
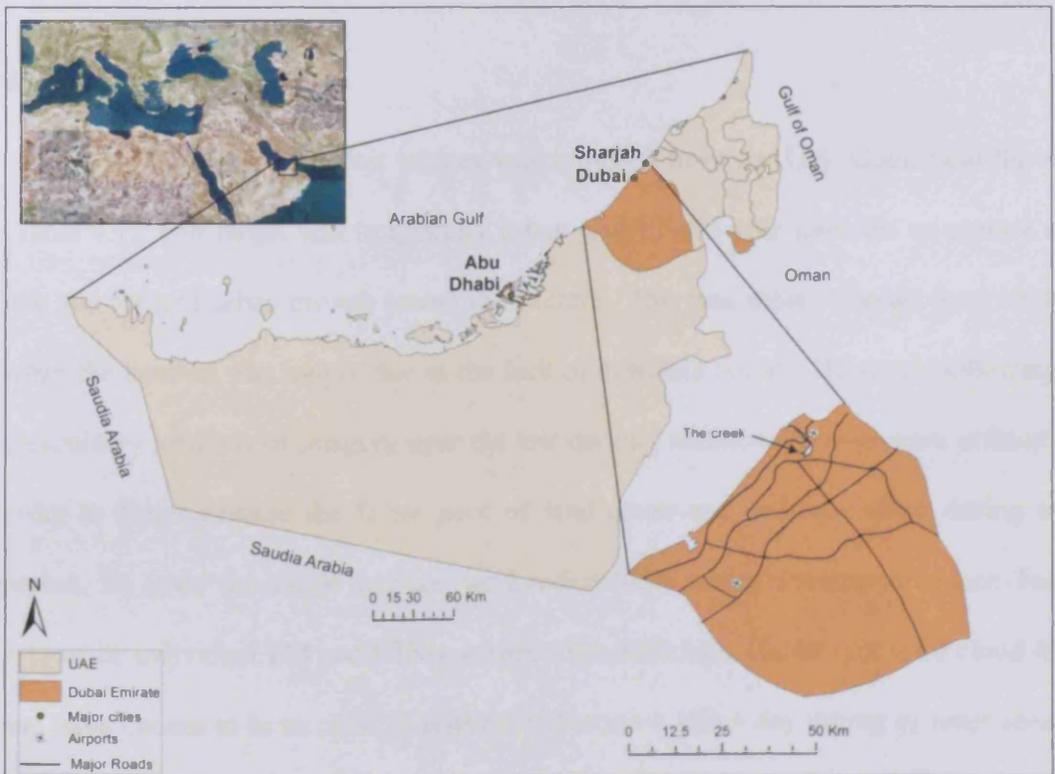
Figure 4.1 Study area, Dubai Emirate, United Arab Emirates. The map of Dubai Emirate shows the major roads that exist at the time of writing (Sources: Vector data: Dubai municipality; Raster data: ESRI online).

Some historians date the origins of Dubai to 1833 when around 800 people settled in the creek area (Pacione, 2005). In this early period the economy was heavily reliant upon fishing and pearling, and Dubai was the transit point for overland trading convoys traveling from Iraq to the Sultanate of Oman and a strategic sea port for trading ships travelling between Asia, Africa and the Gulf region. Population growth accelerated in the 1970's after the discovery of large oil reserves in the emirate which attracted a large labour force, primarily from overseas countries. The Dubai government used the oil revenue to develop infrastructure and industrial projects such as Dubai international airport, Port Rashid, the dry docks and an aluminium smelter (Pacione, 2005). These developments initiated the urbanization process that is the focus of the present investigation.

4.2.2 Data used

A time-series of Landsat images was acquired from the U.S. Geological Survey (Table 4.1). Our target was to quantify urban growth at 5 year intervals to capture the rate and form of urban growth across the emirate. This was achieved apart from 1990's when the interval was longer due to the lack of available scenes. However, following a preliminary analysis of imagery over the last decade, additional scenes were utilised in order to better capture the faster pace of land cover and coastal change during this period. To cover the whole emirate two Landsat MSS scenes were required (see Table 4.1) while individual TM and ETM+ scenes were sufficient. The images were cloud free and were chosen to be as close as possible to the same Julian day during summer season in order to minimise the effects of variations in solar geometry (see Ji, et al., 2001). Supporting data were collected from Dubai municipality, Dubai Statistical Survey Department and the Emirates Institution of Advanced Science and Technology.

Table 4.1 Data used in the study

Data type	Spatial Resolution	Path/Raw	Acquisition date YYYY/MM/DD
Landsat (MSS)	60m	172/042	1972/11/11
Landsat (MSS)	60m	172/043	1972/11/11
Landsat (MSS)	60m	172/042	1976/08/06
Landsat (MSS)	60m	172/043	1976/08/06
Landsat (MSS)	60m	172/042	1980/08/25
Landsat (MSS)	60m	172/043	1980/08/25
Landsat (TM)	30m	160/043	1985/02/11
Landsat (TM)	30m	160/043	1990/08/28
Landsat (TM)	30m	160/043	1992/06/14
Landsat (TM)	30m	160/043	1998/10/13
Landsat (ETM+)	30m	160/043	2000/08/23
Landsat (ETM+)	30m	160/043	2003/08/16
Landsat (ETM+)	30m	160/043	2005/07/22
Landsat (ETM+)	30m	160/043	2008/08/29
Landsat (ETM+)	30m	160/043	2011/08/22
DubaiSat-1	5m	-	2011
IKONOS	1m (Pansharpened)	-	2001, 2005
Aerial photo	1: 50,000	-	1997
Roads	(vector)	-	2008, 2011
Dubai boundary	(vector)	-	2008

4.2.3 Data preparation and pre-processing

All images were pre-processed to remove radiometric, atmospheric and geometric distortions, as discussed in section 2.5. All Landsat bands (1 to 7 covering visible, near and shortwave infrared) were used in subsequent stages, apart from the thermal band because it has coarse spatial resolution and failed to provide useful information for land cover discrimination in the context of this study. The two MSS scenes were mosaicked together to cover the study area for 1972, 1976 and 1980. Landsat images were co-registered precisely with existing map data using a WGS 84 datum/Dubai Local Transverse Mercator projection. This was achieved using 57 ground control points which were collected from road intersections delimited on existing digital maps and these were distributed across the images to provide maximum accuracy (Jensen, 2005). Registered Landsat images were then used to co-register other Landsat images where reference data was unavailable. In all corrections, a 3rd order polynomial transform was

employed and overall RMS errors for all cases were less than half a pixel as recommended by Jensen (2005). The nearest neighbour method was used for image resampling in order to preserve the original pixel digital number values.

4.2.4 Classification

The spectral clusters inherent within the imagery were examined in order to determine which land cover classes could be distinguished that would be of value for addressing the aims of the research. Anderson's Level 2 land cover classification schema (Anderson et al., 1976) has been used in some previous studies that have investigated urban growth using Landsat imagery (see section 2.6). However, our preliminary investigations revealed that for Dubai it was not possible to derive such a detailed classification, in particular the discrimination of urban sub classes (residential, commercial etc.), without the use of supporting data such as aerial photography or ground survey data collected at the same time as each Landsat image. Given the limited availability of such supporting data for Dubai, a modified Level 1 Anderson classification schema was adopted and this was suitable for fulfilling our objective of quantifying the historical trajectory of urban growth. Four land cover classes were mapped: urban, vegetation, water and sand, as seen in Table 4.2.

Table 4.2 Land cover classification schema used in the study

Land cover	Subclass description
Urban	All manmade (built up) surfaces, including roads, commercial, industrial, pavements, etc.
Vegetation	Farms, parks, gardens, mangroves, palm trees, golf courses, etc.
Water	Inland open water and recreational water bodies
Sand	Sand dunes, coastal sands and rock outcrops

A hybrid method of classification using unsupervised and supervised algorithms was adopted in this study. Unsupervised classification techniques were used to aid the selection of the training areas required for the subsequent supervised classification of each image, as this provided the most effective spectral separability of different land covers. Using unsupervised classification in this way can reduce the time required for manual selection of adequate training classes and can reduce the subjectivity of the process (King et al., 1989). This 'hybrid' approach therefore attempts to combine the advantages of both methods and overcome their limitations (Lo & Choi, 2004). The Iterative Self Organizing Data (ISODATA) clustering algorithm was firstly used as it provided maximum separability of different land cover classes. The most important parameters in ISODATA are: number of clusters, convergence threshold and maximum number of iterations. Given the distinctive coastal desert environment of our study site, we conducted trials using a sample image from each Landsat sensor to identify the optimal clustering parameters for achieving maximum land cover separability for each sensor. It was found that 30 clusters and 50 iterations were optimal for TM and ETM+ images and 20 clusters with 40 iterations were optimal for MSS, with a 0.95 convergence threshold for both. All other images in the time series were then classified using the appropriate optimal parameters for the sensor type.

The second step was to apply a maximum likelihood algorithm using spectral signatures derived from training areas within the image to be classified. Training areas should be accurately and carefully selected for all the required output classes to reduce errors of omission and commission and signature extension problems (King et al., 1989). At this stage the output from the unsupervised classification was used to guide the selection of the training areas to improve the efficiency of the selection process and increase the accuracy and representativeness of training areas for the 4 land cover types.

86

Approximately 280 training areas were selected for TM and ETM+ images and 100 for MSS images. Finally, a 3 x 3 kernel size smoothing filter was used to remove "salt and pepper" effects created from classification to minimise errors in areas of mixed land cover (Masek et al., 2000).

4.2.5 Classification Accuracy Assessment

Accuracy assessment was undertaken for the classifications of Landsat images acquired in the four years for which reference data were available (see section 2.7 for full details regarding accuracy assessments and definitions). For each of these years, a total of 60 stratified random samples (image and reference pairs) were collected for each class and these samples were independent from the data used for training in order to avoid the risk of bias (Verbyla & Hammond, 1995). The reference sample classes were identified through manual interpretation of a Dubai Sat1 image for the 2011 Landsat image classification, IKONOS images for 2005 and 2000 and aerial photography for 1998.

The classification accuracy of the 4 images tested was consistently high (Table 4.3). The overall accuracies exceeded the minimum 85% accuracy acceptable for the Level 1 Anderson classification scheme (Anderson et al., 1976) and the kappa coefficients exceeded the values recommended by Janssen and Van Der Wel (1994). These results compare favourably with previous studies in desert cities using different classification techniques where overall accuracies range between 84 and 88% (Stewart et al., 2004; Yagoub, 2004; Yin, et al., 2005). Confusion matrices were produced for the 4 years and the producer and user accuracies were calculated. Detailed definitions and use of these accuracy measures have been discussed extensively (e.g., Congalton & Green, 2009). The matrices showed that there were no constantly high levels of

confusion between different land cover types (Table 4.4 is an example matrix for the 2011 classification). The consistency of these results confirms the transferability of the classification technique across the Landsat image time series and gives us confidence that the land cover maps produced were sufficiently reliable for subsequent analysis and interpretation.

Table 4.3 Land cover classification accuracy

Year	Overall accuracy%	Kappa coefficient
1998	88.75	0.85
2000	87.08	0.83
2005	91.67	0.89
2011	93.33	0.91

Table 4.4 Confusion matrix, users and producers accuracy for the land cover classification for 2011.

Class	Reference pixels				Total	Users Accuracy%
	Vegetation	Urban	Sand	Water		
Vegetation	58	0	2	0	60	96.67
Urban	1	54	5	0	60	90.00
Sand	1	3	56	0	60	93.33
Water	0	0	4	56	60	93.33
Total	60	57	67	56	240	
Producers Accuracy%	96.67	94.74	83.58	100.00		

(Row axis label: Classified pixels)

4.2.6 Urban growth rate and landscape metrics

The pace of change in the areal coverage of urban land cover was quantified using the compound annual growth rate formula (Source: State of New Jersey[7]):

---

[7] http://www.nj.gov/education/archive/abbotts/pbg/pp/cagr.pdf

$$Compound\ Annual\ Growth\ Rate\ (t_0, t_n) = \left(\left(\frac{A(t_n)}{A(t_0)} \right)^{\frac{1}{t_n - t_0}} - 1 \right) \times 100 \qquad (4.1)$$

Where,

$A(t_0)$ is the initial area of urban land cover,

$A(t_n)$ is the area at the end of the analysis period, and

$t_n - t_0$ is the number of years covered by the analysis period.

Hence, this approach could be used to characterise the pace of urban growth over the entire Landsat time series or particular periods within this. The same formula was also used to characterise changes in the other land cover types.

The patterns of urban land cover in Dubai were quantified by analyzing binary grids of urban and non-urban pixels using landscape metrics in Fragstats 3.4 (McGarigal et al., 2002). Although many metrics can be generated, many are highly correlated or unrelated to the objectives of this study. Hence, based on the findings of previous research using landscape metrics for urban studies, five metrics were carefully selected for this study (Table 4.5). These metrics were generated for each of the years for which land cover had been mapped from Landsat data in order to quantify the dynamics of urban growth.

Table 4.5 Landscape metrics used in this study with related authors who used these metrics in their work.

Landscape Metric	Explanation	Range	Recent research focusing on urban pattern
Number of patches (NP)	Number of spatially distinct patches for the urban class	NP $\geq$ 1, without limit.	Aguilera et al., 2011; Araya & Cabral, 2010; Dietzel, Oguz, et al., 2005; Taubenböck et al., 2009; Tian et al., 2011
Largest patch index (LPI)	Percent of the total landscape covered by the largest patch.	0 < LPI $\leq$ 100	Araya & Cabral, 2010; Dietzel, Herold, et al., 2005; Dietzel, Oguz, et al., 2005; Taubenböck et al., 2009
Mean Nearest Neighbour distance (MNN)	Average of the shortest distance (m) from one urban patch to another.	MNN > 0, without limit	Aguilera et al., 2011; Araya & Cabral, 2010; Dietzel, Oguz, et al., 2005; Tian et al., 2011
Landscape Shape Index (LSI)	Total length of urban edges divided by the square root of the total landscape area (square metres).	LSI $\geq$ 1, without limit	Dietzel, Oguz, et al., 2005; Taubenböck et al., 2009; Wu et al., 2011; Yue, Liu, & Fan, 2010
Area Weighted Mean Fractal Patch Dimension (AWMPFD)	Average fractal dimension of patches in the landscape, weighted by patch area	1 $\leq$ AWMPFD $\geq$ 2	Araya & Cabral, 2010; Dietzel, Herold, et al., 2005; Dietzel, Oguz, et al., 2005; Tian et al., 2011; Zhang et al., 2011

4.2.7. Population analysis and drivers of urban growth

The population density for urban areas was calculated for each sampling period by combining annual total population data together with the percentage of population in urban/rural areas and the area of urban land cover determined from the Landsat data. The rate of change in urban population density was calculated using Equation 4.1 in subsection 4.2.6. The changes in urban area and urban population density have been found to be good indicators of the processes of urbanization and urban sprawl (Angel et al., 2010; United Nations, 2012; Yin, et al., 2005). Political and local/global economic factors were also compiled and integrated with the urban land cover time series in order to further understand and interpret the various phases of urban development.

4.3 Results and discussion

4.3.1 Land cover changes

Figure 4.2 illustrates the changes in land cover across Dubai between 1972 and 2011, with an increase in urban, vegetation and water at the expense of sand. There has been a dramatic increase in the area of urban land cover over 39 years ($561 km^2$), which represents a compound annual growth rate of 10.03%. The majority of this urban growth occurred after 2000, with the period 2003-2005 experiencing a peak compound annual growth rate of 13.02%. In comparison, Guangzhou city in China had a compound annual growth rate of 7.72% between 1979 and 2002 according to data published in Ma and Xu (2010). Furthermore, according to estimates by the City Mayors Foundation (n.d.) the fastest growing city in the world is Beihai in China with a compound annual growth rate of

10.58% between 2006-2020 (observed and forecast). Such comparisons confirm that Dubai was one of the fastest growing cities in the world throughout the time period covered in this study, and particularly during the first decade of the 21st century.

Figure 4.2 also illustrates that vegetated areas increased substantially from $0.85km^2$ in 1972 to $41.31km^2$ in 2011, a compound annual growth rate of 10.47%. This occurred in response to government policies to increase the green spaces in Dubai by developing farms, parks, gardens and mangrove forest (Al Marashi & Bhinder, 2008). Likewise the amount of inland water increased from $3.88km^2$ to $18.30km^2$, a compound annual growth rate of 4.06%. This increase was due to creek dredging and expansion, port construction and the development of recreational water bodies. Such large changes in vegetation and water bodies are likely to have ecological and environmental impacts. Maintaining such land covers in a hyperarid region requires continual inputs of energy, water and chemicals and this may have negative environmental consequences. However, these land covers may promote biodiversity and improve microclimate and air quality in a way which mitigates some of the impacts of the urban development. Therefore, it is important that the environmental costs and benefits of these patterns of land cover change are investigated in future research.
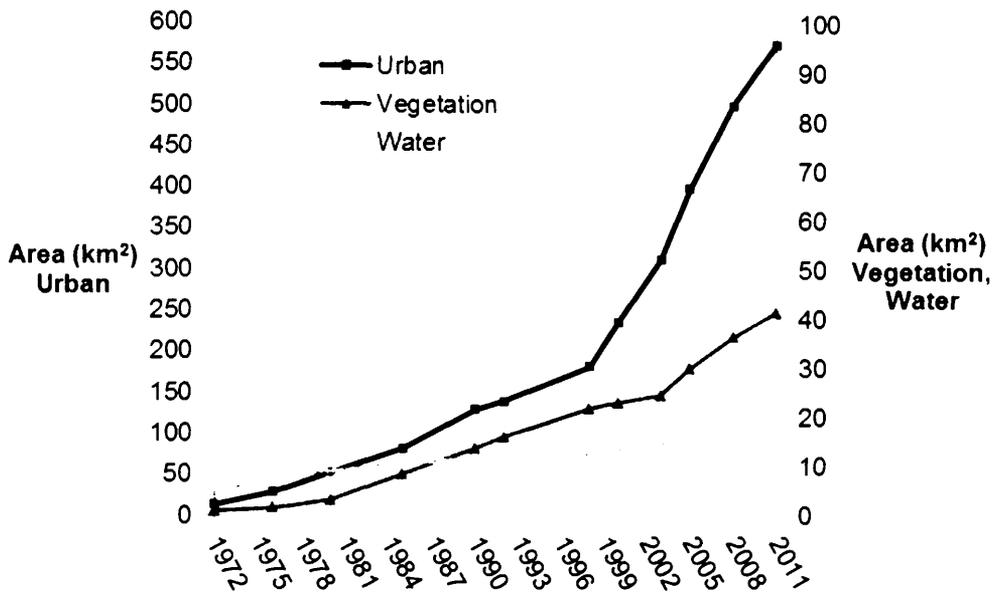
Figure 4.2 The trend of land cover changes in Dubai (1972–2011). Urban area on primary Y-axis, vegetation and water on secondary Y-axis.

4.3.2 Spatiotemporal characteristics of urban growth

Figure 4.3 illustrates how the size and shape of the urban area has changed over time. The majority of the urbanization between 1972 and 1990 was concentrated around Dubai Creek. During this period, the central urban area expanded east of the creek from 2.3km in 1972 to 8km in 1990 and west of the creek from 0.7km in 1972 to 11km in 1990. The rulers ensured that Dubai's oil revenues were directed to implement major infrastructure projects such as Rashid port, Jebel Ali port, Dubai International Airport and Jebel Ali free zone. These developments acted as seeds for subsequent urban growth in the west of the emirate detected in the present study (Fig. 4.3). During this period, the urban area expanded at an annual rate of 11% while the population experienced an annual growth rate of 7%. This meant that urban population density decreased at an annual rate of 5% indicating that a process of urban sprawl was initiated during this period.

93
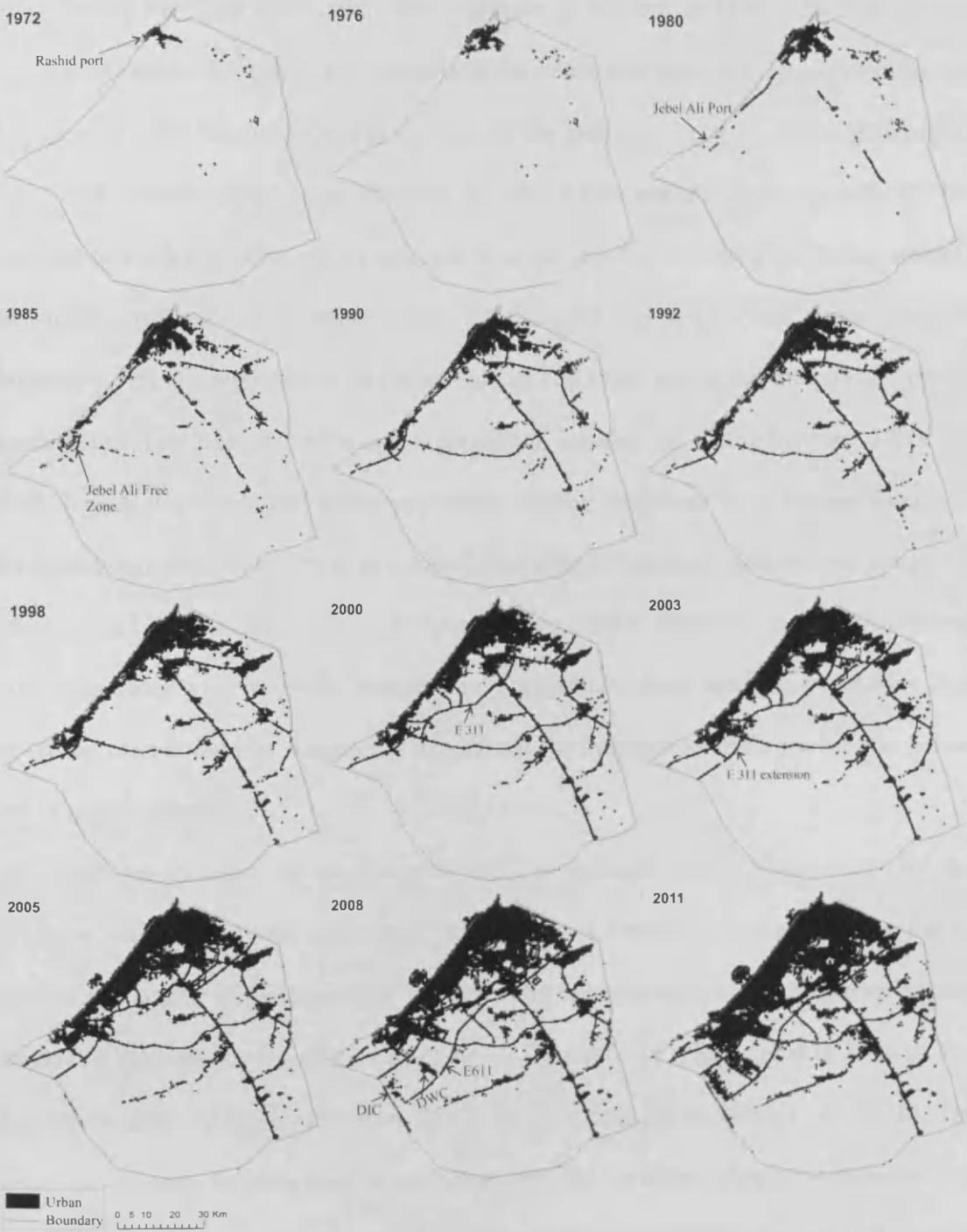
Figure 4.3 Change in urban extent in Dubai Emirate (1972-2011). White areas within the city boundary represent non-urban areas. Emirates road (E311); bypass outer road (E611); Dubai industrial city (DIC); Al Maktoum international airport (DWC).

During the 1990's the urban area expanded in the east of Dubai towards Sharjah Emirate and along the gulf coast, particularly for residential purposes. However, leapfrog developments also occurred towards the west of the emirate (Fig. 4.3). Within this period there were similar annual rates of urban growth (6.2%) and population growth (5.5%) resulting in a much smaller rate of decrease in urban population density (0.7% per annum) than in the previous period. Some context for these findings is provided by the study of Angel et al. (2010) who used a global sample of 120 cities and found an average annual increase in urban area of 3.66% and a population increase of 1.66% between 1990 and 2000. It was also found that urban population density decreased by 1.7% per annum in developing countries and 2.2% in developed countries, indicating a more intense process of urban sprawl in developed countries (Angel et al., 2005). Therefore, during this period Dubai experienced substantially higher rates of growth in urban area and population than the global sample used by Angel et al. (2010) but the intensity of urban sprawl was below that of other countries.

After the collapse of oil prices in 1997, a strategic decision was made by the government to diversify the economy of the emirate to avoid over reliance on the fragile petroleum industry, by building new infrastructure, stimulating real estate marketing and developing tourism. As a result, oil revenue fell from 46% of total income in 1974 to less than 5% in 2005 (Dubai Government, 2007) and less than 2% in 2010 (DSC, 2010). The Dubai government implemented a number of policies to attract foreign businesses, for example, allowing full ownership and 0% corporate and income taxes for up to 25 years in free zones. These initiatives help explain the dramatic increase in the number of urban areas including arterial roads that were detected in the present study between 2000 and 2005 (Fig.

4.3) with the construction of major highways and roads such as Emirates Road (E311) which is 68km long and extends from the east to the west of the emirate. Furthermore, huge ribbon urban developments were observed between 2000 and 2005 along a 5km wide zone along the coast in the west of the Emirate, in addition to the palm development which will be discussed later. In this rapid phase of development, the annual rate of urban growth increased to 12% and while population growth remained very high (7.4% per annum) the declining urban population density (2% per annum) demonstrates that the process of urban sprawl intensified during this period.

In 2002 the ruler of Dubai issued a decree to allow foreign ownership of properties in Dubai which resulted in a boom in the real estate market. Accordingly, the results of this study demonstrate further construction of arterial roads between 2005 and 2008 including the 71km long Bypass Outer road (E611), with associated ribbon and infill urban developments. During this period, the annual rates of urban and population growth remained high (7.9% and 7.6%, respectively) but this was followed by decline in urban and population growth (to 4.7% and 6.8% per annum, respectively) during 2008-2011. This was the first time since the start of the period covered by this study when an increase in urban population density was observed (2% per annum), indicating a decreasing of urban sprawl. This decline in urban growth may be a consequence of the global economic recession which developed towards the end of 2008. Nevertheless, there was still a large expansion of urban area of 74km^2 during this latter period. The urban areas continued to expand primarily towards Jebel Ali port to the west, towards the newly constructed Al Maktoum International Airport (DWC) and Dubai Industrial City (DIC) to the southwest and towards Sharjah in the north east of the emirate (Fig. 4.3).

By 2011, urban areas covered 15% of the total land area of the emirate, a substantially higher proportion than the 5%-10% coverage found in European countries (Milanović, 2007). Alongside this, the percentage of population living in urban areas is very high and has remained so since the 1970s (95-98%). This compares with Europe and China where 74% and 51%, respectively, live in urban areas (United Nations, 2012). Therefore, the high rates of growth in urban area and population and the high proportions of urban land cover and urban population are notable characteristics of Dubai emirate, while the observed process of urban sprawl is common to most cities globally.

4.3.3 Coastal change in Dubai

Our results also show a considerable alteration to the form of the coastline of Dubai since 1972 due to both offshore and onshore construction. Using the land cover classes generated from Landsat data, it was possible to define the offshore developments as either completed urban developments (the urban class) or developments under construction (the sand class). Figure 4.4 shows the extent of coastal development that had taken place by 2011, with considerable areas of completed urban development and even larger areas under construction. The first major coastal developments were observed between 1972 and 1976 with the dredging and filling operations to extend Rashid Port and its dry docks. This was followed during the period 1976-1985 by the excavation of Jebel Ali which is now recognised as the largest inland artificial harbour in the world (Pacione, 2005). Offshore construction for real estate and tourism purposes began during 1992-1998 with the Jumairah beach extension and Burj Al Arab hotel. However, a significant increase in pace

and scale of offshore development took place during 2000-2003, with the construction of Jumairah Palm Island. Even more extensive changes in the coastline appeared between 2003-2011 where 68km^2 was added to the total terrestrial area of Dubai Emirate by offshore reclamation projects in the Arabian Gulf. By 2011 approximately 11km^2 of the marine environment had been converted to urban areas (artificial islands) while approximately 57km^2 were converted to sand where four islands are still under development (Palm Deira, World Islands, Palm Jebel Ali and Dubai Waterfront). This transformation of the form of the coastal landscape is likely to have implications for the aquatic environment, with potential changes in the dynamics of currents, sediments, biogeochemicals and ecosystem functions. Further work is now required to understand the environmental impacts of this coastal change, in order to define environmental management strategies and guide future coastal development.

N

Palm Deira

Port Rashid and Dry Docks

The World Islands

Dubai Creek

Palm Jumairah

Palm Jebel Ali

Jebel Ali Port Waterway

Dubai Waterfront

— 1972 Coastline
Under development
Urban
Water

Kilometers
0 1 2   4   6   8   10
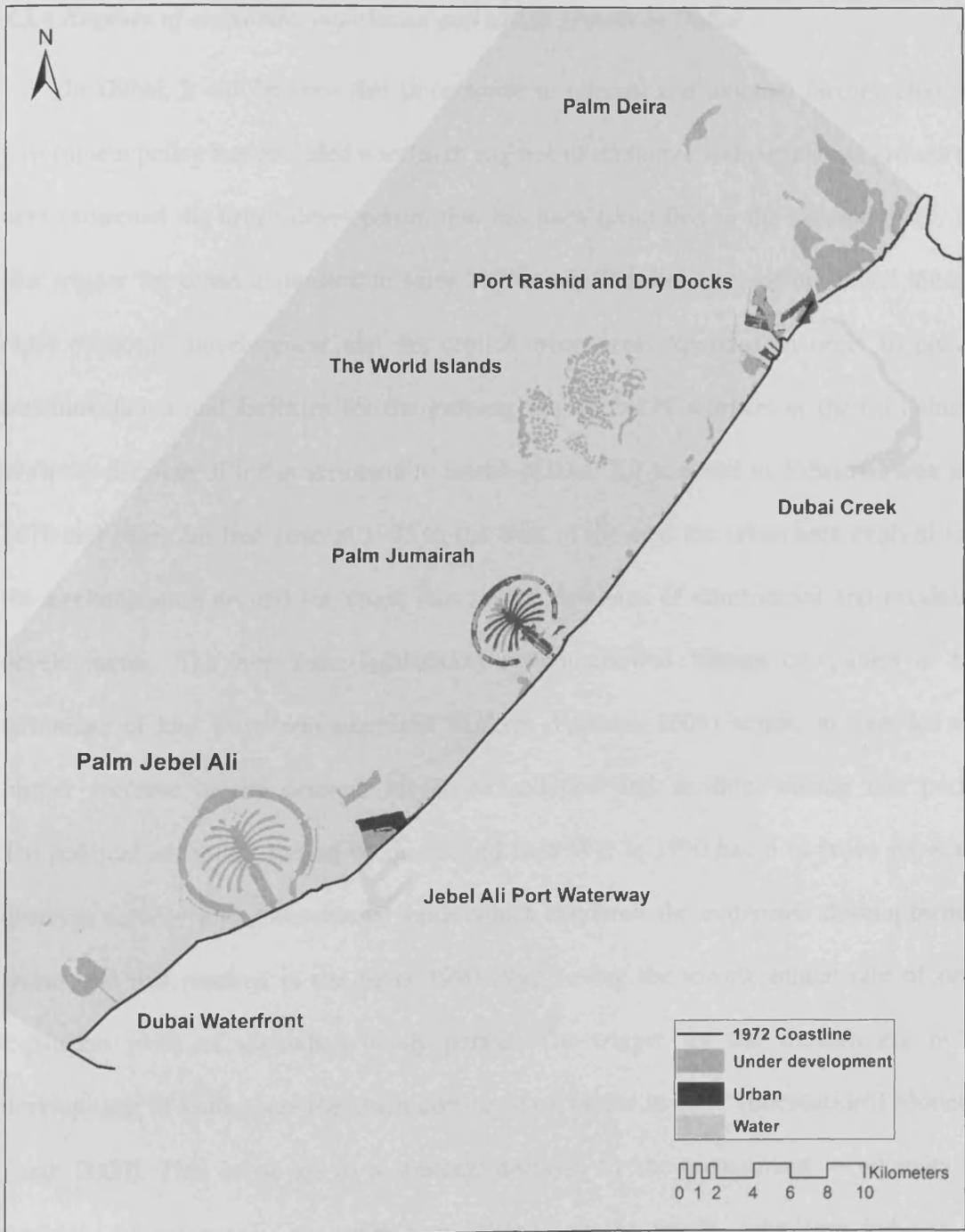
Figure 4.4 Dubai's coastal development by 2011.

4.3.4 Engines of economic, population and urban growth in Dubai

In Dubai, it can be seen that in response to internal and external factors, changing government policy has provided a series of engines of economic and population growth that have promoted the urban development that has been quantified in the present study. The first trigger for urban expansion in early 1970's was the discovery of oil which initiated rapid economic development and the central urban area expanded in order to provide accommodation and facilities for the growing population of workers in the oil industry. With the decision of the government to establish Jebel Ali port and its industrial area after 1976 and Jebel Ali free zone in 1985 to the west of the city, the urban area evolved from the agglomeration around the creek into several satellites of commercial and residential developments. The free zone legalization system allowed foreign companies to take advantage of low wage non-unionized workers (Pacione, 2005) which, in turn, led to a further increase in the demand for accommodation and facilities during this period. The political instability caused by the second Gulf War in 1990 had a negative impact on business activity and international trade which hindered the economic development of Dubai and this resulted in the years 1990-1992 having the lowest annual rate of urban expansion (4%) of the whole study period. The trigger for the modern era in the development of Dubai was the sharp decline of oil prices in 1997 (International Monetary Fund, 2000). This event led to a strategic decision by the government to diversify the economy of the emirate to avoid over reliance on the fragile petroleum industry, by building new infrastructure, stimulating real estate marketing and developing tourism. As a result, the activity of non-governmental establishments and international commercial organisations increased by 41% between 1993 and 2000 (DSC, 2000). This led to the

recruitment of a large international labour force, with consequent demand for residences and facilities leading to rapid urban growth.

Following the 2002 decree by the ruler of Dubai to allow foreign ownership of properties in areas designated by the government, a boom in the real estate market occurred and many 'mega' construction projects took place including Jebel Ali Free Zone extension, Dubai metro, the offshore islands and some developments distant from the city, deep in the desert. These projects reinforced the urban expansion process and demonstrated that the spatial evolution of Dubai was not hindered by the natural geographic barriers presented by the waters of the Gulf or desert sand dunes. However, the global financial recession starting by late 2007 resulted in a decline in economic, population and urban growth rates in Dubai. Total Gross Domestic Product (GDP) decreased by 2.7% between 2008-2009 with greatest declines in the productivity of the construction, real estate and business services sectors (DSC, 2009), but by 2011 productivity and consequently population and urban growth had recovered. Hence, this sequence of phases in the evolution of Dubai demonstrate the interactions between government policy and economic drivers and consequences, the resultant fluctuations in the rate of population growth and the associated variations in urban expansion and form.

4.3.5 Urban growth patterns in Dubai in the context of modern urban growth theory

Previous studies of urban growth by Dietzelet al. (2005a) and Dietzelet al. (2005b) suggest development can take place in oscillating phases of diffusion and coalescence in urban form, and that these phases can be detected using landscape metrics based on the

number of urban patches and distance between them (NP and MNN, respectively). Figure 4.5 illustrates the historical changes in landscape metrics for urban areas in Dubai over the study period. Based on the NP plots, the study period can be divided into recognisable phases of coalescence, when NP is decreasing, and diffusion, when NP is increasing (denoted using vertical shading). The MNN metric is able to confirm these phases, as it also decreases during coalescence and increases during diffusion. There is only one departure from this in the period 1985 to 1990 where MNN decreases during a period of diffusion (as indicated by increasing NP). This indicates that new, separate urban patches were being developed in this phase, but they tended to be in close proximity to existing patches. In all other phases of diffusion, MNN increased, indicating the dispersion of urban development across the emirate. The LPI also provides supporting evidence for the oscillating phases of growth, as it consistently increases during coalescence, when development is concentrated around the historical urban core, and decreases during diffusion, as more distant urban centres start to develop. There is only one departure from this in the period 2008 to 2011, where the decreasing LPI during a phase of coalescence indicates that more extensive urban areas have coalesced away from the historical urban core.
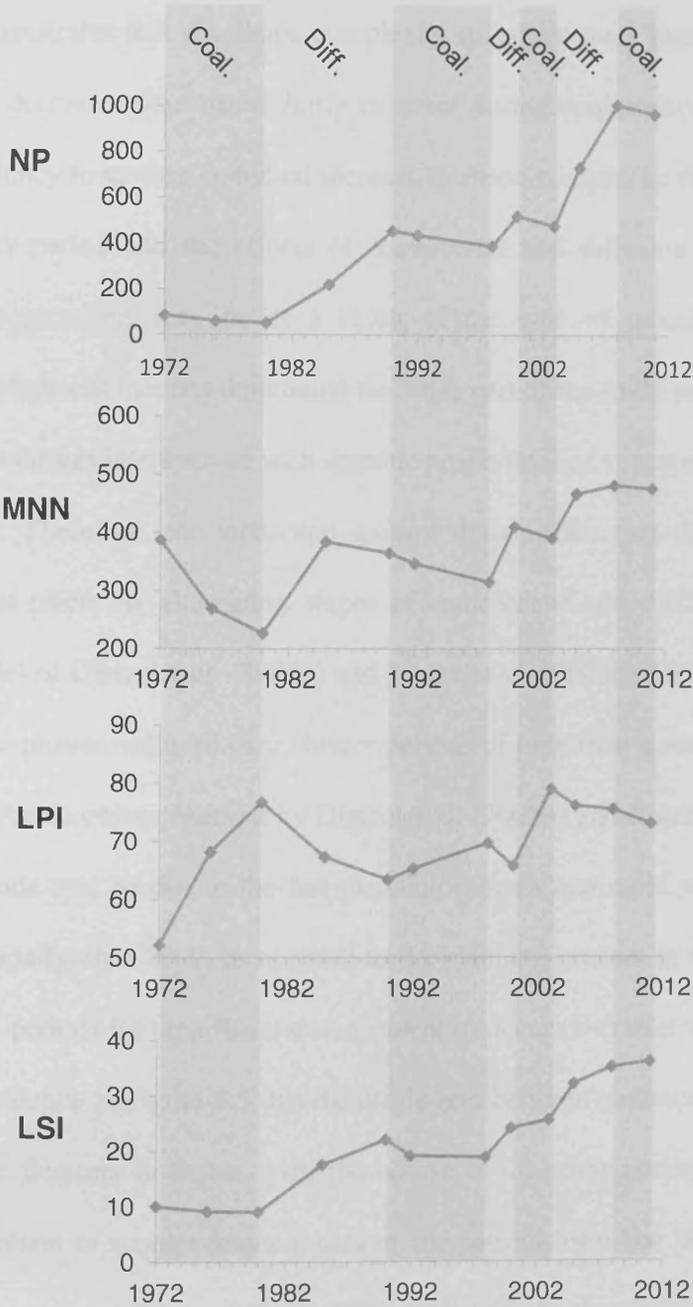
Figure 4.5 Historical changes of the landscape metrics for urban areas in Dubai: Number of Patches (NP); Mean Nearest Neighbour distance (MNN); Largest Patch Index (LPI); Landscape Shape Index (LSI). Differences in vertical shading indicate phases of coalescence (Coal.) and diffusion (Diff.) as interpreted from the NP plot.

103

The LSI metric (AWMPFD is not shown in Fig 4.5. as it showed the same behaviour) demonstrates that the shape complexity of urban areas increases during diffusion phases and decreases or remains fairly constant during coalescence phases. However, there is a tendency towards a continual increase in shape complexity throughout the latter part of the study period and the effects of coalescence and diffusion on urban shape become less apparent. This may be as a result of the type of mixed commercial and residential development that has dominated the latter part of the study period, with a fairly low density of buildings interspersed with sizeable proportions of vegetation and water bodies.

Therefore, the landscape metrics demonstrate that the development of Dubai has taken place via alternating stages of coalescence and diffusion, in accordance with the model of Dietzelet al. (2005a) and Dietzelet al. (2005b). However, the oscillation between these phases occurred over shorter periods of time than Houston and the Central Valley of California cities observed by Dietzelet al. (2005b) and Dietzelet al. (2005a). These shorter periods may be due to the fast planning process and rapid pace of development in Dubai, especially after 2000, as opposed to the planning process in the US which results in longer time periods for significant development to occur (Dietzelet al., 2005b). Furthermore, there is evidence in Figure 4.5 that the oscillation between coalescence and diffusion has become more frequent in Dubai, over the course of the study period. This demonstrates that it is important to acquire frequent data on the patterns of urban land cover, which is likely only to be retrieved from satellite data, in order to fully characterise the process of urban growth in rapidly developing cities, such as Dubai. Indeed, it could be argued that because some of the latter phases of coalescence and diffusion begin and end between consecutive image acquisition dates (i.e. consecutive data points on Figure 4.5), there may be a case for using

more frequent images than those used in the present research. However, as all available/useable scenes from the Landsat archive were used in this study, to increase the frequency would necessitate the use of images from other satellite systems, which could introduce a series of difficulties around comparability issues.

By comparing Figure 4.5 (metrics) with Figure 4.3 (maps of change in urban extent), it is possible to suggest that superimposed upon the basic oscillations between coalescence and diffusion there are particular spatial patterns of development that have taken place within each phase. The correspondence between these phases and patterns is summarised in Figure 4.6. The first phase of coalescence is characterised by a compact bi-central urban growth pattern on each side of the Creek throughout the 1970's. The following stage of diffusion throughout the 1980's largely took of the form of a satellite development pattern, occurring mainly to the west towards Sharjah Emirate and South East of Dubai towards Jebel Ali port. A period of coalescence throughout most of the 1990's was characterised by a ribbon pattern of development along the coastal strip of the Arabian Gulf. A short period of diffusion then ensued where satellite developments arose at various points inland of the coastal strip and in the western side of the emirate.

As Figure 4.3 shows, between 2003 and 2008 the road network expanded rapidly and urban development patterns followed this network. The profusion of road networks into previously non-urban territory which triggers the spatial evolution of the urbanization front has recently been described as the 'exploration' process (Strano et al., 2012). The final coalescence phase is characterised by infill development throughout the emirate, with a 'densification' process (Strano et al., 2012) corresponding to an increase in the local density of roads around existing urban centres.
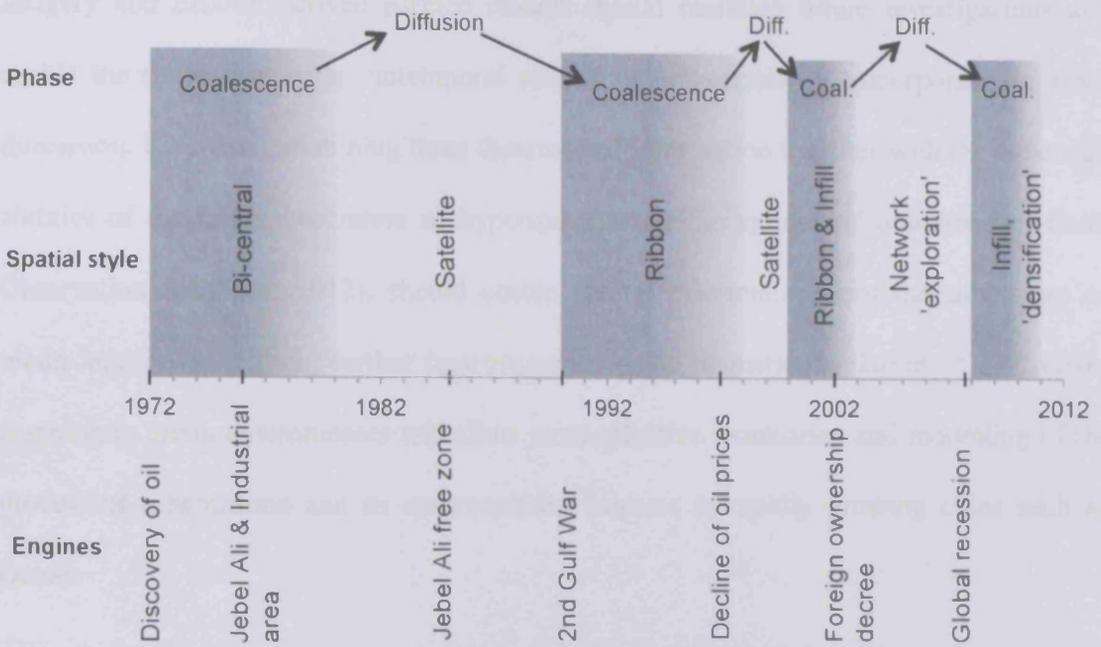
Figure 4.6 Correspondence between phases of coalescence and diffusion and spatial patterns of urban development for Dubai over the study period.

It is important to acknowledge that the methods used in the present study are only able to offer a two dimensional representation of the process of urban growth in Dubai. This does not account for an important aspect of the urbanization of Dubai where several zones within this city have expanded vertically as well as horizontally, with the construction of high rise buildings. According to the Skyscraper Center (2012), 19 skyscrapers in Dubai are among the highest 100 buildings in the world. In terms of magnitude, such vertical expansion is negligible in comparison with the increase in horizontal area of Dubai, nevertheless, quantifying the contribution of high rise construction to the total volume of expansion could be important for further understanding the process and pattern of urbanization. While there is a paucity of remote sensing data to support such analyses over an extended time series, the increasing availability of stereo

106

imagery and LiDAR derived surface models should facilitate future investigations and enable the refinement of spatiotemporal models of urbanization to incorporate the third dimension. Likewise, combining three dimensional information together with the enhanced abilities of the future generation of hyperspectral satellite systems (Committee on Earth Observation Satellites, 2012), should enable greater discrimination of the subclasses of urban land cover. Hence, further improvements in the thematic resolution of land cover mapping in urban environments will allow more effective monitoring and modelling of the process of urbanization and its environmental impacts in rapidly growing cities such as Dubai.

4.3.6 Comparing Dubai to other rapidly growing cities

In order to provide some context for our observations on urban growth in Dubai, it is useful to provide a comparison with other cities. However, such comparisons can be difficult because the data related to urban growth is produced by studies that have widely varying objectives and methodologies for monitoring urbanization; in particular, the length of the study period and sampling interval varies substantially. Although several rapidly growing cities have been documented (e.g. City Mayors Foundation, n.d.), detailed long term studies have not been carried out on many of these cities. Therefore, here we discuss only studies that have presented sufficiently detailed information over an extended study period.

The high rates of urban growth that we have observed in Dubai are comparable to those of the fastest growing cities in the world. For example Angel et al. (2005) reported that the cities with the highest urban growth rates were Yiyang, China between 1994-1999

and Bacolod, Philippines between 1992-2000, with annual growth rates of 14.67% and 12.25%, respectively. Schneider and Woodcock (2008) studied the growth of 25 cities between 1990-2000 and revealed that the highest annual growth rates were in Dongguan and Guangzhou, China with rates of 14.25% and 11.68%, respectively, while the remaining cities had annual growth rates of less than 5%. The major form of Dongguan and Guangzhou was of fragmented patches of urban areas with large amounts of expansion in the fringe and hinterland areas with a decline in population density over the study period. Schneider et al., (2005) showed that Chengdu, China had annual growth rate of 7% between 1978-2002, which comprised of three phases of development. Firstly, prior to 1990, urban expansion occurred in all directions, especially around the core which resulted in unattached urban areas becoming agglomerated; secondly, after 1990, urban areas expanded along road corridors and as satellite patches around the airport; thirdly, there was an infilling process which connected the satellite patches in the late 1990's to 2002. These findings indicate a cycle of diffusion and coalescence during the study period. A similar process of urban evolution to Chengdu has been observed in Guangzhou, China which experienced an annual growth rate of 7.72% between 1979 and 2002 (Ma & Xu, 2010). In Guangzhou growth initially radiated outward from the historic core then became focused along major transport links then the focus of growth shifted from the historic center to a new city center. Hence, the basic forms of spatial evolution in Chengdu and Guangzhou are similar to those in Dubai but Dubai possesses some more complex forms of development such as onshore and offshore satellites, ribbon and gradual infill, which are superimposed on the basic growth forms. However, a major difference between Dubai and most other fast growing cities is that its spatial evolution is linked to increases the area of both vegetation

and water. For example, Seto et al. (2002) reported the high growth rates of the Pearl River Delta cities in China and found substantial decreases in vegetation cover as 1376km^2 of urban area was converted from farmland. Likewise, Pune in India experienced a high annual urban growth rate of 10% at the expense of water bodies and vegetated lands (Bhailume, 2012).

In comparison to other cities that have developed in desert environments, Dubai shows some similarities and some differences in growth characteristics. Greater Muscat in Oman, situated in a coastal desert in the Gulf region, experienced a rapid urban growth with an annual compound rate of 8.11% between 1960-2003 (Al-Awadhi, 2007) which is only slightly lower than that observed for Dubai. However, unlike Dubai which has grown in all directions, Muscat has grown mostly in the coastal strip with three major urban forms: firstly a very narrow urban expansion between major old urban areas; second an accelerated urban expansion along the coastal strip, and finally an infilling urbanization between urban patches. In Muscat, vegetation cover decreased over the study period, in contrast to Dubai, but there was a small increase in inland water cover. Doha in Qatar is another desert city along the Gulf coast which was studied over the period 1972- 2002 and found to experience a decrease in vegetation cover, in contrast to Dubai, but did show an increase in total area of 10km^2 due to land reclamation in a similar, but smaller scale process to that observed in Dubai (Al-Manni et al., 2007). Las Vegas in the desert environment of Nevada is the fastest growing city in the United States (City Mayors Foundation, n.d.). Xian et al., (2005) studied urban expansion in Las Vegas from 1984-2002 and demonstrated an annual growth rate of 4.31%. As in Dubai, urban areas in Las Vegas have sprawled in almost all directions where several roads and transportation systems were built to serve the city. However, the

growth of Las Vegas has been constrained by surrounding mountains whilst the development of Dubai has not been impeded by such restrictions.

4.4. Conclusions

This study has quantified the rapid process of urbanization in Dubai Emirate using a time series of Landsat imagery which was able to capture the key phases of development from 1972 to 2011. Indeed, without satellite remote sensing it is difficult if not impossible to document such large scale changes in land cover, as other sources of information are restricted or non-existent for this region. A hybrid unsupervised and supervised classification method was able to provide an accurate discrimination between urban and other land cover types, even in this challenging desert environment.

There was a rapid rate of development over the entire study period and this was particularly intense after 2000, making Dubai one of the fastest growing cities in the world during this period, but growth has slowed recently. The observed spatiotemporal dynamics of urban growth were closely associated with prevailing local and global economic conditions and the ambitious development strategies implemented by the government of Dubai. The high rates of urban growth have resulted in a notably high proportion of the emirate now being urban landcover and a particularly high proportion of the total population has occupied urban areas throughout the development period. While the population growth rate has been high, this has been outpaced by the rate of increase in urban area and the declining population density is indicative of a process of urban sprawl that has been observed in most cities globally.

A substantial increase in vegetation and inland water bodies was observed and the ecological and environmental impacts of maintaining such land covers in a hyperarid region are worthy of further investigation. While offshore constructions and land reclamation are not unique to Dubai, the pace, scale and complexity of the coastal urban developments observed in this study are unprecedented. Again, it is important that the impacts of such developments on the coastal environment are now investigated.

The analysis of landscape metrics provided evidence that Dubai generally conformed to the model of oscillating phases of urban diffusion and coalescence (Dietzel, Herold, et al., 2005; Dietzel, Oguz, et al., 2005), albeit with much more rapid transitions between these phases than has been observed in other cities. While coalescence and diffusion provided a useful overall description of the urbanization process, each of these basic phases was characterised by specific spatial patterns of development. Earlier phases were dominated by bicentral, satellite and ribbon patterns, while latter stages comprised infill, 'exploration' and 'densification' (Strano et al., 2012).

This study has provided a new insight into the pace and process of urban growth in Dubai. While there are several characteristics in common with the development of other cities, there are many unique spatiotemporal features of urbanization in Dubai. It is now important to evaluate the consequences of this form of rapid urban development on the environment.

Acknowledgements

111

References

Aguilera, F., Valenzuela, L. M., & Leitão, A. B. (2011). Advances in urban ecology: Integrating humans and ecological processes in urban ecosystems. *Landscape and Urban Planning*, 99, 226–238. doi:10.1016/j.landurbplan.2010.10.004

Al-Awadhi, T. (2007). Monitoring and modeling urban expansion using GIS & RS: Case study from Muscat, Oman. *Urban Remote Sensing Joint Event*, IEEE (pp. 1-5). doi: 10.1109/URS.2007.371790

Al-Manni, A. A., Abdu, A. S., Mohammed, N. A., Al-Sheeb, A. E., (2007). Urban growth and land use change detection using remote sensing and geographic information system techniques in Doha City, State of Qatar, *Arab Gulf Journal for Scientific Research*, 25(4), 190-198. <http://cat.inist.fr/?aModele=afficheN&cpsidt=20363607> Retrieved 22.09.13.

Al Marashi, H., & Bhinder, J. (2008). From the Tallest to the Greenest -Paradigm Shift in Dubai. *From The Council on Tall Buildings and Urban Habitat*. <http://www.ctbuh.org/Portals/0/Repository/T1_AlMarashi.ec25feeb-c7e3-4e10-9fed-1fdfac4e74c3.pdf > Retrieved 12.07.12.

Alberti, M. (2008). *Advances in urban ecology: Integrating humans and ecological processes in urban ecosystems*. New York: Springer.

Anderson, J. M., Hardy, E. E., Roach, J. T., & Witmer, R. E. (1976). A Land Use Classification System for Use with Remote Sensing Data. Geological Survey Professional Paper. Washington D. C.: Government Printing Office. <http://landcover.usgs.gov/pdf/anderson.pdf> Retrieved 12.010.12.

Angel, S., Parent, J., Civco, D. L., & Blei, A. M. (2010). The persistent decline of urban densities: Global and historical evidence of sprawl. Cambridge, MA: Lincoln Institute of Land Policy. < http://www.alnap.org/pool/files/1834-1085-angel-final-1.pdf > Retrieved 13.05.13.

Angel, S., Sheppard, S. C., Civco, D. L., Chabaeva, A., Gitlin, L., Kraley, A., et al. (2005). The dynamics of global urban expansion. Washington, DC: The World Bank. <http://www.worldbank.org/urban> Retrieved 02.03.12.

Araya, Y. H., & Cabral, P. (2010). Analysis and Modeling of Urban Land Cover Change in Setúbal and Sesimbra, Portugal. *Remote Sensing*, 2, 1549-1563. doi:10.3390/rs2061549

Badouri, S. (2007). Construction boom in UAE & Saudi Arabia: Opportunities for Asian companies. Master Builders Association Malaysia. <http://www.mbam.org.my/mbam/images/@BOOM%20UAE%20%2880-92%29.pdf> Retrieved 02.11.12.

Bhailume, S. A. (2012). *An assessment of urban sprawl using GIS and remote sensing techniques: A case study of Pune-Pimpri-Chinchwad area* (Doctoral thesis, SNDT Women's University, Pune, India). <http://shodhganga.inflibnet.ac.in/handle/10603/3425> Retrieved 22.09.13.

Boyce, R. R. (1966). *The edge of the metropolis: The wave theory analog approach*. Vancouver. University of British Columbia, Department of Geography.

Burgess, E. W. (1924). The growth of the city: an introduction to a research project. *Publication of the American Sociological Society*, 18, 85-97.

City Mayors Foundation. (n.d.). The world's fastest growing cities and urban areas from 2006 to 2020. <http://www.citymayors.com/statistics/urban_growth1.html> Retrieved 12.07.12.

Clarke, K. C., Hoppen, S., & Gaydos, L. (1997). A self-modifying cellular automata model of historical urbanization in the San Francisco Bay area. *Environment and Planning B*, 24, 247–261. doi:10.1068/b240247

Committee on Earth Observation Satellites.(2012). The earth observation handbook. <http://www.eohandbook.com/> Retrieved 16.11.12.

Congalton, R. G., & Green, K. (2009). *Assessing the Accuracy of Remotely Sensed Data: Principles and Practices* (2nd ed.). Boca Raton, FL: CRC Press/Taylor & Francis Group.

Department of Finance. (2009). Dubai DOF Sukuk Limited. <http://www.dof.gov.ae/en-us/Investor/Lists/InvestorForms/Attachments/3/Sukuk%20Base%20Prospectus%20Oct-2009.pdf> Retrieved 10.03.12.

Dietzel, C., Herold, M., Hemphill, J. J., & Clarke, K. C. (2005). Spatio-temporal dynamics in California's Central Valley: Empirical links to urban theory. *International Journal of Geographical Information Science*, 19(2), 175–195. doi:http://dx.doi.org/10.1080/13658810410001713407

Dietzel, C., Oguz, H., Hemphill, J. J., Clarke, K. C., & Gazulis, N. (2005). Diffusion and coalescence of the Houston Metropolitan Area: Evidence supporting a new urban theory. *Environment and Planning B: Planning and Design*, 32, 231-246. doi:10.1068/b31148

Dubai Airport. (2010). Climate. <http://www.dia.ae/DubaiMet/Met/Climate.aspx> Retrieved 01.10.12.

Dubai Government. (2007). Dubai Stratigic Plan 2015. <http://www.deg.gov.ae/SiteCollectionImages/Content/pubdocs/Dubai_Strategic_Plan_2015.pdf> Retrieved 19.07.12.

Dubai Statistical Centre. (2000). Total population, buildings, housing units & establishments in censuses. < http://www.dsc.gov.ae/Reports/-72238938CSFB00-02-01.pdf> Retrieved 22.09.13.

Dubai Statistical Centre. (2009). Gross Domestic Product at Constant Prices.<http://www.dsc.gov.ae/EN/Themes/Pages/Reports.aspx?TopicId=4&Year=2009> Retrieved 25.09.13.

Dubai Statistical Centre. (2010). Statistical Yearbook-Emirate of Dubai. <http:dsc.gov.ae/Publication/SYB_2010.pdf> Retrieved 21.05.12.

Dubai Statistical Centre. (2011). Population Bulletin: Emirates of Dubai. <http://www.dsc.gov.ae/EN/Themes/Pages/Publications.aspx?TopicId=23> Retrieved 21.05.12.

Gamba, P., Dell'Acqua, F., Stasolla, M., Trianni, G., & Lisini, G. (2011). Limits and challenges of optical very-high-spatial-resolution satellite remote sensing for urban applications. In X. Yang (Ed.), *Urban Remote Sensing: Monitoring, Synthesis and Modeling in the Urban Environment* (1st ed., pp. 35-48). Chichester: John Wiley & Sons, Ltd.

Harris, C. D., & Ullman, E. L. (1945). The nature of Cities. *The Annals of American Academy of Political and Social Science*, 242, 7-17. doi:10.1177/000271624524200103

Hoyt, H. (1939). *The Structure of growth of residential neighbourhoods in American cities.* Washington, D. C.: Federal Housing Administration.

Intercon. (2010). Dubai: The nemesis of sustainability. http://intercongreen.com/2010/02/23/dubai-the-nemesis-of-sustainability> (accessed 16th December, 2014)

International Monetary Fund. (2000). The Impact of higher oil prices on the global economy. < http://www.imf.org/external/pubs/ft/oil/2000/oilrep.pdf> Retrieved 20.09.13.

Janssen, L. L., & Van Der Wel, F. J. (1994). Accuracy assessment of satellite derived land-cover: A review. *Photogrammetric Engineering and Remote Sensing*, 60(4), 419–426. Retrieved from http://cat.inist.fr/?aModele=afficheN&cpsidt=4035219

Jensen, J. R. (2005). *Introductory digital image processing a remote sensing perspective* (Third ed.). USA: Prentice Hall Series in geographic information sciense.

Ji, C. y., Liu, Q., Sun, D., Wang, S., Lin, P., & Li, X. (2001). Monitoring urban expansion with remote sensing in China. *International Journal of Remote Sensing*, 22(8), 1441–1455. doi: 10.1080/01431160117207

Kelbaugh. D. (2012). The environmental paradox of cities: gridded in Manhattan vs. gridless in Dubai. *The Journal of Sustainable Development*, 9(1), 84 – 96.

King, R. B., Lee, M. T., & Singh, K. P. (1989). *Land use/cover classification for the proposed superconducting super collider study area, northeastern Illinois*. Champaign, Illinois: Illinois State Water Survey Division, Surface Water Section.

Leitão, A. B., Miller, J., Ahern, J., & McGarigal, K. (2006). *Measuring Landscape: A Planner's Handbook*. Washington, D.C: Island Press.

Li, L., Sato, Y., & Zhu, H. (2003). Simulating spatial urban expansion based on physical process. *Landscape and Urban Planning*, 64, 67-76. Retrieved from http://www.sciencedirect.com/science/article/pii/S0169204602002013

Lo, C. P., & Choi, J. (2004). A hybrid approach to urban land use/cover mapping using Landsat 7 Enhanced Thematic Mapper Plus (ETM+) images. *International Journal of Remote Sensing*, 25(14), 2687–2700. doi:http://dx.doi.org/10.1080/0143116031000161842 8

Ma, Y., & Xu, R. (2010). Remote sensing monitoring and driving force analysis of urban expansion in Guangzhou City, China. *Habitat International*, 34, 228–235. doi:10.1016/j.habitatint.2009.09.007

Martellozzo, F. & Clarke, K.C. (2011). Measuring urban sprawl, coalescence, and dispersal: a case study of Pordenone, Italy. *Environment and Planning B: Planning and Design*, 38, 1085-1104. doi:10.1068/b36090

Masek, J. G., Lindsay, F. E., & Goward, S. N. (2000). Dynamics of urban growth in the Washington DC metropolitan area, 1973–1996, from Landsat observations. *International Journal of Remote Sensing*, 21, 3473–3486. doi:http://dx.doi.org/10.1080/014311600750037507

McGarigal, k., Cushman, S. A., Neel, M. C., & Ene, E. (2002). Fragstats v4: Spatial Pattern Analysis Program for Categorical Maps. <http://www.umass.edu/landeco/research/fragstats/fragstats.html> Retrieved 12.01.12.

Milanović, N. P. (2007). European urban spawl: Sustainability, cultures of (anti)urbanism and "hybrid cityscapes". *DOAJ*, 27, 101-133.

Moeller, M. S., & Blaschke, T. (2006). Urban change extraction from high resolution satellite image. *ISPRS Technical Commission II Symposium* (pp. 151-156). Vienna.

National Bureau of Statistics. (2010). UAE Population by Emirates, Nationality and Sex. <http://www.uaestatistics.gov.ae/ReportDetailsEnglish/tabid/121/Default.aspx?ItemId=186 9&PTID=104&MenuId=1> Retrieved 21.03.12

National Bureau of Statistics. (2011). Population estimates 2006-2010. http://www.uaestatistics.gov.ae/ReportPDF/Population%20Estimates%202006%20-%202010.pdf> Retrieved 21.03.12

Pacione, M. (2005). City profile Dubai. *Cities*, 22(3), 255–265. doi:10.1016/j.cities.2005.02.001

Patino, J. E., & Duque, J. C. (2013). A review of regional science applications of satellite remote sensing in urban settings. *Computers, Environment and Urban Systems*, 37, 1-17. doi: http://dx.doi.org/10.1016/j.compenvurbsys.2012.06.003

Rajendran, S., Arumugam, M., & Chandras, V. A. (2002). Potential use of high resolution IRS-1C satellite data and detection of urban growth in and around of Tiruchirapalli City, Tamil Nadu State, India. *FIG XXII International Congress* (pp. 1-13). Washington, D.C. USA.

Schneider, A., Seto K. C., & Webster, D. R. (2005). Urban growth in Chengdu, Western China: application of remote sensing to assess planning and policy outcomes, *Environment and Planning B: Planning and Design*, 32, 323 -345. doi:10.1068/b31142

Schneider, A., & Woodcock, C. E. (2008). Compact, dispersed, fragmented, extensive? A comparison of urban growth in twenty-five global cities using remotely sensed data, pattern metrics and census information, *Urban Studies*, 45(3), 659–692. doi:

10.1177/0042098007087340

Seto, K. C., Woodcock, C. E., Song, C., Huang, X., Lu, J. & Kaufmann, R. K. (2002). Monitoring land-use change in the Pearl River Delta using Landsat TM, *International Journal of Remote Sensing*, 23(10), 1985–2004. doi:10.1080/0143116011075532

Skyscraper center. (2012). 100 Tallest completed buildings in the world. <http://www.skyscrapercenter.com/> Retrieved 02.09.12.

Stewart, D. J., Yin, Z. Y., Bullard, S. M., & MacLachlan, J. T. (2004). Assessing the Spatial Structure of Urban and Population Growth in the Greater Cairo Area, Egypt: A GIS and Imagery Analysis Approach. *Urban Studies*, 41(1), 95–116. doi:10.1080/0042098032000155704

Strano, E., Nicosia, V., Latora, V., Porta, S., & Barthélemy, M. (2012). Elementary processes governing the evolution of road networks. *Scientific Reports*, 2, 1-8. doi:10.1038/srep00296

Taubenböck, H., Wegmann, M., Roth, A., Mehl, H. & Dech, S. (2009). Urbanization in India spatiotemporal analysis using remote sensing data. *Computers, Environment and Urban Systems*, 33, 179–188. doi:10.1016/j.compenvurbsys.2008.09.003

Tian, G., Jiang, J., Yang, Z., & Zhang, Y. (2011). The urban growth, size distribution and spatio-temporal dynamic pattern of the Yangtze River Delta megalopolitan region, China. *Ecological Modelling*, 222(3), 865–878. doi:10.1016/j.cities.2005.05.009

United Nations. (2012). World urbanization prospects: The 2011 revision. <http://esa.un.org/unup/> Retrieved 20.08.12.

Verbyla, D. L., & Hammond, T. O. (1995). Conservative bias in classification accuracy assessment due to pixel-by-pixel comparison of classified images with reference grids. *International Journal of Remote Sensing*, 16, 581-587. doi:10.1080/01431169508954424

Wu, J., Jenerette, G. D., Buyantuyev, A., & Redman, C. L. (2011). Quantifying spatiotemporal patterns of urbanization: The case of the two fastest growing metropolitan regions in the United States. *Ecological Complexity*, 8, 1-8. doi:10.1016/j.ecocom.2010.03.002

Xian, G., Crane, M., & McMahon, C. (2005). Assessing urban growth and environmental change using remotely sensed data. *Pecora 16 "Global Priorities in Land Remote Sensing"* (pp. 1-9). Sioux Falls, South Dakota.

Yagoub, M. (2004). Monitoring of urban growth of a desert city through remote sensing: Al-Ain, UAE, between 1976 and 2000. *International Journal of Remote Sensing*, 25(6), 1063-1076. doi:http://dx.doi.org/10.1080/0143116031000156792

Yeh, C. T., & Huang, S. L. (2009). Investigating spatiotemporal patterns of landscape diversity in response to urbanization. *Landscape and Urban Planning*, 93, 151–162. doi:10.1016/j.landurbplan.2009.07.002

Yin, Z. Y., Stewart, D. J., Bullard, S., & MacLachlan, j. T. (2005). Changes in urban built-up surface and population distribution patterns during 1986–1999: A case study of Cairo, Egypt. *Computers, Environment and Urban Systems*, 29, 595–616. doi:10.1016/j.compenvurbsys.2005.01.008

Yue, W., Liu, Y., & Fan, P. (2010). Polycentric urban development: the case of Hangzhou. *Environment and Planning A*, 42, 563-577. doi:10.1068/a42116

Zhang, Q. Ban, Y., Liu, J. & Hu, Y. (2009). Simulation and analysis of urban growth scenarios for the Greater Shanghai Area, China. *Computers, Environment and Urban Systems, 35, 126–139*. doi:10.1016/j.compenvurbsys.2010.12.002

Chapter 5 What controls the magnitude of the daytime heat sink as a desert city grows?

Ahmed K. Nassar, G. Alan Blackburn and J. J. Duncan Whyatt

Lancaster Environment Centre, Lancaster University, Lancaster, UK

Statement of Authorship

I, Ahmed K. Nassar, in my capacity as the first author of the above publication researched, acquired, processed and compiled all data used in this paper. I carried out the various statistical analyses undertaken in this research, analysed the results and drafted the manuscript, which includes the preparation of all figures and tables. I undertook the revisions of the manuscript following comments and advice from the co-authors and already submitted the final version to the journal. This constitutes approximately 85% of the work involved with this publication.

Please find herein signatures of the co-authors confirming my contribution as described above to the paper.

Yours sincerely,

Ahmed Khalaf Nassar

Signature   *Ahmed Khala /*

Co- authors:

Name   G. Alan Blackburn

Signature

Name   J. Duncan Whyatt

Signature
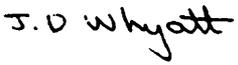
Context

In the previous chapter the rate and form of urbanisation across Dubai was quantified. Such changes in land cover are likely to have impacts upon the natural environment. This chapter explores the relationships between changes in land cover and the daytime thermal characteristics of Dubai over time.

A time-series of Landsat images were used to investigate the surface thermal characteristics during the period of rapid urbanization in Dubai between 1990 and 2011. Landsat thermal images are preferred to other forms of thermal imagery because they cover the full duration of the period under investigation and provide higher spatial resolution thermal data than other satellites (see section 3.5). Changes in land cover and albedo were also quantified from Landsat data and the development of different land use types and variations in urban geometry were characterized using ancillary data. These variables were chosen based on previous studies, as discussed in section 3.3.

The results demonstrate that urban growth has promoted a heat sink and that all urban land use types contributed to this effect. Impervious surfaces dominated the urban environment and are responsible for the majority of the cooling. Changes in albedo, as measured from Landsat, are not causally related to the urban heat sink but variations in urban geometry, particularly the amount of shading cast by buildings, were related to the magnitude of cooling.

The findings of this chapter highlight the importance of urban geometry in developing urban heat sinks. The relationship between urban geometry and urban heat sinks is explored in more detail in the next chapter.

5.1 Introduction

Numerous studies have addressed the issue of the urban heat island (UHI) in different regions of the world, especially where urban areas have replaced naturally vegetated areas in temperate and subtropical environments. The results of these studies have indicated that urban areas show higher temperatures than surrounding rural areas, particularly at night time (e.g. Hu & Brunsell, 2013; Nichol & Hang, 2012; Rajasekar & Weng, 2009). However, in hot arid environments, where urban areas are replacing desert sands (see section 3.4), urban heat sinks (UHS) can be detected, where urban land surface temperature (LST) is lower during the daytime than the surrounding desert (Frey et al., 2007; Imhoff et al., 2010; Lazzarini et al., 2013). For example, Lougeay et al. (1996) reported that the densely urbanized city of Phoenix was 3°C cooler than surrounding natural desert areas during the daytime in summer. Likewise, surface temperature in the city of Las Vegas was 0.46°C lower than in adjacent rural desert areas during the summertime (NASA, 2009). Therefore, such studies demonstrate that urbanization can have opposite effects on surface temperature depending upon the characteristics of the surrounding landscape and time of day.

The magnitude of the observed UHS in desert regions can depend on many factors including weather conditions and the timing of temperature observations, but it has been suggested that the characteristics of the urban land cover exert a major control on variations in land surface temperature (Carnahan & Larson, 1990). The UHS effect has been attributed to an increase in vegetated areas associated with urbanization which generate a cooling effect in urban areas due to the increase in latent heat flux through evapotranspiration and decrease in sensible heat in the urban area compared to the desert

119

surroundings (Lazzarini et al., 2013). However, other research has shown that desert cities can still exhibit an UHS despite containing little vegetation and being primarily composed of impervious surfaces (Frey et al., 2007: Imhoff et al., 2010). This disparity in the literature highlights the need for further research to understand the relationships between land cover and LST in desert cities.

The properties of the urban fabric can also influence the UHS; it has been suggested that highly reflective materials, or those with a low thermal conductivity, can contribute to urban cooling (Erell et al., 2011; US EPA, 2008a). Some cities have made use of highly reflective materials on rooftops, roads and parking lots to increase albedo hence reduce the absorption of solar radiation and surface temperatures (Bretz et al., 1998), see subsection 3.3.3. Mackey et al. (2012) found that increasing the surface reflectivity in urban areas of Chicago had a stronger cooling effect than increasing the amount of vegetation cover. Similarly, increasing the specific heat capacity of urban materials has been shown to decrease daytime summer peak temperatures by postponing the release of stored heat (Hamdi & Schayes, 2009). Urban water bodies can also make a significant contribution to cooling due to their high specific heat capacity and ability to lose heat via evaporation (Omran, 2012). However, the overall contribution of variations in the thermal properties of different surface materials has received little attention in the context of the UHS phenomenon in desert cities.

Evidence concerning the impact of urban geometry on thermal conditions is somewhat unclear. Several studies have demonstrated that an increase in building height and density produces an increase in surface temperature (e.g. Martin et al., 2012; Wu et al., 2013). Conversely, other research suggests that tall buildings and narrow streets generate

120

shadow effects which decrease the absorption of solar energy at the land surface thus lowering temperatures (e.g. Kato et al., 2010; Littlefair et al., 2000). There is also evidence that the variability in building heights is important, whereby areas with a diverse range of building heights generate an increase in wind speeds and natural ventilation at street level leading to a decrease in surface temperature (Johansson and Emmanuel, 2006). Given such divergence in the literature, it is now important to determine the extent to which variations in urban geometry influence the UHS in desert cities.

Although the UHS effect in desert regions has been identified there is considerable uncertainty over the factors which generate this phenomenon. Hence, the aim of this study was to increase knowledge of the causes of cooling in desert cities. The study site was Dubai, United Arab Emirates (UAE), which has experienced rapid urbanization over the period covered by the Landsat data archive. This archive was used to address the following research objectives: (i) to characterize the changes in land cover, land use and albedo that have taken place during urbanization; (ii) to quantify the development of the UHS during urbanization; (iii) to examine whether variability in the magnitude of the cooling effect can be explained by the transitions in land cover and albedo and the type of land use; and (iv) to evaluate the sensitivity of the UHS to variations in urban geometry.

5.2 Study area

Dubai Emirate, situated on the Arabian Gulf (Fig. 5.1), is one of the fastest growing cities in the Middle East (Nassar et al., 2014). The total area of the emirate is approximately 3885 km^2 and it is characterized as a hyper arid environment with an annual average rainfall of only 8mm falling mostly in the late autumn and winter months (Dubai Airport, 2014).

With such limited rainfall, Dubai relies heavily on desalination plants along the Gulf for drinking water and for drip and spark irrigation purposes. The warmest months in Dubai are May to September with an average maximum temperature of 40°C and average minimum of 28°C; the coldest months are December to February with an average maximum temperature of 25°C and average minimum of 15°C (Dubai Airport, 2014).
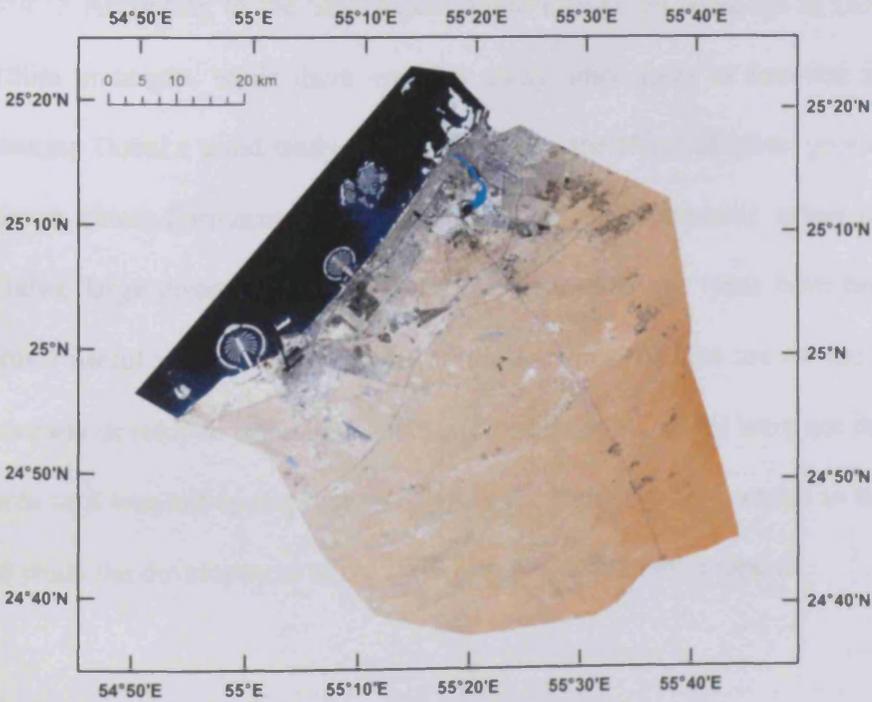
Figure 5.1 Overview map of the Arabian Gulf and map of the study area, Dubai Emirate, United Arab Emirates (Sources: Upper image from ESRI, lower image from Landsat, 2011 (USGS)) .

After the discovery of oil in the late 1960s, Dubai attracted a large labour force from overseas. As a result the population increased from 183,187 in 1975 (National Bureau of Statistics, 2010) to 2,003,790 inhabitants in 2011 (Dubai Statistical Centre, 2011). Furthermore, the physical size of the urban area has grown dramatically as the desert has been transformed into residential, commercial, sports and tourism developments; as a result the urban area increased by 561.4 km^2 between 1972 and 2011 (Nassar et al., 2014). This growth was a consequence of the strategic plan of the Emirate to diversify the economy by stimulating real estate marketing and developing tourism attractions. Indeed, the rapid pace of desert alteration in Dubai has attracted the attention of economists, environmentalists and urban planners.

According to the Skyscraper Centre (2014), 96 buildings in Dubai are greater than 150m in height, while there are also many other areas of low-rise urban development, making Dubai a good study site to investigate the effect of urban geometry on the UHS in desert cities. Furthermore, due to the strong and systematic urban planning process in Dubai, large discrete blocks of different urban land use types have been created, making this a useful study site for investigating the impact of land use on the cooling effect. The recently developed offshore islands (see Nassar et al., 2014) were not included in the study area as it was not appropriate to examine the transition from ocean to urban island in order to study the development of the UHS effect in desert environments.

5.3 Materials and Methods

Figure 5.2 shows the main stages of data processing and details are provided in the following subsections. Landsat images were preprocessed and classified into land cover

(LC) types and processed to retrieve surface albedo and land surface temperature (LST). A map of land use in 2011 was constructed and used to divide the urban area into 55 zones. Using urban zones as the sampling unit data on land cover, albedo and LST were extracted for each of the three sample years. This enabled us to analyse how changes in land cover, albedo and land use have effected LST. Using community areas as the spatial sampling unit, data on urban geometry and LST were extracted for year 2011 in order to analyse the effect of urban geometry on LST.
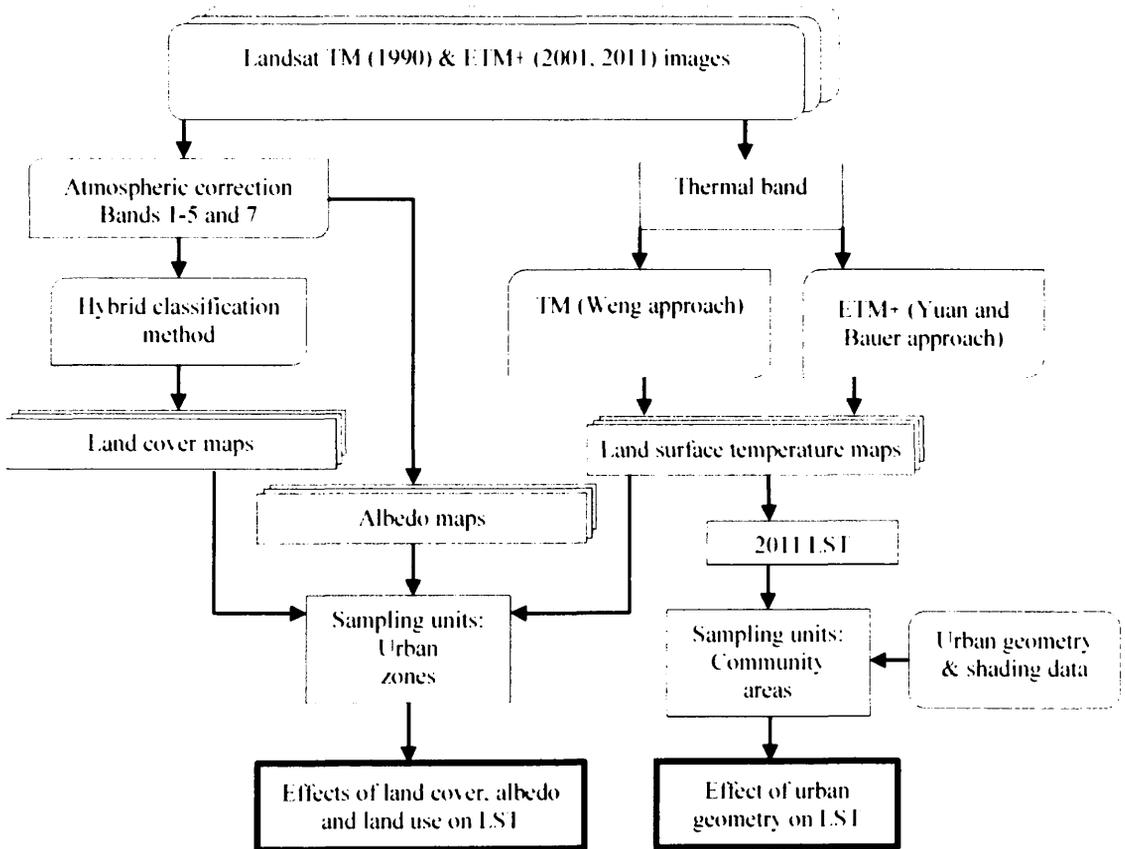
Figure 5.2 Flowchart showing the main stages of data processing and analysis.

5.3.1 Data acquisition and image pre-processing

Three Landsat scenes were obtained from the United States Geological Survey (Table 5.1) which were acquired in August in 1990, 2001 and 2011 and covered the main period of rapid urbanization in Dubai. Previously, the largest UHS effects have been observed in daytime during summer (e.g. Imhoff et al., 2010; Lazzarini et al., 2013), therefore the Landsat scenes chosen for this study were the most appropriate for examining the variability of the UHS in Dubai over space and time. All the images were cloud free, which greatly helped in the LC classification and retrieval of LST and albedo, and the images were acquired as close as possible to the same Julian day in order to minimize the effects of variations in solar geometry and vegetation phenology (Ji, et al., 2001), though the latter effect is small in Dubai as vegetation is maintained by irrigation.

Landsat 7 images for 2011 were affected by Scan Line Corrector (SLC) failure, however, only small areas of Dubai were affected by this failure and it had a very negligible effect on the final product.

Atmospheric correction for bands 1-5 and 7 was conducted using the Fast Line of Sight Atmospheric Analysis of Spectral Hypercubes module within ENVI and the original digital numbers were converted to surface reflectance (Kayadibi, 2011), see section 3.6. The images were then co-registered with existing map data on a WGS 84 datum/Dubai Local Transverse Mercator projection using 57 ground control points which were distributed around the images to maximize registration accuracy (Jensen, 2005).

Table 5.1 Satellite images used in the study

Date YY-MM-DD	Local time overpass	Satellite/Sensor	Sun elevation (degrees)	Sun Azimuth (degrees)	Spatial resolution of bands
90-08-28	10:14:55	Landsat4 (TM)	56.631	110.737	TIR: 120m; other bands:30m
01-08-26	10:35:19	Landsat7 (ETM+)	61.116	114.745	TIR: 60m; other bands:30m
11-08-22	10:39:57	Landsat7 (ETM+)	62.678	113.0399	TIR: 60m; other bands:30m

5.3.2 Land Cover (LC) classification

The atmospherically corrected images were used in a hybrid classification method to map four land cover classes (impervious surface, vegetation, water and sand). It has been noted previously that there are considerable challenges when classifying multispectral images of desert cities as it can be difficult to distinguish between built structures and sand (Flores et al., 2008; Stewart et al., 2004; Yagoub, 2004), as was investigated in section 2.9. The hybrid method of classification is based on a combination of unsupervised and supervised algorithms which exploits the advantages of both approaches to overcome their limitations (Lo & Choi, 2004). This method has proven effective for discriminating urban areas in desert environments (Nassar et al., 2014).

To assess the accuracy of the classified images, 60 stratified random samples (image and reference pairs) were collected for each class and these samples were independent from the data used for training to avoid bias (Verbyla & Hammond, 1995). The reference sample classes were identified through manual interpretation of high resolution imagery from Dubai Sat-1 (for 2011), IKONOS (for 2001) and aerial photography (for 1990). The overall accuracies for the three classified images ranged from

89-93% which exceeded the minimum 85% accuracy recommended by Anderson et al. (1976). As a result three LC maps were produced as shown in Figure 5.3.

1990

The creek

Jebel Ali port waterway

2001

2011

Boundary
Impervious surface
Vegetation
Water
Sand

0 5 10 20km
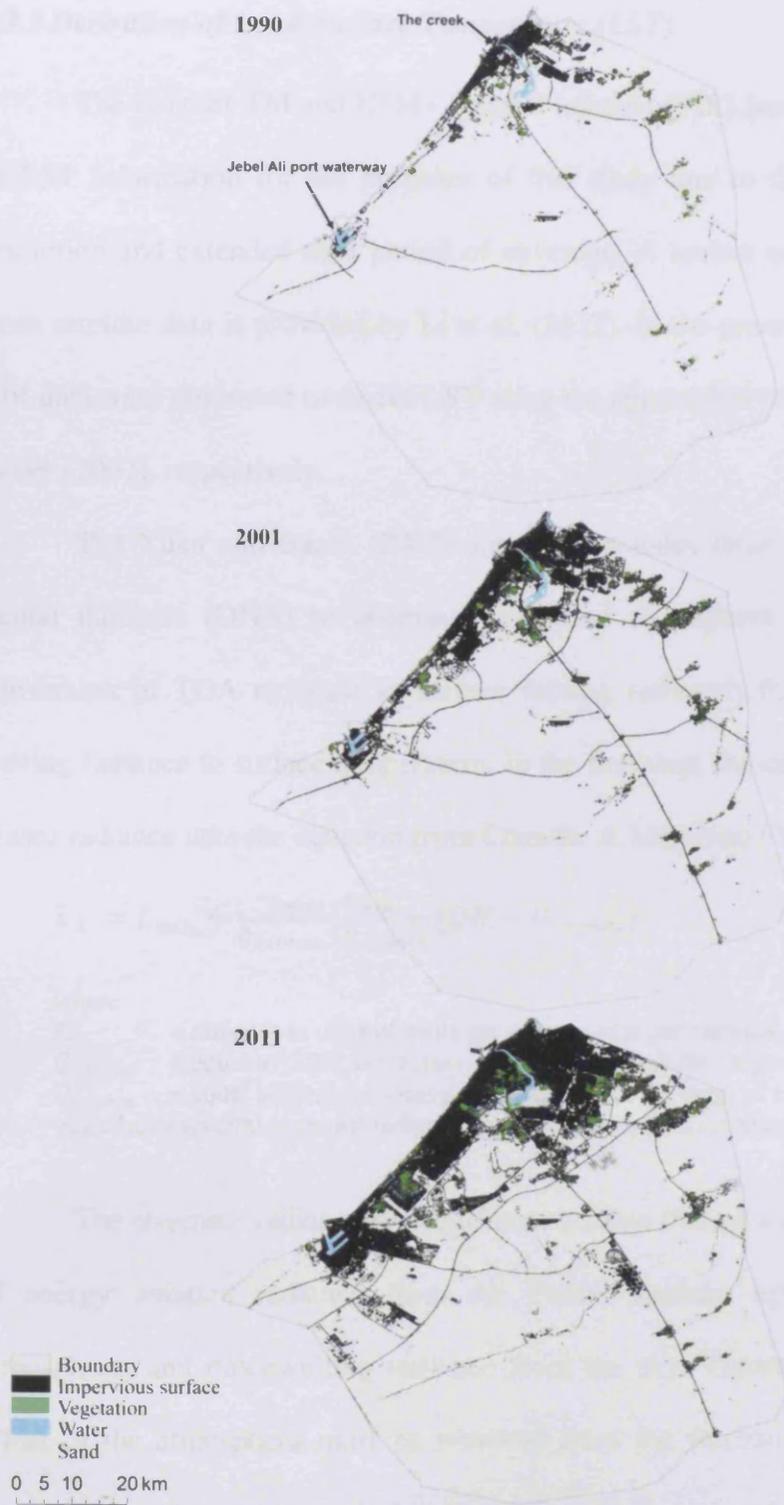
Figure 5.3 Land cover characteristics in Dubai in 1990, 2001 and 2011. The specific locations in the 1990 map are labelled because they are referred to later in the text.

5.3.3 Derivation of Land Surface Temperature (LST)

The Landsat TM and ETM+ thermal infrared (TIR) band data are a valuable source of LST information for the purposes of this study due to their reasonably high spatial resolution and extended time period of coverage. A review of methods for LST retrieval from satellite data is provided by Li et al. (2013). In the present study the TM and ETM+ TIR data were processed to derive LST using the approaches of Weng (2001) and Yuan and Bauer (2007), respectively.

The Yuan and Bauer (2007) approach includes three steps: firstly, conversion of digital numbers (DN's) to at-sensor or top of atmosphere (TOA) radiance; secondly, conversion of TOA radiance to surface leaving radiance; finally, conversion of surface leaving radiance to surface temperature. In the first step, the conversion of raw DN's to at-sensor radiance uses the equation from Chander & Markham (2003):

$$L_\lambda = L_{min} + \frac{L_{max}-L_{min}}{Q_{calmax}-Q_{calmin}} (DN - Q_{\text{calmin}}) \qquad (5.1)$$

where
$L\lambda$ = radiance in units of watts per square meter per steradian per micrometer (W/(m^2 sr μm);
Q_{calmax} = equal to (255), represents maximum point of the range of rescaled radiance in DN;
Q_{calmin} = equal to (0), represents minimum point of the range of rescaled radiance in DN;
L_{min}, L_{max}= spectral at-sensor radiance that is scaled to Q$_{calmin}$ and Q$_{calmax}$ (W/(m^2 sr μm)).

The at-sensor radiance derived from equation (5.1) is a combination of three sources of energy: emitted radiance from the Earth's surface, upwelling radiance from the atmosphere, and downwelling radiance from the sky. Therefore, in studies of LST, the effect of the atmosphere must be removed from the thermal band in which the emitted signal from the surface can be both attenuated and enhanced by the atmosphere. Consequently, the data resulting from step one were atmospherically corrected using an online tool developed by Barsi et al. (2005; http://atmcorr.gsfc.nasa.gov) which is based on

the MODTRAN radiative transfer code and a suite of integration algorithms. The parameters include date, time, location and local surface conditions which incorporates altitude, temperature, pressure and relative humidity. In the present study these parameters were acquired at Dubai international airport at the time of the Landsat overpasses by the National Center of Meteorology & Seismology. As a result, estimates of the transmission and upwelling and downwelling radiance were acquired from the atmospheric correction tool.

In order to calculate surface-leaving radiance a value for the emissivity of the surface material is required. Two main methods have been widely used with Landsat data for emissivity retrieval: the first method employs a land cover classification and assigns an emissivity value for each class (Snyder et al., 1998); the second employs the Normalized Difference Vegetation Index Threshold Method (NDVI THM) where emissivity values are assigned to surfaces based on their position within three NDVI ranges (Sobrino et al., 2004). Due to the heterogeneous land surfaces of Dubai and the arid environment with sparse vegetation cover the Snyder et al. (1998) method was more appropriate for this study. Therefore, impervious surfaces were assigned an emissivity value of 0.91 based on previous literature which investigated a variety of anthropogenic surfaces including asphalt, concrete and roofing materials (Artis & Carnahan, 1982; Stathopoulou et al., 2007). The desert sands of Dubai vary in texture and mineral composition (the majority is Silica) hence a representative emissivity value of 0.84 was adopted after consulting a variety of sources (ASTER spectral library http://asterweb.jpl.nasa.gov, Zhou et al. (2003), Schmugge et al. (2002)). Because Dubai is characterized by sparse vegetation (mainly grass and shrubs) a common feature of many desert cities, an emissivity value of 0.88 was assigned to

vegetation (Schmugge et al., 2002) and an emissivity value of 0.97 was given to inland shallow water bodies. Consequently these emissivity values were used together with the results from equation 5.1 to calculate surface leaving radiance using the following equation:

$$L_T = \frac{L_\lambda - L_\mu - \tau(1-\varepsilon)L_d}{\tau\varepsilon} \qquad (5.2)$$

Where

L_T = radiance of a blackbody target of kinetic temperature T in W/(m² sr μm);

$L\lambda$ = at-sensor radiance in W/(m² sr μm);

L_μ = upwelling atmospheric radiance (path radiance) in W/(m² sr μm)

τ = atmospheric transmissivity (unitless);

ε = emissivity of the surface (unitless);

L_d = downwelling or sky radiance in W/(m² sr μm).

Finally, the surface leaving radiance was converted to surface temperature using Planck's function calibrated for Landsat:

$$LST = \frac{K_2}{\ln\left(\frac{K_1}{L_T+1}\right)} \qquad (5.3)$$

where

LST = temperature in Kelvin;

L_T = radiance of a blackbody target of kinetic temperature;

K_1 = pre-launch thermal calibration constants in W/(m² sr μm), for Landsat 7= 666.09; and

K_2 = pre-launch thermal calibration constants in W/(m² sr μm), for Landsat 7= 1282.71.

For the Landsat TM TIR band for year 1990, the Weng (2001) approach was used which is based on a quadratic model to convert the digital number (DN) of into radiant temperatures, T_B (Malaret et al., 1985):

$$T_B = 209.831 + 0.834DN - 0.00133DN^2 \qquad (5.4)$$

Then emissivity values for the different land cover types were used to calculate land

surface temperature using the following formula (Artis & Carnahan, 1982):

$$LST = \frac{T_B}{1 + \left(\frac{\lambda T_B}{\rho}\right) \ln \varepsilon} \tag{5.5}$$

Where

LST	= surface temperature in Kelvin;
T_B	= black body temperature in Kelvin;
λ	= wavelength of emitted radiance, herein equal 11.5 μm for band 6 TM;
ρ	= hc/σ (1.438 × 10^{-2} mK), where h = Planck constant (6.626 x 10^{-34}Js), c = velocity of light (2.998 ×10^8 s^{-1}), σ = Boltzman constant (1.38 ×10^{-23} J K^{-1})
ε	= emissivity of the surface (unitless).

LST values derived from both the TM and ETM+ data were subsequently converted from Kelvin to degrees Celsius by subtracting 273.15.

5.3.4 Retrieval of albedo

Land surface albedo is a key parameter when modeling the earth's surface energy balance and remote sensing has been widely used to estimate this (Zhao et al., 2001). Land cover (LC), land use (LU), albedo and LST have been used in combination to study the consequences of anthropogenic changes in urban environments on microclimate (Bretz et al., 1998; Mackey et al., 2012). There has been long interest in estimating surface albedo from Landsat as it has the potential to detect variations in albedo from local to regional scales with high spatial resolution (e.g. Otterman & Fraser, 1976). Therefore, several algorithms have been developed to derive surface albedo from Landsat data (e.g. Liang, 2000; Román et al., 2013). In the present study surface albedo was retrieved by using the atmospherically corrected reflectance values from TM and ETM+ assuming a

Lambertian surface. The empirical model of Liang (2000) was used to convert these bands to total shortwave albedo:

$$Albedo = 0.356\alpha_1 + 0.130\alpha_3 + 0.373\alpha_4 + 0.085\alpha_5 + 0.072\alpha_7 + 0.0018 \qquad (5.6)$$

where
Albedo   = shortwave albedo
α_{1-7} = reflectance value in each of Landsat TM and ETM+ bands 1, 3, 4, 5 and 7.

5.3.5 Land use (LU) map and sampling of Land Surface Temperature (LST), albedo and Land Cover (LC).

A LU map for the urban area of Dubai (as of 2011) was constructed by manually digitizing the boundaries of zones of different LU types by incorporating information from the Landsat-derived LC map for 2011, existing land use maps (Source: Dubai Municipality) and through visual interpretation of high resolution images on Google Earth^{TM}. Five urban LU types were mapped in this way (Table 5.2) resulting in 55 different urban zones with a total area of 859km^2 (Fig. 5.4). Six sample areas covering the desert were also digitized (Fig. 5.4) and used as reference sites to represent the original natural land cover in the study area. The boundaries of the urban zones and the desert samples were then used to extract data from the LST maps from 2011, 2001 and 1990. The mean LST was calculated for each zone (i.e. all LST pixels falling within each urban zone and within each desert zone were averaged). For each year, the difference in LST between each urban zone and the desert was calculated in order to express the LST of each urban zone relative to the desert (LST$_r$) (Lazzarini et al., 2013). This avoided the use of absolute LST measurements which can vary between sampling years according to meteorological conditions leading up to and at the time of acquisition of each of the Landsat scenes. Furthermore, the use of LST$_r$

measurements accounted for any residual effects of atmospheric interactions or differences in sensor types between Landsat image acquisitions which may have still been present in absolute LST measurements despite the extensive pre-processing effort. Hence, the use of LST_r data for each of the three sample years allowed us to quantify the changes over time in the magnitude of the UHS effect for each urban zone.

Table 5.2 Land use classification schema employed in this study.

LU type	Description
Residential	All types of distinctive residential communities.
Mixed	Both residential and commercial that cannot be separated.
Recreational	Parks, golf courses and playgrounds.
Industrial	All types of light and heavy industrial plants.
Transportation	Airports and seaports.

Figure 5.4 Map of urban zones in Dubai in 2011. Each zone is represented by an individual polygon (55 in total) and the colour of the polygon represents the land use type within each zone. The areas used to sample desert land surface temperature are also shown. The Landsat ETM+ scene from 2011(RGB-321) is displayed in the background. Example images from IKONOS of the five urban land use types and the desert are inset.

The boundaries of the urban zones in 2011 were then used to extract data from the LC and albedo maps from 2011, 2001 and 1990. For each urban zone the areal percentage of each anthropogenic cover (impervious surface, vegetation and water) and the average albedo was calculated for each year. Generating the datasets in this way meant that we were able to sample across urban zones that have undergone a wide range of different types of transitions, from the extremes of zones which were urban in 2011 but entirely desert in 1990, through to zones which were urban in 2011 and had essentially remained so from

135

1990; the data sampled across all of the different LU types and incorporated a wide variation in the composition of LC. Hence, these data sets were subsequently used to assess (graphically and statistically) how the changes in LU type, LC composition and albedo of the urban zones have influenced LST_r over time.

5.3.6 Urban geometry variables and associated LST

Information on urban geometry was derived from a vector layer of building 'footprints' and associated height attributes (source: Dubai Municipality). These data were only available for 2011 hence we restricted our analysis of the impacts of urban geometry on LST to this year. The buildings data were voluminous and spatially precise but only covered a proportion of the entire study site ($73km^2$) hence it was inappropriate to use the (large) urban zones as the sampling units (as in section 5.3.5) for the analysis of urban geometry effects. Instead, here we used the boundaries of 'communities' as the sampling units; these are defined administrative areas in Dubai, within which, due to the systematic planning process, the form of urban development is consistent. The spatial extent of the buildings layer coincided with 116 community boundaries which contained a total of over 200,000 buildings and incorporated a variety of different urban forms ranging from areas dominated by high rise construction with wide streets through to low-rise, high density buildings with narrow streets. The buildings dataset was used to derive average building height, variability in building height (standard deviation) and building density for each community. The 3D Analyst extension in ArcGIS was then used to simulate the area of shadow cast by the individual buildings, based on the actual solar azimuth and zenith

angles at the time of acquisition of the 2011 Landsat ETM+ image. The areal percentage of shade per community was then summarized. The community boundaries were also used to summarize the average LST per community from the 2011 LST image. Hence, these data sets enabled analysis of the influence of building height, density and shadow on LST.

5.4 Results

5.4.1 LC and LU change in Dubai

Some context for the subsequent results is provided by the LC and LU changes that have taken place during the urbanization of Dubai. From 1990 to 2011, the area of impervious surface increased by $423km^2$ with a compound annual growth rate of 7.5%, while vegetated areas increased by $25km^2$ with an annual growth of 4.9%. Inland water (excluding the Creek and Jebel Ali port waterway) increased from 0 to $2km^2$ but this cover type still only occupied 0.2% of the total area of Dubai in 2011. All of these changes in LC occurred at the expense of desert sand. Table 5.3 summarizes the changes in LC that have taken place within each of the different LU types. By 2011 there was considerable variability in the percentage of impervious surface coverage across the different LU types, with the highest within the mixed type. The recreational LU type had the smallest increase in impervious surface but the largest areal percentage of vegetation. However, the largest total area of increase in impervious surface and vegetation was generated by the residential LU type. Small areas of inland water developed in some LU types but were absent from the industrial and transportation categories.

Table 5.3 Percentage coverage and total area of the different anthropogenic LC types within each LU type for years 1990, 2001, 2011.

1990	Impervious surface		Vegetation		Water	
LU type	Percentage	Area (km²)	Percentage	Area (km²)	Percentage	Area (km²)
Industrial	14.7	25.7	0.0	0.0	0.0	0.0
Mixed	18.5	34.3	1.5	2.9	0.0	0.0
Residential	12.0	45.6	2.9	10.9	0.0	0.0
Transportation	13.8	12.4	0.0	0.0	0.0	0.0
Recreational	1.0	0.3	3.9	1.1	0.0	0.0
2001						
Industrial	27.2	47.5	0.2	0.3	0.0	0.0
Mixed	35.5	66.1	2.8	5.3	0.0	0.0
Residential	25.0	95.2	3.2	12.2	0.0	0.0
Transportation	29.3	26.4	0.0	0.0	0.0	0.0
Recreational	2.3	0.7	20.9	5.9	0.2	0.1
2011						
Industrial	65.3	114.2	0.2	0.4	0.0	0.0
Mixed	74.7	139.0	3.2	5.9	0.8	1.5
Residential	60.4	229.5	5.5	21.0	0.1	0.3
Transportation	63.6	57.2	0.1	0.1	0.0	0.0
Recreational	5.8	1.6	46.2	12.9	0.7	0.2

Note. These are overall values based on all of the urban zones for each LU type. Number of zones of each LU type in each year are: industrial (10), mixed (11), residential (15), transportation (5) and recreational (14).

5.4.2 Spatial and temporal variability of LST and albedo

Figure 5.5 shows the spatial variations over time in LST, the percentage of anthropogenic land cover (combined impervious surface, vegetation and water) and albedo for the extent of the area that became urban by the end of the study period (UA_{2011}). For the UA_{2011}, average LST was highest in 1990 (42.28 ^{0}C), slightly lower in 2001 (41.71 ^{0}C) and lower still in 2011 (41.10 ^{0}C). The average LST relative to the desert sample areas (LST_r) of the UA_{2011} in 1990 was -0.28°C (Standard Deviation (SD)= 0.49°C). This average cooling effect increased to -0.74°C in 2001 (SD= 0.93°C) and was greater still in 2011 (-1.56 °C; SD= 1.3°C). These data demonstrate how the development of the urban area has

138

generated an overall cooling effect and that urban surface temperatures have become more variable. Such findings concerning daytime LST are consistent with the results of other studies in desert cities (Frey et al., 2007) but here we are demonstrating how the UHS has developed as the city has grown.
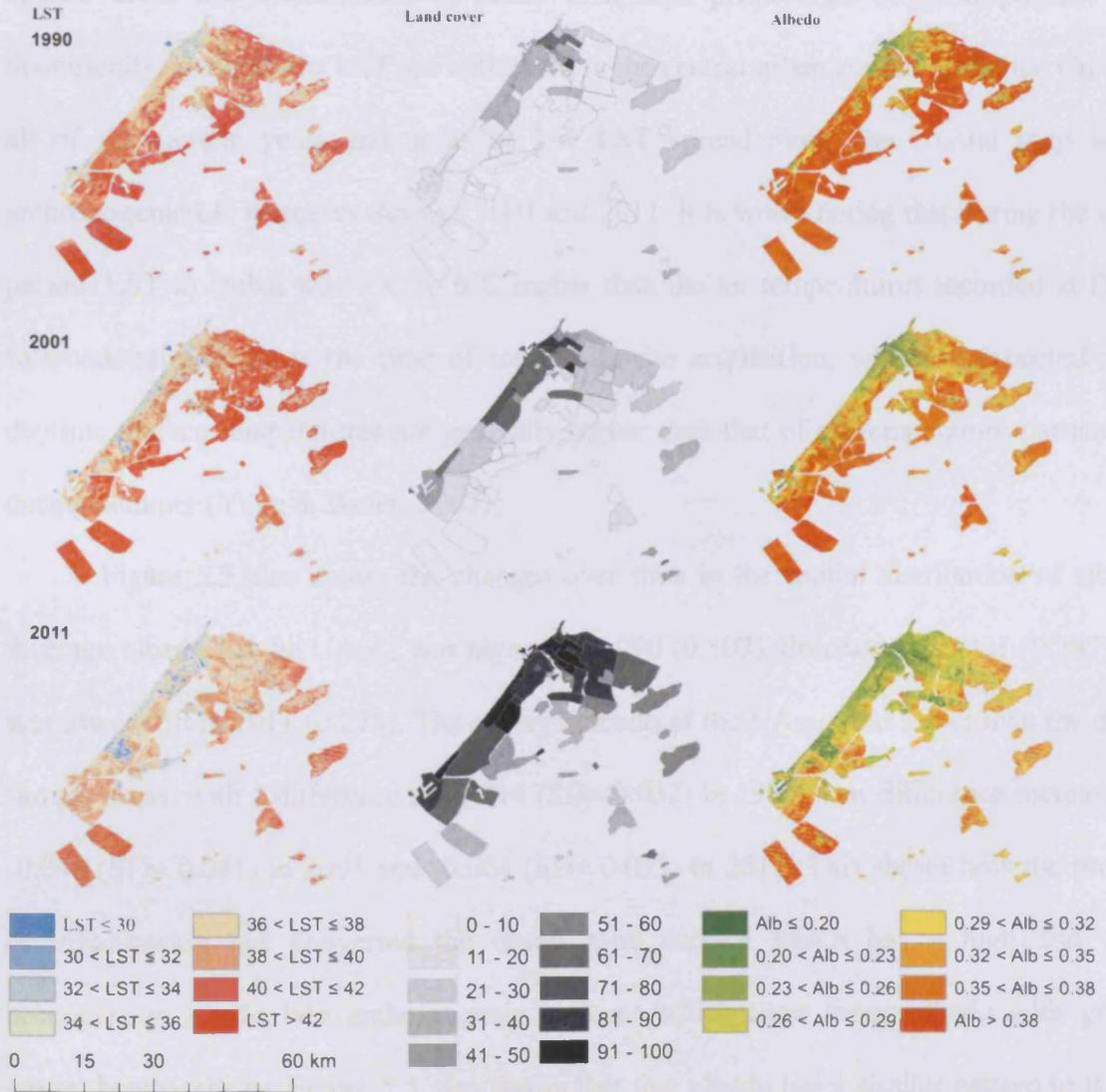
Figure 5.5 For the extent of the urban area in 2011 (UA$_{2011}$) these images show the development over time in LST in ^{0}C (left column), percentage of anthropogenic land cover (combined impervious surface, vegetation and water) in each urban zone (middle column) and albedo (right column).

Visual interpretation of the map of LST (Fig. 5.5) suggests an increase in the extent of surface cooling throughout the study period and a decline in the extent of surfaces with high temperatures. By comparing this to the map of percentage of anthropogenic LC, it can be seen that the areas of highest LST occur over undeveloped natural sands. In contrast, the coolest areas are concentrated in zones with high proportions of anthropogenic LC. Specifically, areas of low LST are noticeable in the central urban zones around the Creek in all of the sample years and areas of low LST spread along the coastal strip where anthropogenic LC increases through 2001 and 2011. It is worth noting that during the study period, LST in Dubai was 4°C to 6°C higher than the air temperatures recorded at Dubai International Airport at the time of satellite image acquisition, which is expected since daytime surface temperatures are generally higher than that of air temperature particularly during summer (Yuan & Bauer, 2007).

Figure 5.5 also shows the changes over time in the spatial distribution of albedo. Average albedo for the UA_{2011} was highest in 1990 (0.307), decreased in 2001 (0.297) and was lower still in 2011 (0.279). The average albedo of the UA_{2011} was lower than the desert sample areas, with a difference of -0.014 (SD= 0.032) in 1990. This difference increased to -0.040 (SD= 0.041) in 2001 and -0.064 (SD= 0.055) in 2011. This shows how the process of urbanization has converted the desert sand surface which has a high and more homogenous albedo into anthropogenic surfaces which have lower albedo with greater spatial heterogeneity. Figure 5.5 also shows that that albedo has a similar pattern to that of LST and that the highest LST and albedo values occur in zones with the lowest proportion of anthropogenic LC. Similar trends in LST and albedo have been noted in other desert

cities by Frey et al. (2007). So despite the decrease in albedo between 1990 and 2011 for the UA$_{2011}$ of Dubai, LST still decreases and, indeed, there is a high positive correlation between albedo and LST (r= 0.651; based on data from the 55 urban zones). As we would normally expect a negative correlation between albedo and LST, with low reflectance surfaces absorbing more solar radiation and therefore experiencing higher temperatures, it would appear that factors other than albedo must be responsible for the decrease in LST as the urban area of Dubai has developed.

5.4.3 Temporal variability of LSTr for the different LU types

Figure 5.6 shows the magnitude of the difference in LST between each of the LU types and the desert (i.e. LST$_r$) for each of the three sample years. This demonstrates that all of the urban LU types had a lower temperature than the desert on all occasions and this cooling effect increased over time but the magnitude of the change varied considerably between LU types. The increase in the cooling effect can be attributed to the increase in the area of the zones converted to urban LU as the city expanded between 1990 and 2011. In 1990 the largest cooling effect was experienced in the mixed LU type, followed by residential, recreational, industrial and transportation. By 2001 the cooling effect was most pronounced in the recreational LU type, then the mixed, residential, industrial and transportation types. A similar ranking was observed in 2011. The error bars in Figure 5.6 demonstrate that there is an increase in the variability of the cooling effect for all LU types over time, implying an increase in the spatial heterogeneity of the UHS within and between different LU types as the city developed.
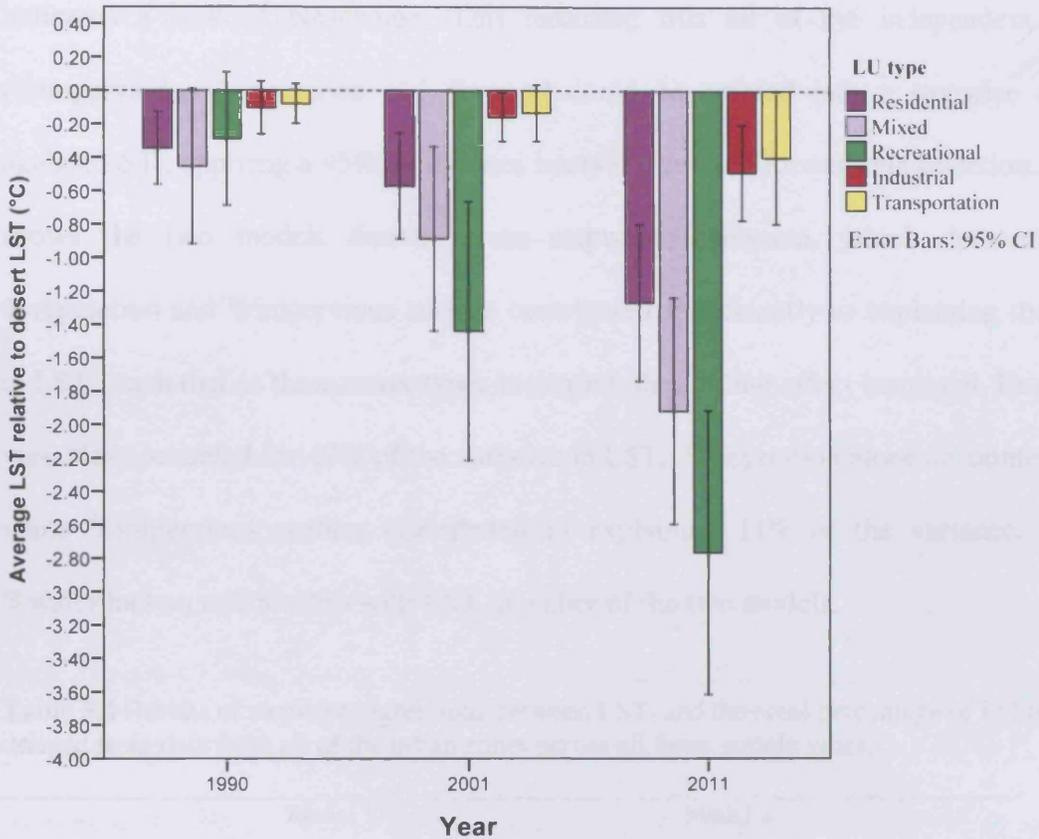
Figure 5.6 Average LST relative to desert (LST$_r$) for the different LU types, with 95% confidence intervals.

5.4.4 Relationships between LSTr and LC

The relationships between LST$_r$ and the three different types of land cover was examined to evaluate how the proportions of impervious surface, vegetation and water contribute to the UHS effect in Dubai. The analysis was based on a combined data set of LST$_r$ and LC percentages for all of the urban zones for all of the sample years. Stepwise multiple regression analysis (see Draper & Smith, 1998) was used to select the LC types (as independent variables) according to their statistical contribution in explaining the variance in LST$_r$ (as the dependent variable). Initially the independent variables were tested for multicollinearity and the variance inflation factor and tolerance value (Brace et al., 2009)

indicated a lack of correlation. This indicated that all of the independent variables (%impervious, %vegetation and %water) could be entered into a stepwise regression against LST$_r$, applying a 95% confidence interval threshold for variable selection. Table 5.4 shows the two models derived from stepwise regression, which demonstrate that %vegetation and %impervious surface contributed significantly to explaining the variance in LST$_r$, such that as these cover types increased, the cooling effect increased. Both of these variables accounted for 43% of the variance in LST$_r$; %vegetation alone accounted for 32% while %impervious surface contributed to explaining 11% of the variance. However, %water had no relationship with LST$_r$ in either of the two models.

Table 5.4 Results of stepwise regressions between LST$_r$ and the areal percentage of LC types, derived from data from all of the urban zones across all three sample years.

	Model 1			Model 2	
Contributor	*B*	95% CI		*B*	95% CI
Constant	-.571**	[- .725, - .416]		-.168	[-.371, -.036]
%vegetation	-3.238**	[- 3.996, - 2.510]		-3.743**	[-4.438, -3.048]
%impervious				-1.192**	[-1.622, -.762]
%water					
R²	.321			.427	
F	77.122**			60.391**	
R² change				.106	
F change				29.958	

Note. *N*= 165, *B*= unstandardized coefficients, CI = confidence interval, **= $p < .01$, R^2=proportion variance explained; *F*= F statistic.

5.4.5 Relationships between LSTr and LC within the different LU types

In order to understand the impacts of LC change on LST$_r$ within each LU type in Dubai, a set of stepwise multiple regression analyses were performed. These regressions

were based on separate data sets of LST_r and LC percentages derived from all of the zones of each LU type across all three of the sample years. All independent variables (%impervious, %vegetation and %water) for each LU type were tested and found not to exhibit multicollinearity. Table 5.5 shows the results of the stepwise regressions where a single statistically significant model emerged for all of the LU types. The results demonstrate that LST_r was relatively well explained by %impervious surface in four LU types (industrial, transportation, residential and mixed), whereby an increase in % impervious surface generates an increased cooling effect, but %vegetation and %water make no contribution to this model. There was a wide variation between LU types in the variance in LST_r that was explained by %impervious surface, ranging from a maximum of 85% in the mixed LU type to 63% in the industrial. This suggests that while the areal percentage of impervious surface is a dominant control on the magnitude of the cooling effect, other factors such as the thermal properties of the impervious materials used or the geometry of the urban environment (dealt with in the next section) may also be influential. As Table 5.5 shows LST_r in the recreational LU type was well explained by the increase in %vegetation, accounting for 72% of the variance, while %impervious surface and %water make no contribution to this model.

Table 5.5 Results of stepwise regressions between LST$_r$ and the areal percentage of LC types, for each LU type.

LU type Model# *B*	Industrial 1	Transportation 1	Recreational 1	Residential 1	Mixed 1
Constant	.016	.127	-.572*	-.131	-.155
%Vegetation			-4.253**		
%impervious	-.627**	-.716**		-2.941**	-3.656**
%Water					
R^2	.627	.769	.721	.763	.852
F	18.059**	54.894 **	42.520**	43.052**	82.282**
R^2 change					
F change					
N	30	15	42	45	33

Note. **= $p < .01$, *= $p < .05$.

5.4.6 Relationships between LST and urban geometry

Figure 5.7 uses a sample area of central Dubai to demonstrate how LST varies in response to the distribution of buildings. To quantify this effect, data from the 116 communities were used to examine the relationships between LST (for the year 2011) and each of the four urban geometry variables (average building height, building height variation, building density and %shading). Bivariate linear regression revealed that LST had a significant negative relationship with all variables (Table 5.6). The weakest correlation was between LST and building height variation, with stronger relationships for building density and average building height. The highest correlation was between LST and %shade. The results of the shadow analysis suggest that 17km^2 of the land surface was shaded by buildings at the time of 2011 Landsat image acquisition (4.3% of the total urban area). Figure 5.8 shows that the shade cast by buildings varies considerably depending upon building height and density and comparison with Figure 5.7 illustrates how variations in shading influence the detected LST.

Table 5.6 Correlation between LST and urban geometry variables.

Variable	Average building height	Building height variation	Building density	%Shade
LST	-.561	-.237	-.426	-.592

Note. N= 116, all correlations are significant at the 0.01 level (2-tailed).

Figure 5.7 Sample area from central Dubai city demonstrating the correspondence between LST (from 2011 Landsat data) and building distribution, demonstrating the cooling effect of dense urban areas. The white lines show the boundaries of the community areas which were used as sampling units for analysing relationships between urban geometry variables and LST. The red square on the inset map of Dubai emirate shows the position of the sample area used in the main map.
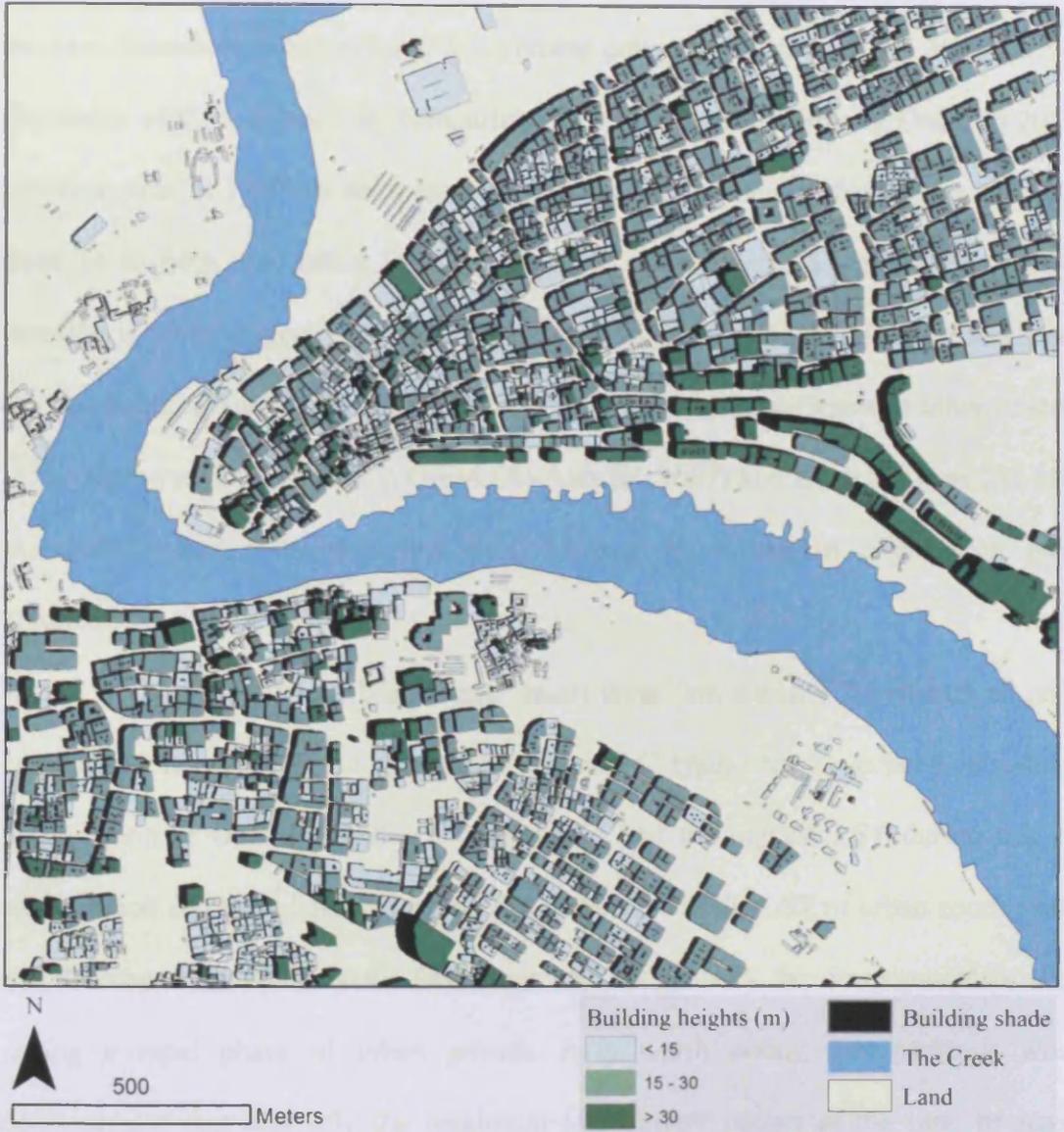
Figure 5.8 Sample area from central Dubai city (same area as Figure 5.7) showing the shade cast by buildings and variation in building heights.

5.5 Discussion

The transition of the desert environment to anthropogenic LC types has resulted in

substantial changes in LST in Dubai. Since 1990, the desert sands have been transformed into impervious surfaces, vegetation and inland water as a consequence of population increase, economic prosperity and government policy (see Nassar et al., 2014 for detailed discussion of these issues). By comparing LC across the urban area of Dubai in 2011 with the same area in 1990 we have demonstrated that impervious surface cover has increased from 14 to 64%, vegetation from 1.5 to 4.7% and water bodies from 0 to 0.2%. This increase in anthropogenic land cover has occurred at the expense of desert sand which is the main natural land cover across the emirate. This is quite different to other desert cities in the region such as Muscat in Oman (Al-Awadhi, 2007) and Doha in Qatar (Al-Manni et al., 2007) which have experienced a decrease in vegetation cover with increased urbanization.

In this study the LST of natural desert areas was set as a benchmark to provide a comparison for the LST of the anthropogenic LC types that have been introduced via urbanization in Dubai. The desert consistently had the highest LST during the 21-year study period and there has been a systematic decrease in the LST of urban zones as the city has developed. In this way we have been able to quantify the development of the UHS during a rapid phase of urban growth. It is worth noting that previous work has demonstrated that diurnally the maximum UHS effect occurs at the time of maximum temperature during the afternoon (Carnahan & Larson, 1990) therefore our measurements from Landsat images acquired during the morning are likely to underestimate the magnitude of the UHS. Nevertheless our findings provide valuable evidence of the spatial variations in the UHS within the city and the temporal variations in response to urban growth.

Our statistical analysis (Table 5.4) revealed that the percentage of vegetation cover explained 32% of the variance in the cooling effect during the study period. Vegetation increases latent heat loss through the evapotranspiration which in turn generates a temperature decrease on and above the vegetated surface (e.g. Voogt & Oke, 2003). This cooling effect of urban vegetation is consistent with previous studies of other cities in desert environments (e.g. Lazzarini et al., 2013). However, water bodies made no significant contribution to cooling in Dubai which is probably explained by the very small amount of water in any of the urban zones.

The increase in the percentage of impervious surface over the study period has also contributed to the UHS, accounting for 11% of the variance in the cooling effect. In contrast to other cities, where cooling has been generated primarily by the presence of impervious surfaces that have a higher albedo than the surrounding environment (e.g Mackey et al., 2012), in Dubai there is no evidence that impervious urban surfaces have generated cooling via increased albedo. Our findings indicate that LST and albedo exhibit similar spatio-temporal patterns and they are positively correlated, which suggests that other factors may be responsible for the UHS effect. It is feasible that the daytime cooling effect of impervious surfaces such as buildings, pavements and roads might be due to differences in specific heat capacity between construction materials and surrounding desert sands. Indeed, it is the case that published values of specific heat capacity for typical construction materials such as asphalt, aluminum, concrete and bricks (920, 897, 880 and 840 J/kgK) are higher than that for sand (835 J/kgK) (Physics Hypertextbook, 2014). This would indicate that for a given input of energy the temperature of desert sand would show a larger increase in temperature than the impervious urban surfaces. It has to be noted that the

observed rate of increase in LST in response to solar radiation input may also be influenced by other factors such as surface reflectivity, thermal conductivity and surrounding materials or objects. Nevertheless, it would appear that the lower specific heat capacity of urban materials may have some contribution to the UHS in desert cities and this is worthy of further investigation. However, the present study has demonstrated that the magnitude of the UHS effect in Dubai is significantly influenced by urban geometry. In particular, LST was negatively correlated with average building height and percentage of shade (Table 5.6) because taller buildings provide greater shadow which reduces the amount of solar energy reaching the land surface (e.g. Kato et al., 2010).

The relative contribution of the specific heat capacity of materials and urban geometry towards the UHS in Dubai can be assessed when we investigate the temporal changes in anthropogenic LC and the magnitude of the cooling effect in the individual LU types. Figure 5.9 shows that all the different urban LU types have experienced some cooling throughout the study period and the cooling effect has increased as the percentage of anthropogenic LC has increased. This figure also shows that LU types containing vegetation have a proportionally larger cooling effect than those containing only impervious surfaces. Nevertheless those LU types with only impervious surfaces (industrial and transport) do show the cooling effect and this increases as the percentage cover of impervious surface increases through the study period. Because vegetation is present in much smaller amounts than impervious surfaces in most LU types, our statistical analysis (Table 5.5) shows that the dominant influence on cooling in industrial, transportation, residential and mixed LU types is the amount of impervious surface cover. Such findings concur with those of Frey et al. (2007) who found that in desert cities even industrial urban

areas with no vegetation and water coverage had lower LST than the surrounding desert environment. This is the case for both transportation and industrial LU types in Dubai where both have negligible vegetation coverage (<0.23%) and low buildings heights, so shading is minimal, yet they still show a cooling effect. Therefore, it is likely that the UHS in these LU types is attributable to the thermal properties of impervious surface materials such as specific heat capacity. As similar materials are used in all of the LU types then their contribution to the UHS effect is likely to be ubiquitous. However, the UHS is considerably enhanced in the residential and mixed LU types due to shading by taller buildings.

The findings of this study call for some consideration of what aspects of the urban surface energy balance are actually being measured from a satellite's perspective. The shading analysis raises questions about the measurement of albedo, the physical property of a surface which describes the fraction of total incoming light that it reflects. In this study, and many others, Landsat waveband reflectance is used to estimate albedo, but surface reflectance is calculated assuming the same amount of incoming radiation across the whole scene. For ground areas that are shaded by buildings this assumption is invalid, so we must be underestimating reflectance and therefore underestimating albedo. Indeed, Frey and Parlow (2009) used radiation modelling to show that shading in dense urban areas can reduce estimates of albedo by up to 50% when the solar incidence angle was low in winter. So from a satellite perspective, we are not estimating the albedo of all areas of the land surface in the urban area, but deriving an estimate of the overall albedo of the wider urban area which Frey and Parlow (2009) term a nadir-view 'regional' albedo. This may explain why our measurements of albedo from Landsat show a decrease in albedo with urbanization, in that the decrease is likely responding to the increase in shading in urban

152

areas in addition to the decrease in the albedo of the actual urban surfaces relative to the highly reflective desert sands. This, in turn, may provide a rationale for our observation that LST decreases despite albedo also decreasing with urban development.
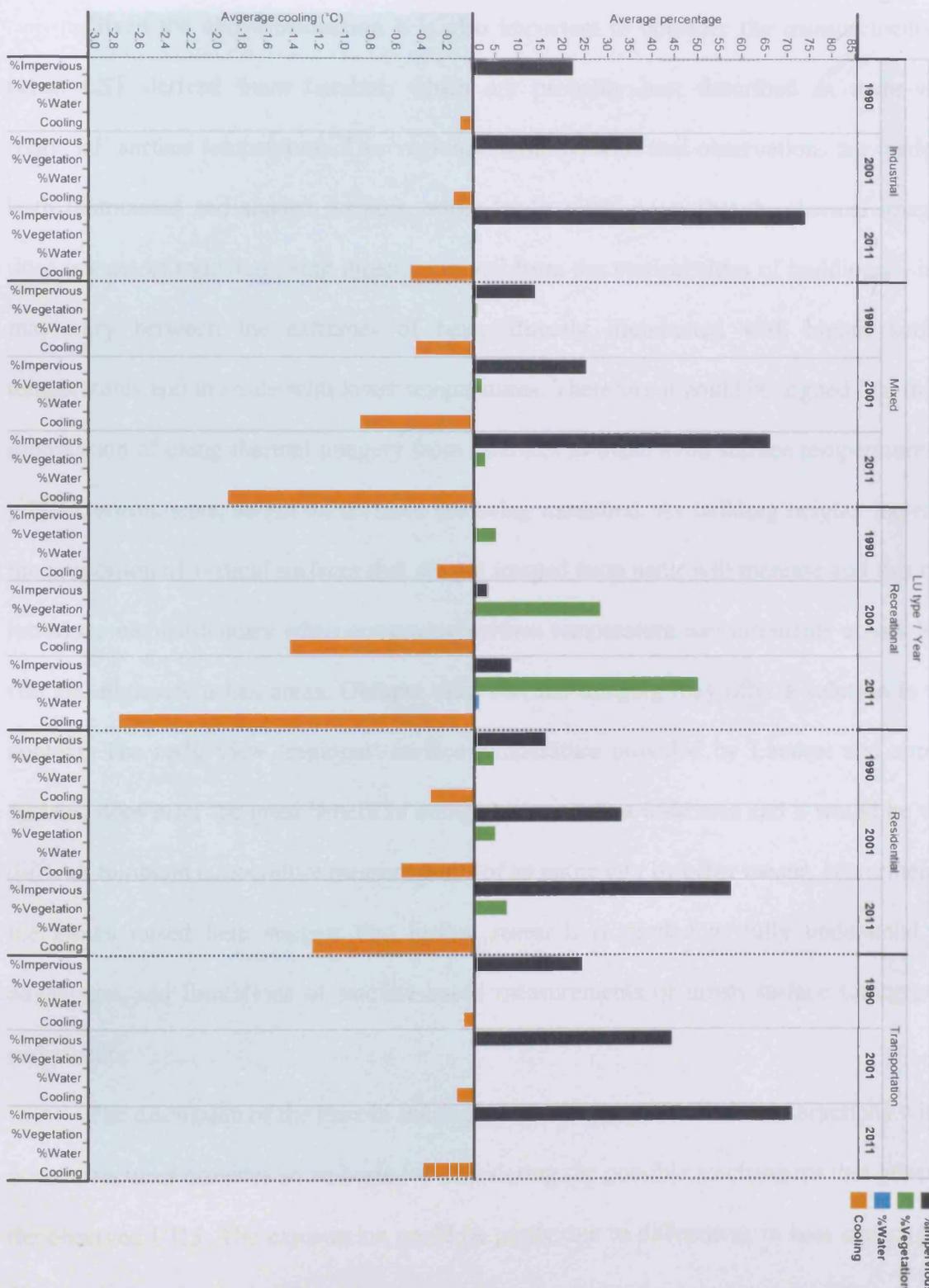
Figure 5.9 Changes over time (1990, 2001 and 2011) in the percentage of anthropogenic land covers (impervious surface, vegetation and water) within each land use type and the magnitude of the associated surface cooling effect (LST$_r$). The figure is best viewed in landscape orientation.

Given the above discussion it is also important to consider the measurements of urban LST derived from Landsat, which are probably best described as nadir-view 'regional' surface temperature. The 'regional' term explains that observations are made of both illuminated and shaded surfaces, while 'nadir view' notes that the thermal imagery does not detect radiation being directly emitted from the vertical sides of buildings, which may vary between the extremes of being directly illuminated with higher surface temperatures and in shade with lower temperatures. Therefore it could be argued that this is a limitation of using thermal imagery from satellites to understand surface temperatures in urban environments, as not all surfaces are being measured. As building heights increase, the proportion of vertical surfaces that are not imaged from nadir will increase and this may introduce inconsistencies when comparing surface temperature measurements across low-rise and high-rise urban areas. Oblique view thermal imaging may offer a solution in this context. The nadir-view 'regional' surface temperature provided by Landsat and similar systems does offer the great benefit of being able to cover a wide area and it would be very difficult to obtain temperature measurements of an entire city by other means. Nevertheless, the issues raised here suggest that further research is needed to fully understand the advantages and limitations of satellite-based measurements of urban surface temperature and albedo.

The discussion of the remote sensing methodology and radiation interactions within urban structures provides some basis for considering the possible mechanisms that generate the observed UHS. The explanation could be partly due to differences in heat capacity, as discussed above, where urban materials require more energy input to raise their surface temperature. However, urban geometry is also likely to be influential. During most of the

daytime, solar radiation will be impinging on the illuminated sides of buildings at a lower incidence angle than it will when reaching largely horizontal desert surfaces. So the same amount of energy will be distributed across a larger surface area on the sides of the buildings, thereby reducing surface temperatures. In addition, the three dimensional urban environment has a larger total surface area than the planar desert surface and while both receive the same solar input, the urban environment has greater capacity to emit thermal radiation and thus reduce surface temperatures, effectively acting like a heat sink on a computer processor. So the greater emissions combined with the effects of the low incidence angles on illuminated building sides, the areas of shadow this creates and higher specific heat capacity of urban materials may produce the heat sink effect relative to the desert observed in the Landsat thermal imagery. Clearly, the validity of this mechanism and the relative contribution of the different processes are worthy of further investigation.

5.6 Conclusions

This study has demonstrated how the development of the desert city of Dubai has generated an overall cooling effect. All urban LU types generated a lower LST than the desert and there was an increase in the spatial heterogeneity of the UHS within and between different LU types as the city developed. Where urban vegetation was planted LST reduced substantially but impervious surfaces dominated the urban environment and are responsible for the majority of the UHS. Albedo, as measured from Landsat, is positively correlated with LST and therefore appears to not be causally related to the UHS effect. However, it was found that the urban geometry was related to the magnitude of cooling of LST, particularly through the effects of shadows cast by buildings. The urban geometry has

implications for the remote sensing of urban albedo and LST which warrant further investigation and future research on the effects of LC transitions and type of LU on LST within desert cities will be valuable. In particular, deeper understanding of the interactions between the thermal properties of construction materials, urban vegetation and urban geometry is now needed in order to determine efficient ways of generating beneficial UHS effects which may reduce the environmental impacts of desert cities.

References

Al-Awadhi, T. (2007). Monitoring and modeling urban expansion using GIS & RS: Case
   study from Muscat, Oman. *Urban Remote Sensing Joint Event, IEEE*. doi:
   10.1109/URS.2007.371790.
Al-Manni, A. A., Abdu, A. S., Mohammed, N. A., & Al-Sheeb, A. E. (2007). Urban growth
   and land use change detection using remote sensing and geographic information
   system
   techniques in Doha City, State of Qatar. *Arab Gulf Journal for Scientific Research*,
   25(4),
   190-198.
Anderson, J. M., Hardy, E. E., Roach, J. T., & Witmer, R. E. (1976*). A land use
   classification system for use with remote sensing Data*. Geological Survey Professional
   Paper. Washington D. C.: Government Printing Office.
Artis, D.A., & Carnahan, W.H. (1982). Survey of emissivity variability in thermography
   of urban areas. *Remote Sensing of Environment, 12*, 313–329.
   http://dx.doi.org/10.1016/0034-4257(82)90043-8.
Barsi, J.A., Schott, J.R., Palluconi, F.D., & Hook, S.J. (2005). Validation of a web-based
   atmospheric correction tool for single thermal band instruments. *Earth Observing
   Systems X, Proc. SPIE Vol. 5882*, August 2005, San Diego, CA. doi:
   10.1117/12.619990.
Brace, N., Kemp, R., & Snelgar, R. (2009). *SPSS for Psychologists: A Guide To Data
   Analysis* (4th ed.). Basingstoke: Palgrave Macmillan Limited.
Bretz, S., Akbari, H., & Rosenfeld, A. (1998). Practical issues for using solar-reflective
   materials to mitigate urban heat islands. *Atmospheric Environment, 32*, 95-101.
   http://dx.doi.org/10.1016/S1352-2310(97)00182-9.
Brown, R.D. (2010). *Design with microclimate: the secret to comfortable outdoor space*.
   Washington, DC: Island Press.
Carnahan, W.H., & Larson, R.C. (1990). An Analysis of an Urban Heat Sink. *Remote
   Sensing of Environment, 33*, 65-71. http://dx.doi.org/10.1016/0034-4257(90)90056-R.
Chander, G., & Markham, B. (2003). Revised Landsat-5 TM radiometric calibration
   procedures and postcalibration dynamic ranges. *IEEE Transactions on Geoscience and
   Remote Sensing, 41(11)*, 2674–2677. doi: 10.1109/TGRS.2003.818464.
Dubai Airport (2014). *Climate*.
   https://services.dubaiairports.ae/DubaiMet/Met/Climate.aspx.
   (accessed May 15, 2014)
Dubai Statistical Centre (2011). *Population Bulletin: Emirates of Dubai*.
   http://www.dsc.gov.ae/EN/Themes/Pages/Publications.aspx?TopicId=23 (accessed
   May 21, 2012)
Draper, N.R, & Smith, H. (1998). *Applied Regression Analysis* (3rd ed., pp.335-339). New
   York: John Wiley & Sons, Inc.
EPA (2008). *Reducing urban heat islands: Compendium of strategies*. United States
   Environmental Protection Agency, Washington, D.C.
   http://www.epa.gov/hiri/resources/compendium.htm (accessed Nov 12, 2013).
Erell, E., Pearlmutter, D., & Williamson, T. (2011). *Urban Microclimate: designing the*

spaces between buildings (1st ed.) London: EarthScan.

Flores, E. S., Olivas, A. G., & Chávez, J. (2008). Land cover change and landscape dynamics in the urbanizing area of a Mexican border city. *ASPRS 2008 Annual Conference, 28 April-2 May, 2008*. Portland, Oregon. (pp. 1-9).

Frey, C. M. & Parlow, E. (2009). Geometry effect on the estimation of band reflectance in an urban area. *Theoretical and Applied Climatology*, 96, 395-406.

Frey, C. M., Rigo, G., & Parlow, E. (2007). Urban radiation balance of two coastal cities in a hot and dry environment, *International Journal of Remote Sensing, 28(12)*, 2695 2712. http://dx.doi.org/10.1080/01431160600993389.

Hamdi, R., & Schayes, G. (2009). Sensitivity study of the urban heat island intensity to urban characteristics. *The seventh International Conference on Urban Climate, 29 June - 3 July*. Yokohama, Japan.

Hu, L., & Brunsell, N.A. (2013). The impact of temporal aggregation of land surface temperature data for surface urban heat island (SUHI) monitoring. *Remote Sensing of Environment, 134*, 162–174. http://dx.doi.org/10.1016/j.rse.2013.02.022.

Imhoff, M.L., Zhang, P., Wolfe, R.E., & Bounoua, L. (2010). Remote sensing of the urban heat island effect across biomes in the continental USA. *Remote Sensing of Environment, 114*, 504–513. http://dx.doi.org/10.1016/j.rse.2009.10.008.

Jensen, J. R. (2005). *Introductory digital image processing a remote sensing perspective* (3rd ed.). USA: Prentice Hall Series in geographic information science.

Ji, C. Y., Liu, Q., Sun, D., Wang, S., Lin, P., & Li, X. (2001). Monitoring urban expansion with remote sensing in China. *International Journal of Remote Sensing, 22(8)*, 1441–1455.
doi: 10.1080/01431160117207.

Jin, M. (2004). Analysis of land skin temperature using AVHRR observations. *Bulletin of the American meteorological society, 85*, 587- 600. doi: 10.1175/BAMS-85-4-587.

Jin, M., & Liang, S. (2006). An improved land surface emissivity parameter for land surface models using global remote sensing observations. *American Meteorological Society, 19*, 2867- 2881. http://dx.doi.org/10.1175/JCLI3720.1.

Johansson, E., & Emmanuel, R. (2006). The influence of urban design on outdoor thermal comfort in the Hot Humid City of Colombo, Sri Lanka. *International Journal of Biometeorology, 51*, 119-133. doi: 10.1007/s00484-006-0047-6.

Kato, S., Matsunaga, T., & Yamaguchi, Y. (2010). Influence of shade on surface temperature in an urban estimated by ASTER data. *International Archives of the Photogrammetry, Remote Sensing and Spatial Information Science, 38*, 925–929.

Kayadibi, O. (2011). Evaluation of imaging spectroscopy and atmospheric correction of multispectral images (Aster and Landsat 7 ETM+). *Proceedings, 5th Int. Conf. Recent Advances in Space Technologies (RAST),9-11 June.*, Istanbul. pp. 154–159. doi: 10.1109/RAST.2011.5966811

Lazzarini, M., Marpu, P.R., & Ghedira, H. (2013). Temperature-land cover interactions: The inversion of urban heat island phenomenon in desert city areas. *Remote Sensing of Environment, 130*, 136–152. http://dx.doi.org/10.1016/j.rse.2012.11.007

Li, Z.L., Tang, B.H., Wu, H., Ren, H., Yan, G., Wan, Z., Trigo, I.F., & Sobrino, J.A. (2013). Satellite-derived land surface temperature: Current status and perspectives.

Remote Sensing of Environment, 131, 14–37.
http://dx.doi.org/10.1016/j.rse.2012.12.008.

Liang, S. (2000). Narrowband to broadband conversions of land surface albedo I Algorithms. *Remote Sensing of Environment, 76,* 213– 238.

Littlefair, P.J., Santamouris, M., Alvarez, S., Dupagne, A., Hall, D., Teller, J., et al. (2000). *Environmental site layout planning: solar access, microclimate and passive cooling in urban areas* (1st ed.). Watford: CRC.

Lo, C. P., & Choi, J. (2004). A hybrid approach to urban land use/cover mapping using Landsat 7 Enhanced Thematic Mapper Plus (ETM+) images. *International Journal of Remote Sensing, 25(14),* 2687–2700. http://dx.doi.org/10.1080/01431160310001618428.

Lougeay, R., Brazel, A., & Hubble, M. (1996). Monitoring intraurban temperature patterns and associated land cover in Phoenix, Arizona using Landsat thermal data. *Geocarto International, 11(4),* 79-90. doi: 10.1080/10106049609354564.

Mackey, C.W., Lee, X., & Smith, R.B. (2012). Remotely sensing the cooling effects of city scale efforts to reduce urban heat island. *Building and Environment, 49,* 348-358. http://dx.doi.org/10.1016/j.buildenv.2011.08.004.

Malaret, E., Bartolucci, L.A., Lozano, D.F., Anuta, P.E., & McGillem, C.D. (1985). Landsat-4 and Landsat-5 Thematic Mapper data quality analysis. *Photogrammetric Engineering and Remote Sensing, 51,* 1407–1416.

Martin, J., Kurc, S.A., Zaimes, G., Crimmins, M., Hutmacher, A., & Green, D. (2012). Elevated air temperatures in riparian ecosystems along ephemeral streams: The role of housing density. *Journal of Arid Environments, 84,* 9-18. http://dx.doi.org/10.1016/j.jaridenv.2012.03.019.

NASA (2009). http://www.nasa.gov/mission_pages/terra/news/heat-islands.html. Edited by Carlowicz, M. (accessed April 3rd, 2014).

Nassar, A.K., Blackburn, G.A., & Whyatt, J.D. (2014). Developing the desert: The pace and process of urban growth in Dubai. *Computers, Environment and Urban Systems, 45,* 50–62. http://dx.doi.org/10.1016/j.compenvurbsys.2014.02.005.

National Bureau of Statistics (2010). UAE Population by Emirates, Nationality and Sex. http://www.uaestatistics.gov.ae/ReportDetailsEnglish/tabid/121/Default.aspx?ItemId=1 869&PTID=104&MenuId=1. (accessed Mar 21, 2012)

Nichol, J. E., & Hang, T. P. (2012). Temporal characteristics of thermal satellite images for urban heat stress and heat island mapping. *ISPRS Journal of Photogrammetry and Remote Sensing*, 74, 153–162. http://dx.doi.org/10.1016/j.isprsjprs.2012.09.007

Omran, E.E. (2012). Detection of land-use and surface temperature change at different resolutions. *Journal of Geographic Information System, 4,* 189-203. http://dx.doi.org/10.4236/jgis.2012.43024.

Otterman, J., & Fraser, R.S. (1976). Earth-atmosphere system and surface reflectivities in arid regions from Landsat MSS data. *Remote Sensing of Environment, 5,* 247-266. http://dx.doi.org/10.1016/0034-4257(76)90054-7.

Physics Hypertextbook (2014). http://physics.info/heat-sensible/ (accessed Feb 1st, 2014)

Qin, Z., Karnieli, A., & Berliner, P. (2001). A mono-window algorithm for retrieving land surface temperature from Landsat TM data and its application to the Israel-Egypt border region. *International Journal of Remote Sensing, 22*, 3719–3746. doi: 10.1080/01431160010006971.

Rajasekar, U., & Weng, Q (2009). Urban heat island monitoring and analysis using a non-parametric model: A case study of Indianapolis. *ISPRS Journal of Photogrammetry and Remote Sensing, 64*, 86-96. doi:10.1016/j.isprsjprs.2008.05.002.

Rogerson, P.A. (2006). *Statistical Methods for Geography: A Students Guide* (2nd ed.). London: Sage Publications.

Román, M. O., Gatebe, C. K., Shuai, Y., Wang, Z., Gao, F., Masek, J., et al. (2013).Use of in-situ and airborne multiangle data to assess MODIS- and Landsat-based estimates of directional reflectance and albedo. *IEEE Transactions on Geoscience and Remote Sensing, 51(3)*, 1393–1404.

Schmugge, T., Frencha, A., Ritchiea, J.C., Rangoa, A., & Pelgrum, H. (2002). Temperature and emissivity separation from multispectral thermal infrared observations. *Remote Sensing of Environment, 79*, 189 – 198.

Seto, K. C., Woodcock, C. E., Song, C., Huang, X., Lu, J., & Kaufmann, R. K. (2002). Monitoring land-use change in the Pearl River Delta using Landsat TM. *International Journal of Remote Sensing, 23(10)*, 1985–2004. doi:10.1080/01431160110075532.

Skyscraper center. (2014). http://www.skyscrapercenter.com/ (accessed Jan 2, 2014).

Snyder, W.C., Wan, Z., Zhang, Y., & Feng, Y.Z. (1998). Classification-based emissivity for land surface temperature measurement from space. *International Journal of Remote Sensing,19 (14)*, 2753-2774. doi:10.1080/014311698214497

Sobrino, J. A., Jiménez-Muñoz, J. C., & Paolini, L. (2004). Land surface temperature retrieval from LANDSAT TM5. *Remote Sensing of Environment, 90(4)*, 434–440. http://dx.doi.org/10.1016/j.rse.2004.02.003

Stathopoulou, M., Cartalis, C., & Petrakis, M. (2007). Integrating Corine Land Cover data and Landsat TM for surface emissivity definition: application to the urban area of Athens, Greece. *International Journal of Remote Sensing, 28(15)*, 3291-3304. doi: 10.1080/01431160600993421.

Stewart, D. J., Yin, Z. Y., Bullard, S. M., & MacLachlan, J. T. (2004). Assessing the spatial structure of urban and population growth in the Greater Cairo Area, Egypt: A GIS and imagery analysis approach. *Urban Studies, 41(1)*, 95–116. http://dx.doi.org/10.1080/0042098032000155704.

Verbyla, D. L., & Hammond, T. O. (1995). Conservative bias in classification accuracy assessment due to pixel-by-pixel comparison of classified images with reference grids. *International Journal of Remote Sensing, 16*, 581–587. http://dx.doi.org/10.1080/01431169508954424.

Voogt, J.R., & Oke, T.R. (2003). Thermal remote sensing of urban climates. *Remote Sensing of Environment*, 86(3), 370-384. http://dx.doi.org/10.1016/S0034-4257(03)00079-8.

Weng, Q. (2001). A remote sensing-GIS evaluation of urban expansion and its impact on surface temperature in the Zhujiang Delta, China. *International Journal of Remote Sensing, 22*, 1999–2014. doi: 10.1080/713860788.

Wu, C., Lung, S. C., Jan , F.(2013). Development of a 3-D urbanization index using digital

terrain models for surface urban heat island effects. *ISPRS Journal of Photogrammetry and Remote Sensing*, 81, 1–11. http://dx.doi.org/10.1016/j.isprsjprs.2013.03.009

Yagoub, M. (2004). Monitoring of urban growth of a desert city through remote sensing: Al-Ain, UAE, between 1976 and 2000. *International Journal of Remote Sensing, 25(6),* 1063–1076. http://dx.doi.org/10.1080/0143116031000156792.

Yuan, F., & Bauer, M.E. (2007). Comparison of impervious surface area and normalized difference vegetation index as indicators of surface urban heat island effects in Landsat imagery. *Remote Sensing of Environment, 106,* 375–386. http://dx.doi.org/10.1016/j.rse.2006.09.003.

Zhao, W., Tamura, M., & Takahashi, H. (2001). Atmospheric and spectral corrections for estimating surface albedo from satellite data using 6S code. *Remote Sensing of Environment, 76,* 202 – 212. http://dx.doi.org/10.1016/S0034-4257(00)00204-2.

Zhou, L., Dickinson, R.E., Tian, Y., Jin, M., Ogawa, K., Yu, H., et al.. (2003). A sensitivity study of climate and energy balance simulations with use of satellite derived emissivity data over Northern Africa and the Arabian Peninsula. *J. Geophys. Res., 108 (D24).* doi:10.1029/2003JD004083.

Chapter 6 Dynamics and controls of urban heat sink and island phenomena in a desert city: development of a local climate zone scheme using remotely-sensed inputs

Ahmed K. Nassar, G. Alan Blackburn and J. J. Duncan Whyatt

Lancaster Environment Centre, Lancaster University, Lancaster, UK

Statement of Authorship

I, Ahmed K. Nassar, in my capacity as the first author of the above publication researched, acquired, processed and compiled all data used in this paper. I carried out the various statistical analyses undertaken in this research, analysed the results and drafted the manuscript, which includes the preparation of all figures and tables. This constitutes approximately 85% of the work involved with this publication.

Please find herein signatures of the co-authors confirming my contribution as described above to the paper.

Yours sincerely,

Ahmed Khalaf Nassar

Signature   Ahmed Khala/

Co- authors:

Name   G. Alan Blackburn

Signature

Name   J. Duncan Whyatt

Signature
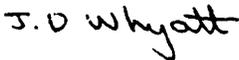
Context

Following the findings concerning the importance of the urban geometry in developing the urban heat sink in Dubai in the previous chapter, this chapter focuses more specifically on the impact of urban geometry and proximity to water on both daytime urban heat sink and night time urban heat island phenomena

Local Climate Zones (LCZ) schema which have previously been to assess air temperature variations across cities have been employed here to characterize the urban environment in Dubai based on a number of geometric parameters. The LCZs are then used to investigate diurnal and seasonal thermal variations across the city using MODIS imagery as opposed to conventional ground-based measurements of temperature. In addition, multivariate analysis techniques are used to better understand the combined impacts of urban geometry and proximity to water on variations of land surface temperatures during different times of the day.

Although the imagery generated by MODIS has relatively low spatial resolution, its temporal resolution provided the opportunity to assess spatial and temporal variations in land surface temperature four times daily, providing greater insights into the characterstics of urban heat sinks and urban heat islands than would have been possible using thermal imagery from other sensors (see section 3.5 for full specifications of MODIS thermal sensors compared to other sensors).

The findings of this study provide a better understanding the impacts of urban geometry and proximity to water on both urban heat sink and urban heat island phenomena in coastal desert environments.

6.1 Introduction

The term "Urban Heat Island (UHI)" is defined as the difference in temperature measurements between urban and rural areas (Stewart and Oke, 2012). It is mostly associated with air temperature data collected from mobile traverses or weather stations 2 meters above ground level (Emmanuel & Kruger, 2012; Pichierri et al., 2012). However, with the advent of thermal infrared (TIR) remote sensing technology, more UHI studies have been employed to investigate surface UHI (SUHI) based on differences in land surface temperature (LST) from various space-borne TIR sensors. Data from space-borne TIR sensors cover larger spatial extents and retrieve temperature measurements for each pixel much more rapidly and cost-effectively than conventional ground-based measurements. Furthermore, remotely-sensed TIR data is particularly useful in areas where the weather stations are sparse or absent altogether (Knight et al., 2010). Although LST is not identical to air temperature, as the former is usually warmer than air temperature especially during the summer and winter months (US EPA, 2008a; Yuan & Bauer, 2007), a study by Coutts and Harris (2012) revealed that trends in LST derived from remotely sensed imagery were relatively similar to trends in air temperature, albeit with differences in absolute values for the city of Melbourne.

With the availability of various TIR sensors on board different satellite platforms, a choice has to be made between using thermal data at high spatial resolution or high temporal resolution. Similarly, a choice has to be made between using a thermal sensor that operates at day and/or one that operates at night. For example, Landsat 8 and ASTER sensors provide medium spatial resolution thermal data (100m and 90m respectively) over a relatively long revisit time (16 days) whilst MODIS and AVHRR sensors provide coarser

resolution thermal data (1km) over short revisit times of less than 24 hours. It is currently unfeasible to estimate LST at both high spatial and temporal resolution (Sattari & Hashim, 2014).

Various satellites and thermal instruments have been used in SUHI studies: Advanced Very High Resolution Radiometer (AVHRR) images have been used at local scales (e.g. Streutker, 2003) and global scales (e.g. Jin, 2004); MODIS data have been used at local scales (e.g. Lazzarini et al., 2013), at continental scales (e.g. Imhoff et al., 2010) and at global scales (e.g. Jin & Dickinson, 2010). However, medium resolution TIR sensors such as Landsat TM (e.g. Sobrino et al., 2004), ETM+ (e.g. Li et al., 2012) and ASTER (e.g. Nichol et al., 2009) have been primarily used at local scales.

While many factors affect the formation of SUHI and its intensity such as local weather conditions and geographical location, the major contributor is urbanization where the natural land cover type is replaced by impervious surfaces (e.g. Imhoff et al., 2010; Rhee et al., 2014; Weng, 2001). As a consequence of urbanization, the evapotranspiration, thermal properties and wind flow of the landscape is altered, which can lead to an increase in surface temperatures in cities (Kato & Yamaguchi, 2005; US EPA, 2008a). The increase in impervious surfaces leads to the increase of absorption of solar energy and its conversion to sensible heat rather than latent heat. This is evident when compared to rural areas through the increase of heat storage in urban areas from the combination of two properties: thermal conductivity and heat capacity (Gartland, 2008; Obiakor, 2012).

In desert environments, SUHI is observed during the night while the surface urban heat sink (SUHS) phenomenon is observed throughout the morning (Frey et al., 2007; Lazzarini et al., 2013). Previous remote sensing studies in desert cities have focused on

investigating the direct relationship between land surface temperature and surface cover (i.e., impervious surface and vegetation) in a two-dimensional perspective (Frey et al., 2007; Lazzarini et al., 2013). However, no research has thoroughly examined the effects of the three-dimensional urban geometry on the formation of SUHS and SUHI in desert cities. Indeed, urban geometry is considered a significant factor in determining the temperature distribution within cities (Unger, 2009; Voogt & Oke, 2003). A detailed investigation of the effects of urban geometry and land cover type on the surface temperature variations in Dubai is motivated by previous studies in desert cities that have found that even areas lacking vegetation and containing large proportions of impervious surfaces exhibit lower surface temperatures than surrounding rural areas (Frey et al., 2007, Imhoff et al., 2010). Proximity to large water bodies has also not been considered in previous studies of UHI in coastal desert cities (Frey et al., 2007; Lazzarini et al., 2013) in spite of its importance (e.g. Coseo & Larsen, 2014).

6.1.1 Local Climate Zones in the urban environment

Stewart and Oke (2012) developed a climate-based classification system called 'local climate zones' (LCZs) in order to standardize the classification and sampling of field sites in urban heat island studies and facilitate the comparison between several sites within the urban landscape. Typically, the study area is classified into a number of LCZs, each with a diameter ranging from hundreds of meters to several kilometres that share relatively similar geometry and land cover types.

A recent study by Stewart et al. (2014) based on three temperate cities concluded that thermal contrasts do exist among different LCZs and are governed primarily by urban

168

geometry, tree heights and pervious surfaces thus the LCZ system was deemed useful to investigate the UHI among various locations within the cities. The system is categorized into 17 LCZs based on their geometrical, land cover and heat emission characteristics (Table 6.1). These classes are categorized according to their geometrical properties: sky view factor (SVF), aspect ratio (h/w), building surface fraction (BSF) and height of roughness elements (HRE). They are also categorized according to their land cover properties: impervious surface fraction (ISF) and pervious surface fraction (PSF). The classes are also categorized according to their thermal, radiative, and metabolic properties such as surface admittance and anthropogenic heat output. For the full list of properties of each LCZ consult Stewart and Oke (2012, p1885-1887).

Several UHI studies have adopted this classification system based on air temperature measurements using fixed or mobile weather stations and the findings are in favour of this classification method (Alexander & Mills, 2014; Leconte et al., 2015; Siu & Hart, 2013; Unger et al., 2014). This study aims to utilize the LCZ classification schema to characterize the urban environment in Dubai then use the resulting LCZs to explore spatial and temporal differences in LST from the MODIS TIR imagery

Table 6.1 LCZ classification system (source: Stewart et al., 2014; p. 1063)

Urban classes	LCZ code	Land cover classes	LCZ code
Compact high-rise	LCZ 1	Dense trees	LCZ A
Compact mid-rise	LCZ 2	Scattered trees	LCZ B
Compact low-rise	LCZ 3	Bush, scrub	LCZ C
Open high-rise	LCZ 4	Low plants	LCZ D
Open mid-rise	LCZ 5	Bare rock or paved	LCZ E
Open low-rise	LCZ 6	Bare soil or sand	LCZ F
Lightweight low-rise	LCZ 7	Water	LCZ G
Large low-rise	LCZ 8		
Sparsely built	LCZ 9		
Heavy industry	LCZ 10		

6.1.2 Aim and objectives

This study aims to examine the use of the local climate zones classification system using remote sensing inputs rather than air temperature measurements. Specifically, the following three objectives are investigated: (i) to develop a technique to classify Dubai into LCZs in accordance with LCZ classification schema; (ii) to study the diurnal dynamics of SUHS and SUHI throughout the four seasons based on Dubai's LCZs; and (iii) to investigate the impact of eight physical variables (related to urban geometry, proximity to the Arabian Gulf and land cover properties) on the LST variations diurnally and seasonally.

6.2 Study Area

Situated on the Arabian Gulf, Dubai emirate (25°16N, 55°20'E) is considered one of the fastest growing cities in the Middle East and has been transformed into a city of global stature (Elsheshtawy, 2010). The total administration area of the emirate before the development of the islands was 3885 km^2 and the population reached 2,213,000 inhabitants in 2013 (Dubai Statistical Centre, 2013).

Dubai Creek divides the city into Deira to the east and Bur Dubai to the west forming bi-central districts comprising of high density buildings. Bur Dubai is generally known for its modern high-rise buildings, however, low-rise to mid-rise building blocks are spreading in both directions from the Creek. In the last two decades, the physical size of the urban area has grown dramatically both horizontally and vertically and the desert has been transformed into residential, commercial, sports and tourism projects. The total urban area has increased horizontally to approximately 560 km^2 in year 2011 (Nassar et al., 2014) while vertically, the Skyscraper Center (2014) stated that 96 buildings in Dubai are above

150m tall. In 2011, approximately 14% of the Emirate was covered by impermeable surfaces (buildings, roads, walking-ways and parking lots) and 1.1% by vegetation (Nassar et al., 2011).

Due to the diversity of building heights in Dubai and systematic urban planning processes, large discrete blocks of different urban land use types and building heights have been created, making this an interesting study site for investigating the impact of urban geometry on SUHS and SUHI. For example, residential areas are usually comprised of low to mid rise buildings; mixed land use areas are usually comprised of mid to high rise buildings while industrial areas are comprised of low-rise buildings.

Dubai is built upon flat terrain and experiences a hot and arid climate. Desert sand is the main land cover type in the emirate. Based on a report in 2013 (Dubai Statistical Centre, 2014), the warmest months in Dubai are July and August with an average maximum temperature of 43°C and an average minimum of 33°C. The coldest months are January and February with an average maximum temperature of 25.5°C and an average minimum of 16°C.

Our specific study area covers the main urban areas in Dubai which consists of a variety of urban structures, configurations, and land cover types with an area of 450km^2 (Fig. 6.1). The study area was also chosen based on the availability of building footprint data for the city which will be used later to compute urban geometry parameters. Furthermore, the study area has been designed to exclude the coastal strip (1km) in order to avoid the land-water mixed pixel problem which is a confounding factor in thermal studies of coastal regions (Lazzarini et al., 2013).

171

Figure 6.1 Overview map of the study area and the Arabian Gulf, Dubai based on a Landsat 8 scene from 2013 acquired from USGS.

6.3 Materials and Methods

To achieve the aims and objectives of the study, the following steps were taken: (1) derivation of urban geometry and land cover parameters from several datasets, (2) creation of LCZs based on the derived parameters according to the LCZ classification scheme, (3) LST retrieval using Dubai's LCZs based on day and night time satellite images, (4) investigation of the SUHI and SUHS intensities diurnally and seasonally, and (5) determination of the relationships between eight physical variables and the seasonal LST variations during day and night time. The schema in Figure 6.2 lists the major steps of the methodology.

172
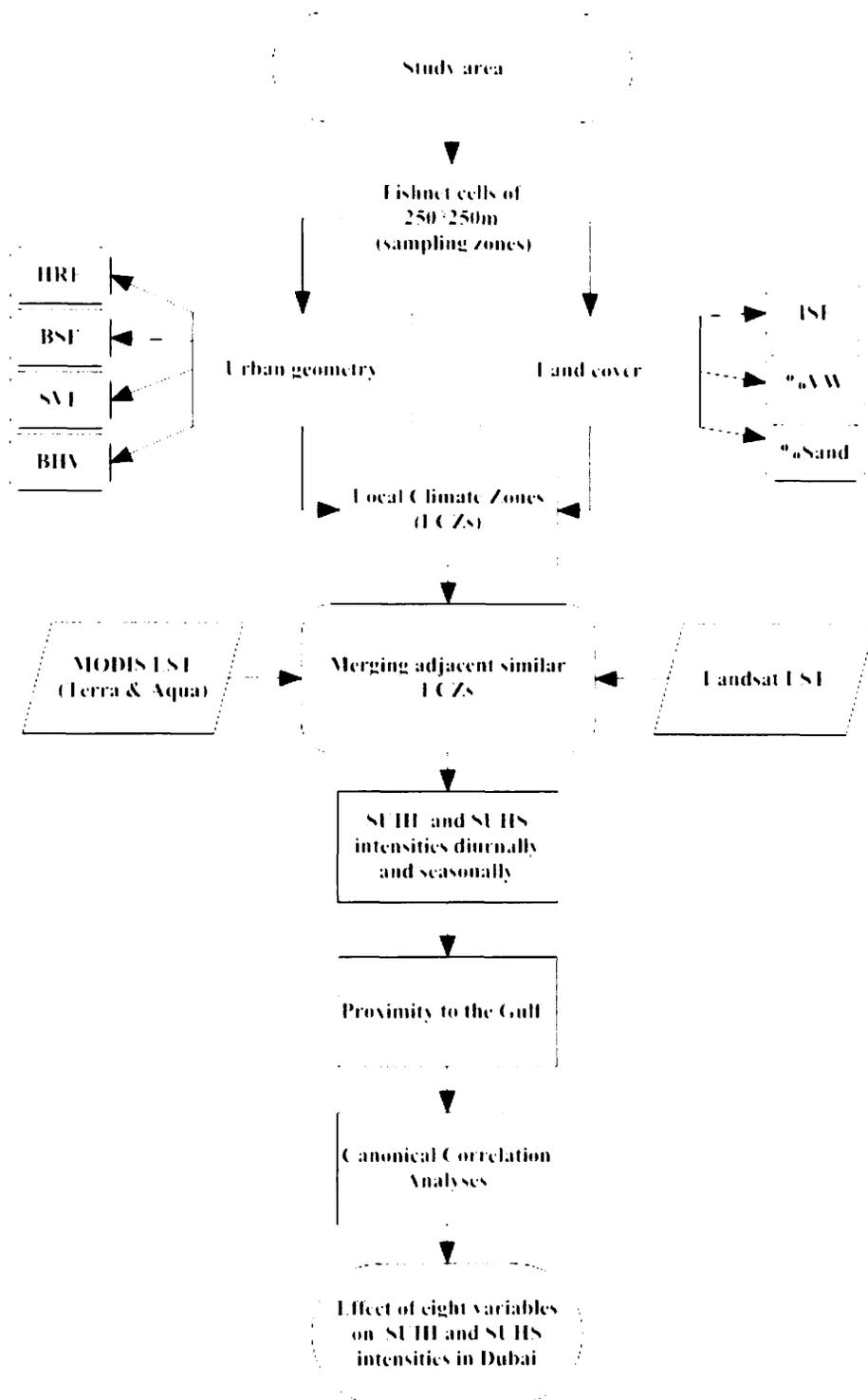
Figure 6.2 Flowchart showing the main stages of LCZs selection process and analysis. HRE: heights of roughness elements, BSF: building surface fraction, SVF: sky view factor, BHV: building height variations, ISF: impervious surface fraction, and %VW: vegetation and water percentage.

6.3.1 Local Climate Zone parameters

Based on the parameters used to classify LCZs in Stewart and Oke (2012) and other parameters used in previous UHI studies, we determined eight different parameters based on the availability of datasets for Dubai. Six parameters relating to urban geometry and land cover type were utilized from the Stewart and Oke classification system (2012). In their system, Pervious Surface Fraction (PSF) is considered a single parameter, however, this parameter actually combines three pervious surfaces: vegetation, water and bare soil, each of which has a different effect on surface temperature. Therefore, in our study, this parameter has been divided into two separate parameters: vegetation/water (VW) and sand. In Dubai, inland water does not play an important role in SUHI intensity due to its very limited coverage; therefore it has been combined with vegetation. On the other hand, sand might play an important role in surface thermal difference due to its large coverage as the main cover type in desert cities.

In addition, we added a building height variations (BHV) parameter because a group of buildings with varying heights tends to increase wind circulation within urban areas which helps in air and surface cooling (Johansson & Emmanuel, 2006). Furthermore, Coseo and Larsen (2014) have used proximity to Lake Michigan to study the UHI intensity in several locations across the city. For example, coastal urban areas that are close to large bodies of water tend to have lower UHI intensity. This is because cold breezes that are generated from water bodies convect heat away from urban surfaces, thus potentially mitigating the effects of UHI in cities (Oda & Kanda, 2009; US EPA, 2008a). However, the sea breeze system is pronounced specifically during daytime due to the difference in air pressure between land and water caused by the variation in surface temperatures. At night

time an inverse land breeze system is formed (Freitas et al., 2007). For this reason, this parameter was also deemed important for Dubai due to the presence of the Arabian Gulf.

In order to compute urban geometry parameters we utilized a vector format buildings database for Dubai which contains individual building 'footprints' (polygons) and associated attributes (including height) acquired from Dubai Municipality. Using these data four parameters were computed: SVF, HRE, BHV and BSF.

SVF (Sky View Factor) is a widely used parameter in urban thermal studies and is considered as an essential controlling factor of the UHI effect. It represents a dimensionless quantity of visible sky (Hwang et al., 2011). This parameter represents the amount of solar radiation that reaches or leaves the surface, thus has an impact of surface cooling and heating during the day and night (Heldens et al., 2013). This geometric variable is preferred over other geometric variables such as the aspect ratio (H/W) because it can describe the complex urban environment more efficiently (Johnson & Watson, 1984). Although many methods have been used to compute SVF, ranging from fish-eye photos to computer modeling software, the vast majority of these methods rely on computing SVF for specific locations excluding building rooftops from the calculation. Since this study examines the impact of SVF on the SUHI from a remote sensing perspective, the value for each ground and rooftop pixel should be computed. For this reason, the SVF was computed using a computer modeling program developed by Zaksek et al. (2011). Using the three dimensional data as an input, a continuous SVF map for the entire urban environment was generated at 1m pixel resolution. The SVF is stored for each pixel with values ranging from 0-1 (0 represents pixels that cannot see the sky while 1 represents pixel that can see the sky) (Fig. 6.3).

Figure 6.3 Sky view factor of a small sample area in Dubai at 1m resolution using a raster based model.

HRE (heights of roughness elements) is defined as the geometric heights of building and trees in meters. Tree heights were excluded from this parameter because these data were unavailable and because there are few trees in Dubai in any case with the exception of parks and farms.. The BHV parameter is computed based on the variation or dispersion of building heights in a given area compared to the mean for that area. The higher the value, the greater the variation in height, with zero representing buildings of uniform height. The standard deviation is used because it is a more reliable measure of variation, and is less susceptible to outliers. Finally, BSF (building surface fraction) is the horizontal area of

176

building footprints per unit area of ground that is computed using existing building footprints polygons.

6.3.2 Land Cover Parameters

In this study, three land cover parameters were employed using Dubai's high-resolution classified map (Source: Dubai's municipality). The roads, walkways and car parking lots were merged into one class of impervious surfaces (ISF) while vegetation and water were merged into a single class (%VW). Finally, the sand class was treated as a separate parameter (%Sand)

6.3.3 Land Surface Temperature Retrieval

In this study, LST data were retrieved from two satellites which have been widely used in thermal studies due to their favourable spatial and temporal resolution and zero cost of acquisition: (i) MODIS thermal bands with low spatial resolution of 1km with twice daily revisit time; (ii) Landsat 8 TIR bands with medium spatial resolution of 100m (resampled to 30 meters to match multispectral bands) and 16 day revisit time.

MODIS (Moderate Resolution Imaging Spectroradiometer) is the instrument on board the Terra (Launched in late 1999) and Aqua (launched in mid-2002) satellites. Terra and Aqua orbits generate different overpass times. Terra passes Dubai in the morning at 1030 a.m. (Gulf Standard Time; GST) and in the evening at 1030 p.m. (GST). However, Aqua passes Dubai in the afternoon at 0130 p.m. (GST) and after mid-night at 0130 a.m. (GST). MODIS data have been widely used in SUHI applications for local areas since the launch of the Terra satellite because both Terra and Aqua data are able to provide LST four times daily. This provides the opportunity to study the variations of SUHI in the the

177

morning, afternoon, evening, and late-night hours (e.g. Cui & Foy, 2012; Nichol, 2005). MODIS bands 31 and 32 are used to retrieve 1km LST data by using the generalized split-window algorithm which corrects both atmospheric effects and surface emissivity (Wan & Dozier, 1996). Eight-day composite 1km LST MODIS Terra (MOD11A2) and Aqua (MYD11A2) V5 products were acquired for year 2013. These LST data were derived from daily clear-sky 1km LST products MOD/MYD_11A1.

Landsat 8 was launched in early 2013. Images are available for Dubai from 13-April-2013 and the local crossing time is approximately 1045 a.m. (GST). Although the Landsat 8 TIRS has two spectrally adjacent thermal bands (bands 10 and 11) which are suitable for the split window techniques in atmospheric correction and LST retrieval, the Landsat scientists team does not recommend using band 11 in split-window techniques due to the larger calibration uncertainty associated with it (USGS, 2014). Thus, a single window technique based on band 10 is preferred at this stage. A total of 9 cloud free scenes were available between the periods of April to December 2013 and were acquired from the NASA archive. The single window method from Yuan and Bauer (2007) was used (equations 5.1, 5.2 and 5.3) to derive LST from TIR band 10 which takes into account the atmospheric parameters and surface emissivity. In the subsequent analysis only MODIS data have been used due to the limited number of Landsat scenes available (see Fig. 6.4 for an example of daytime LST derived from Landsat). Nevertheless, for the limited time period available, we have conducted equivalent analysis on the Landsat data and the results are effectively very similar to those derived from overlapping periods of MODIS Terra (1030 a.m.).
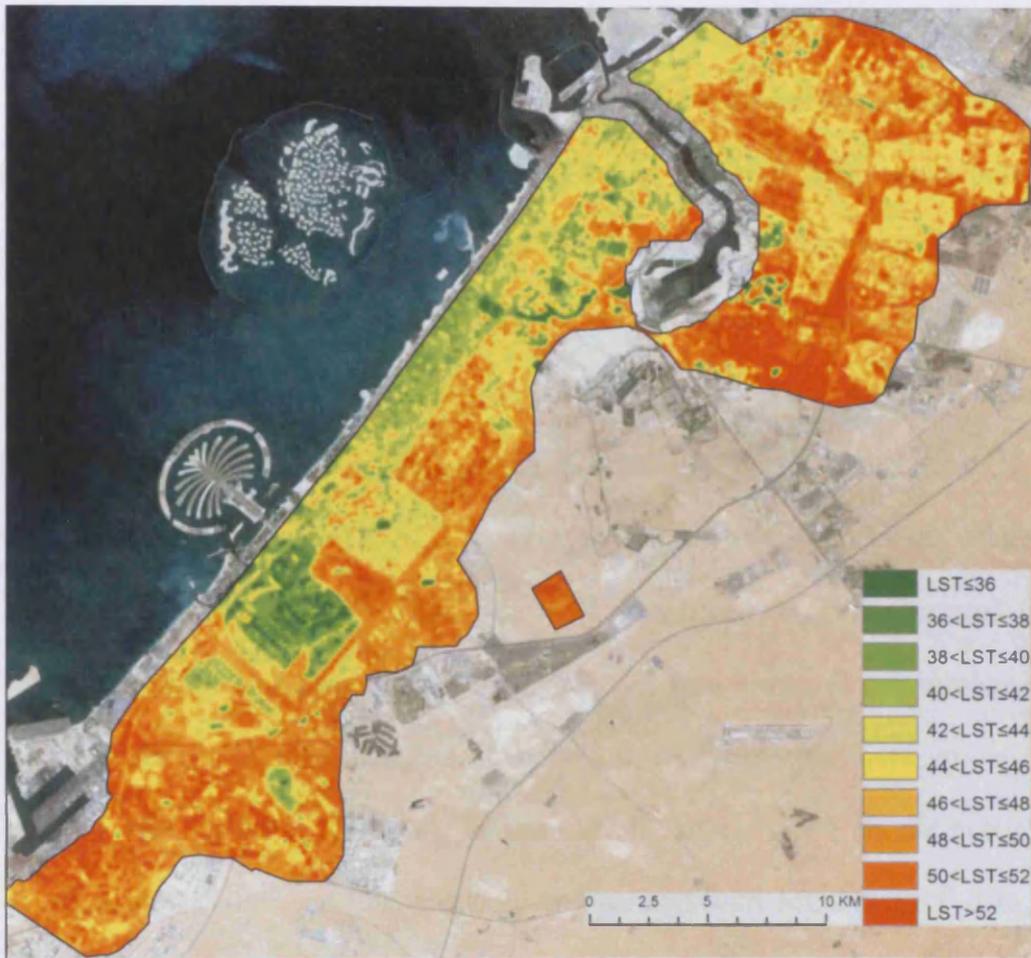
Figure 6.4 Example of daytime LST image for Dubai acquired July, 2013 using Landsat 8 TIR.

6.3.4 LCZs classification in Dubai & LCZs sampling technique

The study area (Fig. 6.1) was divided into a regular grid ('fishnet') with an area of 250*250m per cell. These were used to compute the geometry and land cover parameters for each cell in order to classify the study area into LCZs based on Stewart and Oke (2012) property values system. As a result, 6750 cells were produced including detached bare sand cells with an area of $4km^2$ to represent the main land cover type of Dubai (LCZ F). LCZ F is used for both LST normalization purpose and to represent the rural area.

Subsequently, the HRE parameter was set as the first main benchmark for LCZ classification and the average building heights within each cell were computed. As a result, these cells were categorized into three classes in terms of height according to the LCZ classification system: high-rise, midrise and low-rise cells. The BSF parameter was then used to categorize the cells in terms of compactness (open or compact). This was followed by a sequence of selection analyses based on the pervious surface classes using ISF and PSF (desert and vegetation with water) in order to categorize the percentages of these parameters in each cell. The SVF parameter was not employed in the selection process because in Stewart and Oke (2012) the SVF was based on SVF measured from ground observations. Nevertheless, the SVF for each cell was computed for subsequent analyses. Finally, adjacent cells of more than four cells of the same class were grouped together to comply with Stewart and Oke's recommendation that each LCZ should occupy an area of at least 500-1000m^2 and also to allow comparison with MODIS LST data at a spatial resolution of 1km^2. Based on the computed parameters, six LCZs were extracted from the study area (Fig. 6.5). The detailed list of Dubai's urban LCZs classification scheme characteristics in terms of configuration, land cover and construction materials is given in Tables 6.2 and 6.3.

Following the classification process, the average daytime and night-time LST from both Terra and Aqua was extracted for each LCZ. To study the magnitude of the SUHI amongst various LCZs, the differences between LST for the six urban LCZs (LCZ$_{1-6}$) and LST for rural area (LCZ$_F$; sand) were computed using equation (6.1) (Stewart et al.; 2014) :

$$\Delta_{SUHI} = LST\ LCZ\ _{1-6} - LST\ LCZ_F \qquad (6.1)$$

Where, LST LCZ$_{1-6}$ is the average surface temperature for each urban LCZ and LST LCZ$_F$ is the average surface temperature for the sand zone.

Figure 6.5 The fishnet of 250*250m cells and the obtained LCZ map of Dubai with Landsat 8 scene from 2013 is displayed in the background. CMR= large low-rise large low-rise large low-rise, LLR= large low-rise, OHR= open high-rise, OLR= open low-rise, OMR= open mid-rise, SB= sparsely built.

Table 6.2 Geometry & land cover properties of LCZs of both Stewart and Oke, (2012) and a modified LCZs of Dubai.

LCZs	HRE (m)	HRE_Dubai	%BSF	BSF_Dubai	SVF	SVF_Dubai	%ISF	ISF_Dubai	%PSF	PSF_Dubai	BHV_Dubai	Proximity to the ocean (km)
CMR	10-25	18-25 (22)	40-70	49-64 (56)	0.3-0.6	0.70-0.80 (.73)	30-50	34-36 (35)	<20	02-16 (9)	5-8 (7)	1.5-3 (2.3)
OHR	>25	23-58 (44)	20-40	25-33 (29)	0.5-0.7	0.60-0.75 (.72)	30-40	32-39 (34)	30-40	32-41 (36)	12-20 (15)	1.6-5 (2.5)
OMR	10-25	12-23 (19.4)	20-40	21-34 (26)	0.5-0.8	0.70-0.85 (.76)	30-50	26-48 (33)	20-40	17-50 (41)	4-8 (6)	1-15 (7)
OLR	3-10	6-12 (8)	20-40	22-34 (27)	0.6-0.9	0.70-0.90 (.83)	20-50	17-29 (21)	30-60	41-57 (52)	3-5 (3.5)	1.1-13 (6)
LLR	3-10	5-9 (7)	30-50	35-51 (40)	>0.7	0.84-0.91 (.87)	40-50	46-53 (51)	<20	4-15 (9)	2-4 (2.9)	3-11 (7)
SB	3-10	6-11 (7.8)	10-20	13-19 (16)	>0.8	0.88-0.95 (.93)	<20	08-14 (10)	60-80	67-79 (74)	2 -4 (2.6)	2-14 (9)

Note. Numbers in brackets are the average values.

Table 6.3 Dubai's urban LCZs classification characteristics in terms of configuration, land cover and construction materials.

Urban local climate zones in Dubai	Configuration & land cover	Construction material
Compact midrise (LCZ 2)	Dense mix of midrise buildings with low-medium height variations and relatively narrow roads. Sparse or no pervious cover types.	Bricks, concrete, steel and some glass. Pavements of asphalt and concrete for roadways and walkways
Open high-rise (LCZ 4)	Open configuration of tall buildings with large height variations and wide roads. Plenty of pervious land covers of sand and some vegetation.	Comprised of mostly modern high-rise buildings made from glass, steel and other metal construction materials with mostly sharp edges.
Open midrise (LCZ 5)	Open configuration of midrise buildings with low-medium height variations. Plenty of pervious land covers of sand and some of vegetation and trees.	Bricks, concrete, steel and some glass. Pavements of asphalt and concrete for roadways and walkways.
Open low-rise (LCZ 6)	Open configuration of low-rise buildings with below medium height variations and narrow roads. Plenty of pervious land covers of sand and some vegetation and trees.	Found mostly in residential areas and made of bricks, stone and concrete. Pavements of asphalt, concrete and sand for roadways and walkways.
Large low-rise (LCZ 8)	Open configuration of large low-rise buildings with low height variations. Majority of paved land cover and no or very sparse vegetation.	Found mainly in industrial areas and made mostly of metal corrugated sheets and steel hangers. Pavements of asphalt and concrete for roadways and walkways.
Sparsely built (LCZ 9)	Sparse configuration of low rise buildings with low height variations. Abundance of sand as the major land cover type.	Found in residential areas and made of bricks, stone and concrete. Pavements of sand and some asphalt for roadways and walkways.
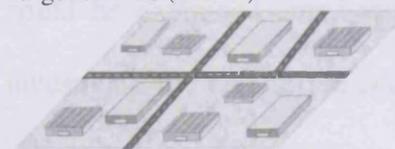
183

6.3.5 Multivariate Correlation Analysis

In order to investigate the factors influencing the LST variations amongst the different LCZs, we performed a canonical correlation analysis. Canonical correlation analysis is a multivariate analysis technique that is used to analyze the relationship between two sets of variables, a predictor set and a criterion set (Guarino, 2004). In the case of our study, this technique is used to investigate the impact of physical variables (surface geometry, land covers and proximity to water) on LST variations during daytime and night time.

Despite the similarities between canonical correlation and techniques such as bivariate and multiple regression analysis, the canonical correlation overcomes the limitations of other techniques (Tabachnick & Fidell, 2012). The bivariate technique can handle a relationship between two variables, while the canonical technique can handle two sets of variables. Furthermore, the major difference between the canonical technique and multiple regression analysis is that in the canonical the relationships between more than one variable as predictors and more than one variable as criteria could be examined simultaneously. Therefore, the canonical technique was used to investigate the correlation between a set of physical variables (8 variables) from one side and a set of temperatures variables (4 variables) from another side during the day and night for both Terra and Aqua. Both sets (predictor and criterion variables) were not independent, and the variables within each set were also related in some way. Given the characteristics of our data, the canonical correlation analysis seems the best suited method (Tabachnick & Fidell, 2012; p. 571).

6.4 Results

6.4.1 Dynamics of the surface urban heat island

Eight-day MODIS LST data for both Terra and Aqua have been analyzed by observing the temporal variation of LST amongst the six urban LCZs (LCZ_{1-6}) and the sandy desert zone (LCZ_F) in Dubai. Subsequently, the SUHI magnitude of each LCZ was computed based on the average LST difference using equation (6.1) (LCZ_{1-6}–LCZ_F). The objective is to investigate the trends of SUHS during daytime and SUHI during night-time at four times (morning, afternoon, evening and after mid-night) for Dubai's urban LCZs based on averaged 8-day, monthly and seasonally during the year 2013.

6.4.2 Daytime Surface Urban Heat Sink

The daytime LST variations detected by Terra at 1030 a.m. and Aqua at 0130 p.m. (GST) are shown in Figure 6.6 (based on the 8-day composite LST products) using LCZs over urban and sand zones in Dubai. The LST variations for both times were fairly consistent, with peaks of temperature observed especially during summer periods (June to August). However, the afternoon LST measurements are higher than mornings by 3-5 °C for all urban LCZs. The highest monthly average LST for urban LCZs was noted in August at 1030 a.m. and in July at 0130 p.m. Conversely, the lowest LST are noted during winter periods (January, February and December) with the afternoon measurements showing higher LST than mornings by 1-3°C. The lowest monthly average LST for urban LCZs was noted in January for both times. The sand LCZ shows

the highest LST values during most of the periods at both times with the highest values in the afternoon due to the acquisition of data during the peak sun hour.
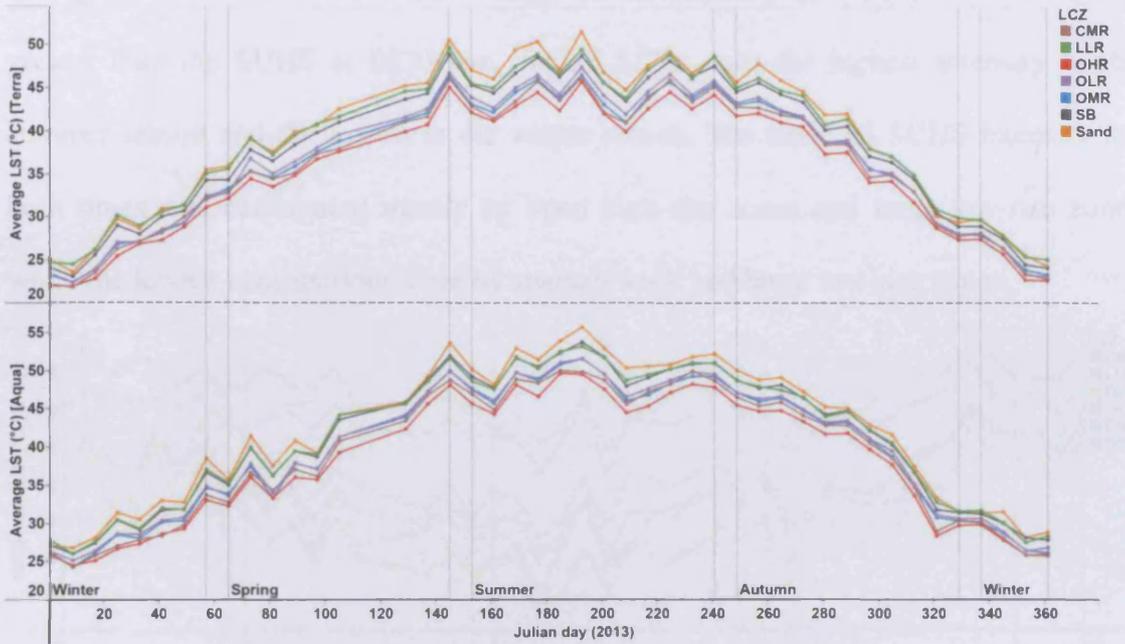
Figure 6.6 Daytime 8-day average LST variations amongst LCZs for Terra 1030 a.m. (above) and Aqua 0130 p.m. (below) GST, 2013.

In the analysis of the SUHI difference ($LCZ_{1-6} - LCZ_F$) at 1030 a.m. (Terra) and at 0130 p.m. (Aqua) (Fig. 6.7), a surface urban heat sink (SUHS) was noted during the daytime for the majority of urban LCZs. The LST values show lower temperatures than sand with the exception of some periods in both sparsely built and large low-rise zones. Furthermore, the monthly averaged data (Fig. 6.8) clearly indicates that SUHS contrasts do exist among all LCZ classes for both times with less contrast between sparsely built and large low-rise zones at 0130 p.m. It also shows that the highest SUHS intensity was noted in June at 1030 a.m. and in July at 0130 p.m. While the weakest SUHS intensities occurred mainly during cold months.

186

The analysis of the average seasonal magnitudes of SUHS for urban LCZs during both times is shown in Figure 6.9. With the exception of large low-rise zones during the summer, the seasonal average SUHS intensity at 1030 a.m. was slightly greater than the SUHS at 0130 p.m. for all LCZs with the highest intensity in the summer season and the lowest in the winter season. The seasonal SUHS intensity for both times was contributed mostly by open high-rise zones and large low-rise zones while the lowest contributions were by sparsely built and large low-rise zones.
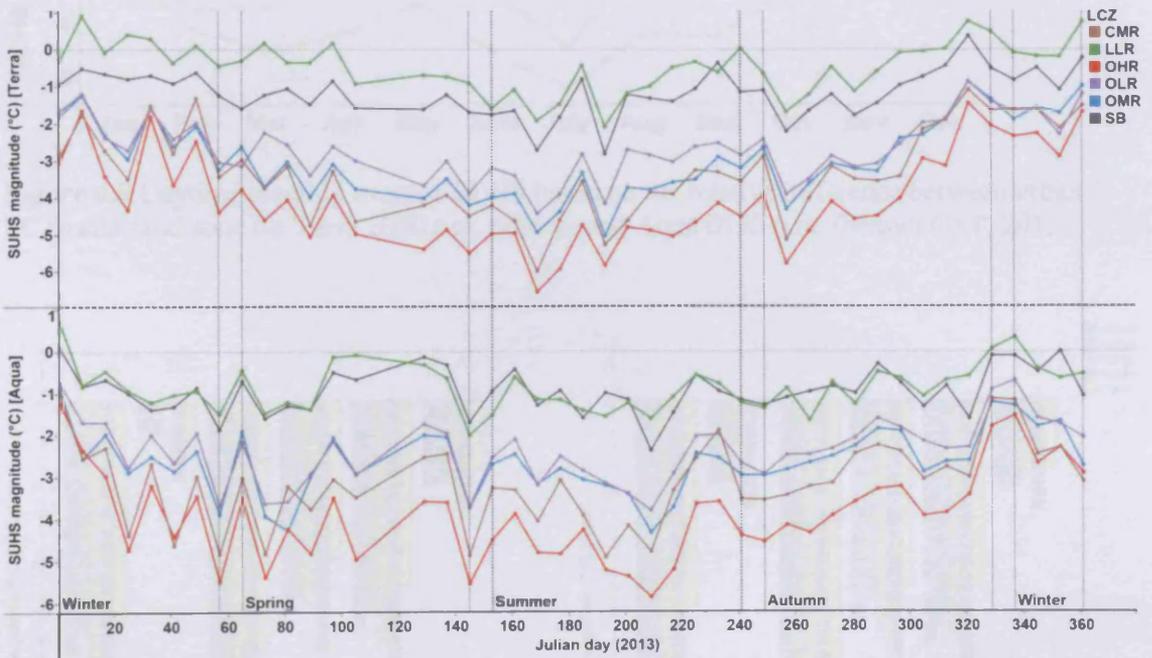
Figure 6.7 Daytime 8-day average SUHS based on the relative difference between urban LCZs and sand for Terra 1030 a.m. (above) and Aqua 0130 p.m. (below) GST, 2013.
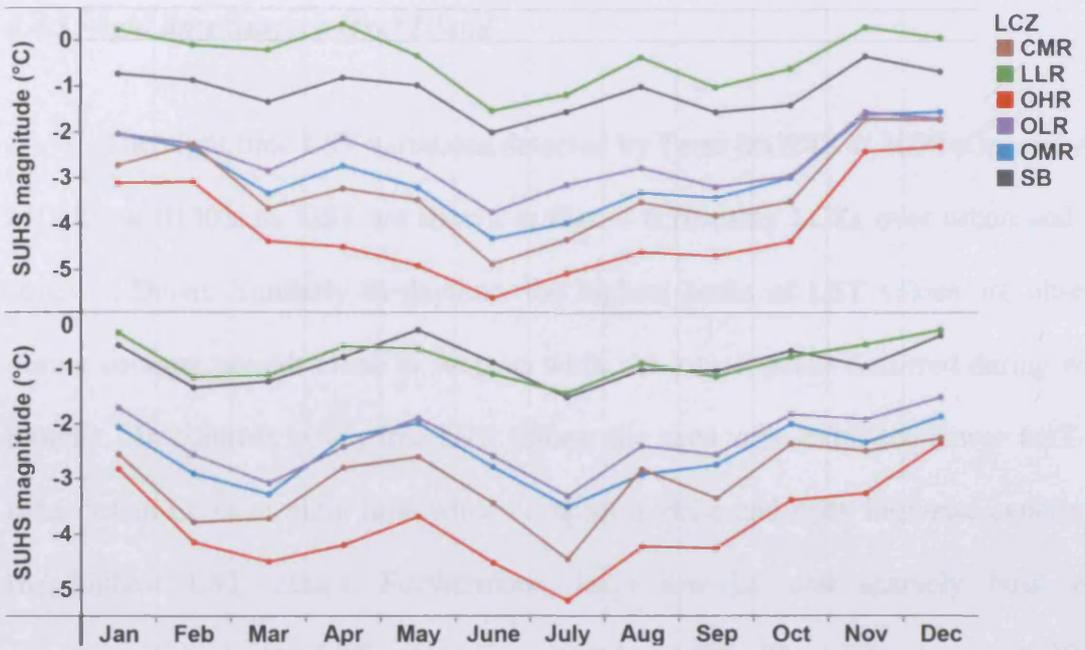
Figure 6.8 Daytime monthly average SUHS based on the relative difference between urban LCZs and sand zone for Terra 1030 a.m. (above) and Aqua 0130 p.m. (below) GST, 2013.
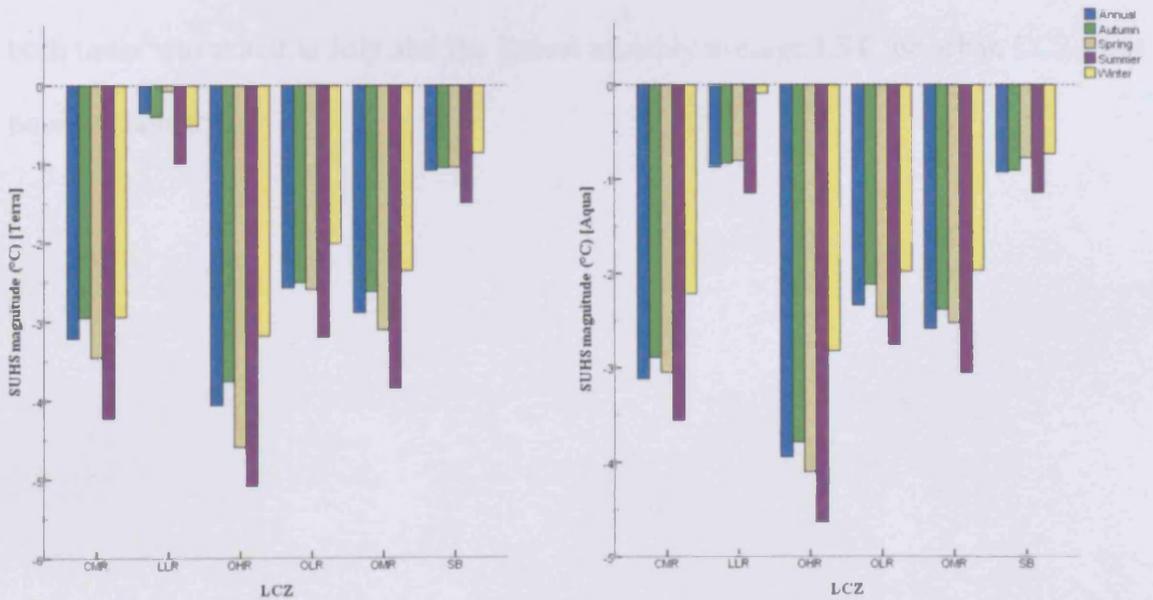
Figure 6.9 Daytime seasonal and annual average SUHS based on the relative difference between urban LCZs and sand for Terra 1030 a.m. (left) and Aqua 0130 p.m. (right) GST, 2013.

6.4.3 Night time Surface Heat Island

The night time LST variations detected by Terra MODIS at 1030 p.m. and Aqua MODIS at 0130 a.m. GST are shown in Figure 6.10 using LCZs over urban and sand zones in Dubai. Similarly to daytime, the highest peaks of LST values are observed during summer periods (June to August) while the lowest peaks occurred during winter months. In contrast to daytime LST values, the sand zone exhibited lower LST than other urban LCZs at night time while compact midrise and open high-rise experienced the highest LST values. Furthermore, large low-rise and sparsely built zones experienced the lowest LST values amongst urban LCZs. The LST values at 1030 p.m. were higher than the values at 0130 a.m. by 1-2.5°C during the summer months and 2-4°C during the winter months. The highest monthly average LST for urban LCZs in both times was noted in July and the lowest monthly average LST for urban LCZs was noted in January.
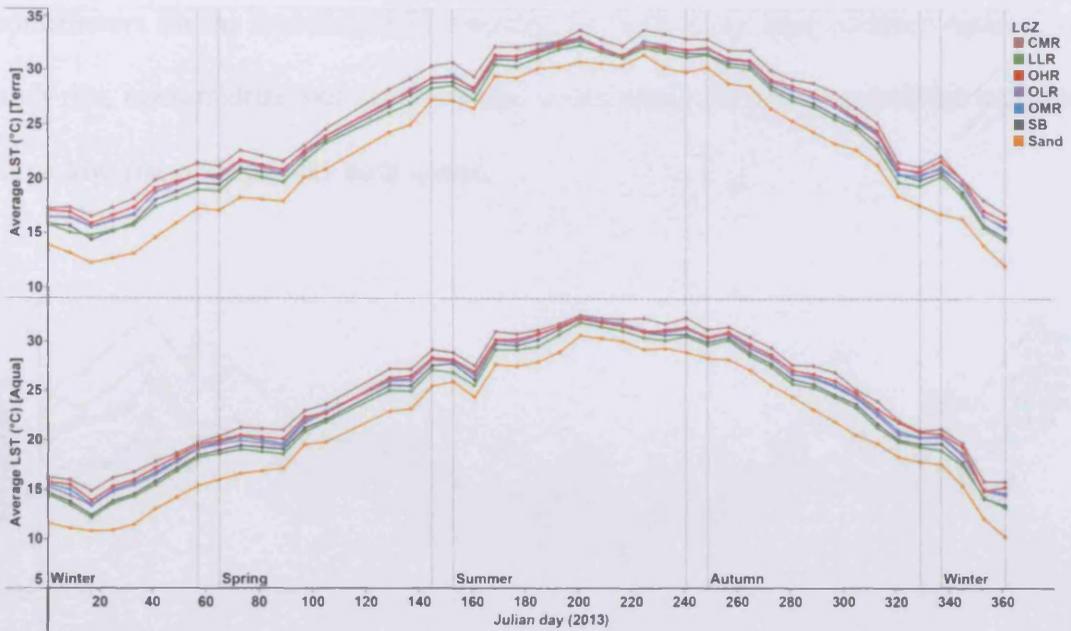
Figure 6.10 Nighttime 8-day average LST variations amongst LCZs for Terra 1030 p.m. (above) and Aqua 0130 a.m. (below) GST), 2013.

A night-time SUHI is noted for all LCZs, where all LST values for all LCZs are higher than LST for desert sand (Fig. 6.11). Compact mid-rise and open high-rise zones show the highest SUHI intensity across the months while large low-rise and sparsely built zones experienced the lowest SUHI intensity. Contrary to the SUHS during daytime, the weakest SUHI intensity was noted in the summer while the highest was noted during the winter. Furthermore, the monthly SUHI for open high-rise, open midrise and open low-rise show less contrasts during relatively hot months (May-September) at 10.30 p.m. and July-August at 0130 a.m. while other LCZs show clear contrasts for both times (Fig. 6.12).

The analysis of the average seasonal variations of SUHI magnitude for urban LCZs for both times is shown in Figure 6.13. The annual average SUHI intensity at 1030 p.m. was slightly higher than the SUHI at 0130 a.m. for all LCZs with the highest intensity in winter season and lowest in summer season for both times. The major

190

contributors for the seasonal SUHI intensity for both times were compact midrise, open high-rise, open midrise and open low-rise zones while the lowest contributions were by large low-rise and sparsely built zones.
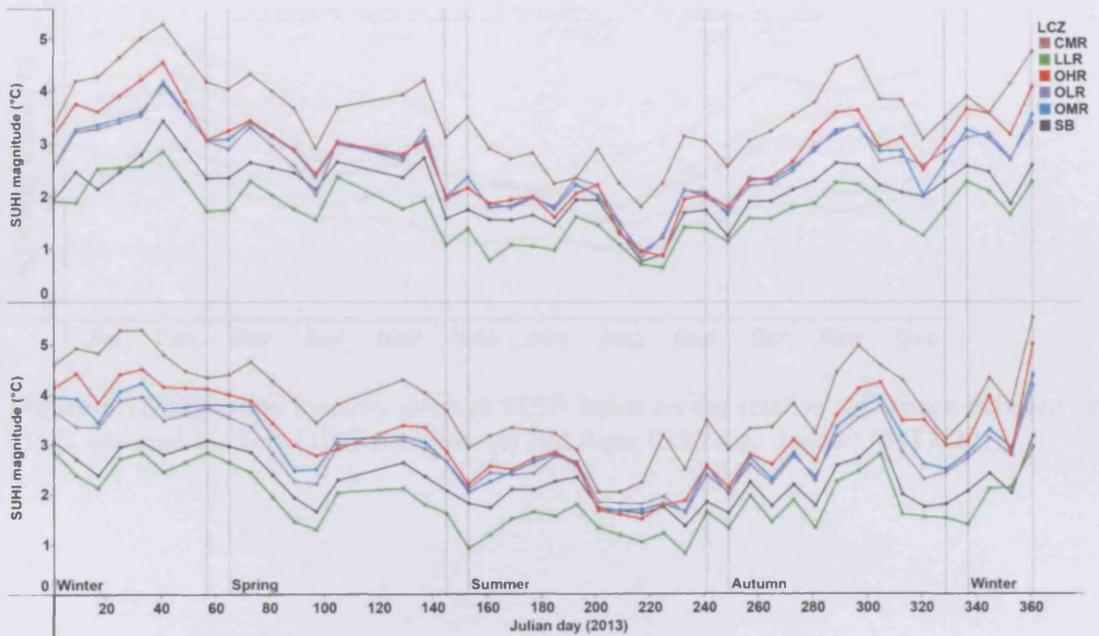
Figure 6.11 Nighttime 8-day average SUHI based on the relative difference between urban LCZs and sand for Terra 1030 p.m. (above) and Aqua 0130 a.m. (below) GST), 2013.
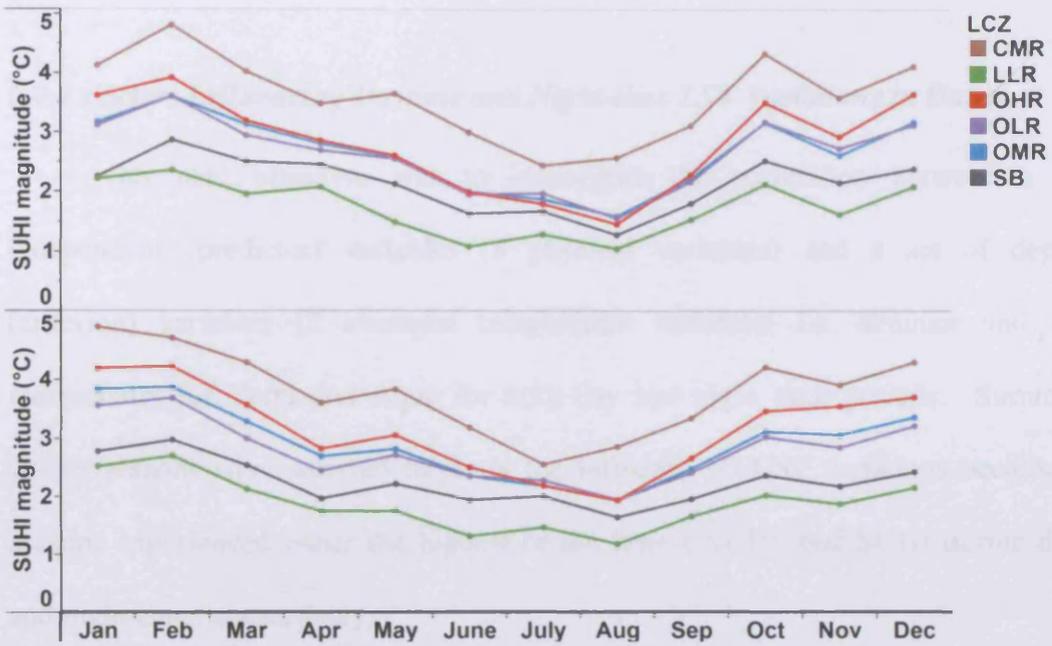
Figure 6.12 Nighttime monthly average SUHI based on the relative difference between urban LCZs and sand for Terra 1030 p.m. (above) and Aqua 0130 a.m. (below) GST), 2013.
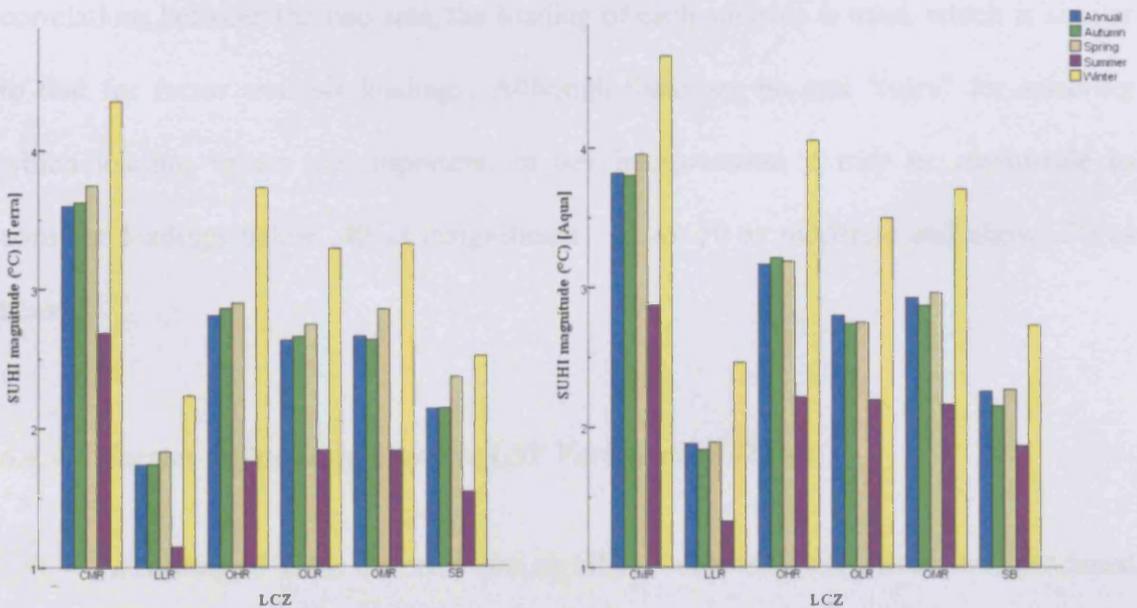
Figure 6.13 Nighttime seasonal and annual average SUHI based on the relative difference between urban LCZs and sand for Terra 1030 p.m. (left) and Aqua 0130 a.m. (right) GST, 2013.

6.4.4 Factors Influencing Daytime and Night-time LST Variations in Dubai

Our next objective was to investigate the correlation between a set of independent (predictor) variables (8 physical variables) and a set of dependent (criterion) variables (2 averaged temperature variables; i.e. summer and winter) individually for Terra and Aqua for both day and night time periods. Summer and winter seasons were selected to study the influence on LST variations because these seasons experienced either the highest or the lowest SUHS and SUHI during daytime and night-time, respectively.

The number of canonical correlations produced will be equal to the number of variables in the smaller data set of the predictor or criterion variables. Consequently, not all of the canonical correlations produced from a particular data are likely to be statistically significant. Furthermore, in order to interpret the meaning of the correlations between the two sets, the loading of each variable is used, which is similar to that for factor analysis loadings. Although there are no real "rules" for selecting which loading values are important, in our interpretation it may be reasonable to consider loadings below .40 as insignificant, .41 to .70 as moderate and above .70 as heavy.

6.4.4.1 Factors Influencing Daytime LST Variations in Dubai

According to Table 6.4, only one significant canonical correlation was produced for both Terra (1030 a.m.) and Aqua (0130 p.m.) data according to significance Chi-square significance values. However the correlation between the predictor variables set

and criterion variables set at both times are similar with more variability at 0130 p.m. than 1030 a.m.

For both daytime periods, the first linear combination of physical predictors loaded heavily and positively on proximity to gulf; however with higher magnitude at 0130 p.m. Urban geometry variables (HRE, SVF and BHV) for both time periods loaded higher than other land cover variables. At 1030 a.m., HRE and BHV variables loaded moderately and negatively, while positively with SVF. However, the %VW loaded moderately and negatively at 1030 a.m. while ISF loaded moderately and positively at 0130 p.m. Furthermore, the remaining variables (BSF, and %Sand) were insignificant over both time periods. Finally, summer LST loaded higher than winter LST for both time periods.

Table 6.4 Canonical correlations between physical variables and daytime LST variations during summer and winter seasons at 1030 a.m. (Terra) and 0130 p.m. (Aqua).

	Canonical solution for predicting daytime LST (1030 a.m.)		Canonical solution for predicting daytime LST (0130 p.m.)	
	1st can. Corr.	2nd Can. Corr.	1st can. Corr.	2nd Can. Corr.
Canonical correlation Coefficient	.88	.70	.88	.55
Chi-square significance	.0001	.165	.0001	.0832
Variability (%)	61.50	38.50	73.97	26.03
	Loadings			
Predictor variables				
HRE	-.58	-.29	-.60	-.43
SVF	.65	.28	.64	.38
BSF	-.24	.39	-.25	-.21
ISF	.07	.47	.41	.23
%VW	-.44	.09	-.37	-.12
%Sand	.27	.07	.17	.04
BHV	-.61	-.16	-.56	-.48
Proximity to Gulf	.82	.21	.92	-.14
Criterion Variables				
Summer LST	.95	.32	.99	.12
Winter LST	.83	.68	.64	.81

6.4.4.2 Factors Influencing Nighttime LST Variations in Dubai

According to Table 6.5, only one significant canonical correlation was produced for Terra (1030 p.m.) and Aqua (0130 a.m.) data according to Chi-square significance values. The correlation coefficients for both night time periods are lower than the correlations during both day time periods which indicates that the correlation between the two set of independent (predictor) and dependent (criterion) variables are weaker during nightime. Furthermore, the influence of urban geometry and proximity to the gulf on LST variations is inverted during night-time.

Similarly to daytime, urban geometry and proximity to the gulf variables had the highest loading magnitude. At 1030 p.m., the first linear combination of physical predictors loaded heavily and negatively on proximity to the gulf and SVF while proximity to the gulf loaded heavily and SVF loaded moderately at 0130 a.m. With the exception of ISF (which is already insignificant), all loadings at 0130 a.m. were lower in magnitude than 1030 p.m. This indicates a weaker influence of these variables on the LST variations at 0130 a.m. In contrast to the daytime, the loadings for winter LST were higher than summer LST for both times.

Table 6.5 Canonical correlations between Physical variables and night-time LST variations during summer and winter at 1030 p.m. (Terra) and 0130 a.m. (Aqua).

	Canonical solution for predicting night-time LST (1030 p.m.)		Canonical solution for predicting night-time LST (0130 a.m.)	
	1st can. Corr.	2nd Can. Corr.	1st can. Corr.	2nd Can. Corr.
Canonical correlation Coefficient	.74	.57	.71	.57
Chi-square significance	.0001	.082	.0001	.070
Variability (%)	63.02	36.98	60.43	39.57
	Loadings			
Predictor variables				
HRE	.60	-.10	.52	-.09
SVF	-.75	-.08	-.57	.29
BSF	.33	.24	.31	.08
ISF	.12	.28	-.08	.45
%VW	-.21	-.41	-.19	-.23
%Sand	-.28	-.14	-.05	-.28
BHV	.15	-.37	.11	.02
Proximity to Gulf	-.87	-.08	-.78	.51
Criterion Variables				
Summer LST	.40	.91	.75	.66
Winter LST	.87	.50	.91	.42

6.5 Discussion

The urban geometry and land cover properties that were utilized to classify Dubai's urban enviornment into LCZs have effectively charactized the landscape into distinctive surface thermal responses diurnally and seasonally. As expected, the SUHS phenomenon was noted during the daytime while the SUHI phenomenon was noted during the nighttime for the majority of LCZs. One reason these phenomena exist might relate to differences in specific heat capacity between the urban materials of the LCZs and the natural sands of the desert. Indeed, the specific heat capacity for typical urban surface materials such as asphalt, aluminum, concrete and bricks are higher than those for sand (Physics Hypertextbook, 2014). This means that sand shows a larger increase in LST than the urban surfaces during the daytime (Fig. 6.6) and a larger decrease in LST than the urban surfaces during the night time (Fig. 6.10). The differences in

magnitudes of SUHS and SUHI depending on LCZ type, time of the day and season, suggest that the properties used to characterize the LCZs influence the LST variations differently. The SUHS was clearer for zones with medium to high-rise buildings, thus these zones are most advantageous for daytime cooling (Figs. 6.7 to 6.9). However, during the night the SUHI was higher in zones with medium to high rise buildings, with the highest intensity in compact-midrise zones, while cooler for sparsely built and large low-rise zones (Figs. 6.11 to 6.13). This indicates that some or all of the LCZs' properties (Table 6.2) behave differently during nighttime.

The multivariate correlation analyses (Tables 6.4 and 6.5) revealed that differences in urban geometry and proximity to the gulf explain most of the variation in LST during the day and the night for both Terra and Aqua data. This finding underscores the importance of integrating urban geometry into urban heat studies (Hwang et al., 2011; Voogt & Oke, 2003). It also emphasizes the importance of including proximity to large water bodies as an essential factor in urban heat studies for coastal cities.

During daytime, building heights (HRE) loaded negatively with LST variations; this indicates that taller buildings produce greater shadows which reduce the amount of solar energy reaching the land surface thus decreasing the surface temperature (e.g. Kato et al., 2010). Similarly, building height variations (BHV) loaded negatively, this indicates that buildings with more height variations produce stronger surface wind circulation thus helping to cool the urban surface (Johansson & Emmanuel, 2006). On the other hand, SVF loaded positively with LST variations which indicates that lower SVF leads to fewer urban surfaces that are exposed to the sun (lower income of solar radiation) therefore decreasing surface temperature. Additionally, proximity to the gulf has

contributed strongly and positively to the SUHS during the daytime which indicates that zones closer to the coast exhibit lower LST. This influence is due to the presence of sea breeze which helps cool nearby urban surfaces; however with higher magnitude at 0130 p.m. Indeed, at noon and especially during the summer season, the solar radiation increases to its maximum thus the temperature contrast maximizes between the inland and the Gulf which promotes stronger sea breeze (Dailey & Fovell, 1999). Similarly, Coseo and Larsen (2014) reported that lake breezes from Lake Michigan cooled nearby urban shore areas.

At 1030 a.m., the average SUHS magnitude was higher than at 0130 p.m. (Fig. 6.9). This might be due to the greater influence of impervious surface fraction (ISF) on LST, as a heat source, at 0130 p.m. than 1030 a.m. The greater influence of ISF at 0130 p.m. might be due to the fact that the impervious surfaces of roads, walk-ways and parking lots have much higher LST at 0130 p.m. than 1030 a.m. due to longer exposure to the sun. In addition, the percentage of vegetation and water (%VW), as a heat sink source, has a slightly more influence on LST mitigation at 1030 a.m. than 0130 p.m. due to its slightly higher loading level at 1030 a.m. Finally, the higher loading for summer LST than winter LST during daytime, indicates that the combined physical variables are more predictive of LST variations during the summer than winter.

Figure 6.9 (Daytime Seasonal and Annual Average SUHS) and Tables 6.2 & 6.3 (Geometry and Land Cover Properties of Dubai's LCZs) illustrate the above findings. Open high-rise zones and midrise zones (compact midrise and open midrise) showed higher SUHS than other zones not only due to the effect of urban geometry but also due to their close proximity to the gulf compared to other zones (see Fig. 6.5). However, it

was expected that compact midrise zones have less potential to absorb heat during the day than most of the zones especially at 0130 p.m. because they have no or very sparse vegetation and higher ISF. Nevertheless, they exhibited the second coolest zones because of their close proximity to the gulf and due to their small SVF. Furthermore, the narrow streets and building height average of 22m in compact midrise zones help to generate relatively more shadow effect than other LCZs especially during the sun peak hours thus lowering the LST (Littlefair et al., 2000). In addition to the influence of urban geometry, proximity to water and land cover variables on the LST variations, other factors have also contributed to the variations. For example, the industrial activities and the surface materials of large low-rise zones (made of metal corrugated sheets and steel hangers) tend to heat up the urban areas faster than other zones.

Relative to night time, SVF and proximity to gulf have strongly negatively influenced the LST variations. This indicates that the zones with higher SVF or/and large distance to the gulf exhibit a decrease in LST. During nighttime, high SVF of urban areas increases the chance of the radiative heat loss thus lowering the LST in urban areas. Conversely, HRE has moderately positively influenced the LST variation while other variables were insignificant. In addition, the proximity to the gulf has majorly contributed to the SUHI intensity, especially for zones close to water. This is due to the presence of land breeze phenomenon during the night which is the opposite of the sea breeze phenomenon noticed earlier in the morning. Figure 6.13 (Nighttime Seasonal and Annual Average SUHI) and Table 6.2 (Geometry and Land Cover Properties of Dubai's LCZs) illustrate these findings. Compact midrise, open high-rise and open midrise zones exhibited the highest SUHI intensity due to their taller buildings

and lower SVF compared to other zones. During nighttime, taller buildings with low SVF trap the heat near the surface which keeps the skin surface warm thus increasing their LST (Hamdi & Schayes, 2008). Furthermore, these zones are closer to the water than other LCZs hence the larger increase in LST. Despite the fact that the average proximity to the gulf for large low-rise zones is less than open low-rise and sparsely built zones, large low-rise zones exhibited lower SUHI during nighttime. This might be attributed to the surface materials for large low-rise that are primarily made of thin metal corrugated sheets which help to lose the heat faster than the construction materials for open low-rise and sparsely built zones thus the surface cools faster than other materials. In contrast to the daytime, the loadings for winter LST were higher than summer LST for both times which indicates that the physical variables are more predictive of the LST variations during the winter than the summer.

In highly urbanized desert cities like Dubai, the unbuilt surfaces of LCZs are still covered majorly by sand while vegetation and inland water cover less than 2% of the studied LCZs. It is important to mention that the vast majority of vegetation and plants are found in parks, farms and golf courses that contain a very limited amount of impervious surfaces and buildings (Nassar et al., 2014), thus these areas were not selected in the LCZ selection process as per the classification schema in Stewart and Oke (2012). This fact might explain the lower contribution of vegetation on LST variations during most of the study periods.

Finally, the overall influence of urban geometry properties (HRE, SVF, BHV) on the SUHS during daytime and SUHI during nighttime have both beneficial and negative impacts on the thermal behavior of LCZs. During the daytime, these properties could

generate shadow effects which decrease the absorption of solar energy at the land surface and increase wind speeds and natural ventilation at street level leading to a decrease in LST within the urban environment. However during the nighttime, the urban geometry properties could trap heat near the surface thus increases the LST.

6.6 Conclusions

The major contribution of this research is the development of a Local Climate Zone (LCZ) classification schema that was primarily used to explore spatial and temporal variations in LST across the city by day and night. We have also systematically analyzed how various urban zones with varying structures, cover types and proximity to water influence urban cooling and heating in the desert city of Dubai through the use of remote sensing and statistical analysis. In this study, the major factors affecting thermal change in coastal desert cities have been taken into account by employing urban geometry, land cover and proximity to water factors in the analysis. This provides a valuable extension to previous studies in coastal desert cities which have considered only land cover factors (Frey et al., 2007; Lazzarini et al., 2013).

In terms of the SUHS and SUHI intensities, we have found that different LCZs exhibited different responses in intensity, both diurnally and seasonally, which clearly indicates that the predictor variables affecting those intensities behave differently. On average, we found that the summer daytime SUHS magnitude was significantly higher than other seasons and that the winter daytime SUHS was the lowest. Conversely, during the night time, winter SUHI magnitude was significantly higher than other seasons while summer night time SUHI was the lowest. We have demonstrated that

proximity to the gulf, sky view factor, heights of roughness elements and building height variations are the major factors governing the zonal surface temperature varations in Dubai.

To further investigate the factors influencing the surface thermal variation of LCZs, we encourage other researchers to use other LCZ characteristics such as traffic loads, anthropogenic activities and albedo.

Acknowledgement

References

Alexander, P.J., & Mills, G. (2014). Local Climate Classification and Dublin's Urban Heat Island. *Atmosphere*, 5 (4), 755-774. doi: 10.3390/atmos5040755

Coseo, P., & Larsen, L. (2014). How factors of land use/land cover, building configuration, and adjacent heat sources and sinks explain Urban Heat Islands in Chicago. *Landscape and Urban Planning*, 125, 117–129. doi: 10.1016/j.landurbplan.2014.02.019

Coutts, A., & Harris, R. (2013). *Urban Heat Island Report: A multi-scale assessment of urban heating in Melbourne during an extreme heat event: policy approaches for adaptation.* Victorian Centre for Climate Change Adaptation Research.

Cui, Y.Y., & Foy, D.E. (2012). Seasonal variations of the urban heat island at the surface and the near-surface and reductions due to urban vegetation in Mexico City. *Journal of Applied Meteorology and Climatology*, 51(5), 855-868. doi: 10.1175/JAMC-D-11-0104.1

Dailey, P.S., & Fovell, R.G. (1999). Numerical simulation of the interaction between the sea-breeze front and horizontal convective rolls. part 1: offshore ambient flow. *American Meteorological Society*, 127, 858-878. doi: http://dx.doi.org/10.1175/1520-0493(1999)127<0858:NSOTIB>2.0.CO;2

Dubai Statistical Centre (2013). Population Bulletin: Emirates of Dubai. https://www.dsc.gov.ae/en-us/Themes/Pages/Population-and-Vital-Statistics.aspx?Theme=42 (accessed 23rd June, 2015).

Dubai Statistical Centre (2014). Population Bulletin: Emirates of Dubai. https://www.dsc.gov.ae/en-us/Themes/Pages/Climate-and-Environment.aspx?Theme=35 (accessed 9th May, 2015).

Elsheshtawy, Y. (2010). *Dubai: Behind an Urban Spectacle*. Routledge; 1 ed. Oxfordshire.

Emmanuel, R., & Kruger, E. (2012). Urban heat island and its impact on climate change resilience in a shrinking city: The case of glasgow, UK. *Building and Environment*, 53, 137-149. doi:10.1016/j.buildenv.2012.01.020

Freitas,E., Rozoff, C., Cotton, W., & Dias, P. (2007). Interactions of an urban heat island and sea-breeze circulations during winter over the metropolitan area of São Paulo, Brazil. *Boundary-Layer Meteorology*, 122(1), 43-65. doi: 10.1007/s10546-006-9091-3

Frey, C. M., Rigo, G., & Parlow, E. (2007). Urban radiation balance of two coastal cities in a hot and dry environment, *International Journal of Remote Sensing*, 28(12), 2695 2712. http://dx.doi.org/10.1080/01431160600993389

Gartland, L. (2008). *Heat Islands: Understanding and mitigating heat in urban areas*. Washington, DC: Earthscan.

Guarino, J. (2004). A comparison of first and second generation multivariate analyses: canonical correlation analysis and structural equation modeling. *Florida Journal of Educational Research*, 42, 22 – 40.

Heldens W., Taubenböck H., Esch T., Heiden U., & Wurm M. (2013). Analysis of surface thermal patterns in relation to urban structure types: a case study for the city of Munich. In: Kuenzer C., & Dech S. (eds). *Thermal infrared remote sensing – sensors, methods, applications. Remote sensing and digital image processing series 17*. Springer, Netherlands, p. 475–495.

Hu, L., & Brunsell, N. A. (2013). The impact of temporal aggregation of land surface temperature data for surface urban heat island (SUHI) monitoring. *Remote Sensing of Environment*, 134, 162–174. doi: 10.1016/j.rse.2013.02.02

Hwang, R-L., Lin, T-P., Lin, T-P., & Matzarakis, A. (2011). Seasonal effects of urban street shading on long-term outdoor thermal comfort. *Building and Environment*, 46, 863-870. doi: 10.1016/j.buildenv.2010.10.017

Imhoff, M.L., Zhang, P., Wolfe, R.E., & Bounoua, L. (2010). Remote sensing of the urban heat

island effect across biomes in the continental USA. *Remote Sensing of Environment, 114,* 504–513. doi: 10.1016/j.rse.2009.10.008

Jin, M. (2004). Analysis of Land Skin Temperature Using AVHRR observations. *Bulletin of the American Meteorological Society,* 85, 587–600. doi: http://dx.doi.org/10.1175/BAMS-85-4-587

Jin, M., & Dickinson , R.E. (2010). Land surface skin temperature climatology: benefitting from the strengths of satellite observations. *Environmental Research Letter,* 5 (4), 1-13. doi:10.1088/1748-9326/5/4/044004

Johansson, E., & Emmanuel, R. (2006). The influence of urban design on outdoor thermal comfort in the Hot Humid City of Colombo, Sri Lanka. *International Journal of Biometeorology,* 51, 119-133. doi: 10.1007/s00484-006-0047-6

Johnson, G.T., & Watson, I.D. (1984). The determination of view-factors in urban canyons. *Journal of Climate and Applied Meteorology,* 23, 329–335. doi: http://dx.doi.org/10.1175/1520-0450(1984)023<0329:TDOVFI>2.0.CO;2

Kato, S., & Yamaguchi, Y. Analysis of urban heat-island effect using ASTER and ETM+ data: Separation of anthropogenic heat discharge and natural heat radiation from sensible heat flux. *Remote Sensing of Environment,* 99, 44–54. doi: 10.1016/j.rse.2005.04.026

Kato, S., Matsunaga, T., & Yamaguchi, Y. (2010). Influence of shade on surface temperature in an urban estimated by ASTER data. *International Archives of the Photogrammetry, Remote Sensing and Spatial Information Science,* 38, 925–929.

Knight, S., Claire, S., & Michael, R. (2010). Mapping Manchester's urban heat island. *Weather,* 65(7), 188-193. doi: 10.1002/wea.542

Lazzarini, M., Marpu, P.R., & Ghedira, H. (2013). Temperature-land cover interactions: The inversion of urban heat island phenomenon in desert city areas. *Remote Sensing of Environment, 130,* 136–152. doi: 10.1016/j.rse.2012.11.007

Leconte, F., Bouyer, J., Claverie, R., Pétrissans, M. (2015) Using Local Climate Zone scheme for UHI assessment: Evaluation of the method using mobile measurements. *Building and Environment,* 83, 39-49. doi: 10.1016/j.buildenv.2014.05.005

Li, Y.y., Zhang, H., & Kainz, W. (2012). Monitoring patterns of urban heat islands of the fast-growing Shanghai metropolis, China: Using time-series of Landsat TM/ETM+ data. *International Journal of Applied Earth Observation and Geoinformation,* 12, 127–138. doi: 10.1016/j.jag.2012.05.001

Littlefair, P.J., Santamouris, M., Alvarez, S., Dupagne,A., Hall, D., Teller, J., et al. (2000). *Environmental site layout planning: solar access, microclimate and passive cooling in urban areas* (1st ed.). Watford: CRC.

Nassar, A.K., Blackburn, G.A., & Whyatt, J.D. (2014). Developing the desert: The pace and process of urban growth in Dubai. *Computers, Environment and Urban Systems,* 45, 50–62. doi: 10.1016/j.compenvurbsys.2014.02.005

Nichol, J. E., Fung, W.Y., Lam, K., & Wong, M.S. (2009). Urban heat island diagnosis using ASTER satellite images and 'in situ' air temperature. *Atmospheric Research,* 94(2), 276-284. doi: 10.1016/j.atmosres.2009.06.011

Obiakor, M.O.; Ezeonyejiaku, C.D. & Mogbo, T.C. (2012). Effects of Vegetated and Synthetic (Impervious) Surfaces on the Microclimate of Urban Area. *Journal of Applied Sciences and Environmental Management,* Vol. 16, No. 1, 2012, pp. 85-94

Oda, R., & Kanda, M. (2009). Cooling effect of sea surface temperature of Tokyo bay on urban air temperature. *The seventh International Conference on Urban Climate,* 1-4, 29 June - 3 July 2009, Yokohama, Japan.

Physics Hypertextbook (2014). http://physics.info/heat-sensible/ (accessed 1st February, 2014).

Pichierri, P., Bonafoni, S., & Biondi, B. (2012). Satellite air temperature estimation for monitoring the canopy layer heat island of Milan. *Remote Sensing of Environment,* 127, 130–138. doi: 10.1016/j.rse.2012.08.025

Unger, J. (2009). Connection between urban heat island and sky view factor approximated by a software tool on a 3D urban database. *Int. J. Environment and Pollution.* 36, 59-80. doi: 10.1504/IJEP.2009.021817

Unger, J., Lelovics, E., & Gál, T. (2014). Local Climate Zone mapping using GIS methods in Szeged. *Hungarian Geographical Bulletin,* 63 (1) , 29–41. doi: 10.15201/hungeobull.63.1.3

US EPA. (2008a). Urban Heat Island basics. In Reducing Urban Heat Islands: Compendium of Strategies. Washington. http://www.epa.gov/heatisland/resources/pdf/BasicsCompendium.pdf (accessed 8th June, 2013).

USGS (U.S. Geological Survey). (2014). http://landsat.usgs.gov/calibration_notices.php. http://landsat.usgs.gov/calibration_notices.php (accessed 9th September, 2014).

Rhee, J., Seonyoung, P., & Zhenyu, Lu. (2014). Relationship between land cover patterns and surface temperature in urban areas. *GIScience & Remote Sensing,* 51(5), 521-536. doi:10.1080/15481603.2014.964455

Sattari, F., & Hashim, M. (2014). A brief review of land surface temperature retrieval methods from thermal satellite sensors. *Middle-East Journal of Scientific Research,* 22 (5), 757-768. doi: 10.5829/idosi.mejsr.2014.22.05.21934

Siu, L.W., & Hart, M.A. (2013). Quantifying urban heat island intensity in Hong Kong SAR, China. *Environmental Monitoring and Assessment* 185, 4383–4398. doi: 10.1007/s10661-012-2876-6

Sobrino, J. A., Jiménez-Muñoz, J. C., & Paolini, L. (2004). Land surface temperature retrieval from LANDSAT TM5. *Remote Sensing of Environment,* 90(4), 434–440. :10.1016/j.rse.2004.02.003

Stewart, I. D., & Oke, T. R. (2012). Local climate zones for urban temperature studies. *Bulletin of the American Meteorological Society,* 93(12), 1879-1900. doi: http://dx.doi.org/10.1175/BAMS-D-11-00019.1

Stewart, I.D., Oke, T. R., & Krayenhoff, E. S. (2014). Evaluation of the 'local climate zone' scheme using temperature observations and model simulations. *International Journal of Climatology,* 34(4), 1062-1080. doi: 10.1002/joc.3746

Streutker, D.R. (2003). Satellite-measured growth of the urban heat island of Houston, Texas. *Remote Sensing of Environment,* 85, 282-289. doi: 10.1016/S0034-4257(03)00007-5

Tabachnick, B.G., Fidell L.S. (2012). *Using Multivariate Statistics* (6 ed.). Boston: Pearson Education Inc.

Voogt, J.A., & Oke, T.R. (2003). Thermal remote sensing of urban climates. *Remote Sensing of Environment,* 86, 370–384. doi: 10.1016/S0034-4257(03)00079-8

Wan, Z., & Dozier, J. (1996). A generalized split-window algorithm for retrieving land-surface temperature from space. *IEEE Transactions on Geoscience and Remote Sensing,* 34(4), 892–905. doi: 10.1109/36.508406

Weng, Q. (2001). A remote sensing-GIS evaluation of urban expansion and its impact on surface temperature in the Zhujiang Delta, China. *International Journal of Remote Sensing,* 22, 1999–2014. doi: 10.1080/713860788

Yuan, F., & Bauer, M.E. (2007). Comparison of impervious surface area and normalized difference vegetation index as indicators of surface urban heat island effects in Landsat imagery. *Remote Sensing of Environment,* 106, 375–386. doi: 10.1016/j.rse.2006.09.003.

Zakšek, K., Oštir, K., Kokalj, Ž. (2011). Sky-View Factor as a Relief Visualization Technique. *Remote Sensing,* 12, 398-415. doi: http://dx.doi.org/10.3390/rs3020398

Chapter 7 Conclusion and perspectives on future research

7.1 Thesis conclusions

Researchers studying the environmental impacts of urbanisation on the Dubai emirate have been hampered by limited access to official information on the scale of urbanization and supporting ground-based temperature measurements. This study used satellite remote sensing to overcome such difficulties. It investigated the evolution of Dubai over time to subsequently study the impacts of land cover/use change and urban geometry on the formation of urban heat sinks and urban heat islands. The results have provided valuable insights into the interaction of both land cover and urban geometry variables on the modification of diurnal and seasonal land surface temperature variations in a desert environment.

The thesis has specifically described the urbanisation process in the emirate since the origins of modern Dubai following the discovery of oil in the late 1960s. It has explored the urban evolution over an extended of approximately 40 years (1972-2011) and has efficiently captured the rate and form of urbanisation across the city and the drivers of such urbanisation. Although several techniques have previously been used to classify the urban environment from medium spatial resolution Landsat data, discriminating urban classes from other classes in arid environments has remained particularly challenging. Adoption of a hybrid classification technique initially proposed by Lo and Choi (2004) for the city of Atlanta, USA, proved successful in discriminating between urban areas and other classes of land cover around Dubai. It is recommended that other researchers now test this technique in other desert cities.

The result of the classification indicated a dramatic increase in urban area over time, making Dubai one of the fastest growing cities in the world. This gave insights into the rapid pace of urbanization and the unprecedented rate of construction of offshore islands in the region that have not been revealed previously. Landscape metrics were used to link patterns of urbanisation to local and global economic conditions, and regional conflicts to better explore the drivers of urban growth in Dubai. Furthermore, these metrics were used to compare and contrast the style of urban growth in Dubai with that of other cities using an empirical growth theory proposed by Dietzel et al. (2005). Pertinently, urban growth in Dubai did not occur in response to population growth unlike many other cities in the region and around the world including Cairo in Egypt (Yin et al., 2005) and Xuzhow city in China (Zhao et al., 2007). Urban growth occurred as a result of diversification of economy to avoid over reliance on the fragile petroleum industry by stimulating real estate marketing and developing tourism.

In contrast to other cities in the Gulf region (Al-Awadhi, 2007; Al-Manni et al., 2007) this growth has been accompanied by significant increases in vegetation. The substantial increase in all anthropgenically-introduced land cover types (impervious surfaces, vegetation and inland water) at the expense of the sand has prompted an investigation of the influence of these changes on the daytime thermal urban environment. Consequently, the influence of changes in land use, land cover and albedo on the land surface temperature variations were explored for three periods between 1990 and 2011 using Landsat images. In contrast to previous studies conducted in desert cities, which have related an increase in urban cooling exclusively to increases in vegetation cover (Frey et al., 2007; Lazzarini et al., 2013), this study found that both the

amount of vegetation cover and impervious surface contributed to the cooling effect based on the results of stepwise multiple regression analysis. It was anticipated that the increase in cooling caused by impervious surfaces would be linked to an increase in surface albedo, however, this was not the case. Therefore, it was concluded that other factor (s) must be responsible for urban cooling.

The combined influences of urban geometry, land cover and proximity to water on daytime cooling (SUHS) and night-time warming (SUHI) were then explored on a daily and seasonal basis. Further motivation for this study came from Frey et al. (2007) and Lazzarini et al. (2013) who had not investigated the impact of proximity to large water bodies on the surface temperature variations, despite its importance (Coseo & Larsen, 2014).

Therefore, eight variables were used in conjunction with MODIS data to evaluate spatial and temporal changes in SUHS and SUHI across the city. Although the LST derived from MODIS lacked the spatial accuracy of the LST derived from Landsat, it provided information at much higher temporal resolution. The increased frequency of observations from the MODIS Aqua and Terra platforms was therefore used to better understand the underlying factors of SUHI and SUHS in desert cities.

A local climate zone (LCZ) classification schema developed by Stewart & Oke (2012) was adopted for this study using remotely sensing inputs rather than traditional ground-based measurements of air temperature. Over four time periods (morning, afternoon, evening, and late-night), proximity to water and urban geometry proved to be most influential on seasonal variations in LST based on a multivariate canonical correlation analysis. However, the urban geometry variables (building height, sky view

factor; building surface fraction; and building height variation) varied in the nature of their effects. In contrast, land cover variables showed generally lower correlations with LST variations than the majority of the urban geometry variables. The findings of this research suggests that other researchers in desert cities should incorporate urban geometry variables into future urban thermal studies and incorporate distance to large water bodies for studies conducted in coastal cities.

7.2 Contributions to the knowledge

This thesis makes several contributions to the literature. Firstly, it has used remote sensing and spatial metrics to study aspects of landscape change and provide insights into the processes and potential problems associated with rapid urbanization in desert cities. Using a combination of inputs from spatial urban metrics, recent empirical urban theory, socio-economic data and historic local, regional and global events, this study has shown the growth of Dubai to be very dynamic, with phases and drivers that are distinct from other rapidly growing cities. It has investigated the rate and form of urbanization and coastal change in Dubai emirate over the last four decades, identifying unique spatial characteristics of the development and highlighting the need for further research on its environmental impacts.

Secondly, this is the first study that assesses the combined influences of changes in land use, land cover, albedo and urban geometry on the developing urban heat sink in desert cities as demonstrated through Dubai. The findings provided important insights into the causes of cooling in desert cities and have implications for the design of urban areas within arid environments. This study has extended previous studies of urban heat

island phenomena in desert environments through exploring more influencing factors and using a statistical approach to measure the magnitude of influence rather than simple visual analysis (Frey et al., 2007) or a limited number of sample sites (Lazzarini et al., 2013).

Finally, a key development of the thesis has been the use of a combination of variables from both remote sensing and urban climatology literature on the local climate zone classification schema (Stewart and Oke, 2012) to investigate their impact on the diurnal and seasonal variations of temperature. In this research, a technique has been developed to employ the classification schema which was primarily developed for air temperature measurements into thermal urban studies using remotely sensed data inputs. Urban geometry and proximity to water variables have not previously been used in assessments of coastal desert cities. This should therefore provide a useful addition to urban thermal literature and our understanding of interactions between different variables responsible for thermal change. Furthermore, this study should be useful in standardizing the sampling units in remotely sensed thermal studies to better understand the underlying factors that govern the LST variations in different environments.

7.3 Limitations

In the course of this study a number of issues may have limited some aspects of the research. The application of Landsat imagery to monitor urban growth and other land cover types was limited by the Scan Line Corrector (SLC) failure that affected the Landsat 7 images used in chapter 4 of this study. SLC failure also affected land surface temperature and albedo retrieval for 2011 reported in chapter 5. Nevertheless, in chapter

4 the problem was overcome by filling the SLC gaps with temporally adjacent images of 16 days. This procedure had minimal effect on the amount of urban and other land cover types quantified per sampling unit because 16 days is a very short period for urban expansion to occur. In addition, vegetation in Dubai is heavily reliant on drip and spark irrigation thus the effect of gap-filling was minimal on the vegetation amount in the city.

However, no filling was applied in chapter five because filling the gaps from adjacent images would have altered the land surface temperature and albedo values and potentially affecting the outcomes of the statistical analysis. Fortunately, the recently launched Landsat 8 does not suffer from the SLC problem, hence offers scope for future monitoring of land surface temperature and albedo retrieval. The problems of SLC and relatively low temporal resolution of Landsat were overcome through the use of MODIS imagery, which has a higher temporal resolution (2 times daily) and no SLC issues. With MODIS it was possible to obtain four images daily to better understanding the urban heat sink and urban heat island phenomena in Dubai.

7.4 Future directions

Further work to extend the research presented in this thesis is highly dependent on the availability of reliable ground-based measurements. For example, air quality in Dubai is likely to have deteriorated in response to the fast pace of urban growth and the increasing population (Hansen, 2013; Prasad et al., 2005; UNEP, 2012). Increases in particulate matter (i.e. $PM_{2.5}$ and PM_{10}), NO_2, SO_2 and O_3 resulting from urbanisation can have negative effects on human health, animals, plants and other organisms (Fan et

al., 2012; Honour et al., 2009; Singh et al., 1991; Winters et al., 2015). However, in order to efficiently monitor and assess ambient air quality across urban and rural areas in Dubai, several fixed and/or mobile air quality monitoring stations will be required. In addition, to investigate the effect of urban growth on air quality, historical air quality data would be also required.

The substantial dredging and filling operations which have resulted in the construction of 68 km^2 of artificial islands in Dubai between 2003 and 2011 are likely to have implications for the aquatic environment, with potential changes in the dynamics of currents, sediments, biogeochemicals and ecosystem functions (e.g. Butler, 2005; Cressey, 2011; Duan et al., 2007; Hu et al., 2004). Several marine indices could be employed to assess the impact of the artificial island formations on the water quality such as suspended sediments, salinity, turbidity and chlorophyll-a.

Although many approaches have been developed to employ satellite remote sensing images in the estimation of air and marine indices, these approaches are heavily reliant on in-situ data for calibration in order to come up with a best fit model for index estimations. These approaches are based on finding the relationships between values measured from in-situ data and the reflectance values from satellite images. These approaches have been used in air measurements by primarily estimating $PM_{2.5}$ and PM_{10} through developing aerosol retrieval algorithms. Several satellites have been used based on primarily the optical aerosol characteristics in the atmosphere such as MODIS (e.g. Hashim and Yap, 2012; Lin et al., 2014; Yao and Lu, 2014) and Landsat (e.g. Luo et al., 2015; Zhao et al., 2011). For marine index estimations, chlorophyll-a has been estimated using MODIS 250m (e.g. Chen et al., 2013; Huang et al., 2011), Landsat TM

(e.g. Duan et al., 2007; Markogianni et al., 2014) and Landsat ETM+ (Allan et al., 2015; Han and Jordan, 2005). Suspended sediments have been estimated using MODIS (Jun et al., 2014; Wang & Lu, 2010) and Landsat (Cai et al., 2015; Montanher et al., 2014). Turbidity characterization has been conducted on MODIS data (Maltese, 2013; Wang et al., 2012) and Landsat data (Bustamante et al., 2009; Gan et al., 2004). Salinity estimation has also been conducted using MODIS data (e.g. Daqamseh et al., 2010; Qing et al., 2013) and Landsat data (Zhang et al., 2012). Hence, the further use of satellite remote sensing holds considerable promise for developing a comprehensive understanding of the full range of environmental impacts of the rapid urban growth in Dubai.

References

Aguilera, F., Valenzuela, L. M., & Leitão, A. B. (2011). Advances in urban ecology: Integrating humans and ecological processes in urban ecosystems. *Landscape and Urban Planning*, 99, 226–238. doi:10.1016/j.landurbplan.2010.10.004

Akbari, H. (2002). Shade trees reduce building energy use and CO2 emissions from power plants. *Environmental Pollution*, 116, 119–S126

Al-Awadhi, T. (2007). Monitoring and modeling urban expansion using GIS & RS: Case study from Muscat, Oman. *Urban Remote Sensing Joint Event*, IEEE (pp. 1-5). doi: 10.1109/URS.2007.371790

Al-Awadhi, T., & Azaz, L. (2005). Monitoring Urban Growth in Oman Using Remote Sensing and GIS, Seeb Wilayat Case Study. In M. Moeller, & E. Wentz (Ed.), *The International Symposium Remote Sensing of Urban Areas (URS 2005). XXXVI.* Tempe, AZ: International Archives of Photogrammetry, Remote Sensing and Spatial Information Sciences.

Al-Manni, A. A., Abdu, A. S., Mohammed, N. A., Al-Sheeb, A. E., (2007). Urban growth and land use change detection using remote sensing and geographic information system techniques in Doha City, State of Qatar, *Arab Gulf Journal for Scientific Research*, 25(4), 190-198. http://cat.inist.fr/?aModele=afficheN&cpsidt=20363607 (accessed 22nd September, 2013).

Al-Marashi, H., & Bhinder, J. (2008). From the Tallest to the Greenest -Paradigm Shift in Dubai. *From The Council on Tall Buildings and Urban Habitat.* http://www.ctbuh.org/Portals/0/Repository/T1_AlMarashi.ec25feeb-c7e3-4e10-9fed-1fdfac4e74c3.pdf (accessed 12 July, 2012).

Alexander, P.J., & Mills, G. (2014). Local Climate Classification and Dublin's Urban Heat Island. *Atmosphere*, 5 (4), 755-774. doi: 10.3390/atmos5040755

Alberti, M. (2008). *Advances in urban ecology: Integrating humans and ecological processes in urban ecosystems.* New York: Springer.

Allan, M., Hamilton, D., Hicks, B., Brabyn, L. (2015). Empirical and semi-analytical chlorophyll a algorithms for multi-temporal monitoring of New Zealand lakes using Landsat. *Environmental Monitoring and Assessment*, 187(6), 1-24. doi: 10.1007/s10661-015-4585-4

Anderson, J. M., Hardy, E. E., Roach, J. T., & Witmer, R. E. (1976). *A land use classification system for use with remote sensing Data.* Geological Survey Professional Paper. Washington D. C.: Government Printing Office.

Angel, J. M., Hardy, E. E., Roach, J. T., & Witmer, R. E. (1976). A Land Use Classification System for Use with Remote Sensing Data. *Geological Survey Professional Paper.* Washington D. C.: Government Printing Office. http://landcover.usgs.gov/pdf/anderson.pdf (accessed 12 October, 2012).

Angel, S., Parent, J., Civco, D. L., & Blei, A. M. (2010). The persistent decline of urban densities: Global and historical evidence of sprawl. Cambridge, MA: Lincoln Institute of Land Policy. http://www.alnap.org/pool/files/1834-1085-angel-final-1.pdf (accessed 13th May, 2013).

Angel, S., Sheppard, S. C., Civco, D. L., Chabaeva, A., Gitlin, L., Kraley, A., et al. (2005). The dynamics of global urban expansion. Washington, DC: The World Bank. http://www.worldbank.org/urban (accessed 2nd March, 2012).

Araya, Y. H., & Cabral, P. (2010). Analysis and Modeling of Urban Land Cover Change in Setúbal and Sesimbra, Portugal. *Remote Sensing*, 2, 1549-1563. doi:10.3390/rs2061549

Artis, D.A., & Carnahan, W.H. (1982). Survey of emissivity variability in thermography of urban areas. *Remote Sensing of Environment*, 12, 313–329. doi: http://dx.doi.org/10.1016/0034-4257(82)90043-8.

Assimakopoulus, D.N., Assimakopoulos, V.D., Chrisomallidou, N., Klitsikas, N., Mangold, D., Michel, P., Santamouris, M., Tsangrassoulis, A. 2001. Energy and Climate in the Urban Built Environment. Routledge: London, UK.

Avery, T.E., & G.L. Berlin, (1992). *Fundamentals of remote sensing and airphoto interpretation* (5th ed.). Upper Saddle River, New Jersey: Prentice Hall.

Badouri, S. (2007). Construction boom in UAE & Saudi Arabia: Opportunities for Asian companies. Master Builders Association Malaysia. http://www.mbam.org.my/mbam/images/@BOOM%20UAE%20%2880-92%29.pdf (accessed 2nd November, 2012)

Banzhaf, E., Grescho, V., & Kindler, A. (2009). Monitoring urban to peri-urban development with integrated remote sensing and GIS information: a Leipzig, Germany case study. *International Journal of Remote Sensing, 30*(7), 1675–1696.

Barredo, J., & Demicheli, l. (2003). Urban sustainability in developing countries' megacities: modelling and predicting future urban growth in Lagos. *Cities, 20*(5), 297-310.

Barsi, J.A., Schott, J.R., Palluconi, F.D., & Hook, S.J. (2005). Validation of a web-based atmospheric correction tool for single thermal band instruments. *Earth Observing Systems X, Proc. SPIE,* Vol. 5882, August 2005, San Diego, CA. Doi: 10.1117/12.619990

Basith, A., Matori, A. B., Hara, I. S., & Talib, J. A. (2010). Application of land use changes detection for identification of landslide risk areas in pulau penang using a decade of landsat 7 etm+ images. *MRSS*, (pp. 1-11). PWTC, Malaysia.

Belaid, M. A. (2003, December 2-5). *Urban-Rural Land Use Change Detection and Analysis Using GIS & RS Technologies. Urban-Rural Land Use Change Detection and Analysis Using GIS & RS Technologies*, 2nd FIG Regional Conference. Marrakech, Morocco: Geographic Information for Planning.

Bhailume, S. A. (2012). *An assessment of urban sprawl using GIS and remote sensing techniques: A case study of Pune-Pimpri-Chinchwad area* (Doctoral thesis, SNDT Women's University, Pune, India). http://shodhganga.inflibnet.ac.in/handle/10603/3425 (accessed 22nd September, 2013).

Bhaskaran, S., Paramananda, S., & Ramnarayan, M. (2010). Per-pixel and object-oriented classification methods for mapping urban features using Ikonos satellite data. *Applied Geography*, 30(4), 650–665. doi:10.1016/j.apgeog.2010.01.009

Bhatta, B. (2009). Analysis of urban growth pattern using remote sensing and GIS: a case study of Kolkata, India. *International Journal of Remote Sensing, 30*(18), 4733 -4746. doi: 10.1080/01431160802651967

Bhatta, B., Saraswati, S., & Bandyopadhyay , D. (2010). Quantifying the degree-of-freedom, degree-of-sprawl, and degree-of-goodness of urban growth from remote sensing data. *Applied Geography*, 30, 96–111. doi: 10.1016/j.apgeog.2009.08.001

Böer, B. (1997). An introduction to the climate of the United Arab Emirates. *Journal of Arid Environments*, 35(1), 3-16. doi: 10.1006/jare.1996.0162

Boyce, R. R. (1966). *The edge of the metropolis: The wave theory analog approach.* Vancouver. University of British Columbia, Department of Geography.

Brace, N., Kemp, R., & Snelgar, R. (2009). *SPSS for Psychologists: A Guide To Data Analysis* (4th ed.). Basingstoke: Palgrave Macmillan Limited.

Bretz, S., Akbari, H., & Rosenfeld, A. (1998). Practical issues for using solar-reflective materials to mitigate urban heat islands. *Atmospheric Environment*, 32, 95-101. doi: http://dx.doi.org/10.1016/S1352-2310(97)00182-9

215

Burgess, E. W. (1924). The growth of the city: an introduction to a research project. *American Sociological Society*, 18, 85-97.

Bustamante, J., Pacios, F., Díaz-Delgado, R., Aragonés, D. (2009). Predictive models of turbidity and water depth in the Doñana marshes using Landsat TM and ETM+ images. *Journal of Environmental Management*, 90 (7), 2219-2225. doi: 10.1016/j.jenvman.2007.08.021

Butler, T. (2005). Dubai's artificial islands have high environmental cost. *Mongabay.* http://news.mongabay.com/2005/08/dubais-artificial-islands-have-high-environmental-cost/ (accessed 22nd May, 2015).

Cai, L., Tang, D., & Li, C. (2015). An investigation of spatial variation of suspended sediment concentration induced by a bay bridge based on Landsat TM and OLI data. *Advances in Space Research*, 56(2), 293-303. doi: 10.1016/j.asr.2015.04.015

Carnahan, W.H., & Larson, R.C. (1990). An Analysis of an Urban Heat Sink. *Remote Sensing of Environment*. 33, 65-71. doi: http://dx.doi.org/10.1016/0034-4257(90)90056-R

Chander, G., & Markham, B. (2003). Revised Landsat-5 TM radiometric calibration procedures and postcalibration dynamic ranges. *IEEE Transactions on Geoscience and Remote Sensing, 41(11),* 2674–2677. doi: 10.1109/TGRS.2003.818464.

Chen, Y.C., Tan, C.H., Wei, C., & Su, Z.W. (2014). Cooling Effect of Rivers on Metropolitan Taipei Using Remote Sensing. *International Journal of Environmental Research and Public Health*, 11, 1195-1210; doi:10.3390/ijerph110201195

Cheng, P., & Sustera, J. (2009). Using RapidEye data without round control: Automated high-speed high-accuracy. *Geoinformatics*, 36-40. http://www.gisat.cz/images/upload/69ba4_geoinformatics-rapideye.pdf (accessed 9th December, 2013).

Chi, M. V., Thi, L. P., & Si, S. T. (2009). Monitoring urban space expansion using Remote sensing data in Ha Long city, Quang Ninh province in Vietnam. *7th FIG Regional Conference*. Hanoi, Vietnam.

Christen, A., & Vogt, R. (2004). Energy and Radiation Balance of a Central European City. *International Journal of Climatology*, 24(11):1395-1421. doi: 10.1002/joc.1074

City Mayors Foundation. (n.d.). The world's fastest growing cities and urban areas from 2006 to 2020. http://www.citymayors.com/statistics/urban_growth1.html (accessed 12 July, 2013).

Clarke, K. C., Hoppen, S., & Gaydos, L. (1997). A self-modifying cellular automata model of historical urbanization in the San Francisco Bay area. *Environment and Planning B*, 24, 247–261. doi:10.1068/b240247

Cohen, B. (2006). Urbanization in developing countries: Current trends,future projections, and key challenges for sustainability. *Technology in Society, 26*, 63–80.

Committee on Earth Observation Satellites.(2012). The earth observation handbook. http://www.eohandbook.com/ (accessed 16th November, 2012).

Congalton, R. G., & Green, K. (2009). *Assessing the Accuracy of Remotely Sensed Data: Principles and Practices* (2nd ed.). Boca Raton, FL: CRC Press/Taylor & Francis Group.

Coutts, A., & Harris, R. (2013). *Urban Heat Island Report: A multi-scale assessment of urban heating in Melbourne during an extreme heat event: policy approaches for adaptation.* Victorian Centre for Climate Change Adaptation Research.

Coseo, P., & Larsen, L. (2014). How factors of land use/land cover, building configuration, and adjacent heat sources and sinks explain Urban Heat Islands in Chicago. *Landscape and Urban Planning*, 125, 117–129. doi: 10.1016/j.landurbplan.2014.02.019

Crane, M., Xian, G., & McMahon, C. (2005). Estimation of Sub-Pixel Impervious Surfaces Using Landsat and Aster Imagery for Assessing Urban GrowthAGERY FOR

ASSESSING URBAN GROWTH. In M. Moeller, & E. Wentz (Ed.), *Proceedings of the ISPRS joint conference.* Tempe, AZ: International Archives of Photogrammetry, Remote Sensing and Spatial Information Sciences.

Cressey, D. (2011). Gulf ecology hit by coastal development Dubai's artificial islands are affecting marine eco. *Nature*, 479, 277. http://www.nature.com/polopoly_fs/1.9374!/import/pdf/479277a.pdf (accessed 18th January, 2015).

Cristobal, J. Jimenez-Munoz, J. C., Sobrino, J. A., Ninyerola, M., & Pons, X. (2009). Improvements in land surfacetemperature retrieval from the Landsat series thermal band using water vapor and air temperature. *J. Geophys. Res.*, 114. doi:10.1029/2008JD010616.

Cui, L., & Shi, J., (2012). Urbanization and its environmental effects in Shanghai, China. *Urban Climate*, 2, 1-15. doi: 10.1016/j.uclim.2012.10.008

Cui, Y.Y., & Foy, D.E. (2012). Seasonal variations of the urban heat island at the surface and the near-surface and reductions due to urban vegetation in Mexico City. *Journal of Applied Meteorology and Climatology*, 51(5), 855-868. doi: 10.1175/JAMC-D-11-0104.1

Czajkowski, K. P., Goward, S. N., Mulhern, T., Goetz, S. J., Walz, A., Shirey, D., Stadler, S., Prince; S.D., & Dubayah, R.O. (2004). Estimating environmental variables using thermal remote sensing. In: *Thermal Remote Sensing in Land Surface Processes.* Quattrochi, D. A., & Luvall, J. C. (Eds.) CRC Press: Washington D.C., pp. 11-32.

Dailey, P.S., & Fovell, R.G. (1999). Numerical simulation of the interaction between the sea-breeze front and horizontal convective rolls. part 1: offshore ambient flow. *American Meteorological Society*, 127, 858-878. doi: http://dx.doi.org/10.1175/1520-0493(1999)127<0858:NSOTIB>2.0.CO;2

Daqamseh, S. T ; Mansor, S. ; Mahmud, A., & Pirasteh, S. (2010). Monitoring sea surface salinity season variation from MODIS satellite data. IEEE International Geoscience and Remote Sensing Symposium, 628-63. doi: 10.1109/IGARSS.2010.5651823

Dash, P., Göttsche, F.-M., Olesen, F.-S., & Fischer, H. (2002). Land surface temperature and emissivity estimation from passive sensor data: Theory and practice-current trends. *International Journal of Remote Sensing*, 23(13), 2563-259.

Department of Finance. (2009). Dubai DOF Sukuk Limited. http://www.dof.gov.ae/en-us/Investor/Lists/InvestorForms/Attachments/3/Sukuk%20Base%20Prospectus%20Oct-2009.pdf (accessed 10th March, 2012).

Dewan, A. M., & Yamaguch, Y. (2009). Land use and land cover change in Greater Dhaka, Bangladesh: Using remote sensing to promote sustainable urbanization. *Applied Geography*(29), 390–401.

Dietzel, C., Herold, M., Hemphill, J. J., & Clarke, K. C. (2005). Spatio-temporal dynamics in California's Central Valley: Empirical links to urban theory. *International Journal of Geographical Information Science*, 19(2), 175–195. doi:http://dx.doi.org/10.1080/13658810410001713407

Dietzel, C., Oguz, H., Hemphill, J. J., Clarke, K. C., & Gazulis, N. (2005). Diffusion and coalescence of the Houston Metropolitan Area: Evidence supporting a new urban theory. *Environment and Planning B: Planning and Design*, 32, 231-246. doi:10.1068/b31148

Draper, N.R, & Smith, H. (1998). *Applied Regression Analysis* (3rd ed., pp.335-339). New York: John Wiley & Sons, Inc.

Duan, H., Zhang, Y., Zhang , B., Song, K., & Wang, Z. (2007). Assessment of chlorophyll-a concentration and trophic state for Lake Chagan using Landsat TM and Field Spectral Data. *Environmental Monitoring and Assessment* , (129), 295–308. doi: 10.1007/s10661-006-9362-y

Dubai Airport. (2010). *Climate*. http://www.dia.ae/DubaiMet/Met/Climate.aspx (accessed 1st October, 2012).

Dubai Airport (2014). *Climate*. https://services.dubaiairports.ae/DubaiMet/Met/Climate.aspx. (accessed 15th May, 2014).

Dubai Government. (2007). Dubai Stratigic Plan 2015. http://www.deg.gov.ae/SiteCollectionImages/Content/pubdocs/Dubai_Strategic_Plan_2 015.pdf (accessed 19th July, 2012).

Dubai Statistical Centre. (2000). Total population, buildings, housing units & establishments in censuses. http://www.dsc.gov.ae/Reports/-72238938CSFB00-02-01.pdf (accessed 22nd September, 2013).

Dubai Statistical Centre. (2009). Gross Domestic Product at Constant Prices. http://www.dsc.gov.ae/EN/Themes/Pages/Reports.aspx?TopicId=4&Year=2009 (accessed 25th September, 2013).

Dubai Statistical Centre. (2010*)*. Statistical Yearbook-Emirate of Dubai. http:dsc.gov.ae/Publication/SYB_2010.pdf (accessed 21st May, 2012).

Dubai Statistical Centre. (2011). Population Bulletin: Emirates of Dubai. http://www.dsc.gov.ae/EN/Themes/Pages/Publications.aspx?TopicId=23 (accessed 21st May, 2012).

Dubai Statistical Centre (2013). Population Bulletin: Emirates of Dubai. https://www.dsc.gov.ae/en-us/Themes/Pages/Population-and-Vital-Statistics.aspx?Theme=42 (accessed 23rd June, 2015).

Dubai Statistical Centre (2014). Population Bulletin: Emirates of Dubai. https://www.dsc.gov.ae/en-us/Themes/Pages/Climate-and-Environment.aspx?Theme=35 (accessed 9th May, 2015).

Elsheshtawy, Y. (2010). *Dubai: Behind an Urban Spectacle*(1st ed.). Routledge: Oxfordshire.

Emmanuel, R. (2005). *An Urban approach to climate sensitive design: strategies for the tropics*. London: Spon Press.

Emmanuel, R., & Kruger, E. (2012). Urban heat island and its impact on climate change resilience in a shrinking city: The case of Glasgow, UK. *Building and Environment*, 53, 137-149. doi:10.1016/j.buildenv.2012.01.020

Emmanuel, R., Rosenlund, H., & E. Johansson. (2007). Urban shading – a design option for the tropics? A study in Colombo, Sri Lanka. *International Journal of Climatology*, 27(14), 1995–2004. doi: 10.1002/joc.1609

Erell, E., Pearlmutter, D., & Williamson, T. (2011). *Urban Microclimate: designing the spaces between buildings* (1st ed.) London: EarthScan.

Exelis (2013). Vegetation Analysis: Using Vegetation Indices in ENVI. (accessed 5th December, 2015).

Fan, X., Lam, K., & Yu, Q. (2012). Differential exposure of the urban population to vehicular air pollution in Hong Kong. Science of the Total Environment, 427, 211-219. doi: 10.1016/j.scitotenv.2012.03.057

Flores, E. S., Olivas, A. G., & Chávez, J. (2008). Land cover change and landscape dynamics in the urbanizing area of a Mexican border city. *ASPRS 2008 Annual Conference*, 28 April-2 May, 2008. Portland, Oregon. (pp. 1-9).

Foody, G. M., 2002, Status of land cover classification accuracy assessment. *Remote Sensing of Environment*, 80, 185- 201.

Freitas,E., Rozoff, C., Cotton, W., & Dias, P. (2007). Interactions of an urban heat island and sea-breeze circulations during winter over the metropolitan area of São Paulo, Brazil. *Boundary-Layer Meteorology*, 122(1), 43-65. doi: 10.1007/s10546-006-9091-3

Frey, C. M. & Parlow, E. (2009). Geometry effect on the estimation of band reflectance in an urban area. *Theoretical and Applied Climatology*, 96, 395-406.

Frey, C. M., Rigo, G., & Parlow, E. (2007). Urban radiation balance of two coastal cities in a hot and dry environment. *International Journal of Remote Sensing*, 28(12), 2695 2712. doi: http://dx.doi.org/10.1080/01431160600993389

Frumkin, H. (2002). Urban sprawl and public health. *Public health reports*, 117(3), 202-217. http://www.ncbi.nlm.nih.gov/pmc/articles/PMC1497432/pdf/12432132.pdf (accessed 2nd May, 2013).

Gal, T., Lindberg, F., & Unger, J. (2009). Computing continuous sky view factors using 3D urban raster and vector databases: comparison and application to urban climate. *Theoretical and Applied Climatology*, 95: 111–123. doi: 10.1007/s00704-007-0362-9

Gamba, P., Dell'Acqua, F., Stasolla, M., Trianni, G., & Lisini, G. (2011). Limits and challenges of optical very-high-spatial-resolution satellite remote sensing for urban applications. In X. Yang (Ed.), *Urban Remote Sensing: Monitoring, Synthesis and Modeling in the Urban Environment* (1st ed., pp. 35-48). Chichester: John Wiley & Sons, Ltd.

Gan, T. Y., Kalinga, O. A., Ohgushi, K., & Araki, H. (2004). Retrieving seawater turbidity from Landsat TM data by regressions and an artificial neural network. *International Journal of Remote Sensing*, 25(21), 4593-4615. doi: 10.1080/01431160410001655921

Gartland, L. (2008). Heat Islands: *Understanding and Mitigating Heat in Urban Areas*. Washington, DC: Earthscan.

Gerometta, M., Kazmierczak, P., Lacey, M., Oldfield, P., &, Wood, A. (2009). World's tallest 50 urban agglomerations. *CTBUH Journal*, 5, 1-3. http://www.ctbuh.org/LinkClick.aspx?fileticket=XJiOhTaJjTE%3d&tabid=1006&language=en-GB (accessed 14th April, 2013).

Gillespie, A., Rokugawa, S., Matsunaga, T., Cothern, J.S., Hook, S., & Kahle, A.B. (1998). A temperature and emissivity separation algorithm for Advanced Spaceborne Thermal Emission and Reflection Radiometer (ASTER) images. *IEEE Transactions on Geoscience and Remote Sensing*, 36(4), 1113-1126. doi: 10.1109/36.700995

Gillies, A. V., Taconet O., & Carlson, T.N. (1995). Workshop on thermal remote sensing of the energy and water balance over vegetation in conjunction with other sensors. *The Earth Observer*, September/October, 1995.

Gillies, R. R., Box, J. B., Symanzik, J., & Rodemaker, E. J. (2003). Effects of urbanization on the aquatic fauna of the Line Creek. *Remote Sensing of Environment, 86*, 411–422. doi:10.1016/S0034-4257(03)00082-8

Gonçalves, H., Gonçalves, J.A., Corte-Real, L., 2009. Measures for an objective evaluation of the geometric correction process quality. *IEEE Geoscience and Remote Sensing Letters*, 6(2), 292–296. doi: 10.1109/LGRS.2008.2012441

Gosling, S.N., Bryce, E.K., Dixon, P.G., Gabriel, K.M.A., Gosling, E.Y., Hanes, J.M., Hondula, D.M., Liang, L., Bustos Mac Lean, P.A., Muthers, S., Nascimento, S.T., Petralli, M., Vanos, J.K., & Wanka, E.R. (2014). A glossary for biometeorology, *International Journal of Biometeorology*, 58 (2), 277-308. doi:10.1007/s00484- 013-0729-9

Goward, S.N., (1981). Thermal behavior of urban landscapes and the urban heat island. *Physical Geography*, 2, 19-33. doi: 10.1080/02723646.1981.10642202

Grey, W., Luckman, A., & Holland, D. (2003). Mapping urban change in the UK using satellite radar interferometry. *Remote Sensing of Environment, 87*, 16–22. doi:10.1016/S0034-4257(03)00142-1

Grimmond, S. (2007). Urbanization and global environmental change: local effects of urban warming. The *Geographical Journal*, 173 (1), 83-88. doi: 10.1111/j.1475-4959.2007.232_3

Guarino, J. (2004). A comparison of first and second generation multivariate analyses: canonical correlation analysis and structural equation modeling. *Florida Journal of Educational Research*, 42, 22 – 40.

Haack, B., Craven, D., & Jampoler, S. M. (1997). Processing techniques for mapping urban growth: Kathmandu, Nepal. *Geocarto International, 12*(1), 5-12.

Hailu, A., & VanEenwyk, J. (2009). *Guidelines for Using Rural-Urban Classification Systems for Public Health Assessment.* Hong Kong: Geocarto International Centre, G.P.O. Box 4122. http://www.doh.wa.gov/Portals/1/Documents/5500/RuralUrbGuide.pdf (accessed 17th January, 2014).

Han, L., & Jordan, Karenj. (2005). Estimating and mapping chlorophyll- a concentration in Pensacola Bay, Florida using Landsat ETM+ data. *International Journal of Remote Sensing*, 26(23), 5245-525. doi:10.1080/01431160500219182

Hansen, K. (2013). NASA scientists relate urban population to air pollution. https://www.nasa.gov/content/goddard/nasa-scientists-relate-urban-population-to-air-pollution/#.VbuvlE9VhBc (accessed 18th August, 2014).

Hamdi, R., & Schayes, G. (2009). Sensitivity study of the urban heat island intensity to urban characteristics. *The seventh International Conference on Urban Climate, 29 June - 3 July.* Yokohama, Japan.

Hanberry B O, 2007 *Birds and small mammals, intensively established pine plantations, and landscape metrics of the coastal plain* PhD thesis, Mississippi State University.

Hara, Y., Takeuchi, K., & Okubo, S. (2005). Urbanization linked with past agricultural landuse patterns in the urban fringe of a deltaic Asian mega-city: a case study in Bangkok. *Landscape and Urban Planning, 73*(1), 16-28.

Harris, C. D., & Ullman, E. L. (1945). The nature of Cities. *The Annals of American Academy of Political and Social Science*, 242, 7-17. doi:10.1177/000271624524200103

Hashim, M., & Yap, X. Q. (2012). A robust calibration approach for PM10 prediction from MODIS aerosol optical depth. *Atmospheric Chemistry and Physics Discussions*, 12 (12), 31483-31505. doi: 10.5194/acpd-12-31483-2012

Heldens W., Taubenböck H., Esch T., Heiden U., & Wurm M (2013). Analysis of surface thermal patterns in relation to urban structure types: a case study for the city of Munich. In: Kuenzer C., & Dech S. (eds). *Thermal infrared remote sensing – sensors, methods, applications. Remote sensing and digital image processing series 17.* Springer, Netherlands, p. 475–495.

Herold, M., Scepan, J., & Clarke, C. K. (2002). The use of remote sensing and landscape metrics to describe structures and changes in urban land uses. *Environment and Planning A*, 34, 1443 -1458. doi:10.1068/a3496

Honnay O, Piessens K, Van Landuyt W, Hermy M, Gulinck H, 2003, "Satellite based land use and landscape complexity indices as predictors for regional plant species diversity" *Landscape and Urban Planning* **63** 241–250

Honour, S. L., Bell, J. N. B., Ashenden, T. W., Cape, J. N., & Power, S. A. (2009). Responses of herbaceous plants to urban air pollution: Effects on growth, phenology and leaf surface characteristics, *Environmental Pollution*, 157(4), 1279-1286. doi: 10.1016/j.envpol.2008.11.049

Howard, L. (1833). *The Climate of London.* London Harvey and Dorton: London, UK, 1833, V. 2, pp. 1818-1820.

Hoyt, H. (1939). *The Structure of growth of residential neighbourhoods in American cities.* Washington, D. C.: Federal Housing Administration.

Hu, C., Chen, Z., Clayton, T., Swarnzenski, P., Brock, J., & Muller-Karger, F. (2004). Assessment of estuarine water-quality indicators using MODIS medium-resolution bands: Initial results from Tampa Bay, FL. *Remote Sensing of Environment*, (93): 423-441. doi:10.1016/j.rse.2004.08.007

Hu, L., & Brunsell, N.A. (2013). The impact of temporal aggregation of land surface temperature data for surface urban heat island (SUHI) monitoring. *Remote Sensing of Environment, 134,* 162–174. http://dx.doi.org/10.1016/j.rse.2013.02.022.

Hwang, R-L., Lin, T-P., Lin, T-P., & Matzarakis, A. (2011). Seasonal effects of urban street shading on long-term outdoor thermal comfort. *Building and Environment*, 46, 863-870. doi: 10.1016/j.buildenv.2010.10.017

Imhoff, M.L., Zhang, P., Wolfe, R.E., & Bounoua, L. (2010). Remote sensing of the urban heat island effect across biomes in the continental USA. *Remote Sensing of Environment, 114*, 504–513. http://dx.doi.org/10.1016/j.rse.2009.10.008

Intercon. (2010). Dubai: The nemesis of sustainability. http://intercongreen.com/2010/02/23/dubai-the-nemesis-of-sustainability> (accessed 16th December, 2014).

International Monetary Fund. (2000). The Impact of higher oil prices on the global economy. http://www.imf.org/external/pubs/ft/oil/2000/oilrep.pdf (accessed 20th September, 2013).

IPCC (The Intergovernmental Panel on Climate Change). (2007). TS.3.1.1 *Global Average Temperatures, Climate Change 2007: Working Group I: The Physical Science Basis*, IPCC Fourth Assessment Report: Climate Change 2007. https://www.ipcc.ch/publications_and_data/ar4/wg1/en/tssts-3-1-1.html (accessed 7th, February, 2013)

Janssen, L. L., & Van Der Wel, F. J. (1994). Accuracy assessment of satellite derived land-cover: A review. *Photogrammetric Engineering and Remote Sensing*, 60(4), 419–426. http://cat.inist.fr/?aModele=afficheN&cpsidt=4035219 (accessed 18th March, 2012).

Jat , M. K., Garg, P., & Khare, D. (2008). Monitoring and modelling of urban sprawl using remote sensing and GIS techniques. *International Journal of Applied Earth Observation, 10*, 26–43. doi:10.1016/j.jag.2007.04.002

Jensen, J. R. (2005). *Introductory digital image processing a remote sensing perspective* (3rd ed.). USA: Prentice Hall Series in geographic information science.

Jensen, J.R. (2007). *Remote sensing of the environment: An earth resource perspective* (2nd ed.). NJ: Prentice-Hall: Upper Saddle River.

Ji, C. y., Liu, Q., Sun, D., Wang, S., Lin, P., & Li, X. (2001). Monitoring urban expansion with remote sensing in China. *International Journal of Remote Sensing*, 22(8), 1441–1455. doi: 10.1080/01431160117207

Jimenez-Muooz, J. C., & Sobrino, J. A. (2006), Error sources on the land surface temperature retrieved from thermal infrared single channel remote sensing data. *International Journal of Remote Sensing*, 27 (5),999–1014. doi: 10.1080/01431160500075907

Jimenez-Munoz, J. C., Sobrino, J. A., Skokovic, D., Mattar, C., Cristobal, J. (2014). Land surface temperature retrieval methods from Landsat-8 thermal infrared sensor data. *IEEE Geoscience and Remote Sensing Letters*, 11(10), 1840-1843. doi: 10.1109/LGRS.2014.2312032

Jin, M. (2004). Analysis of land skin temperature using AVHRR observations. *Bulletin of the American Meteorological Society*, 85(4), 587-600. doi: http://dx.doi.org/10.1175/BAMS-85-4-587

Jin, M., & Dickinson , R.E. (2010). Land surface skin temperature climatology: benefitting from the strengths of satellite observations. *Environmental Research Letter*, 5 (4), 1-13. doi: 10.1088/1748-9326/5/4/044004

Jinghui, L., Yang, S., Xiangtao, F., Chudong, H., & Yun, S. (2006). Retrieval and correlation analysis of urban land surface temperature and vegetation fraction using ASTER data. *IEEE International Symposium on Geoscience and Remote Sensing*, July Aug. 2006, pp.1451-1453.

Johansson, E., Emmanuel, R. (2006). The influence of urban design on outdoor thermal comfort in the Hot Humid City of Colombo, Sri Lanka. *International Journal of Biometeorology*, 51, 119-133. doi: 10.1007/s00484-006-0047-6

Johnson, D., Lulla, V., Stanforth, A., & Webber, J. (2011). Remote sensing of heat-related health risks: The trend toward coupling socioeconomic and remotely sensed data. *Geography Compass*, 5(10), 767–780. doi: 10.1111/j.1749-8198.2011.00442.x

Johnson, G.T., & Watson, I.D. (1984). The determination of view-factors in urban canyons. *Journal of Climate and Applied Meteorology*, 23, 329–335. doi: http://dx.doi.org/10.1175/1520-0450(1984)023<0329:TDOVFI>2.0.CO;2

Jong, S. M., Bagre, A., Van Teeffelen, P. B., & van Deursen, W. P. (2000). Monitoring Trends in Urban Growth and Surveying City Quarters in Ouagadougou, Burkina Faso Using SPOT-XS. *Geocarto International*, 15(2), 63-70.

Julien, Y., Sobrino, J. A., & Verhoef, W. (2006). Changes in land surface temperatures and NDVI values over Europe between 1982 and 1999. *Remote Sensing of Environment*, 103 (1), 43-55. doi: 10.1016/j.rse.2006.03.011

Jun, C., Tingwei, C., Zhongfeng, Q., & Changsong, L. (2014). Split-Window Model for deriving total suspended sediment matter from MODIS data in the Bohai Sea. *IEEE Journal of Selected Topics in Applied Earth Observations and Remote Sensing*, 7(6), 2611-2618. doi: 10.1109/JSTARS.2013.2297692

Kakon, A.N., Nobuo, M., Kojima, S., Yoko, T. (2010). Assessment of Thermal Comfort in Respect to Building Height in a High-Density City in the Tropics. *American J. of Engineering and Applied Sciences*. 3(3), 545-551. doi: http://dx.doi.org/10.3844/ajeassp.2010.545.551

Kalnay, E. & Cai, M.(2003). Impact of urbanization and land-use change on climate. *Nature*, 423, 528 – 53. http://www.nature.com/nature/journal/v423/n6939/full/nature01675.html (accessed 22nd December, 2013).

Kaloush, K. E., Carlson, J. D.,Golden, J. S., & Phelan, P.E. (2008). The thermal and radiative characteristics of concrete pavements in mitigating urban heat island effects. *Global Institute of Sustainability, final report*. Arizona State University, Tempe, Arizona, Portland Cement Association.

Kasimu, A., & Tateishi, R. (2008). Global urban mapping using coarse resolution remote sensing data with the reference of landsat imagers Alimujiang. *The International Archives of the Photogrammetry, Remote Sensing and Spatial Information Sciences*, *XXXVII. Part B7*, pp. 1523-1528. Beijing.

Kato, S., Matsunaga, T., & Yamaguchi, Y. (2010). Influence of shade on surface temperature in an urban estimated by ASTER data. *International Archives of the Photogrammetry*, Remote Sensing and Spatial Information Science. 38, 925–929.

Kato, S., & Yamaguchi, Y. (2005). Analysis of urban heat-island effect using ASTER and ETM+ data: Separation of anthropogenic heat discharge and natural heat radiation from sensible heat flux. *Remote Sensing of Environment*, 99, 44–54. doi: 10.1016/j.rse.2005.04.026

Kayadibi, O. (2011). Evaluation of imaging spectroscopy and atmospheric correction of multispectral images (Aster and Landsat 7 ETM+). *Proceedings, 5th Int. Conf. Recent Advances in Space Technologies (RAST),9-11 June.*, Istanbul. pp. 154–159. doi: 10.1109/RAST.2011.5966811

Kelbaugh. D. (2012). The environmental paradox of cities: gridded in Manhattan vs. gridless in Dubai. *The Journal of Sustainable Development*, 9(1), 84 – 96.

Khandelwal, S., & Goyal, R. (2010). Effect of Vegetation and Urbanization over Land Surface Temperature: Case Study of Jaipur City. Remote Sensing for Science, Education and Culture. *30th EARSeL Symposium*, P. 177-183. http://www.conferences.earsel.org/abstract/show/2067 (accessed 12 February, 2013).

Kharol, S.K., Kaskaoutis, D.G., Badarinath, K. V. S., Sharma, A. R., & Singh, A. R. (2013). Influence of land use/land cover (LULC) changes on atmospheric dynamics over the arid region of Rajasthan state, India. *Journal of Arid Environments*, 88, 90-101. doi:

10.1016/j.jaridenv.2012.09.006

King, R. B., Lee, M. T., & Singh, K. P. (1989). *Land use/cover classification for the proposed superconducting super collider study area, northeastern Illinois.* Champaign, Illinois: Illinois State Water Survey Division, Surface Water Section.

Knight , J., & Voth, M. (2010). Mapping Impervious Cover Using Multi-Temporal MODIS NDVI Data. *Ieee journal of selected topics in applied earth observations and remote sensing*, 1-7.

Knight, S., Claire, S., & Michael, R. (2010). Mapping Manchester's urban heat island. *Weather*, 65(7), 188-193. doi: 10.1002/wea.542

Kurucu, Y., & Kucukyilmaz, N. C. (2008). monitoring the impact of urbanization and industrialization on the agricultural land and environment of the Torbali, Izmir region, Turkey. *Environ Monit Assess, 139*, 289-297.

Lamaro, A. A., Mariñelarena, A. , Torrusio, S. E. ; Sala, S. E. (2013). Water surface temperature estimation from Landsat 7 ETM+ thermal infrared data using the generalized single-channel method: Case study of Embalse del Río Tercero (Córdoba, Argentina). *Advances in Space Research,* 51(3), 492-500. doi: 10.1016/j.asr.2012.09.032

Lazzarini, M., Marpu, P.R., & Ghedira, H. (2013). Temperature-land cover interactions: The inversion of urban heat island phenomenon in desert city areas. *Remote Sensing of Environment, 130,* 136–152. doi: 10.1016/j.rse.2012.11.007

Leconte, F., Bouyer, J., Claverie, R., Pétrissans, M. (2015). Using Local Climate Zone scheme for UHI assessment: Evaluation of the method using mobile measurements. *Building and Environment,* 83, 39-49. doi: 10.1016/j.buildenv.2014.05.005

Leitão, A. B., Miller, J., Ahern, J., & McGarigal, K. (2006). *Measuring Landscape: A Planner's Handbook.* Washington, D.C: Island Press.

Li, D., Bou-Zeid, E., Oppenheimer, M. (2014). The effectiveness of cool and green roofs as urban heat island mitigation strategies. *Environmental Research Letters,* 9 (5). doi: 10.1088/1748-9326/9/5/055002

Li, L., Sato, Y., & Zhu, H. (2003). Simulating spatial urban expansion based on physical process. *Landscape and Urban Planning,* 64, 67-76. doi: 10.1016/S0169-2046(02)00201-3

Li, Y.y., Zhang, H., & Kainz, W. (2012). Monitoring patterns of urban heat islands of the fast-growing Shanghai metropolis, China: Using time-series of Landsat TM/ETM+ data. *International Journal of Applied Earth Observation and Geoinformation,* 12, 127–138. doi: 10.1016/j.jag.2012.05.001

Li, Z.L., Tang, B.H., Wu, H., Ren, H., Yan, G., Wan, Z., Trigo, I.F., Sobrino, J.A. (2013). Satellite-derived land surface temperature: Current status and perspectives. *Remote Sensing of Environment,* 131, 14–37. doi: http://dx.doi.org/10.1016/j.rse.2012.12.008

Liang, B, & Weng, Q. (2011). Assessing Urban Environmental Quality Change of Indianapolis, United States, the Remote Sensing and GIS Integration. *IEEE Journal of Selected Topics in Applied Earth Observations and Remote Sensing,* 4 (1), 43-55. doi:10.1109/JSTARS.2010.2060316

Liang, S. (2000). Narrowband to broadband conversions of land surface albedo I Algorithms. *Remote Sensing of Environment, 76,* 213– 238. doi: 10.1016/S0034-4257(00)00205-4

Lillesand, T., M., Kiefer, R., W., & Chipman, J., W. (2004). *Remote Sensing and Image Interpretation* (5th ed.). New York: John Wiley and Sons.

Lin, G., Fu, J., Jiang, D., Hu, W., Dong, D., Huang, Y., & Zhao, M. (2014). Spatio-Temporal Variation of PM2.5 Concentrations and Their Relationship with Geographic and Socioeconomic Factors in China. *Int. J. Environ. Res. Public Health*, 11, 173-186. doi:10.3390/ijerph110100173

Lin, T.-P., Tsai, K.-T., Hwang, R.-L., & Matzarakis, A. (2012). Quantification of the effect of thermal indices and sky view factor on park attendance. *Landscape and Urban*

Planning, 107, 137– 146. doi:10.1016/j.landurbplan.2012.05.011

Lin, Y. P., Chang, T. K., Wu. C .F., chiang, T. C., & Lin S. H. (2006). Assessing impacts of typhoons and the Chi-Chi earthquake on Chenyulan watershed landscape pattern in central Taiwan using landscape metrics. *Environmental Management, 38*, 108-125.

Littlefair, P.J., Santamouris, M., Alvarez, S., Dupagne,A., Hall, D., Teller, J., et al. (2000*). Environmental site layout planning: solar access, microclimate and passive cooling in urban areas* (1st ed.). Watford: CRC.

Liu, L., & Zhang, Y. (2011). Urban heat island analysis using the Landsat TM data and ASTER data: A case study in Hong Kong. *Remote Sensing, 3*, 1535-1552. doi:10.3390/rs3071535

Liu, Y., Zhang, X., & Lei, J. (2010). Urban expansion of oasis cities between 1990 and 2007 in Xinjiang, China. *International Journal of Sustainable Development & World Ecology, 17*(3), 253–262.

Lo, C. P., & Choi, J. (2004). A hybrid approach to urban land use/cover mapping using Landsat 7 Enhanced Thematic Mapper Plus (ETM+) images. *International Journal of Remote Sensing, 25*(14), 2687–2700. doi: http://dx.doi.org/10.1080/0143116031000161842 8

Lougeay, R., Brazel, A., Hubble, M., (1996). Monitoring intraurban temperature patterns and associated land cover in Phoenix, Arizona using Landsat thermal data. *Geocarto International, 11*(4), 79-90. doi: 10.1080/10106049609354564

Loughner, C. P., Allen, D. J., Zhang, D., Pickering, K. E., Dickerson, R. R., & Landry, L. (2012). Roles of urban tree canopy and buildings in urban heat island effects: parameterization and preliminary results. *Journal of Applied Meteorology and Climatology, 51*, 1775-1793. doi: 10.1175/JAMC-D-11-0228.1

Lowry, J.H., & Lowry, M.B. (2014).Comparing spatial metrics that quantify urban form. *Computers, Environment and Urban Systems, 44*: 59-67. doi: 10.1016/j.compenvurbsys.2013.11.005

Luo, N, Wong, M.S, Zhao, W., Yan, X., & Xiao, F. (2015). Improved aerosol retrieval algorithm using Landsat images and its application for PM10 monitoring over urban areas. *Atmospheric Research, 153*, 264-275. doi: 10.1016/j.atmosres.2014.08.012

Ma, Y., & Xu, R. (2010). Remote sensing monitoring and driving force analysis of urban expansion in Guangzhou City, China. *Habitat International, 34*, 228–235.

Mackey, C.W., Lee, X., & Smith, R.B. (2012). Remotely sensing the cooling effects of city scale efforts to reduce urban heat island. *Building and Environment, 49*, 348-358. doi: http://dx.doi.org/10.1016/j.buildenv.2011.08.004

Maktav, D., & Erbek, F. S. (2005). Analysis of urban growth using multi-temporal satellite data in Istanbul,Turkey. *International Journal of Remote Sensing, 26*(4), 797–810.

Malaret, E., Bartolucci, L.A., Lozano, D.F., Anuta, P.E., & McGillem, C.D. (1985). Landsat-4 and Landsat-5 Thematic Mapper data quality analysis. *Photogrammetric Engineering and Remote Sensing, 51*, 1407–1416.

Maltese, A. (2013). Coastal zone water quality: calibration of a water-turbidity equation for MODIS data. *European Journal of Remote Sensing*, 46, 333-347. doi: http://dx.doi.org/10.5721/EuJRS20134619

Markogianni, V., Dimitriou, E., & Karaouzas, I. (2014). Water quality monitoring and assessment of an urban Mediterranean lake facilitated by remote sensing applications. *Environmental Monitoring and Assessment*, 186(8), 5009-5026. doi: 10.1007/s10661-014-3755-0

Martellozzo, F. & Clarke, K.C. (2011). Measuring urban sprawl, coalescence, and dispersal: a case study of Pordenone, Italy. *Environment and Planning B: Planning and Design*, 38, 1085-1104. doi:10.1068/b36090

Martin, J., Kurc, S.A., Zaimes, G., Crimmins, M., Hutmacher, A., & Green, D. (2012). Elevated air temperatures in riparian ecosystems along ephemeral streams: The role of housing

density. *Journal of Arid Environments, 84,* 9-18. http://dx.doi.org/10.1016/j.jaridenv.2012.03.019

Martinuzzi, S., Gould, W. A., & Gonzalez, O. M. (2007). Land development, land use, and urban sprawl in Puerto Rico integrating remote sensing and population census data. *Landscape and Urban Planning, 79,* 288–297.

Maselli, F., Bottai, L., Ercole, T., & Terpessi, C. (2002). Use of multitemporal spot HRV-PAN images for mapping urban expansion processes. *Remote Sensing Reviews,* 20(4), 323-345. doi:10.1080/02757250109532441

Masek, J. G., Lindsay, F. E., & Goward, S. N. (2000). Dynamics of urban growth in the Washington DC metropolitan area, 1973–1996, from Landsat observations. *International Journal of Remote Sensing,* 21, 3473–3486. doi: http://dx.doi.org/10.1080/014311600750037507

Masser, I. (2001). Managing our urban future: the role of remote sensing and geographic information systems. *Habitat International*(25), 503–512.

McCarthy, M.P., Best, M.J., Betts, R.A. (2010). Climate change in cities due to global warming and urban effects. *Geophysical Research Letters,* 37 (9), 1-5. doi: 10.1029/2010GL042845

McGarigal, K. (2006). *Landscape pattern metrics.* In: El-Shaarawi AH and Piegorsch WW (eds.) Encyclopedia of Environmetrics. Wiley: Chichester, UK

McGarigal, k., Cushman, S. A., Neel, M. C., & Ene, E. (2002). Fragstats v4: Spatial Pattern Analysis Program for Categorical Maps. http://www.umass.edu/landeco/research/fragstats/fragstats.html (accessed 12 January, 2012).

McMahon, C., Xian, G., & Crane, M. (2005). Mapping Urban Imperviousness Using Remotely Sensed Data and Regression Tree Models. *Global Priorities in Land Remote Sensing.* Sioux Falls, South Dakota.

Miao, Y., Liu, S., Zheng, Y., Wang, S., Chen, B. (2014). Numerical Study of the Effects of Topography and Urbanization on the Local Atmospheric Circulations over the Beijing-Tianjin-Hebei, China. *Advances in Meteorology,* 2014. doi: 10.1155/2014/397070

Milanović, N. P. (2007). European urban spawl: Sustainability, cultures of (anti)urbanism and "hybrid cityscapes". *DOAJ,* 27, 101-133.

Mirzaei, P. A., & Haghighat, F. (2010). Approaches to study Urban Heat Island – Abilities and limitations. *Building and Environment,* 45(10), 2192-2201. doi: 10.1016/j.buildenv.2010.04.001

Moeller, M. S. (2005). Remote sensing for the monitoring of urban growth patterns. *Scientific Paper.* Trimble website. http://www.ecognition.com/sites/default/files/253_moeller_urs2005.pdf (accessed 13th April, 2011).

Moeller, M. S., & Blaschke, T. (2006). Urban change extraction from high resolution satellite image. *ISPRS Technical Commission II Symposium,* Vienna, (pp. 151-156).

Montanher, O. C., Novo, E M., Barbosa, C. C. F., Rennó, C. D., & Silva, T. S. F. (2014). Empirical models for estimating the suspended sediment concentration in Amazonian white water rivers using Landsat 5/TM. *International Journal of Applied Earth Observations and Geoinformation,* 29, 67-77. doi: 10.1016/j.jag.2014.01.001

Mundia, C., & Aniya, M. (2005). Analysis of land use/cover changes and urban expansion of Nairobi city using remote sensing and GIS. *International Journal of Remote Sensing,* 26(13), 2831–2849.

NASA (2009). <http://www.nasa.gov/mission_pages/terra/news/heat-islands.html.> Edited by Carlowicz, M. (accessed 3rd May, 2014).

NASA (2013). Landsat 7. http://landsat.gsfc.nasa.gov/?p=3184 (accessed 20th May, 2015).

Nasrallah, H.A., Brazel, A.J., Balling, R.C., (1990). Analysis of the Kuwait-City urban heat island. *International Journal of Climatology*, 10, 401–405. doi: 10.1002/joc.3370100407

Nassar, A.K., Blackburn, G.A., & Whyatt, J.D. (2014). Developing the desert: The pace and process of urban growth in Dubai. *Computers, Environment and Urban Systems, 45*, 50–62. doi: http://dx.doi.org/10.1016/j.compenvurbsys.2014.02.005.

National Bureau of Statistics. (2010). UAE Population by Emirates, Nationality and Sex. http://www.uaestatistics.gov.ae/ReportDetailsEnglish/tabid/121/Default.aspx?ItemId=1 869&PTID=104&MenuId=1 (accessed 21st March, 2012).

National Bureau of Statistics. (2011). Population estimates 2006-2010. http://www.uaestatistics.gov.ae/ReportPDF/Population%20Estimates%202006%20-%202010.pdf (accessed 21st March, 2012).

Ngie, A., Abutaleb, K., Ahmed, F., Darwish, A., & Ahmed, M. (2014). Assessment of urban heat island using satellite remotely sensed imagery: A review. *South African Geographical Journal*, 96(2), 198-214. doi: 10.1080/03736245.2014.924864

Nichol, J.E. (1996). High-resolution surface temperature patterns related to urban morphology in a tropical city: A satellite-based study. *Journal of Applied Meteorology*, 35:135–146. doi: http://dx.doi.org/10.1175/1520-0450(1996)035<0135:HRSTPR>2.0.CO;2

Nichol, J. E., Fung, W.Y., Lam, K., & Wong, M.S. (2009). Urban heat island diagnosis using ASTER satellite images and 'in situ' air temperature. *Atmospheric Research*, 94(2), 276-284. doi: 10.1016/j.atmosres.2009.06.011

Niero, M., Foresti, C., & Lombardo, M. A. (1982). The Use of LANDSAT Data to Monitor the Urban Growth of Sao Paulo Metropolitan Area. *Information for the Defence community online publishing*.

Nikolakopoulos, K.G.; Vaiopoulos, D.A.; Skianis, G.A., 2002. A Comparative Study of Different Atmospheric Correction Algorithms Over An Area With Complex Geomorphology in Western Peloponnese, Greece. *Geoscience and Remote Sensing Symposium*, IGARSS '02, IEEE International, 4, pp. 2492 – 2494.

Obiakor, M.O.; Ezeonyejiaku, C.D. & Mogbo, T.C. (2012). Effects of Vegetated and Synthetic (Impervious) Surfaces on the Microclimate of Urban Area. *Journal of Applied Sciences and Environmental Management*, Vol. 16, No. 1, 2012, pp. 85-94

Oda, R., & Kanda, M. (2009). Cooling effect of sea surface temperature of Tokyo bay on urban air temperature. *The seventh International Conference on Urban Climate*, 1-4, 29 June - 3 July 2009, Yokohama, Japan.

Oke, T.R. (1982). The energetic basis of the urban heat island. *Quarterly Journal of the Royal Meteorological Society*, 108 (455), 1-24. doi: 10.1002/qj.49710845502

Oke, T.R., (1987). *Boundary Layer Climates* (2nd ed.). London: Routledge, pp. 435.

Oke, T.R. (1988). Street design and urban canopy layer climate. *Energy and Buildings*, 11: 103–113. doi:10.1016/0378-7788(88)90026-6

Omran, E.E. (2012). Detection of land-use and surface temperature change at different resolutions. *Journal of Geographic Information System, 4,* 189-203. doi: http://dx.doi.org/10.4236/jgis.2012.43024

Ouaidrari, H., Goward, S. N, Czajkowski, K. P., Sobrino, J. A., & Vermote, E. (2002). Land surface temperature estimation from AVHRR thermal infrared measurements: An assessment for the AVHRR Land Pathfinder II data set. *Remote Sensing of Environment*, 81, 114 – 128. doi: 10.1016/S0034-4257(01)00338-8

Otterman, J., & Fraser, R.S. (1976). Earth-atmosphere system and surface reflectivities in arid regions from Landsat MSS data. *Remote Sensing of Environment, 5,* 247-266. doi: http://dx.doi.org/10.1016/0034-4257(76)90054-7

Pacione, M. (2005). City profile Dubai. *Cities*, 22(3), 255–265. doi:10.1016/j.cities.2005.02.001

Patino, J. E., & Duque, J. C. (2013). A review of regional science applications of satellite remote sensing in urban settings. *Computers, Environment and Urban Systems*, 37, 1-17. doi: http://dx.doi.org/10.1016/j.compenvurbsys.2012.06.003

Peng, L.L.H, & Jim, C.Y. (2013). Green-Roof effects on neighbourhood microclimate and human thermal sensation. *Energies*, 6, 598-618. doi:10.3390/en6020598

Physics Hypertextbook (2014). http://physics.info/heat-sensible/ (accessed 1st February, 2014).

Pichierri, P., Bonafoni, S., & Biondi, B. (2012). Satellite air temperature estimation for monitoring the canopy layer heat island of Milan. *Remote Sensing of Environment*, 127, 130–138. doi: 10.1016/j.rse.2012.08.025

Pielke, R.A.S. (2005). Land use and climate change. *Science*, 310 (5754), 1625-1626. doi: 10.1126/science.1120529

Pitman, A. J.(2003). The evolution of, and revolution in, land surface schemes designed for climate models. *International Journal of Climatology*, 23(5), 479-510. doi: 10.1002/joc.893

Prata, A. J., Caselles, V., Coll, C., Sobrino, J., & Ottle, C. (1995). Thermal remote sensing of land surface temperature from satellites: Current status and future prospects. *Remote Sensing Reviews*, 12, 175-224. doi: 10.1080/02757259509532285

Qian, J., & Zhou , Q. (2009). *Spatio-Temporal Pattern Analysis of the Built-Up Area Expansion in China's Aridzone.* Hong Kong: Prepared By The Centre for China Urban and Regional Studies Hong Kong Baptist University.

Qin, Z., Karnieli, A., & Berliner, P. (2001). A mono-window algorithm for retrieving land surface temperature from Landsat TM data and its application to the Israel-Egypt border region. *International Journal of Remote Sensing*, 22, 3719–3746. doi: 10.1080/01431160010006971.

Qing, S., Zhang, J., Cui, T., & Bao, Y. (2013). Retrieval of sea surface salinity with MERIS and MODIS data in the Bohai Sea. *Remote Sensing of Environment*, 136, 117-125. doi: 10.1016/j.rse.2013.04.016

Radhi, H., Assem, E., Sharples, S. (2014). On the colours and properties of building surface materials to mitigate urban heat islands in highly productive solar regions. *Building and Environment*, 72, 162-172. doi: 10.1016/j.buildenv.2013.11.005

Rajendran, S., Arumugam, M., & Chandras, V. A. (2002). Potential use of high resolution IRS-1C satellite data and detection of urban growth in and around of Tiruchirapalli City, Tamil Nadu State, India. *FIG XXII International Congress* (pp. 1-13). Washington, D.C. US

Ramadan, E., Z, C., & FENG, X. Z. (2004). Satellite remote sensing for urban growth assessment in Shaoxing City, Zhejiang Province. *Journal of Zhejiang University SCIENCE*, 5(9), 1095-1101.

Reeves, M., Zhao, M., & Running, S. (2006). Applying improved estimates of MODIS productivity to characterize grassland vegetation dynamics. *Rangeland Ecology & Management, 59*(1), 1-10.

Ren., Z., He, X., Zheng, H., Zhang, D., Yu, X., Shen, G. (2013). Estimation of the Relationship between Urban Park Characteristics and Park Cool Island Intensity by Remote Sensing Data and Field Measurement. *Forests*, 4, 868-886. doi: 10.3390/f4040868

Rhee, J., Seonyoung, P., & Zhenyu, Lu. (2014). Relationship between land cover patterns and surface temperature in urban areas. *GIScience & Remote Sensing*, 51(5), 521-536. doi: 10.1080/15481603.2014.964455

Richardson, G.R., Otero, J., Lebedeva, J., Chan, C.F. (2009). Developing climate change adaptation strategies: A risk assessment and planning tool for urban heat islands in Montreal. *Canadian Journal of Urban Research*, 18(1), 74-93.

Román, M. O., Gatebe, C. K., Shuai, Y., Wang, Z., Gao, F., Masek, J., et al. (2013).Use of in-situ and airborne multiangle data to assess MODIS- and Landsat-based estimates of

directional reflectance and albedo. *IEEE Transactions on Geoscience and Remote Sensing, 51(3),* 1393–1404.

Rosenthal, J.K., Crauderueff, R., Carter, M. (2008). urban heat island mitigation can improve New York city's environment: Research on the impacts of mitigation strategies on the urban environment. *Sustainable South Bronx Working Paper.* <http://nrs.harvard.edu/urn-3:HUL.InstRepos:12361745> Retrieved 15.June.14

Sailor, D.J., & L. Lu. (2004). A top-down methodology for developing diurnal and seasonal anthropogenic heating profiles for urban areas. *Atmospheric Environment,* 38: 2737–2748. doi: 10.1016/j.atmosenv.2004.01.034

Salman, A. A., Ali, A. E., & Mattar, H. E. (2008). Mapping land-use/land-cover of Khartoum using fuzzy classification. *Emirates Journal for Engineering Research, 13*(2), 27-43.

Salamanca, F., Georgescu, M., Mahalov, A., Moustaoui, M., & Wang, M. (2014). Anthropogenic heating of the urban environment due to air conditioning. *Journal of Geophysical Research: Atmospheres,* 119(10), 5949-5965. doi: 10.1002/2013JD021225

San, B. T. and M. L. Suzen, 2010. Evaluation of different atmospheric correction algorithms for EO-1 Hyperion imagery. *Internat Archives Photogrammetry, Rem. Sens. Spatial Info. Sci.,* XXXVIII (Part 8), Kyoto, Japan.

Sattari, F., & Hashim, M. (2014). A brief review of land surface temperature retrieval methods from thermal satellite sensors. *Middle-East Journal of Scientific Research,* 22 (5), 757-768. doi: 10.5829/idosi.mejsr.2014.22.05.21934

Schmugge, T., Frencha, A., Ritchiea, J.C., Rangoa, A., & Pelgrum, H. (2002). Temperature and emissivity separation from multispectral thermal infrared observations. *Remote Sensing of Environment, 79,* 189 – 198.

Schneider, A., Friedl, M., McIver, D., & Woodcock, C. (2003). Mapping urban areas by fusing multiple sources of coarse resolution remotely sensed data. *Photogrammetric Engineering and Remote Sensing,* 69 (12), 1377-1386.

Schneider, A., Seto K. C., & Webster, D. R. (2005). Urban growth in Chengdu, Western China: application of remote sensing to assess planning and policy outcomes, *Environment and Planning B: Planning and Design,* 32, 323 -345. doi:10.1068/b31142

Schneider, A., & Woodcock, C. E. (2008). Compact, dispersed, fragmented, extensive? A comparison of urban growth in twenty-five global cities using remotely sensed data, pattern metrics and census information, *Urban Studies,* 45(3), 659–692. doi: 10.1177/0042098007087340

Schwarz, N., Lautenbach, S., & Seppelt, R. (2011). Exploring indicators for quantifying surface urban heat islands of European cities with MODIS land surface temperatures. *Remote Sensing of Environment,* 115, 3175–3186. doi: 10.1016/j.rse.2011.07.003

Schwarz, N., Schlink, U., Franck, U., & Grobmann, K. (2012). Relationship of land surface and air temperatures and its implications for quantifying urbanheat island indicators—An application for the city of Leipzig (Germany). *Ecological Indicators,* 18, 693-704. doi: 10.1016/j.ecolind.2012.01.001

Seto, K. C., Woodcock, C. E., Song, C., Huang, X., Lu, J. & Kaufmann, R. K. (2002). Monitoring land-use change in the Pearl River Delta using Landsat TM, *International Journal of Remote Sensing,* 23(10), 1985–2004. doi:10.1080/01431160110075532

Shashua – Bar, L., & Hoffman, M.E. (2002). Vegetation as a climatic component in the design of an urban street; an empirical model for predicting the cool effect of urban green areas with trees. *Energy and Building,* 31 (3), 221 – 235. doi: 10.1016/S0378-7788(99)00018-3

Singh, S.K., Rao, D.N., Agrawal, M., Pandey, J., & Naryan, D. (1991). Air pollution tolerance index of plants. *Journal of Environmental Management,* 32(1), 45-55. DOI: 10.1016/S0301-4797(05)80080-5

Siu, L.W., & Hart, M.A. (2013). Quantifying urban heat island intensity in Hong Kong SAR,

China. *Environmental Monitoring and Assessment* 185, 4383–4398. doi: 10.1007/s10661-012-2876-6

Skyscraper Center. (2012). 100 Tallest completed buildings in the world. http://www.skyscrapercenter.com/ (accessed 2nd September, 2012).

Skyscraper Center. (2014). http://www.skyscrapercenter.com (accessed 2nd January, 2014).

Snyder, W.C., Wan, Z., Zhang, Y., & Feng, Y.-Z. (1998). Classification-based emissivity for land surface temperature measurement from space. *International Journal of Remote Sensing*, 19, 2753-2574. doi: 10.1080/014311698214497

Sobrino, J., Oltra-Carrió, R. , Sòria, G., Jiménez-Muñoz, J. C., Franch, Belén, Hidalgo, V., Mattar, C., et al., (2013). Evaluation of the surface urban heat island effect in the city of Madrid by thermal remote sensing. *International Journal of Remote Sensing*, 34(9-10), 3177-3192. doi: 10.1080/01431161.2012.716548

Sobrino, J. A., Jiménez-Muñoz, J. C., & Paolini, L. (2004). Land surface temperature retrieval from LANDSAT TM5. *Remote Sensing of Environment*, 90(4), 434–440. doi:10.1016/j.rse.2004.02.003

Song, C., Woodcock, C.E., Seto, K.C., Lenney, M.P., Macomber, S.A., 2001. Classification and Change Detection Using Landsat TM Data: When and How to Correct Atmospheric Effects?. *Remote Sensing of the Environment*, 75, pp. 230-244. doi:10.1016/S0034-4257(00)00169-3

Song, X., & Li, J. (2009). Land Cover Change Detection Using MSS and MODIS Data: A Case Study for Liangshan-Xiangling Region in Southwestern China. *Journal of Environmental Informatics, 13*(2), 119-126. doi: 10.3808/jei.200900147

Speak, A.F., Rothwell, J.J., Lindley, S.J., Smith, C.L. (2013). Reduction of the urban cooling effects of an intensive green roof due to vegetation damage. *Urban Climate*, 3: 40-55.

Stathopoulou, M., Cartalis, C., & Petrakis, M. (2007). Integrating Corine Land Cover data and Landsat TM for surface emissivity definition: application to the urban area of Athens, Greece. *International Journal of Remote Sensing*, 28(15), 3291-3304. doi: 10.1080/01431160600993421.

Stewart, D. J., Yin, Z. Y., Bullard, S. M., & MacLachlan, J. T. (2004). Assessing the Spatial Structure of Urban and Population Growth in the Greater Cairo Area, Egypt: A GIS and Imagery Analysis Approach. *Urban Studies*, 41(1), 95–116. doi:10.1080/0042098032000155704

Stewart, I. D., & Oke, T. R. (2012). Local climate zones for urban temperature studies. *Bulletin of the American Meteorological Society*, 93(12), 1879-1900. doi: http://dx.doi.org/10.1175/BAMS-D-11-00019.1

Stewart, I.D., Oke, T. R., & Krayenhoff, E. S. (2014). Evaluation of the 'local climate zone' scheme using temperature observations and model simulations. *International Journal of Climatology*, 34(4), 1062-1080. doi: 10.1002/joc.3746

Strahler, A., Muchoney, D., Borak, J., Friedl, M., Gopal, S., Lambin, E., Moody, A., (1999). *MODIS land cover product algorithm theoretical basis document, version 5.0*. Center for Remote Sensing, Boston University, Boston, Massachusetts, pp 72

Strano, E., Nicosia, V., Latora, V., Porta, S., & Barthélemy, M. (2012). Elementary processes governing the evolution of road networks. *Scientific Reports*, 2, 1-8. doi:10.1038/srep00296

Streutker, D.R. (2003). Satellite-measured growth of the urban heat island of Houston, Texas. *Remote Sensing of Environment*, 85, 282-289. doi: 10.1016/S0034-4257(03)00007-5

Strugnell, N.C., & Lucht, W. (2001). An algorithm to infer continental-scale albedo from AVHRR data, land cover class, and field observations of typical BRDFs. *Journal of climate*, 14, 1360–1376. doi: http://dx.doi.org/10.1175/1520-0442(2001)014<1360:AATICS>2.0.CO;2

Sudhira, H. S., Ramachandra, T. V., Raj, K. S., & Jagadish, K. S. (2010). Urban growth

analyses using spatial and temporal data. Centre for ecological sciences Indian institute of science. From ERNET: http://www.ces.iisc.ernet.in/energy/water/paper/urbangrowth_analysis/Urban_Growth_Analysis.pdf (accessed 4th January, 2011).

Svensson, M. K. 2004. Sky View Factor analysis–implications for urban air temperature differences. *Meteorological Applications*, 11: 201–211. doi: 10.1017/S1350482704001288

Tabachnick, B.G., Fidell L.S. (2012). *Using Multivariate Statistics* (6 ed.). Boston: Pearson Education Inc.

Taha, H. (1997). Urban climates and heat islands: Albedo, evapotranspiration, and anthropogenic heat. *Energy and Buildings*, 25(2), 99-103. doi: 10.1016/S0378-7788(96)00999-1

Taubenböck H, Wegmann M, Berger C, Breu M, 2008, "Spatiotemporal analysis of Indian mega cities", in *The International Archives of the Photogrammetry, Remote Sensing and Spatial Information Sciences* Eds. H Taubenböck, M Wegmann, C Berger, M Breunig Beijing pp 75-82

Taubenböck, H., Wegmannb, M., Roth, A., Mehl, H., & Dech, S. (2009). Urbanization in India – Spatiotemporal analysis using remote sensing data. *Computers, Environment and Urban Systems, 33*, 179–188. doi:10.1016/j.compenvurbsys.2008.09.003

Tian, G., Jiang, J., Yang, Z., & Zhang, Y. (2011). The urban growth, size distribution and spatio-temporal dynamic pattern of the Yangtze River Delta megalopolitan region, China. *Ecological Modelling*, 222(3), 865–878. doi:10.1016/j.cities.2005.05.009

Tian, G., Liu, J., Xie, Y., Yang, Z., Zhuang, D., & Niu, Z. (2005). Analysis of spatio-temporal dynamic pattern and driving forces of urban land in China in 1990s using TM images and GIS. *Cities, 12*(6), 400–410. doi:10.1016/j.cities.2005.05.009

Tiangcot, M., Lagmay, A. M. F., & Argete, J. (2008). ASTER-based study of the night-time urban heat island effect in Metro Manila. *International Journal of Remote Sensing*, 29 (10), 2799–2818. doi: 10.1080/01431160701408360

Thiel, M., Esch, T., & Schenk, A. (2008). Object-oriented detection of urban areas from TERRASAR-X data. *The International Archives of the Photogrammetry, Remote Sensing and Spatial Information Sciences*, XXXVII. Part B8., pp. 23-26. Beijing.

Tole, L. (2008). Changes in the built vs. non-built environment in a rapidly urbanizing region: A case study of the Greater Toronto Area. *Computers, Environment and Urban Systems, 32*, 355–364.

Tomlinson, C. J., Chapman, L., Thornes, J. E., & Baker, C. J. (2012). Derivation of Birmingham's summer surface urban heat island from MODIS satellite images. *International Journal of Climatology*, 32 (2), 214-224. doi: 10.1002/joc.2261

Tonkaz, T., Çetin, M., (2007). Effects of urbanization and land-use type on monthly extreme temperatures in a developing semi-arid region, Turkey. *Journal of Arid Environments*, 68, 143–158. http://dx.doi.org/10.1016/j.jaridenv.2006.03.020

UNEP -united Nations Environment Programme - (2012). Sustainable, resource efficient cities – making it happen! http://www.unep.org/urban_environment/PDFs/SustainableResourceEfficientCities.pdf (accessed 25th November, 2014).

Unger, J. (2009). Connection between urban heat island and sky view factor approximated by a software tool on a 3D urban database. *Int. J. Environment and Pollution*. 36, 59-80. doi: 10.1504/IJEP.2009.021817

Unger, J., Lelovics, E., & Gál, T. (2014). Local Climate Zone mapping using GIS methods in Szeged. *Hungarian Geographical Bulletin*, 63 (1), 29–41. doi: 10.15201/hungeobull.63.1.3

United Nations. (2012). World urbanization prospects: The 2011 revision. http://esa.un.org/unup/ (accessed 20th August, 2012).

United Nations (2014). World urbanization prospects: The 2014 revision. http://esa.un.org/unpd/wup/Highlights/WUP2014-Highlights.pdf (accessed 18th March, 2015).

US EPA. (2008a). Urban Heat Island basics. In *Reducing Urban Heat Islands: Compendium of Strategies*. Washington. http://www.epa.gov/heatisland/resources/pdf/BasicsCompendium.pdf (accessed 8th June, 2013).

US EPA (2008b). *Reducing urban heat islands: Compendium of strategies*. United States Environmental Protection Agency, Washington, D.C. http://www.epa.gov/hiri/resources/compendium.htm. (accessed 12 November, 2013).

USGS (United States Geological Survey). (2013). SLC-off Products: Background. http://landsat.usgs.gov/products_slcoffbackground.php (accessed 12 January, 2014).

USGS (U.S. Geological Survey) (2014). http://landsat.usgs.gov/calibration_notices.php. (accessed 9th September, 2014).

Valor, E., & Caselles, V. (1996). Mapping land surface emissivity from NDVI: Application to European, African, and South American areas. *Remote Sensing of Environment*, 57 (3), 167-184. doi: 10.1016/0034-4257(96)00039-9

Van De Griend, A. A., & Owe, M. (1993). On the relationship between thermal emissivity and the normalized difference vegetation index for natural surfaces. *International Journal of Remote Sensing*, 14 (6), 1119-1131. doi: 10.1080/01431169308904400

Vargo, J., Habeeb, D., & Stone, B. (2013). The Importance of land cover change across urban rural typologies for climate modelling. *Journal of Environmental Management*, 114, 243-52. doi:10.1016/j.jenvman.2012.10.007

Vayda, E. (2010). Green roofs and living walls. *A Guide for Small Businesses. Strategic Sustainability Consulting*.

Verbyla, D. L., & Hammond, T. O. (1995). Conservative bias in classification accuracy assessment due to pixel-by-pixel comparison of classified images with reference grids. *International Journal of Remote Sensing*, 16, 581-587. doi:10.1080/01431169508954424

Verzosa, L., & Gonzalez, R. (2010). Remote sensing, geographic information systems and shannon's entropy: measuring urban sprawl in a mountainous environment. In W. Wagner, & B. Székely (Ed.), *ISPRS TC VII Symposium. Vienna*, pp. 269-274. IAPRS.

Vilanova, A., Telea, A., Scheuermann, G., & Möller, T. (2008). Visual Analysis and Semantic Exploration of Error Aware Urban Change Detection. *Eurographics/ IEEE-VGTC Symposium on Visualization, 27*(3).

Voogt, J.A., & Oke, T.R. (2003). Thermal remote sensing of urban climates. *Remote Sensing of Environment*, 86, 370–384. doi: 10.1016/S0034-4257(03)00079-8

Wan, Z., & Dozier, J. (1996). A generalized split-window algorithm for retrieving land-surface temperature from space. *IEEE Transactions on Geoscience and Remote Sensing*, 34(4), 892–905. doi: 10.1109/36.508406

Wan, Z., Zhang, Y., Zhang, Q., & Li, Z.-L. (2004). Quality assessment and validation of the MODIS global landsurface temperature. *International Journal of Remote Sensing*, 25 (1), 261-274. doi: 10.1080/0143116031000116417

Wang, J.-J., & Lu, X.X. (2010). Estimation of suspended sediment concentrations using Terra MODIS: An example from the Lower Yangtze River, China. *Science of the Total Environment*, 408(5), 1131-1138. doi: 10.1016/j.scitotenv.2009.11.057

Wang, M., Nim, C. J., Son, S., & Shi, W. (2012). Characterization of turbidity in Florida's Lake Okeechobee and Caloosahatchee and St. Lucie Estuaries using MODIS-Aqua measurements. *Water Research*, 46(16), 5410-5422. doi: 10.1016/j.watres.2012.07.024

Wang, N., Wu, H., Nerry, F., Li, C., Li, Z.-L. (2011). Temperature and Emissivity Retrievals From Hyperspectral Thermal Infrared Data Using Linear Spectral Emissivity Constraint. *IEEE T. Geoscience and Remote Sensing*, 49(4), 1291-1303. doi: 10.1109/TGRS.2010.2062527

Ward., D., Phinn, S., & Murray, A. T. (2000). Monitoring Growth in Rapidly Urbanizing Areas Using Remotely Sensed Data. *Professional Geographer, 52*(3), 371 –386.

Wark, D. Q., Yamamoto, G., & lienesch, J. (1962). Infrared flux and surface temperature determinations from TIROS radiometer measurements, *Report (US Weather Bureau Meteorological Satellite Laboratory)*, no. 10. M07.362.2 U587re no.10, Washington, D.C. http://docs.lib.noaa.gov/rescue/TIROS/QC8795U45no10.pdf (accessed 18th July, 2012).

Watson, I. D., & Johnson, G. T. (1987). Graphical estimation of sky view-factors in urban environments. *Journal of Climatology*, 7: 193–197. doi: 10.1002/joc.3370070210

Weng, Q. (2001). A remote sensing-GIS evaluation of urban expansion and its impact on surface temperature in the Zhujiang Delta, China. *International Journal of Remote Sensing*, 22, 1999–2014. doi: 10.1080/713860788

Weng, Q., Dengsheng, L., & Schubring, J. (2004). Estimation of land surface temperature–vegetation abundance relationship for urban heat island studies. *Remote Sensing of Environment*, 89, 467–483. doi: 10.1016/j.rse.2003.11.005

Weng, Q., & Larson, R.C. (2005). Satellite Remote Sensing of Urban Heat Islands: Current Practice and Prospects. In: Jensen, R.R., Gatrell, J.D., & McLean, D.D. (eds). *Geospatial technologies in urban environments*. Springer, Berlin, pp 91–111

Winters, N., Goldberg, M. S., Hystad, P., Villeneuve, P. J., & Johnson, K. C. (2015). Exposure to ambient air pollution in Canada and the risk of adult leukemia. *Science of the Total Environment*, 526, 153-176. doi: 10.1016/j.scitotenv.2015.03.149

Wu, C., Lung, S. C., Jan , F.(2013). Development of a 3-D urbanization index using digital terrain models for surface urban heat island effects. *ISPRS Journal of Photogrammetry and Remote Sensing*, 81, 1–11. doi: http://dx.doi.org/10.1016/j.isprsjprs.2013.03.009

Wu, J., Jenerette, G. D., Buyantuyev, A., Redman, C. L. (2011). Quantifying spatiotemporal patterns of urbanization: The case of the two fastest growing metropolitan regions in the United States. *Ecological Complexity*, 8, 1-8. doi:10.1016/j.ecocom.2010.03.002

Wu, W., Courel, M., & LE, Rhun, L. J. (2003). Application of Remote Sensing to the Urban Expansion Analysis for Nouakchott, Mauritania. *Geocarto International, 18*(1). doi:10.1080/10106040308542259

Xian, G., Crane, M., & McMahon, C. (2005). Assessing urban growth and environmental change using remotely sensed data. *Pecora 16 "Global Priorities in Land Remote Sensing"* (pp. 1-9). Sioux Falls, South Dakota.

Xiao, R., Weng, Q., Ouyang, Z., Li, W., Schienke, E.W., Zhang, Z. (2008). Land Surface Temperature Variation and Major Factors in Beijing, China. *Photogrammetric Engineering & Remote Sensing*. 74(4), 451–461.

Xiuwan, C., (2002). Using remote sensing and GIS to analyze land cover change and its impacts on regional sustainable development. *International Journal of Remote Sensing*, 23 (1),107-124. doi: 10.1080/01431160010007051

Xu, H. Q., & Chen, B.Q. (2004). Remote sensing of the urban heat island and its changes in Xiamen City of SE China. *Journal of Environmental Sciences*, 16 (2), 276 —281.

Yagoub, M. (2004). Monitoring of urban growth of a desert city through remote sensing: Al-Ain, UAE, between 1976 and 2000. *International Journal of Remote Sensing*, 25(6), 1063-1076. doi: http://dx.doi.org/10.1080/0143116031000156792

Yang, L., Xian, G., Klaver, J. M., & Deal, B. (2003). Urban land-cover change detection through sub-pixel imperviousness mapping using remotely sensed data. *Photogrammetric Engineering & Remote Sensing, 69*(9), 1003-1010.

Yang, X., & Lo, C. (2003). Modelling urban growth and landscape changes in the Atlanta metropolitan area. *International Journal of Geographical Information Science*, 17, 463-488.

Yang, S., Zha, Y., & Gao, J. (2001). Applications of remote sensing and gis to monitoring of urban sprawl: a case study in Wuxi City, China. *Geographic Information Sciences*, 7(2), 137-141.

Yao, L., & Lu, N. (2014). Particulate matter pollution and population exposure assessment over mainland China in 2010 with remote sensing. *Int. J. Environ. Res. Public Health*, 11, 5241-5250. doi:10.3390/ijerph110505241

Yeh, C. T., & Huang, S. L. (2009). Investigating spatiotemporal patterns of landscape diversity in response to urbanization. *Landscape and Urban Planning*, 93, 151–162. doi:10.1016/j.landurbplan.2009.07.002

Yin, Z. Y., Stewart, D. J., Bullard, S., & MacLachlan, j. T. (2005). Changes in urban built-up surface and population distribution patterns during 1986–1999: A case study of Cairo, Egypt. *Comput., Environ. and Urban Systems, 29*, 595–616. doi:10.1016/j.compenvurbsys.2005.01.008

Yuan, F. (2008). Land-cover change and environmental impact analysis in the Greater Mankato area of Minnesota using remote sensing and GIS modelling. *International Journal of Remote Sensing, 29*(4), 1169–1184. doi:10.1080/01431160701294703

Yuan, F., & Bauer, M.E. (2007). Comparison of impervious surface area and normalized difference vegetation index as indicators of surface urban heat island effects in Landsat imagery. *Remote Sensing of Environment*, 106, 375–386. doi: 10.1016/j.rse.2006.09.003.

Yue, W., Liu, Y., & Fan, P. (2010). Polycentric urban development: the case of Hangzhou. *Environment and Planning A*, 42, 563-577. doi:10.1068/a42116

Zakšek, K., Oštir, K., Kokalj, Ž. (2011). Sky-View Factor as a Relief Visualization Technique. *Remote Sensing*, 12, 398-415. doi: http://dx.doi.org/10.3390/rs3020398

Zhang, C., Xie, Z., Roberts, C., Berry, L., & Chen, G. (2012). Salinity assessment in northeast Florida Bay using Landsat TM data. *Southeastern Geographer*, 52(3), 267-281. doi: 10.1353/sgo.2012.0027

Zhang, Q. Ban, Y., Liu, J. & Hu, Y. (2009). Simulation and analysis of urban growth scenarios for the Greater Shanghai Area, China. *Computers, Environment and Urban Systems*, 35, 126–139. doi:10.1016/j.compenvurbsys.2010.12.002

Zhang, X., Zhong, T., Wang, K., & Cheng, Z. (2009). Scaling of impervious surface area and vegetation as indicators to urban land surface temperature using satellite data. *International Journal of Remote Sensing*, 30 (4), 841–859. doi: 10.1080/01431160802395219

Zhao, H., Due, J., & Guo, D. (2007). Analysis of Urban Expansion and Driving Forces in Xuzhou City Based on Remote Sensing. *Journal of China University of Mining & Technology, 17*(2), 267-271.

Zhao, W., Gong, H., Zhao, W., & Li, X. (2011). The distribution of aerosol optical depth retrieved by TM imagery over Beijing urban area, China. *IEEE International Geoscience and Remote Sensing Symposium*, July 2011, pp.2185-2188. doi: 10.1109/IGARSS.2011.6049600

Zhao, W., Tamura, M., & Takahashi, H. (2001). Atmospheric and spectral corrections for estimating surface albedo from satellite data using 6S code. *Remote Sensing of Environment, 76*, 202 – 212. doi: http://dx.doi.org/10.1016/S0034-4257(00)00204-2.

Zhou, D., Zhao, S., Liu, S., Zhang, L., & Zhu, C. (2014). Surface urban heat island in China's 32 major cities: Spatial patterns and drivers. *Remote Sensing of Environment*, 152, 51–61. doi: 10.1016/j.rse.2014.05.017

Zhou, L., Dickinson, R.E., Tian, Y., Jin, M., Ogawa, K., Yu, H., et al.. (2003). A sensitivity

study of climate and energy balance simulations with use of satellite derived emissivity data over Northern Africa and the Arabian Peninsula. *J. Geophys. Res., 108 (D24)*. doi:10.1029/2003JD004083

Zhou, Q., Li, B., & Kurban, A. (2008). Trajectory analysis of land cover change in arid environment of China. *International Journal of Remote Sensing, 29*(4), 1093–1107. doi: 10.1080/01431160701355256